Institute of Fundamental Technological Research

Polish Academy of Sciences

Doctoral thesis

Stimuli-Responsive Polymer Nanomaterials for Biomedical Applications

Mohammad Ali Haghighat Bayan, M.Sc. Eng.

Discipline of science: Materials Engineering

Supervisor: Dr. Hab. Filippo Pierini

Co-supervisor: Dr. Pawel Nakielski

Warsaw 2024

I would like to express my sincere thanks to

Dr. Filippo Pierini and Dr. Pawel Nakielski, thank you for your time and assistance throughout my Ph.D. journey.

To all my colleagues, who always provided valuable advice and help.

To my parents, I wouldn't have been able to reach this point without their support, motivation, and encouragement.

Table of contents

Abstract 6

1- Electrospinning 7

2- Stimuli-Responsive Materials 9

2-1- Principles of Stimuli-Responsive Materials 9

3- Background on Face Masks and the Pandemic 12

4- Nanotechnology in Personal Protective Equipment 14

5- Electrospinning and Drug Delivery 16

5-1- Methods of Drug Incorporation into the Fiber 16

5-2- Core-Shell Nanofibrous Systems in Drug Delivery 18

6- Smart Drug Delivery Systems 20

7- Aim of the Study 23

8-1- Publications Included in the Cycle of the Dissertations 25

8-2- Summary of the Publications Included in the Publication Cycle of the Dissertation 27

10- References 38

11- Original Publications 43

12- Statement of the Co-Authors 111

Abstract

This doctoral thesis investigates the development and application of stimuli-responsive polymer nanomaterials for advanced biomedical applications, mainly focusing on fabricating electrospun nanofibers that change their properties under the influence of external stimulation. The electrospinning technique forms the basis of this study. This technique facilitates the production of micro- to nanofibers, which are highly valued in the healthcare system.

This study extensively discusses the integration of plasmonic nanoparticles into nanofibers to provide them with photothermal and photodynamic properties. This integration facilitates the development of antibacterial face masks and smart drug delivery systems. Incorporating indocyanine green (ICG) in nanofibers further enhances these nanomaterials' functionality, significantly improving pathogen eradication and filtration upon light activation.

Moreover, the research delves into the on-demand drug delivery capabilities of the developed nanofibers. By utilizing near-infrared (NIR) light-activated core-shell structures, the study displayed a novel approach to achieve controlled and sustained drug release, highlighting the potential for these materials to advance treatments.

In conclusion, this Ph.D. thesis presents significant improvements in the design and application of stimuli-responsive polymer nanomaterials, emphasizing their potential to enhance biomedical applications such as protective face masks and smart drug delivery systems. The findings contribute to the broader materials engineering field and pave the road to future research and development in nanotechnology-driven biomedical solutions.

1- Electrospinning

Electrospinning is a method used to make fibers with diameters spanning from a few nanometers to several micrometers. This technique allows for the creation of very fine fibers of various sizes. The electrospinning setup involves applying a high-voltage electrical field to a polymer solution, causing the formation of an electrically charged jet (Figure 1).[1–5] As this jet goes towards a grounded collector, it undergoes stretching and thinning, resulting in the deposition of ultrafine fibers. These nanofibers exhibit unique properties such as high surface area, tunable porosity, and the ability to incorporate various functional materials, making electrospinning a critical method in nanotechnology.[3,4] Electrospinning involves several key components: a high-voltage source of power, a spinneret, a syringe pump, and a grounded collector. The syringe is then filled with the polymer solution and equipped with spinneret at a controlled rate. When a high voltage is applied, the polymer droplet at the tip of the spinneret becomes charged, forming a Taylor cone. A fine polymer jet is ejected once the electrostatic force overcomes the surface tension. As the jet travels towards the collector, it undergoes rapid solvent evaporation, solidifying into fibers. The spun fibers are formed a non-woven mat on the collector. Depending on the desired fiber alignment and mat architecture, the collector can be a flat, rotating drum or other geometries.[6]

Electrospinning is a method in nanotechnology used to produce ultrafine fibers with unique properties such as high surface area, tunable porosity, and the ability to incorporate various functional materials.[1-3] The setup consists of several essential components: a high-voltage power source, a syringe pump, a spinneret, and a grounded collector, as seen in Figure 1. To begin, the syringe is filled with a polymer solution and connected to the spinneret, which dispenses the solution at a controlled rate. A high voltage between the spinneret and the grounded collector creates an electric field. This field charges the polymer droplet at the tip of the spinneret, forming

a Taylor cone. When the applied voltage surpasses a critical threshold, the electrostatic forces overcome the droplet's surface tension, resulting in the ejection of a fine polymer jet. As the jet travels toward the grounded collector, it undergoes rapid stretching and thinning, driven by the electric field. During this journey, solvent evaporation occurs, solidifying the jet into ultrafine fibers.[4-6] The process results in the deposition of nanofibers on the collector, characterized by their high surface area, customizable porosity, and the potential for incorporating functional additives, making electrospinning a versatile and widely used technique in nanotechnology.

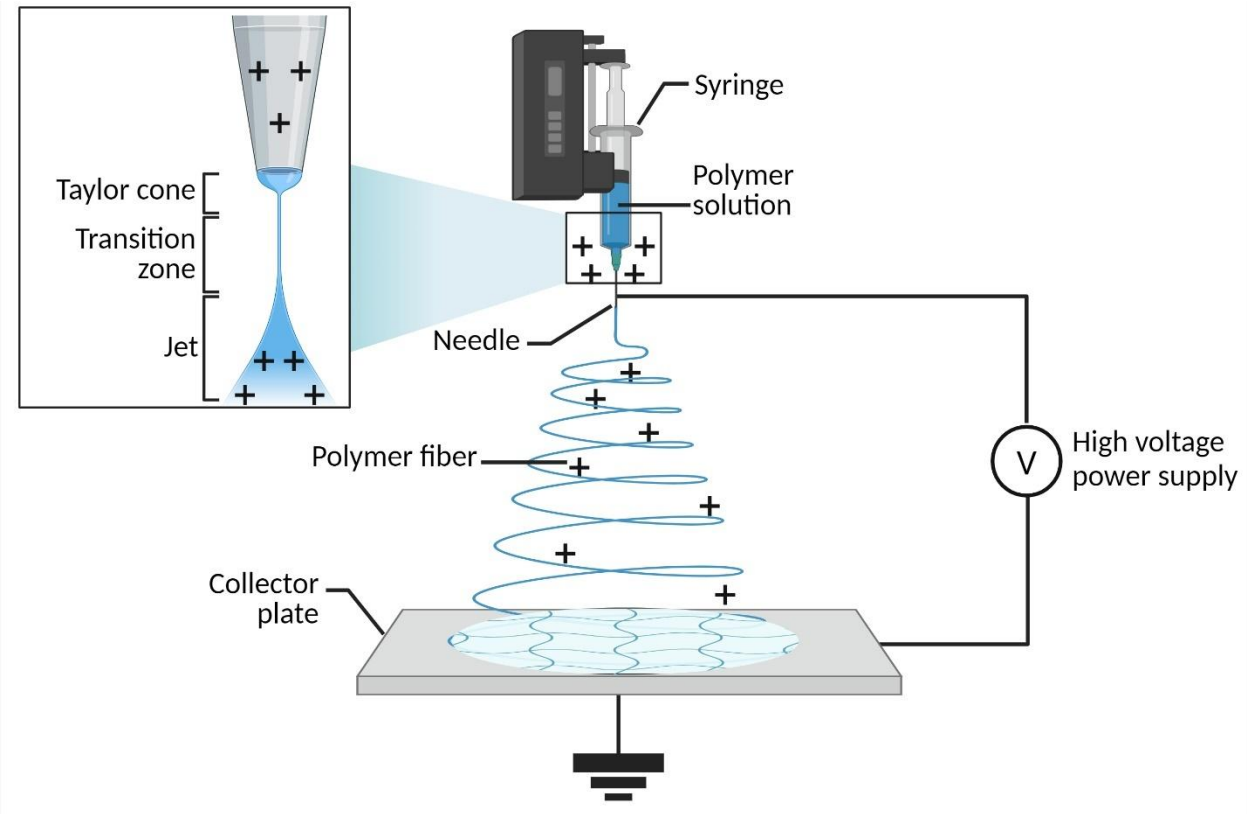

Figure 1. *Schematic of the electrospinning process. Key components include a high-voltage power supply, syringe pump, spinneret, and collector.*

2- Stimuli-Responsive Materials

Stimuli-responsive materials, also known as smart materials, are designed to undergo considerable and predictable changes in their properties in response to stimuli.[7,8] These stimuli include temperature[8], pH[9], light[10,11], electric[12], magnetic[13], and mechanical forces[14]. The ability of these materials to adapt and respond dynamically to environmental changes makes them invaluable in various applications, from biomedical devices and drug delivery systems to sensors, actuators, and adaptive textiles.[15–20] The development of stimuli-responsive materials has a rich history that spans over a century.[21] The early 20th century saw the initial exploration of materials that could change properties in response to external influences, such as temperature-sensitive polymers and piezoelectric materials. However, it was only in the late 20th and early 21st centuries that significant advancements were made, driven by innovations in polymer chemistry, nanotechnology, and materials science.[22,23] These advancements have enabled the design and control of materials with tailored responsiveness to specific stimuli, opening up many new applications.

2-1- Principles of Stimuli-Responsive Materials

When stimuli-responsive materials are exposed to stimuli, they undergo reversible changes in their physical or chemical properties. This change leads to shifts in shape, volume, temperature, conductivity, color, or mechanical properties.[8,11,13–15] The response mechanisms are broadly classified based on the type of stimulus: external stimuli and internal stimuli (Figure 2). External stimuli include thermo-responsive materials like poly(N-isopropyl acrylamide) (PNIPAM), which transition from hydrophilic to hydrophobic above its lower critical solution temperature [24]; photo-responsive materials like azobenzene-containing polymers, which undergo reversible trans-cis isomerization under UV light[25]; electro-responsive materials like polyaniline and polypyrrole,

which change their conductivity and mechanical properties under electric fields[26,27]; and magneto-responsive materials like magnetorheological fluids, which transition from liquid to solid-like states in magnetic fields[28]. Internal stimuli include pH-responsive materials like poly(acrylic acid) (PAA), which swell or shrink depending on the surrounding pH[9]; redox-responsive materials, which alter their properties in response to oxidation-reduction potential[29], such as disulfide bonds cleaving under reducing conditions; and enzyme-responsive materials, which change structure or properties in the presence of specific enzymes, such as polymer hydrogels degrading in the presence of matrix metalloproteinases (MMPs)[30].

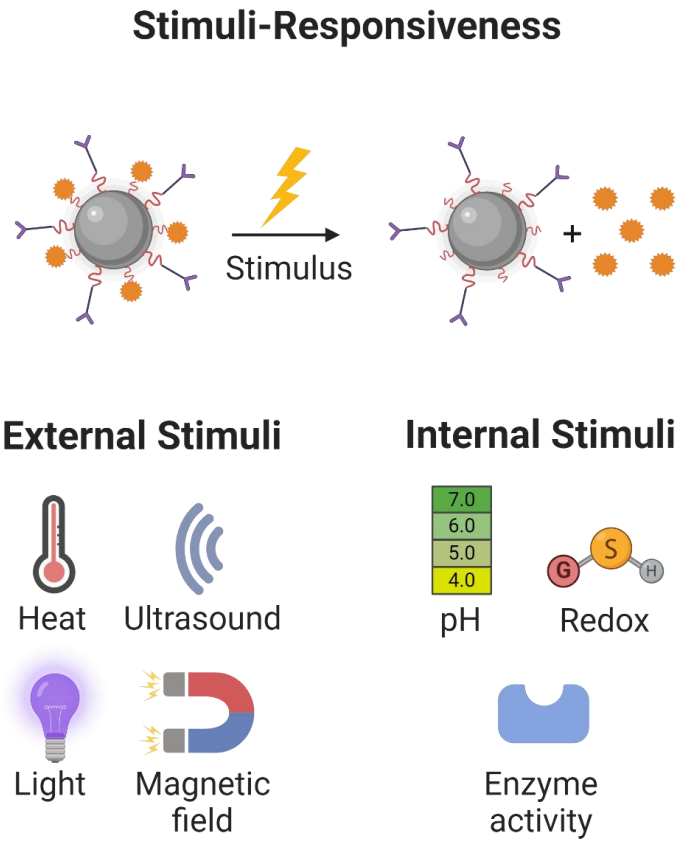

Figure 2. *Illustration of various stimuli-responses. Thermo-responsive, photo-responsive, magneto-responsive, and ultrasound-responsive materials are in the category of external stimuli, while pH-responsive, redox-responsive, and enzyme-responsive materials are in the category of internal stimuli-responsive materials.*

Innovations in material synthesis and processing techniques are expected to enhance the performance and applicability of stimuli-responsive materials. Additionally, integrating these materials with other advanced technologies, such as nanotechnology and biotechnology, will open up new possibilities in fields like personalized medicine, smart infrastructure, and environmental sustainability.[31–36] Stimuli-responsive materials represent a dynamic and versatile class of materials that have the potential to revolutionize various industries. While challenges remain in scalability, ongoing research and technological advancements are aimed toward overcoming these hurdles and expanding the horizons of stimuli-responsive materials, exhibiting their role as key enablers of future innovations.

2-2- Applications of Electrospun Nanofibers

The unique properties of electrospun nanofibers have led to various applications across several fields, as seen in Figure 3. In biomedical applications, electrospun fibers mimicking the extracellular matrix can provide a suitable environment for growing cell and tissue regeneration. Additionally, the nanofibers are used to engineer skin, bone, cartilage, and vascular tissues.[37] Nanofibers can be loaded with therapeutic agents and designed for controlled release, enhancing the efficacy and reducing the side effects of drugs.[38] Additionally, electrospun mats can protect wounds, promote healing, and deliver antimicrobial agents.[39] In environmental applications, the high surface area and tunable porosity of electrospun fibers make them ideal for air and water filtration applications, effectively removing particulate matter, bacteria, and other contaminants.[40] These fibers can also support catalysts, providing high surface area and accessibility for catalytic reactions.[41] Nanofibers have applications in batteries, solar cells, and supercapacitors in energy storage due to their high surface area, which enhances charge storage

capacity and efficiency.[42] In textiles, electrospun fabrics can be engineered to provide protection against chemical, biological, and environmental hazards while maintaining breathability and comfort.[43]

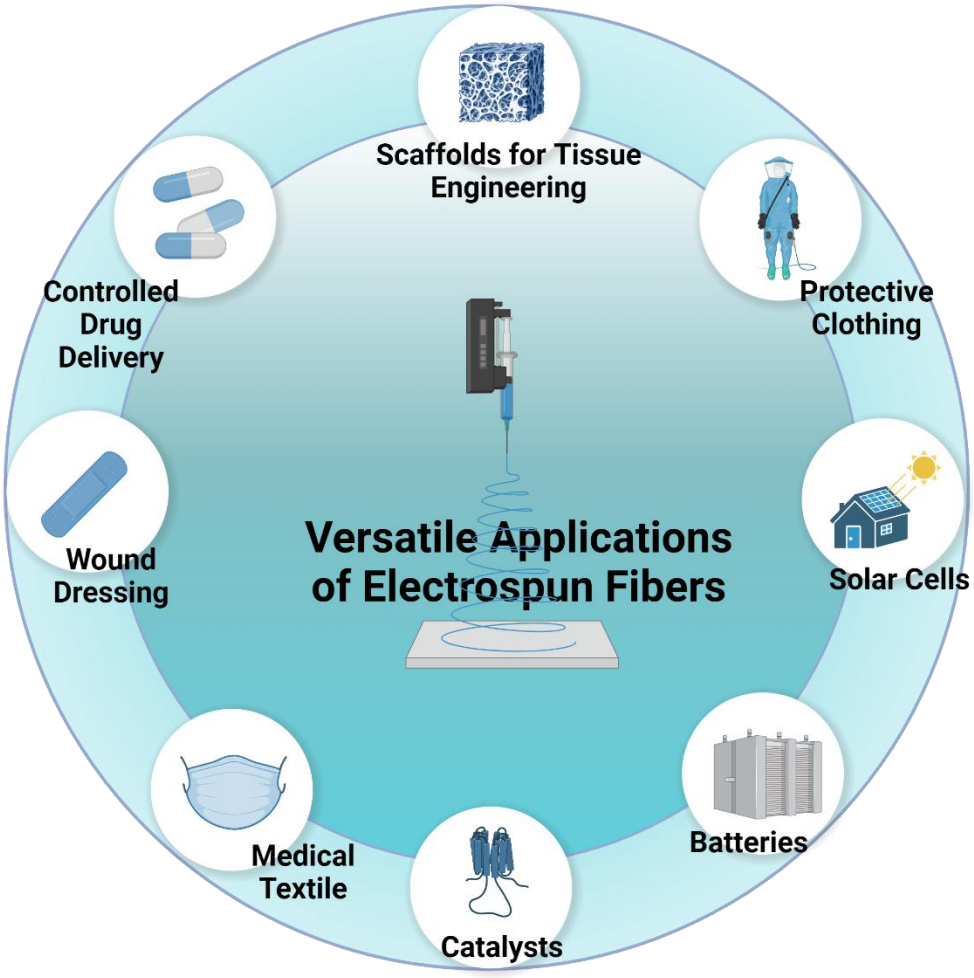

Figure 3. *Schematic of various applications of electrospun nanofibers.*

3- Background on Face Masks and the Pandemic

Personal protective equipment (PPE) has always been crucial for ensuring safety. Still, the COVID-19 pandemic underscored its vital role in protecting healthcare workers and the public from infectious diseases.[44–46] The pandemic exposed critical deficiencies in existing PPE,

especially face masks, leading to a demand for research to enhance their efficacy. The rapid transmission of the virus necessitated widespread mask use, but conventional masks often lacked suitable protection in high-risk environments like hospitals. Healthcare workers needed masks that provided continuous protection during long shifts without causing discomfort or compromising breathability.[47]

Nevertheless, many face masks led to skin irritation, breathing difficulties, and reduced efficacy over time. The pandemic also revealed vulnerabilities in PPE supply chains, highlighting the need for alternative manufacturing techniques using readily available materials to produce high-quality protective equipment.[48,49] Beyond basic filtration, there was a demand for multifunctional PPE with antibacterial properties and self-cleaning. To achieve the mentioned facial mask characteristics, we introduced stimuli-responsive materials on the available face masks to enhance protection and comfort.[50] Nanotechnology, particularly electrospinning, emerged as a critical solution, producing nanofibers with properties ideal for advanced face masks (Figure 4). During the pandemic, my research focus was on developing high-performance masks by employing the antibacterial properties of stimuli-responsive materials and multi-layered structures of electrospun mats to improve filtration efficiency while maintaining breathability.

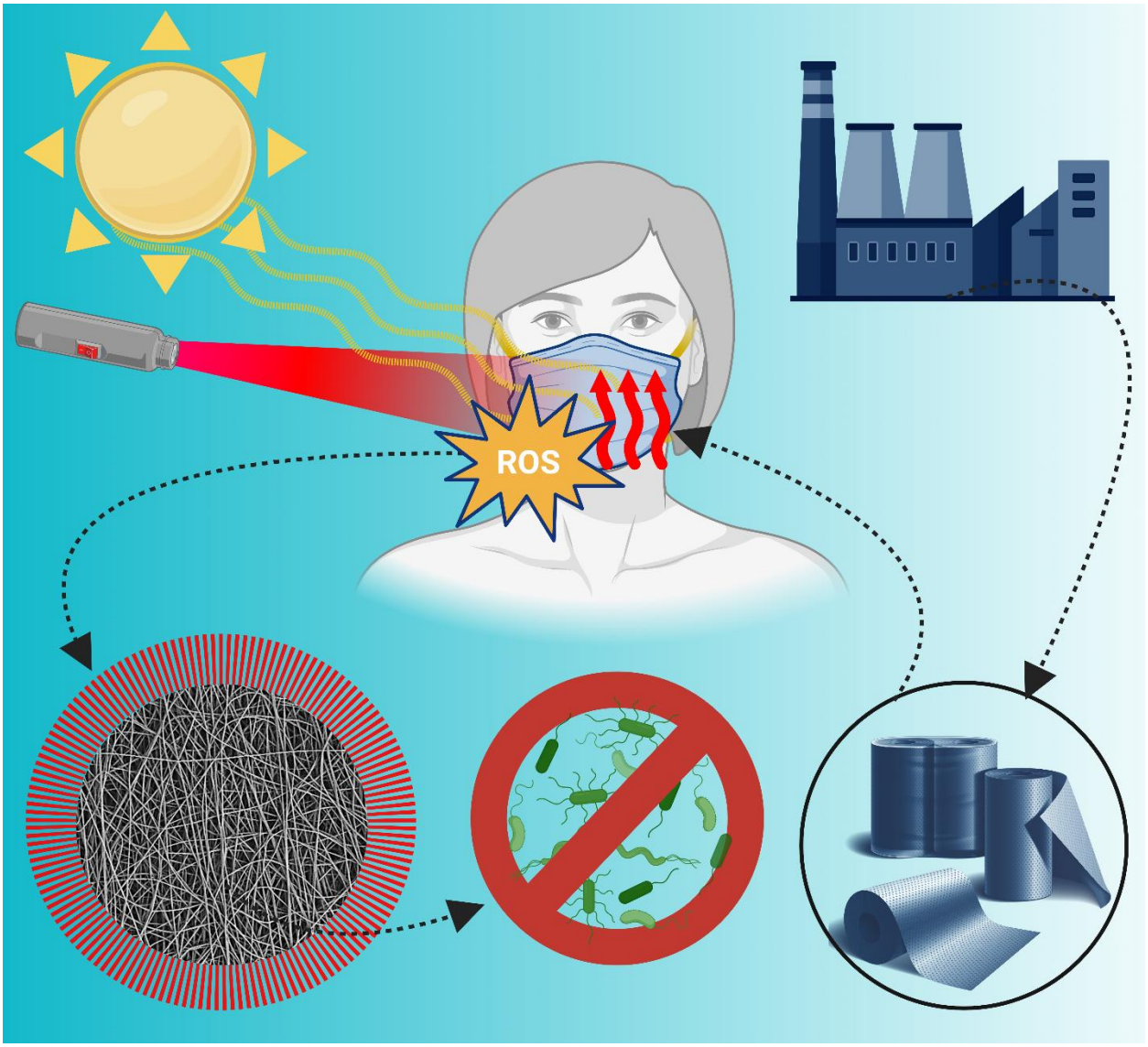

Figure 4. *Schematic showing the multifunctional electrospun mat for on-demand photothermal antibacterial eradication.*

4- Nanotechnology in Personal Protective Equipment

PPE has long been critical in protecting individuals from hazardous environments, infectious agents, and workplace dangers. Nanotechnology has transformed the development and enhancement of PPE, offering extraordinary levels of safety, functionality, and comfort.[51-53] One of the most significant contributions of nanotechnology to PPE is incorporating antimicrobial and

antiviral properties. Nanoparticles such as silver, copper, and gold have been extensively studied and utilized for their potent antimicrobial effects, as seen in Figure 5. These nanoparticles can be embedded into PPE materials, such as masks, gloves, and clothes, to inhibit the growth and transmission of harmful microorganisms.[54-60]

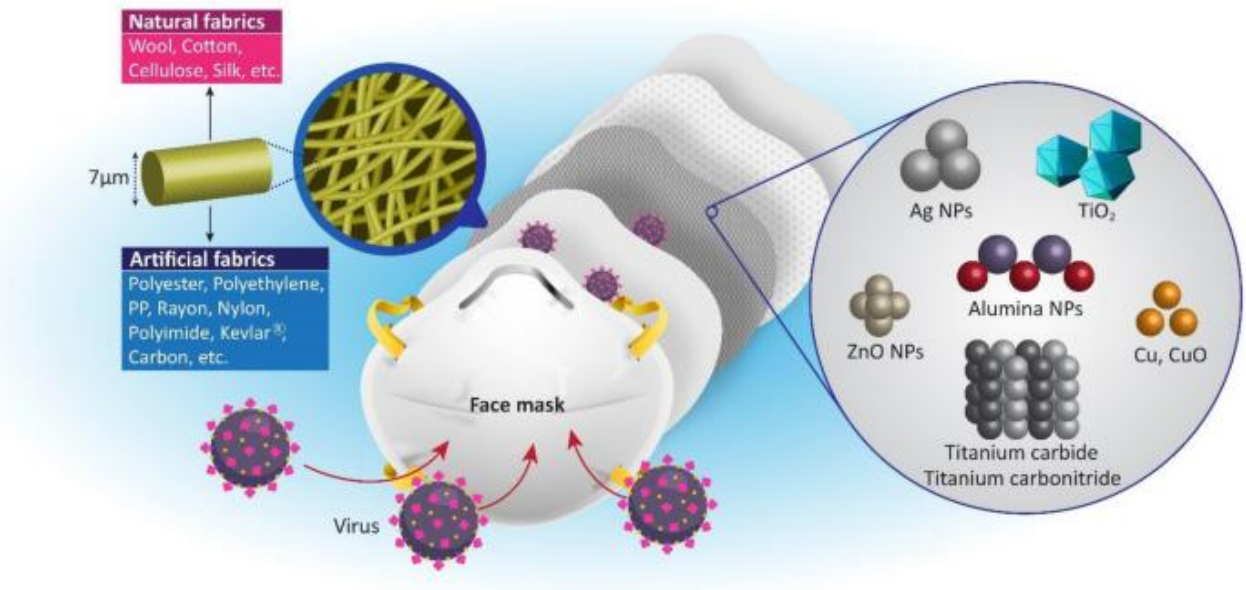

Figure 5. *The schematic structure of multi-layered anti-virus face masks incorporated with metallic nanoparticles and reproduced from ref.* [46] *with permission.*

Gold nanoparticles, in particular, have shown exceptional efficacy in destroying many bacteria, viruses, and fungi. Their small size allows them to penetrate microbial cells, disrupting vital processes and leading to cell inactivation.[61-63] This feature is valuable in infectious disease outbreaks, such as the COVID-19 pandemic, where preventing the spread of viruses is vital. Nanotechnology also enhances the barrier properties of PPE. Traditional materials can be augmented with nanofibers, creating a dense yet breathable barrier that effectively filters out pathogens, particulates, and hazardous chemicals. Electrospun nanofibers, for example, can be used to produce masks and respirators with superior filtration efficiency while maintaining

breathability and comfort for extended use. These nanofiber-based filters can capture particles as small as viruses and fine dust, protecting a broad spectrum of airborne threats. Moreover, the increased surface area of nanofibers improves the entrapment of contaminants, further enhancing the protective capabilities of PPE.[64-66] Traditional PPE often faces criticism for being uncomfortable, reducing compliance and effectiveness. Nanotechnology addresses these issues by enabling the development of lightweight and flexible materials that do not compromise protection.

5- Electrospinning and Drug Delivery

In drug delivery, electrospinning offers new paths for developing advanced therapeutic systems. By engineering materials at the nanoscale, scientists can create drug delivery systems with improved efficacy, targeted delivery, and controlled release profiles.[67-71] One of the most promising developments in this area is using core-shell nanofibrous systems, which combine the advantages of nanofibers and core-shell structures to create highly efficient drug carriers.[72-74] Electrospinning offers several advantages in drug delivery, including enhanced bioavailability, as nanofibers improve the solubility and stability of poorly water-soluble drugs, thereby increasing their therapeutic efficacy. Additionally, nanofibers facilitate controlled release, with nanoparticles engineered to release drugs sustainably for prolonged therapeutic effects. Moreover, nanocarriers can be functionalized with targeting ligands, imaging agents, and therapeutic molecules, providing multifunctionality that enables simultaneous diagnosis and treatment.[75,76]

5-1- Methods of Drug Incorporation into the Fiber

There are several strategies for incorporating drugs into electrospun fibers, as illustrated in Figure 6. The most common method is blend electrospinning, which combines the drug into the polymer solution before fiber production.[77-79] This method requires finding a solvent compatible with the

polymer and the drug or reaching a homogeneous dispersion of drug molecules in the polymer solution. In this approach, polymer features such as solubility and degradability may influence the drug release profile, depending on the polymer used. Water-soluble polymers and drugs are used for immediate release, leading to rapid drug release when the electrospun membrane is placed in an aqueous medium. Conversely, when the polymer and drug are dissolved in an organic solvent, the initial burst release is followed by a more sustained elution. Core-shell, multi-layer, or emulsion spinning are used for more controlled release. Drugs can be encapsulated in either the fibers' core or shell. However, the drug in core encapsulation provides a prolonged release due to a more extended diffusion pathway. Emulsion electrospinning is another method for incorporating drugs into electrospun fibers.[80,81] In this technique, a water-in-oil or oil-in-water emulsion is prepared, where the drug is dissolved in the droplets of the dispersed phase. The prepared emulsion is subsequently subjected to the electrospinning process, during which it is transformed into fibrous structures. This method can form fibers with core-shell structure depending on the composition and processing parameters.[82] The primary advantage of emulsion electrospinning is that it allows the incorporation of hydrophilic drugs within the hydrophobic polymer matrix. This method can sustain the drug's release, as the drug molecules are steadily released from the core as the polymer degrades.

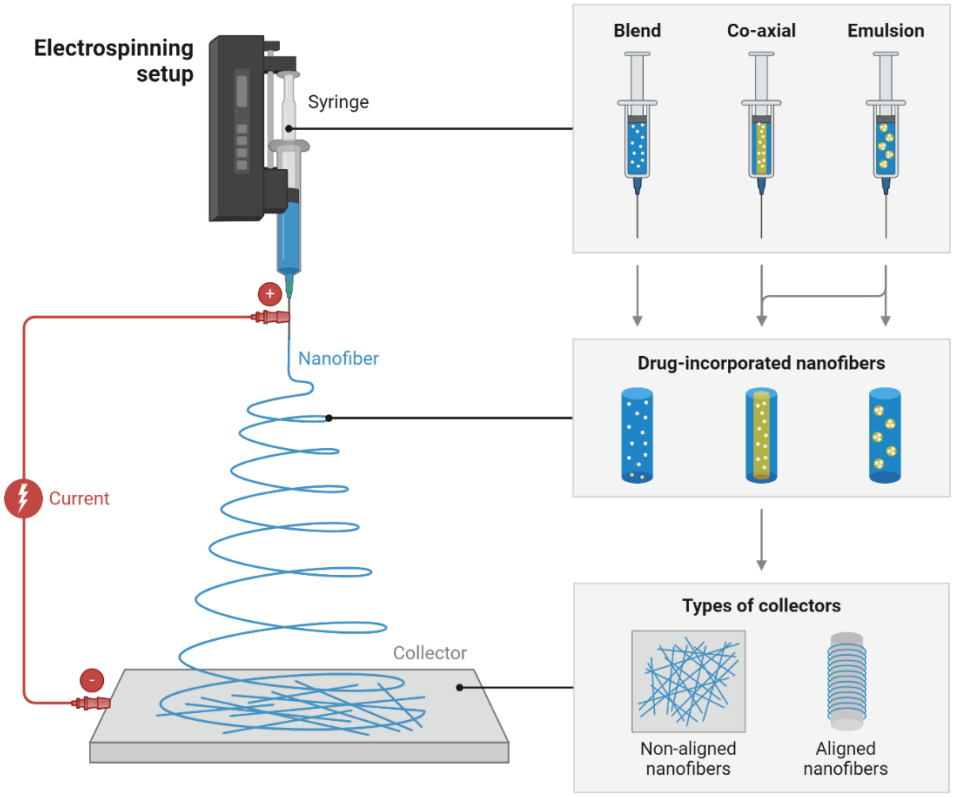

Figure 6. *Schematics of drug incorporation into electrospun fibers: polymer and drug blend in a solution, core-shell fibers, where a drug can be loaded in both the core and shell into a coaxial needle and emulsion electrospinning, where a drug emulsion can be loaded into the polymer solution.*

5-2- Core-Shell Nanofibrous Systems in Drug Delivery

Core-shell nanofibrous systems represent a significant advancement in nanotechnology for drug delivery.[83] These systems consist of a core material encapsulated within a shell, creating a unique structure that offers several advantages over traditional nanofibers and other drug delivery systems. Core-shell nanofibers are typically produced using coaxial electrospinning, a process that involves the simultaneous extrusion of two different polymer solutions through a coaxial needle. This technique allows for the precise control of the core and shell materials, enabling the incorporation of various functionalities into each layer (Figure 7).

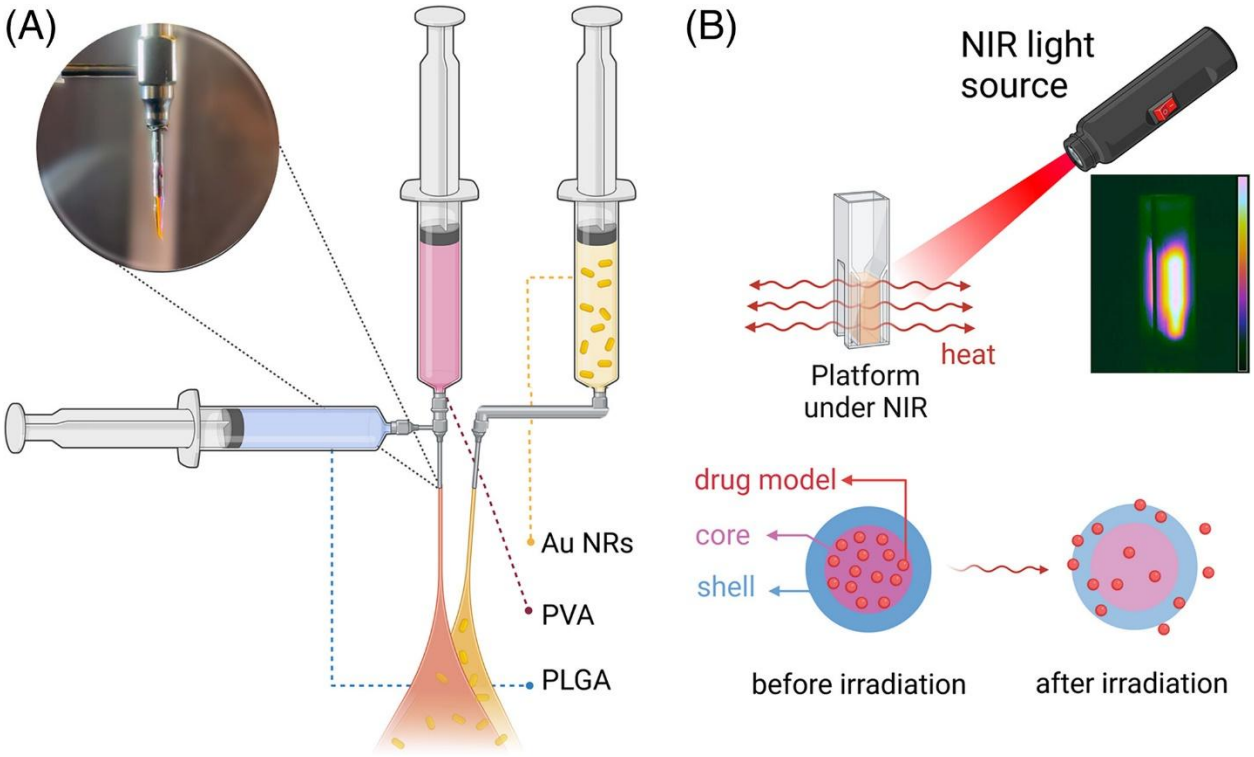

Figure 7. *Schematics core-shell nanofibers fabrication via coaxial electrospinning. It is reproduced from ref.* [15] *with permission.*

Core-shell nanofibrous systems offer several advantages, including the protection of bioactive agents by providing a stable, protective environment within the core, which shields them from degradation. They enable controlled drug release, as the shell material can be engineered to regulate the drug release rate from the core, facilitating sustained and controlled delivery. These systems also support dual functionality, allowing the core and shell to be functionalized independently, thereby incorporating multiple therapeutic agents or functionalities within a single nanofiber. Additionally, the surface of the shell can be modified with targeting ligands to enhance the specificity of drug delivery to diseased tissues or cells.[84-87]

6- Smart Drug Delivery Systems

Core-shell electrospun nanofibers offer an innovative approach to smart drug delivery systems, providing distinct advantages over traditional methods. These nanofibers feature a unique structure, where a core material is encapsulated by a shell layer, allowing for precise control over the encapsulation and release of therapeutic agents. Unlike conventional methods, which often release drugs in a less controlled manner, core-shell nanofibers enable fine-tuning of drug release profiles through the strategic selection and modification of core and shell materials. This level of control ensures a more consistent and targeted delivery, leading to improved therapeutic efficacy. One of the key benefits of these smart materials is the enhancement of patient compliance. The controlled and sustained release of drugs reduces the frequency of dosing, minimizing the burden on patients and ensuring a steadier therapeutic effect. Moreover, these nanofibers can be engineered to respond to external stimuli, such as light, temperature, or pH changes, which allows for on-demand drug release tailored to the patient's needs. Further enhancing their functionality, core-shell nanofibers can be decorated with photoactive plasmonic nanoparticles, which possess unique optical properties like localized surface plasmon resonance (LSPR). This feature enables precise, externally triggered drug release, providing an additional layer of control that is not possible with traditional drug delivery methods.

Near-infrared (NIR) light is a particularly advantageous external stimulus for activating smart drug delivery systems, chosen for its unique properties that set it apart from other stimuli like ultraviolet light, magnetic fields, or chemical triggers. NIR light stands out due to its special tissue penetration capabilities, allowing it to reach deeper layers of the body with minimal effects. [88-90] This deep penetration is coupled with its low absorption by water and biological tissues. This minimizes the risk of damage to healthy cells and reduces the side effects commonly associated with other

external stimuli. In contrast to ultraviolet light, which can be harmful to tissues and has limited penetration depth, NIR light offers a safer and more effective means of activating drug release. Similarly, magnetic fields and ultrasound can serve as external triggers, but they often require more complex equipment. They may not provide the same level of control and precision as NIR light.[91,92] When NIR light interacts with plasmonic nanoparticles incorporated within core-shell nanofibers, it induces localized heating through the LSPR effect (Figure 8). This localized heating can be harnessed to trigger the release of drugs encapsulated within the nanofibers. Upon exposure to NIR light, plasmonic particles absorb the light and convert it into heat, creating small pockets of increased temperature. This thermal response can then induce changes in the surrounding materials, such as the shell of the nanofibers, leading to the controlled release of the encapsulated drugs. By leveraging the unique properties of NIR light, this approach ensures precise and localized drug release. It enhances the safety and efficacy of the drug delivery system compared to other stimuli. This makes NIR light a highly suitable and strategic choice for smart drug delivery applications.

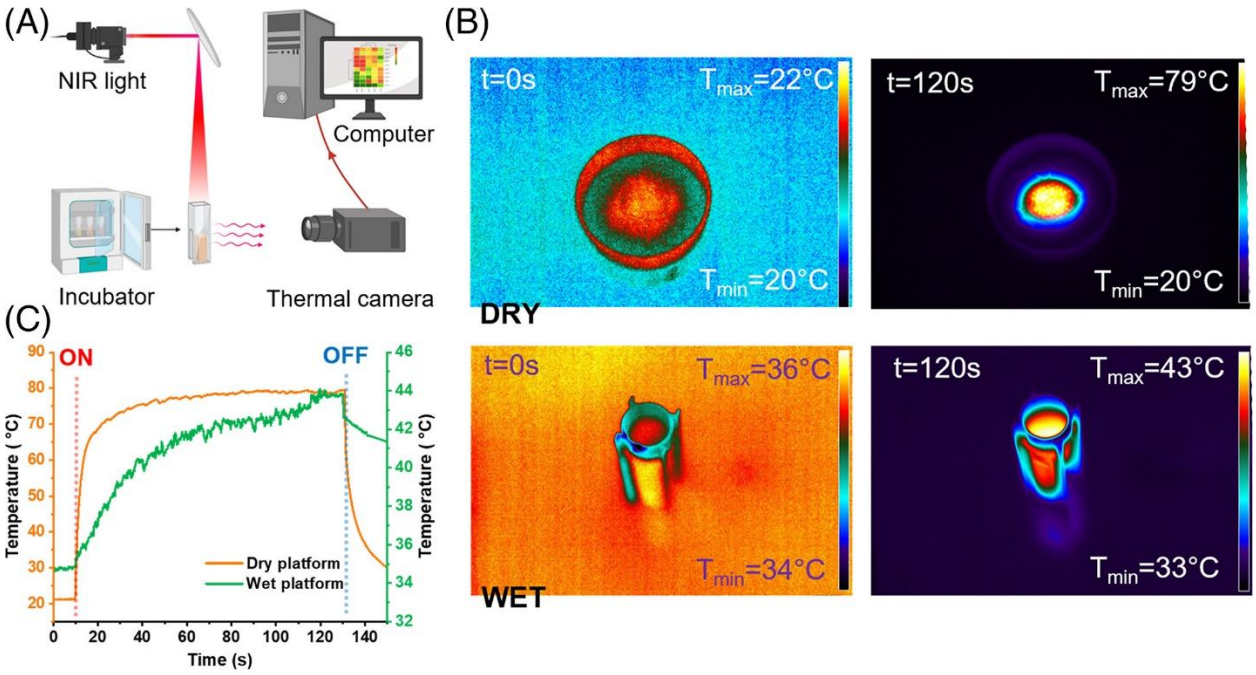

Figure 8. *The photo-responsive platform features the fast and on-demand responsiveness of the fabricated material. a) The schematic of the experimental setup illustrates a thermal camera capturing the temperature of the samples taken out from an incubator and irradiated by a NIR laser. b) The IR thermogram images of the dry and wet platforms before and after 2 min of irradiation were captured with a thermal camera. Wet samples were analyzed on a hot plate to maintain the platform's temperature at around 37 °C. c) Temporal plots of the platform's behaviors under the NIR illustration for wet and dry samples show the photo-response property of the material. They are reproduced from ref.* [15] *with permission.*

Core-shell electrospun nanofibers, decorated with photoactive plasmonic nanoparticles, represent a promising advancement in smart drug delivery systems. The unique core-shell structure offers enhanced protection and controlled release of therapeutic agents while incorporating plasmonic nanoparticles, which enables on-demand drug delivery through NIR light activation. This approach provides a versatile, efficient, and customizable method for targeted drug delivery, potentially revolutionizing the treatment of various diseases and improving patient outcomes.

7- Aim of the Study

The study aimed to design advanced electrospun nanofibers with multifunctional properties for biomedical applications, focusing on enhanced protection and on-demand therapeutic delivery by addressing the following key objectives:

1- Manufacturing and Characterization:
   - Development of face masks using electrospun polymer nanofibers.
   - Integration of plasmonic nanoparticles into nanofibers to enable photothermal and photodynamic properties.
   - Utilization of ICG within nanofibers for the creation of antibacterial face masks.
   - Production of core-shell electrospun nanofibers decorated with photoactive plasmonic gold nanostars and nanorods for use as drug delivery carriers.

2- Physicochemical Property Analysis:
   - Detailed characterization of the mechanical and chemical properties of nanofibrous mats.
   - Evaluation of fiber morphology, structure, and surface wettability through contact angle measurements.

3- Functional Evaluation:
   - Testing the antibacterial efficacy of face masks under NIR and solar irradiation.
   - Analyzing filtration efficiency and the capacity for pathogen eradication.
   - Examining the photothermal effects and their impact on antibacterial properties.

4- On-Demand Drug Delivery:
   - Creation of NIR light-activated core-shell nanofibers for smart drug delivery applications.

- Characterization of controlled and sustained drug release profiles under NIR irradiation.
- Investigation of the thermal response of nanofibers for efficient drug release.

5- Innovative Applications:

- Exploration of electrospinning and electrospraying techniques to enhance face mask functionality.
- Development of light-responsive drug carriers.
- Combination of antiviral, antibacterial, and thermal dissipation properties into multifunctional face masks.

This study successfully achieved its objectives by designing advanced electrospun nanofibers with multifunctional properties for biomedical applications, including the development of antibacterial face masks and smart drug delivery systems.

8-1- Publications Included in the Cycle of the Dissertations

1. Anna Zakrzewska†, **Mohammad Ali Haghighat Bayan**†, Paweł Nakielski, Francesca Petronella, Luciano De Sio, and Filippo Pierini. "Nanotechnology transition roadmap toward multifunctional stimuli-responsive face masks." ACS Applied Materials & Interfaces (2022): 46123-46144.

2. **Mohammad Ali Haghighat Bayan**, Yasmin Juliane Dias, Chiara Rinoldi, Paweł Nakielski, Daniel Rybak, Yen B. Truong, Alexander L. Yarin, and Filippo Pierini. "Near-infrared light activated core- shell electrospun nanofibers decorated with photoactive plasmonic nanoparticles for on-demand smart drug delivery applications." Journal of Polymer Science 61, no. 7 (2023): 521-533.

3. **Mohammad Ali Haghighat Bayan**, Chiara Rinoldi, Daniel Rybak, Seyed Shahrooz Zargarian, Anna Zakrzewska, Olga Cegielska, Kaisa Põhako-Palu, Shichao Zhang, Agata Stobnicka-Kupiec, Rafał L Górny, Paweł Nakielski, Karin Kogermann, Luciano De Sio, Bin Ding, and Filippo Pierini. "Engineering surgical face masks with photothermal and photodynamic plasmonic nanostructures for enhancing filtration and on-demand pathogen eradication." Biomaterials Science 12, no. 4 (2024): 949-963.

4. **Mohammad Ali Haghighat Bayan**, Chiara Rinoldi, Alicja Kosik-Kozioł, Magdalena Bartolewska, Daniel Rybak, Seyed Shahrooz Zargarian, Syed Ahmed Shah, Zuzanna J. Krysiak, Shichao Zhang, Massimiliano Lanzi, Paweł Nakielski, Bin Ding,and Filippo Pierini. "Solar-to-NIR Light Activable PHBV/ICG Nanofiber-Based Face Masks with On-Demand Combined Photothermal and Photodynamic Antibacterial Properties." Advanced Materials Technologies: 2400450.

† Contributed equally to this work

8-2- Summary of the Publications Included in the Publication Cycle of the Dissertation

Nanotechnology Transition Roadmap Toward Multifunctional Stimuli-Responsive Face Masks

Before starting the experimental part of the Ph.D. research, drawing a roadmap for applying stimuli-responsive materials for face mask application was performed. In this paper, we discuss the value of personal protective equipment (PPE), especially face masks, due to the beginning of the COVID-19 pandemic. We explored the development of advanced face masks using electrospun polymer nanofibers, which offer exceptional filtration properties and can be engineered to respond to specific stimuli. It helped me understand that these masks can incorporate additional components to acquire antibacterial and antiviral properties and self-sterilize. The review outlined the historical context of face masks, from their early use during the “Black Death” to the modern N95 respirators. The COVID-19 pandemic has accelerated innovation in face mask technology, emphasizing the need for masks that filter effectively, reduce waste, and enhance user comfort. Electrospinning, a versatile nanofiber production technique, is central to this innovation. It allows the incorporation of various materials into nanofibers, making them suitable for multiple applications, including filtration. We reviewed the electrospinning process, its historical development, and the potential of electrospun nanofibers in creating high-performance, stimuli-responsive face masks. A significant focus of our research was studying the development of masks that can actively respond to environmental changes and reduce pathogens. We discuss integrating advanced materials and technologies into mask design to create reusable, safe, and multifunctional PPE. Prospects and challenges in this dynamic field are also considered, highlighting the ongoing need for innovation to address public health and environmental concerns. This comprehensive

literature review identified a critical gap in existing research, as no studies have reported the integration of on-demand antibacterial properties in face masks using stimuli-responsive materials. This insight has significantly influenced the direction of future work, motivating us to investigate and develop face masks that leverage these advanced materials for dynamic antibacterial functionality.

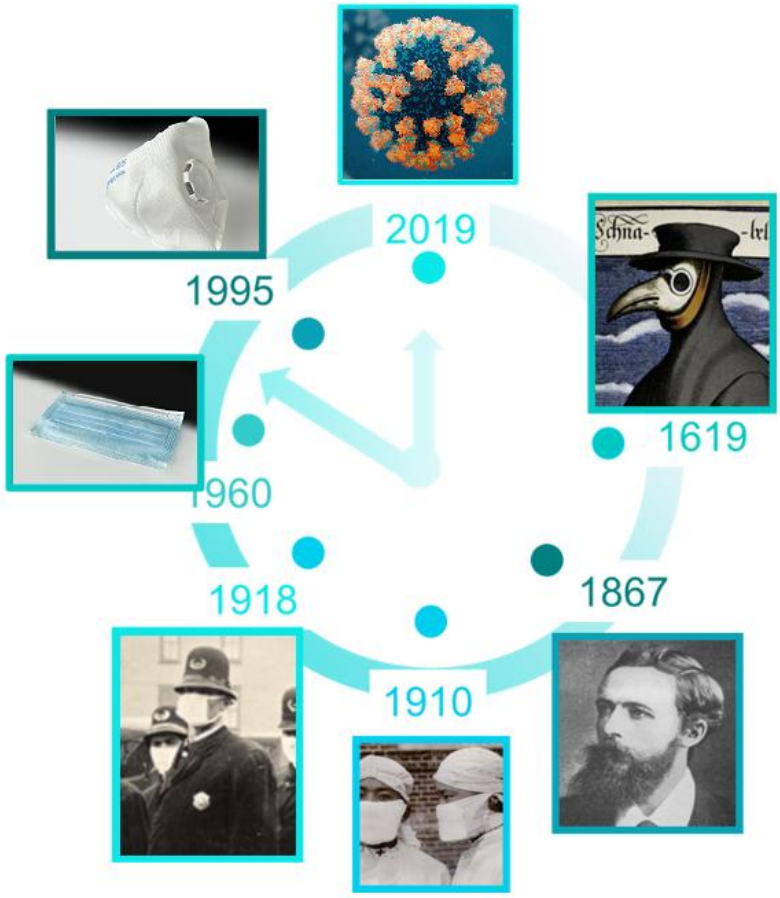

Figure 9. *The evolution of face masks is associated with the milestones of human history: from the "Black Death" bubonic plague of 1619 to the COVID-19 era beginning in 2019. It is reproduced with permission from ref* [40].

Near-infrared light-activated Core-Shell Electrospun Nanofibers Decorated With Photoactive Plasmonic Nanoparticles for On-Demand Smart Drug Delivery Applications

Our research in this paper explores the development of NIR light-activated core-shell electrospun nanofibers. These fibers are decorated with photoactive plasmonic nanoparticles for on-demand smart drug delivery applications. Traditional drug delivery systems have evolved into smart drug delivery systems (DDSs), leveraging biomedical nanotechnology to enhance drug release efficacy and minimize side effects through stimuli-responsive mechanisms. Our study focuses on creating an electrospun nanofibrous photo-responsive DDS, allowing on-demand drug release and preventing burst release and high drug concentrations. We employed a coaxial electrospinning setup and an electrospraying technique to fabricate core-shell PVA-PLGA nanofibers decorated with gold nanorods. The PVA-Rhodamine B (RhB) core provides hydrophilicity, while the PLGA shell offers hydrophobic protection. Incorporating Au NRs enables significant heat generation under NIR light, facilitating controlled and sustained drug release. Our morphological and physio-chemical characterizations confirm the core-shell structure and the successful integration of Au NRs. Cell studies demonstrate the biocompatibility of the electrospun substrates, showing high viability and proliferation of L929 fibroblasts. Thermal-response characterizations using a thermal camera indicate rapid temperature increases in the fibers under NIR light, essential for the photo-responsive drug release. Drug release studies reveal that our core-shell nanofibers exhibit a sustained and controlled release profile, with NIR irradiation significantly enhancing the drug release rate. Our findings suggest that the photo-responsive PVA-PLGA nanofibers decorated with Au NRs hold great promise as on-demand drug carriers, combining effective stimuli-responsive drug delivery with excellent biocompatibility and structural stability.

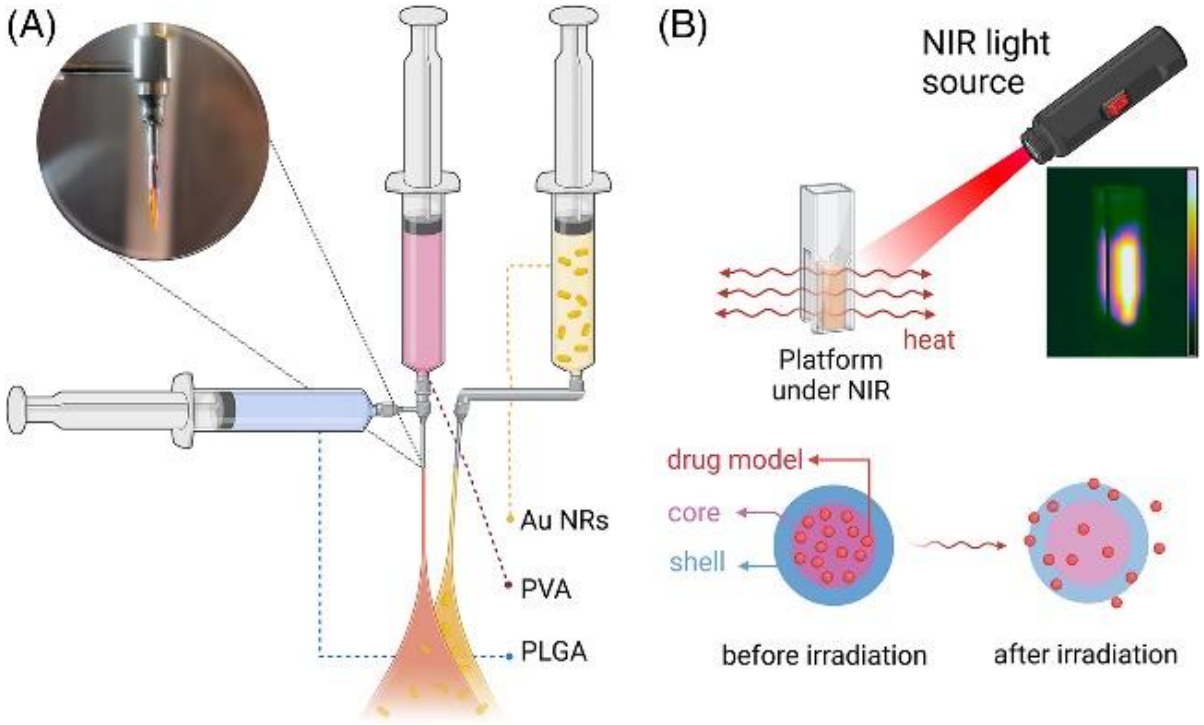

Figure 10. *Illustration of material preparation. a) Schematic presenting the fabrication by coaxial Electrospinning. b) A representative scheme of photo-responsiveness of the fabricated material under the NIR light. It is reproduced from ref.* [15] *with permission.*

Engineering Surgical Face Masks with Photothermal and Photodynamic Plasmonic Nanostructures for Enhancing Filtration and On-Demand Pathogen Eradication

This research paper addresses the urgent need for more effective and reusable face masks due to the COVID-19 pandemic and environmental concerns associated with disposable masks. We propose an innovative approach to upgrading surgical masks by integrating plasmonic nanoparticles that enable photothermal and photodynamic functionalities. Our method decorates surgical masks with gold nanorods (Au NRs) between the electrospun polymer nanofibrous layers. When exposed to NIR light, the Au NRs provide on-demand pathogen eradication, generating heat that can kill bacteria and viruses on the mask surface. This modification significantly enhances the mask's filtration efficiency for particles and bacteria without increasing the pressure drop, ensuring breathability and comfort. We detail the fabrication process, starting with electrospinning a polyacrylonitrile (PAN) nanofiber layer onto the surgical mask. The Au NRs are then electrosprayed onto this layer, followed by another layer of PAN to protect the nanoparticles and prevent leaching. Our structural and morphological characterizations confirm the successful integration and distribution of Au NRs within the nanofibers. Thermal activity tests using a NIR laser demonstrate that our modified masks can reach temperatures sufficient to eradicate pathogens, achieving up to 99.95% bacterial inactivation. Additionally, we conduct extensive bacterial filtration efficiency (BFE) and particle filtration efficiency (PFE) tests, showing that our masks achieve significantly higher filtration rates than standard surgical masks. Our study proves the feasibility of creating multifunctional, reusable face masks with enhanced protective capabilities and environmental benefits.

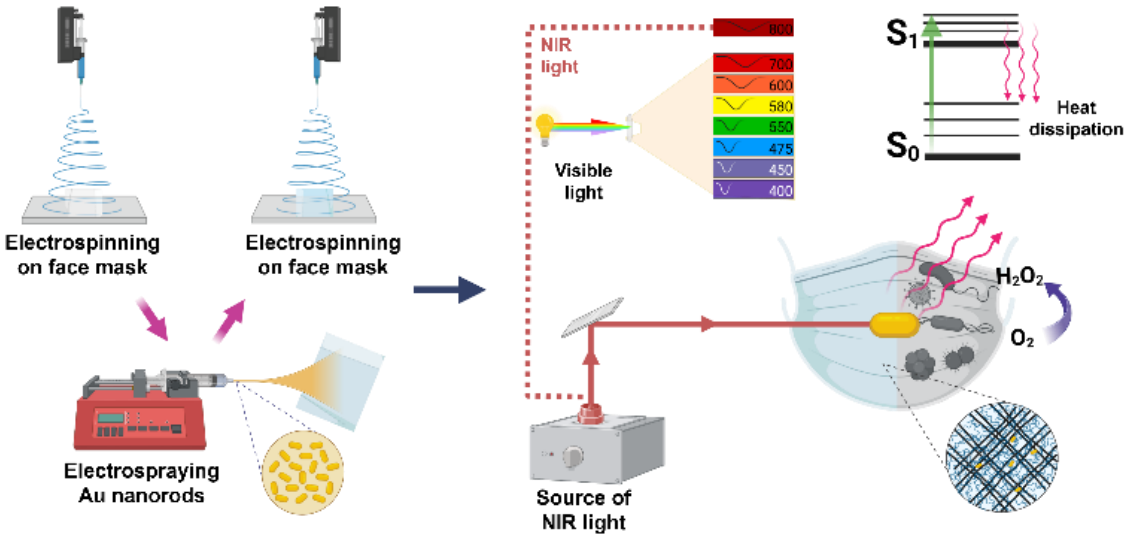

Figure 11. *Sketch of fabricating antibacterial nanofibrous face mask via electrospinning and electrospraying. The schematic illustration shows the concept and structure design of the photo-response and photodynamic face mask fabrication. It is reproduced from ref.* [19] *with permission.*

Solar-to-NIR Light Activable PHBV/ICG Nanofiber-Based Face Masks with On-Demand Combined Photothermal and Photodynamic Antibacterial Properties

In this study, we developed a cutting-edge antibacterial face mask utilizing PHBV (poly(3-hydroxybutyrate-co-3-hydroxyvalerate)) nanofibers integrated with indocyanine green (ICG). This innovation focuses on the urgent need for effective antimicrobial protection for community health workers, especially significant during health crises such as the COVID-19 pandemic. By employing electrospinning, we created a nanofibrous structure that combines mechanical robustness, a vast surface area, and inherent flexibility. The resulting face mask demonstrates substantial bacterial inactivation under both NIR and solar irradiation, attributed to the photothermal response of the nanofibers. Our research focused on fabricating and characterizing this nanofibrous material, evaluating its mechanical and chemical properties, particle filtration, and antibacterial efficacy under photothermal conditions. Electrospinning produced the PHBV/ICG nanofibers, and their morphology, structure, and photothermal response were thoroughly investigated. The antibacterial efficacy was tested using Escherichia coli as a model organism, showing a significant reduction in bacterial viability upon NIR and solar irradiation. This confirms the bactericidal efficiency of the material, making it a promising candidate for combating microbial infections on demand. Moreover, the photothermal effect facilitated by the material's ability to convert light into heat further enhances its antibacterial properties. The study highlights the synergistic impact of PHBV and ICG in creating a biocompatible and environmentally friendly solution. In summary, our study presents an innovative approach to developing nanofibrous face masks with on-demand antibacterial properties, addressing critical public health challenges and paving the way for future advancements in antibacterial materials.

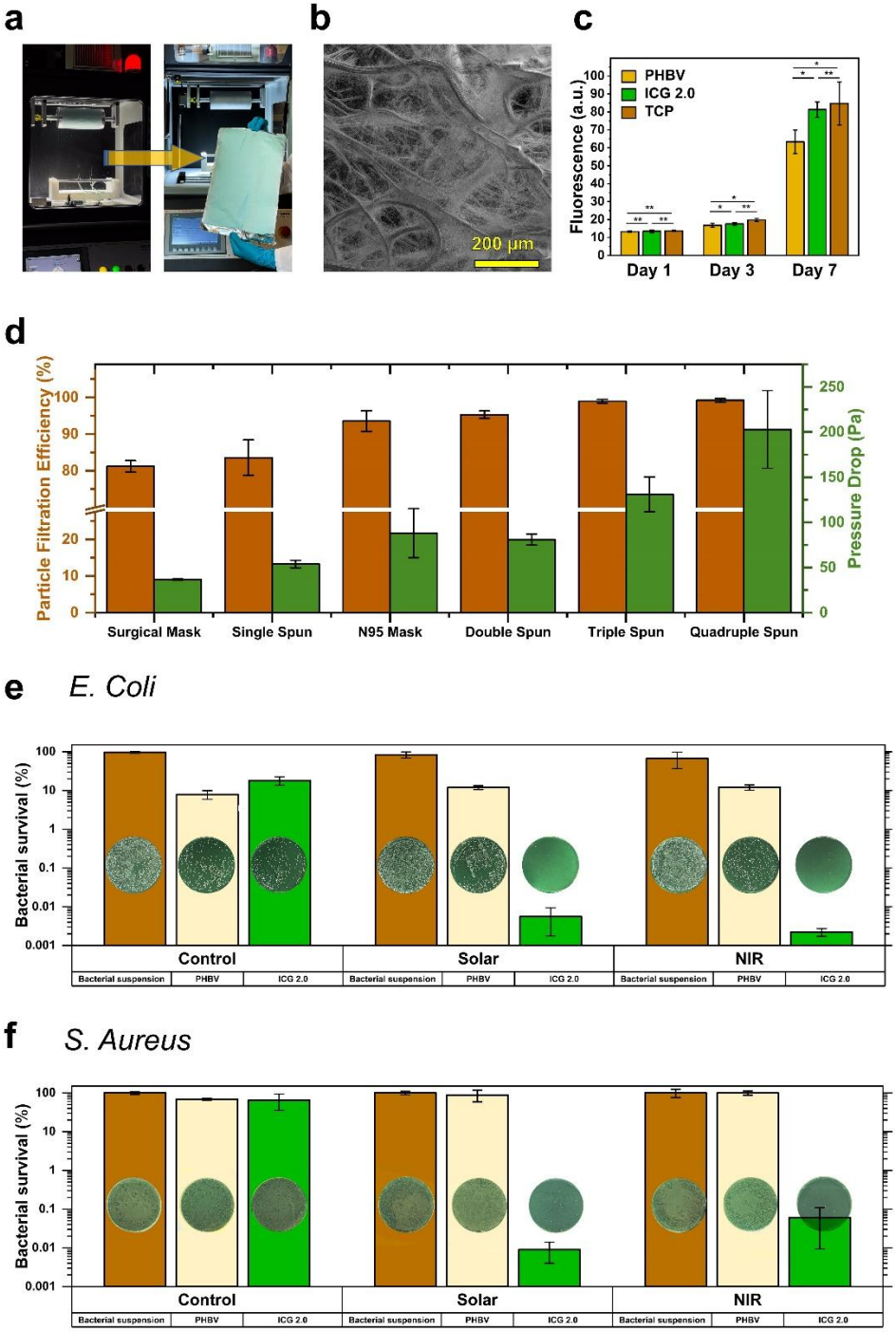

Figure 12. *a) Photographs representing the fabricated textile of ICG 2.0 during and after the electrospinning process, b) SEM image of PHBV nanofibers on PP mask fibers, c) In vitro biological response of L929 fibroblast cells seeded on PHBV, ICG, and TCP up to 7 days of culture, d) PFE and pressure drop comparison between the standard surgical face mask, N95 mask, and masks with single, double, triple, and quadruple electrospun material layers, e) Percentage of bacteria survival when in contact with PHBV and ICG 2.0 nanofibrous materials subjected to NIR or solar irradiations and incubation at RT in the dark for E. Coli and f) S. Aureus survival when in contact with PHBV and ICG 2.0 nanofibrous materials subjected to NIR or solar irradiations.*

9- Conclusions

This thesis has presented a comprehensive investigation into the development and application of stimuli-responsive electrospun nanofiber-based materials, primarily focusing on their use in advanced biomedical applications. In biomedical applications, the research aimed to design advanced multifunctional nanofibers for application in face masks, offering enhanced protection and on-demand bacterial inactivation capabilities. By developing electrospun polymer nanofibers integrated with plasmonic nanoparticles, this study has shown the potential for face masks to achieve enhanced filtration efficiency and antibacterial properties. Incorporating ICG in nanofibers has proven effective in creating antibacterial face masks that respond to NIR and solar irradiation, enabling on-demand pathogen eradication. These nanofibers' successful synthesis and characterization highlight their potential for real-world applications, particularly in light of the ongoing need for effective PPE due to global health crises like the COVID-19 pandemic.

Moreover, the research explored core-shell electrospun nanofibers in drug delivery applications. Core-shell nanofibrous systems, produced via coaxial electrospinning, offer significant advantages in drug delivery, such as enhanced protection of bioactive agents, controlled drug release, and targeted delivery. These systems were designed to incorporate therapeutic agents within the core while the shell provided a protective barrier and functional interface for controlled release. The study demonstrated that these core-shell nanofibers could achieve sustained and controlled drug release, enhancing therapeutic efficacy and patient compliance. Additionally, incorporating photoactive plasmonic nanoparticles enabled on-demand drug delivery through NIR light activation, offering a versatile and customizable method for targeted drug delivery.

The studies presented in this dissertation collectively contribute to the broader scientific understanding of electrospun nanofiber technology and its applications. This work has laid the groundwork for further exploration and development in these critical areas by bridging the gap between material science and practical applications. Future research could build upon these findings by exploring additional materials and configurations, optimizing the production processes, and conducting long-term performance evaluations under real-world conditions.

The doctoral thesis allowed for the following conclusions:

1- The development of stimuli-responsive electrospun nanofiber-based materials for advanced biomedical applications was successfully achieved, demonstrating potential in both personal protective equipment and drug delivery systems.

2- The integration of electrospun polymer nanofibers with plasmonic nanoparticles showed enhanced filtration efficiency and antibacterial properties in face masks, offering on-demand bacterial inactivation capabilities through NIR and solar irradiation. This method holds significant promise for real-world applications, particularly in light of the global need for effective PPE during health crises such as the COVID-19 pandemic.

3- Core-shell nanofibers produced via coaxial electrospinning proved effective in drug delivery systems, offering:

   a) Enhanced protection of bioactive agents.

   b) Controlled and sustained drug release, improving therapeutic efficacy and patient compliance.

c) On-demand drug delivery through NIR light activation, presenting a customizable method for targeted drug delivery.

4- The study provides fundamental knowledge of electrospun nanofiber technology for biomedical applications:

a) Incorporating ICG in nanofibers enabled effective antibacterial activity triggered by NIR light, highlighting their potential in creating advanced antibacterial face masks.

b) Core-shell systems demonstrated significant advantages in controlled release and targeted drug delivery, bridging the gap between material science and practical biomedical applications.

5- The findings contribute to the broader understanding of electrospun nanofiber technology, establishing a foundation for further research and optimization of production processes. Future work could explore new materials, configurations, and long-term performance evaluations under real-world conditions.

In conclusion, this thesis has successfully fabricated various stimuli-responsive nanomaterials that address societal needs in healthcare, laying the groundwork for continued innovation in the field of electrospun nanofiber technology.

10- References

[1] J. Xue, T. Wu, Y. Dai, Y. Xia, *Chem Rev* **2019**, *119*, 5298.

[2] S. Agarwal, A. Greimer, J. H. Wendorff, *Adv Funct Mater* **2009**, *19*, 2863.

[3] A. Keirouz, Z. Wang, V. S. Reddy, Z. K. Nagy, P. Vass, M. Buzgo, S. Ramakrishna, N. Radacsi, *Adv Mater Technol* **2023**, *8*, 2201723.

[4] Y. Dong, S. Fu, J. Yu, X. Li, B. Ding, *Adv Funct Mater* **2024**, *34*, 2311199.

[5] S. A. Hosseini Ravandi, M. Sadrjahani, A. Valipouri, F. Dabirian, F. K. Ko, *https://doi.org/10.1177/00405175211069880* **2022**, *92*, 5130.

[6] A. J. Robinson, A. Pé Rez-Nava, S. C. Ali, J. Betzabe Gonzá Lez-Campos, J. L. Holloway, E. M. Cosgriff-Hernandez, **2021**, DOI 10.1016/j.matt.2020.12.022.

[7] P. Theato, B. S. Sumerlin, R. K. O'reilly, T. H. Epp, *Chem Soc Rev* **2013**, *42*, 7055.

[8] M. A. C. Stuart, W. T. S. Huck, J. Genzer, M. Müller, C. Ober, M. Stamm, G. B. Sukhorukov, I. Szleifer, V. V. Tsukruk, M. Urban, F. Winnik, S. Zauscher, I. Luzinov, S. Minko, *Nature Materials 2010 9:2* **2010**, *9*, 101.

[9] A. Chan, R. P. Orme, R. A. Fricker, P. Roach, *Adv Drug Deliv Rev* **2013**, *65*, 497.

[10] A. Abdollahi, H. Roghani-Mamaqani, B. Razavi, M. Salami-Kalajahi, *Polym Chem* **2019**, *10*, 5686.

[11] M. Mrinalini, S. Prasanthkumar, *Chempluschem* **2019**, *84*, 1103.

[12] G. A. Leith, C. R. Martin, A. Mathur, P. Kittikhunnatham, K. C. Park, N. B. Shustova, *Adv Energy Mater* **2022**, *12*, 2100441.

[13] S. F. Medeiros, A. M. Santos, H. Fessi, A. Elaissari, *Int J Pharm* **2011**, *403*, 139.

[14] L. D. Zarzar, J. Aizenberg, *Acc Chem Res* **2014**, *47*, 530.

[15] M. A. Haghighat Bayan, Y. J. Dias, C. Rinoldi, P. Nakielski, D. Rybak, Y. B. Truong, A. L. Yarin, F. Pierini, *Journal of Polymer Science* **2023**, *61*, 521.

[16] L. Hu, Q. Zhang, X. Li, M. J. Serpe, *Mater Horiz* **2019**, *6*, 1774.

[17] D. Rybak, C. Rinoldi, P. Nakielski, J. Du, M. A. Haghighat Bayan, S. S. Zargarian, M. Pruchniewski, X. Li, B. Strojny-Cieślak, B. Ding, F. Pierini, *J Mater Chem B* **2024**, *12*, 1905.

[18] J. Hu, H. Meng, G. Li, S. I. Ibekwe, *Smart Mater Struct* **2012**, *21*, 053001.

[19] M. A. Haghighat Bayan, C. Rinoldi, D. Rybak, S. S. Zargarian, A. Zakrzewska, O. Cegielska, K. Põhako-Palu, S. Zhang, A. Stobnicka-Kupiec, R. L. Górny, P. Nakielski, K. Kogermann, L. De Sio, B. Ding, F. Pierini, *Biomater Sci* **2024**, *12*, 949.

[20] M. Wei, Y. Gao, X. Li, M. J. Serpe, *Polym Chem* **2016**, *8*, 127.

[21] E. M. White, J. Yatvin, J. B. Grubbs, J. A. Bilbrey, J. Locklin, *J Polym Sci B Polym Phys* **2013**, *51*, 1084.

[22] Z. Li, Y. Yin, *Advanced Materials* **2019**, *31*, 1807061.

[23] J. M. Korde, B. Kandasubramanian, *Ind Eng Chem Res* **2019**, *58*, 9709.

[24] Y. Hiruta, *Polymer Journal 2022 54:12* **2022**, *54*, 1419.

[25] A. Khan, *Chemical Communications* **2024**, DOI 10.1039/D4CC02311K.

[26] S. Sen, G. T. R. Palmore, *Macromolecules* **2016**, *49*, 8479.

[27] A. R. Peringath, M. A. H. Bayan, M. Beg, A. Jain, F. Pierini, N. Gadegaard, R. Hogg, L. Manjakkal, *J Energy Storage* **2023**, *73*, 108811.

[28] K. Minagawa, K. Koyama, *Curr Org Chem* **2005**, *9*, 1643.

[29] N. Vijayakameswara Rao, H. Ko, J. Lee, J. H. Park, *Front Bioeng Biotechnol* **2018**, *6*, 366431.

[30] A. Bratek-Skicki, *Applied Surface Science Advances* **2021**, *4*, 100068.

[31] L. Hu, T. Shu, Y. Wan, C. Fang, F. Gao, M. J. Serpe, *Mol Syst Des Eng* **2021**, *6*, 108.

[32] S. Municoy, M. I. Álvarez Echazú, P. E. Antezana, J. M. Galdopórpora, C. Olivetti, A. M. Mebert, M. L. Foglia, M. V. Tuttolomondo, G. S. Alvarez, J. G. Hardy, M. F. Desimone, *International Journal of Molecular Sciences 2020, Vol. 21, Page 4724* **2020**, *21*, 4724.

[33] P. Vinchhi, S. U. Rawal, M. M. Patel, *Drug Delivery Devices and Therapeutic Systems* **2021**, 267.

[34] M. Panahi-Sarmad, E. Chehrazi, M. Noroozi, M. Raef, M. Razzaghi-Kashani, M. A. Haghighat Baian, *ACS Appl Electron Mater* **2019**, *1*, 198.

[35] P. Nakielski, D. Rybak, K. Jezierska-Woźniak, C. Rinoldi, E. Sinderewicz, J. Staszkiewicz-Chodor, M. A. Haghighat Bayan, W. Czelejewska, O. Urbanek, A. Kosik-Kozioł, M. Barczewska, M. Skomorowski, P. Holak, S. Lipiński, W. Maksymowicz, F. Pierini, *ACS Appl Mater Interfaces* **2023**, *15*, 58103.

[36] C. Rinoldi, Y. Ziai, S. S. Zargarian, P. Nakielski, K. Zembrzycki, M. A. H. Bayan, A. B. Zakrzewska, R. Fiorelli, M. Lanzi, A. Kostrzewska-Księyk, R. Czajkowski, E. Kublik, L. Kaczmarek, F. Pierini, *ACS Appl Mater Interfaces* **2023**, *15*, 6283.

[37] S. Sell, C. Barnes, M. Smith, M. McClure, P. Madurantakam, J. Grant, M. McManus, G. Bowlin, *Polym Int* **2007**, *56*, 1349.

[38] Y. J. Son, W. J. Kim, H. S. Yoo, *Arch Pharm Res* **2014**, *37*, 69.

[39] K. A. Rieger, N. P. Birch, J. D. Schiffman, *J Mater Chem B* **2013**, *1*, 4531.

[40] A. Zakrzewska, M. A. Haghighat Bayan, P. Nakielski, F. Petronella, L. De Sio, F. Pierini, *ACS Appl Mater Interfaces* **2022**, *14*, 46123.

[41] S. Zhu, L. Nie, *Journal of Industrial and Engineering Chemistry* **2021**, *93*, 28.

[42] M. A. Haghighat Bayan, F. Afshar Taromi, M. Lanzi, F. Pierini, *Scientific Reports 2021 11:1* **2021**, *11*, 1.

[43] A. Raza, Y. Li, J. Sheng, J. Yu, B. Ding, **2014**, 355.

[44] Z. Zhang, S. Liu, M. Xiang, S. Li, D. Zhao, C. Huang, S. Chen, *Front Med* **2020**, *14*, 229.

[45] B. Kea, A. Johnson, A. Lin, J. Lapidus, J. N. Cook, C. Choi, B. P. Chang, M. A. Probst, J. Park, C. Atzema, B. Coll-Vinent, G. Constantino, D. Pozhidayeva, A. Wilson, A. Zell, M. Hansen, *J Am Coll Emerg Physicians Open* **2021**, *2*, e12392.

[46] F. Hadinejad, H. Morad, M. Jahanshahi, A. Zarrabi, H. Pazoki-Toroudi, E. Mostafavi, *Advanced Fiber Materials* **2023**, *5*, 1273.

[47] L. De Sio, B. Ding, M. Focsan, K. Kogermann, P. Pascoal-Faria, F. Petronela, G. Mitchell, E. Zussman, F. Pierini, *Chemistry – A European Journal* **2021**, *27*, 6112.

[48] J. Cohen, Y. van der M. Rodgers, *Prev Med (Baltim)* **2020**, *141*, 106263.

[49] M. Tarfaoui, M. Nachtane, I. Goda, Y. Qureshi, H. Benyahia, *Materials 2020, Vol. 13, Page 3339* **2020**, *13*, 3339.

[50] D. Saber, K. Abd El-Aziz, *Journal of Industrial Textiles* **2022**, *51*, 246S.

[51] R. A. M. Basodan, B. Park, H. J. Chung, *Flexible and Printed Electronics* **2021**, *6*, 043004.

[52] N. El-Atab, R. B. Mishra, M. M. Hussain, *Nanotechnology* **2021**, *33*, 062006.

[53] Z. X. Phuna, B. P. Panda, N. K. Hawala Shivashekaregowda, P. Madhavan, *Int J Environ Health Res* **2023**, *33*, 670.

[54] T. Ahmed, R. T. Ogulata, S. Sezgin Bozok, *The Journal of The Textile Institute* **2022**, *113*, 2825.

[55] O. N. Aguda, A. Lateef, *Heliyon* **2017**, e09761.

[56] N. Karim, S. Afroj, K. Lloyd, L. C. Oaten, D. V. Andreeva, C. Carr, A. D. Farmery, I. D. Kim, K. S. Novoselov, *ACS Nano* **2020**, *14*, 12313.

[57] T. J. Lopes, G. R. Rosa, G. A. Fernandes, C. W. Scheeren, A. H. da Silva Júnior, M. L. Martins, *Protective Textiles from Natural Resources* **2022**, 649.

[58] Z. A. Raza, M. Taqi, M. R. Tariq, *The Journal of The Textile Institute* **2022**, *113*, 515.

[59] J. Shi, H. Li, F. Xu, X. Tao, *Mater Today Adv* **2021**, *12*, 100171.

[60] G. Pullangott, U. Kannan, G. S., D. V. Kiran, S. M. Maliyekkal, *RSC Adv* **2021**, *11*, 6544.

[61] D. C. Vodnar, L. Mitrea, L. F. Călinoiu, K. Szabo, B. E. Ştefănescu, *Advanced Nanostructures for Environmental Health: Micro and Nano Technologies* **2020**, 465.

[62] D. Pereira, T. S. Carreira, N. Alves, Â. Sousa, J. F. A. Valente, *International Journal of Molecular Sciences 2022, Vol. 23, Page 1165* **2022**, *23*, 1165.

[63] E. O. Mikhailova, K. Thakur, *Journal of Functional Biomaterials 2021, Vol. 12, Page 70* **2021**, *12*, 70.

[64] S. Gatadi, Y. V. Madhavi, S. Nanduri, *J Mol Struct* **2021**, *1228*, 129750.

[65] W. K. Essa, S. A. Yasin, I. A. Saeed, G. A. M. Ali, *Membranes 2021, Vol. 11, Page 250* **2021**, *11*, 250.

[66] A. Damokhi, S. Yousefinejad, A. Fakherpour, M. Jahangiri, *Journal of Nanoparticle Research* **2022**, *24*, 1.

[67] A. R. S. Rossin, L. Spessato, F. da S. L. Cardoso, J. Caetano, W. Caetano, E. Radovanovic, D. C. Dragunski, *Polymer Bulletin 2023 81:3* **2023**, *81*, 1957.

[68] S. Singh, *J Nanosci Nanotechnol* **2010**, *10*, 7906.

[69] A. Kumar, F. Chen, A. Mozhi, X. Zhang, Y. Zhao, X. Xue, Y. Hao, X. Zhang, P. C. Wang, X. J. Liang, *Nanoscale* **2013**, *5*, 8307.

[70] P. Vega-Vásquez, N. S. Mosier, J. Irudayaraj, *Front Bioeng Biotechnol* **2020**, *8*, 507143.

[71] M. Goldberg, R. Langer, X. Jia, *J Biomater Sci Polym Ed* **2007**, *18*, 241.

[72] S. Yadav, A. K. Sharma, P. Kumar, *Front Bioeng Biotechnol* **2020**, *8*, 500966.

[73] L. E. Sperling, K. P. Reis, P. Pranke, J. H. Wendorff, *Drug Discov Today* **2016**, *21*, 1243.

[74] M. Monfared, S. Taghizadeh, A. Zare-Hoseinabadi, S. M. Mousavi, S. A. Hashemi, S. Ranjbar, A. M. Amani, *Drug Metab Rev* **2019**, *51*, 589.

[75] R. A. Perez, H. W. Kim, *Acta Biomater* **2015**, *21*, 2.

[76] J. H. Ryu, H. Koo, I. C. Sun, S. H. Yuk, K. Choi, K. Kim, I. C. Kwon, *Adv Drug Deliv Rev* **2012**, *64*, 1447.

[77] M. E. Gindy, R. K. Prud'homme, *Expert Opin Drug Deliv* **2009**, *6*, 865.

[78] A. Luraghi, F. Peri, L. Moroni, *Journal of Controlled Release* **2021**, *334*, 463.

[79] A. Repanas, S. Andriopoulou, B. Glasmacher, *J Drug Deliv Sci Technol* **2016**, *31*, 137.

[80] A. Khalf, S. V. Madihally, *European Journal of Pharmaceutics and Biopharmaceutics* **2017**, *112*, 1.

[81] R. Kumar, K. Mondal, P. K. Panda, A. Kaushik, R. Abolhassani, R. Ahuja, H. G. Rubahn, Y. K. Mishra, *J Mater Chem B* **2020**, *8*, 8992.

[82] A. A. Yetisgin, S. Cetinel, M. Zuvin, A. Kosar, O. Kutlu, *Molecules 2020, Vol. 25, Page 2193* **2020**, *25*, 2193.

[83] AL. Yarin, *Polymers for Advanced Technologies* **2011**, 22(3):310-7.

[84] M. Das, C. Mohanty, S. K. Sahoo, *Expert Opin Drug Deliv* **2009**, *6*, 285.

[85] M. Liu, Y. Zhang, S. Sun, A. R. Khan, J. Ji, M. Yang, G. Zhai, *J Drug Target* **2019**, *27*, 270.

[86] N. Nikmaram, S. Roohinejad, S. Hashemi, M. Koubaa, F. J. Barba, A. Abbaspourrad, R. Greiner, *RSC Adv* **2017**, *7*, 28951.

[87] M. Zamani, M. P. Prabhakaran, S. Ramakrishna, *Int J Nanomedicine* **2013**, *8*, 2997.

[88] B. Sana, A. Finne-Wistrand, D. Pappalardo, *Mater Today Chem* **2022**, *25*, 100963.

[89] G. Yang, J. Liu, Y. Wu, L. Feng, Z. Liu, *Coord Chem Rev* **2016**, *320–321*, 100.

[90] Y. Wang, D. S. Kohane, *Nature Reviews Materials 2017 2:6* **2017**, *2*, 1.

[91] A. Saneja, R. Kumar, D. Arora, S. Kumar, A. K. Panda, S. Jaglan, *Drug Discov Today* **2018**, *23*, 1115.

[92] A. Karmakar, A. Silswal, A. L. Koner, *J Mater Chem B* **2024**, *12*, 4785.

11- Original Publications

ACS APPLIED MATERIALS & INTERFACES

www.acsami.org Review

Nanotechnology Transition Roadmap toward Multifunctional Stimuli-Responsive Face Masks

Anna Zakrzewska,[†] Mohammad Ali Haghighat Bayan,[†] Paweł Nakielski, Francesca Petronella, Luciano De Sio, and Filippo Pierini*

Cite This: *ACS Appl. Mater. Interfaces* 2022, 14, 46123−46144 Read Online

ACCESS | Metrics & More | Article Recommendations

ABSTRACT: In recent times, the use of personal protective equipment, such as face masks or respirators, is becoming more and more critically important because of common pollution; furthermore, face masks have become a necessary element in the global fight against the COVID-19 pandemic. For this reason, the main mission of scientists has become the development of face masks with exceptional properties that will enhance their performance. The versatility of electrospun polymer nanofibers has determined their suitability as a material for constructing "smart" filter media. This paper provides an overview of the research carried out on nanofibrous filters obtained by electrospinning. The progressive development of the next generation of face masks whose unique properties can be activated in response to a specific external stimulus is highlighted. Thanks to additional components incorporated into the fiber structure, filters can, for example, acquire antibacterial or antiviral properties, self-sterilize the structure, and store the energy generated by users. Despite the discovery of several fascinating possibilities, some of them remain unexplored. Stimuli-responsive filters have the potential to become products of large-scale availability and great importance to society as a whole.

KEYWORDS: *nanostructured face masks, stimuli-responsive nanomaterials, electrospun nanofibers, active filtration, smart filters, COVID-19, antipathogen*

■ INTRODUCTION

The ongoing coronavirus (COVID-19) disease outbreak initially appeared in China at the end of 2019 and triggered a rapid rise in the incidence of severe acute respiratory syndrome coronavirus 2 (SARS-CoV-2) cases.[1] The ensuing viral respiratory disease-based pandemic is considered the most significant global public health issue of the 21st century so far.[2] The World Health Organization (WHO) suggested wearing properly fitted masks to prevent and slow down the transmission of COVID-19.[3] Significant advancements in the development of dedicated vaccines reduced the impact of SARS-CoV-2 on the health of patients affected by this disease.[4] Nevertheless, even though additional infection reduction measures, such as social distancing and bans on large gatherings have been implemented, after more than two years of the spread of the pandemic, wearing appropriate face masks is still the most effective strategy for protecting people from the inhalation of viral matter and the consequent infection.[5,6] Therefore, wearing face masks became part and parcel of everyday life for the overwhelming majority of humankind. Additionally, it is worth remembering that using face masks has always been at the core of standard safety practices for workers exposed to flying ashes/powders and healthcare workers. It is also the typical protection method in the presence of high concentrations of airborne pollution.[7]

In this perspective, the production of face masks rose considerably in the last couple of years, bringing to light some significant problems connected with the extensive use of these protective devices.[8] The membranes filtering the air to decontaminate it from solid matters such as ashes, powders, and biological materials (e.g., viruses, bacteria, and fungi) should meet the technical requirements on filtration properties relevant to the final targeted applications.[9]

The scientific achievements obtained in the previous decades have made it possible to produce face masks with outstanding filtration performances. Nevertheless, the extensive and continuous use of this personal protective equipment (PPE) revealed a few unexpected issues.[10] The large-scale consumption of face masks caused a massive amount of waste materials.[8,11] This problem can be tackled by designing

Received: June 14, 2022
Accepted: September 13, 2022
Published: September 26, 2022

https://doi.org/10.1021/acsami.2c10335
ACS Appl. Mater. Interfaces 2022, 14, 46123−46144

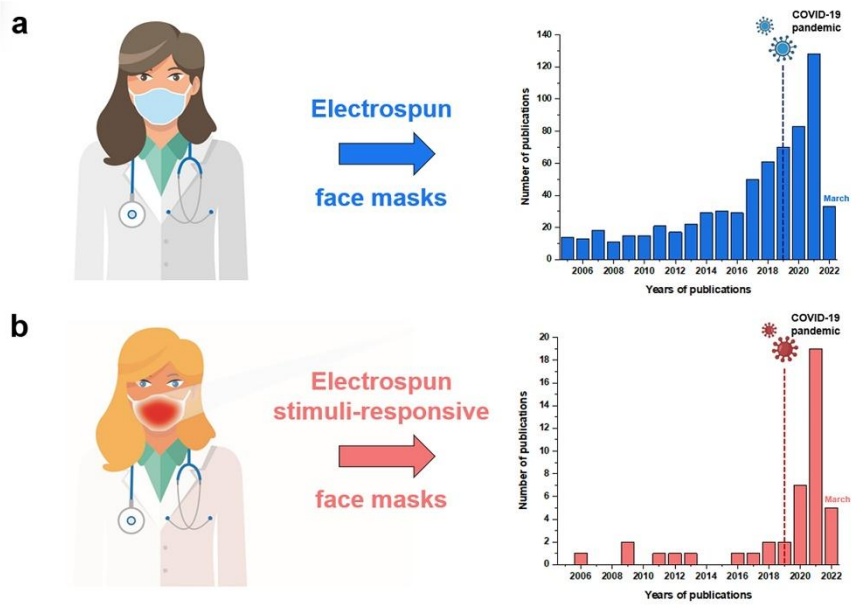

Figure 1. Impact of COVID-19 pandemic on the development of protective face masks. (a) Sketch of an electrospun face mask for passive filtration and the number of published articles relating to passive filtering face masks in 2005−2022. Data were obtained from the Scopus database on 2022-03-14 and have been reproduced with permission from ref 18. Copyright 2020 Wiley−VCH. (b) Representative illustration of an electrospun face mask for active filtration and the number of published articles relating to "smart" face masks in 2005−2022. Data were obtained from the Scopus database on 2022-03-14 and have been reproduced with permission from ref 18. Copyright 2020 Wiley−VCH.

membranes produced with environmentally safe polymers. In any case, one of the basic principles of chemistry and physics, the law of conservation of mass, has taught us that "nothing is lost, nothing is created, everything is transformed."[12] Many scientists have attempted to develop a recycling strategy for single-use masks. Crespo et al. developed a recyclable mixture of polypropylene (PP), polyethylene (PE), and polyethylene terephthalate (PET) with satisfactory mechanical and thermal properties that allow it to be used as an alternative polymeric blend for face mask fabrication.[13] Although the development of recyclable polymer-based masks is advisable,[14] partly biodegradable polymers are environmentally hazardous, as confirmed by the extensive distribution of polymer microparticles throughout the ecosystem.[15] Considering the environment, biostable polymers should be abandoned in favor of biodegradable polymers to produce filtration media. It is worth reminding that natural fibers have better biocompatibility while synthetic fibers have better mechanical properties.[16] The latter are also important in the case of nanofiber membranes for filtration applications as they require the materials to be bent in all directions.[17] It should be noted that the biodegradation process of natural fibers is initiated by an enzymatic or hydrolytic breakdown of bonds, and then other natural biological processes lead to decomposition into nontoxic gases, water, and carbon soil.[16]

In recent years, researchers have been exploring an entirely different strategy aiming to solve this issue, as well as other related problems. The approach presented in this paper is based on the idea that waste reduction is possible by introducing novel capabilities aimed at enhancing face mask performance for specific applications while extending their lifetime.[18] In this perspective, it is necessary to develop fibrous membranes with unique features that can be either constantly active or triggered on demand.[19] One of the most requested properties is the possibility of reducing the number of pathogens deposited onto face masks, thus enhancing the lifetime of face masks for frontline healthcare workers while reducing the possibility of cross-infection.[16] The ability to decontaminate the face mask structure without reducing the filter performance and stability opens the door to the development of long-term reusable and safe PPE.[20] In addition, nanotechnology-based strategies endow filter membranes with novel unique features, thus opening the field to brand-new devices such as energy-harvesting face masks with self-powered properties.[21]

Over the past decades, the entire scientific community of material scientists, working on both fundamental and applied research, has focused its efforts on developing innovative fibrous filtering materials, and this has led to innovative technologies.[22] The constantly growing effort and commitment spent by researchers in this field have focused on certain techniques through which it is possible to produce nanometric polymer fibers with a high surface-to-volume ratio,[23] high porosity,[24] exceptional mechanical properties, and stability, such as the electrospinning technique.[25] Most importantly, electrospinning is a versatile technique that ensures the possibility of incorporating additional materials, including inorganic,[26] metal,[27] and organic nanomaterials, in the produced nanofibrous structures.[28] This electrospinning-based approach to fabricate smart nanofibers can find

https://doi.org/10.1021/acsami.2c10335
ACS Appl. Mater. Interfaces 2022, 14, 46123−46144

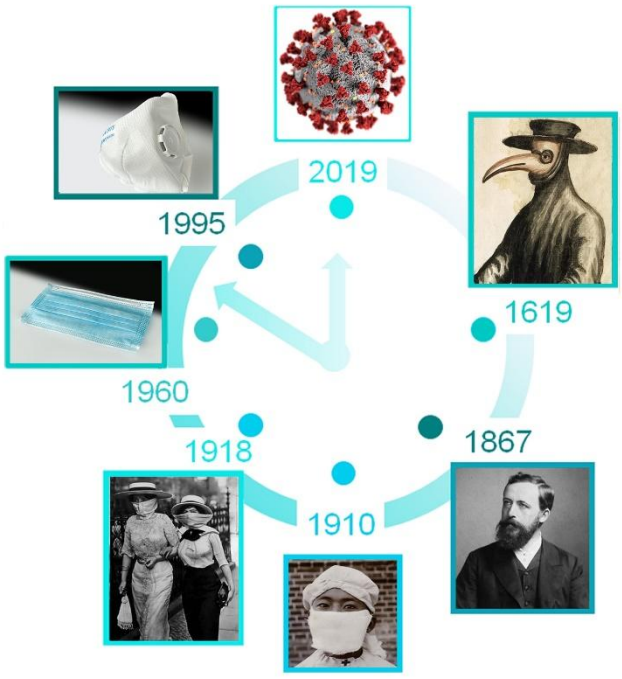

Figure 2. Evolution of face masks associated with the milestones of human history: from the "Black Death" bubonic plague of 1619 to the COVID-19 era beginning in 2019. 1619: a section of the picture "Doctor Schnabel von Rom" from Paulus Fürst illustrating the first face mask for medical use, designed by Charles de l'Orme in 1619. Reproduced from ref 54 under a CC BY-SA license. Copyright 2022 the authors. 1867: portrait of the surgeon Jan Mikulicz-Radecki, who was the first to wear a face mask in an operating room. Reproduced from ref 55 under a CC BY license. Copyright 2012 the authors. 1910: multilayer face mask invented by Doctor Wu Lien-teh, designed for the health management of the pneumonic plague in Manchuria. Reproduced from ref 39 under a CC-BY-NC-ND license. Copyright 2018 the author. 1918: Women wearing masks protecting them from influenza germs. The massive use of face masks among the general public made a crucial contribution toward reducing "Spanish Flu" infections. 1960: the disposable face mask. Since the 1960s, disposable face masks fabricated with artificial materials have replaced the use of cotton-fiber face masks. 1995: the N95 respirator patented by Prof. Peter Tsai. 2019: a graphic representation of the morphology of the SARS-CoV-2 virus, causing the COVID-19 disease. The COVID-19 outbreak opened up a new era for the widespread use of face masks, leading to the design of new face masks with multiple capabilities. Reproduced with permission from ref 56. Copyright 2022 American Chemical Society.

application in different fields, indeed, it was recently used by Xiong et al. to overcome the limitations occurring during intracellular delivery of therapeutics using the advantages given by photoporation.[29] Li et al. showed in their research that smart electrospun membranes also have great potential for water purification.[30] They fabricated a hydrophilic and visible light-responsive hydrolyzed polyacrylonitrile (HPAN) nanofiber membrane containing oxygen clusters that, under the influence of visible light, can destroy organic pollutants' structure. The stimuli that trigger a smart material response can be different and include ultrasounds, light, mechanical force, temperature, electric or magnetic field, and internal, such as a local change in pH.[31]

The unique properties of electrospun nanofibers enable their various, wide applications. In recent decades, electrospun nanomaterials have also been extensively investigated to produce high-performance face masks (Figure 1a). The combination of active compounds and stimuli-responsive nanomaterials with electrospun nanofibers opened the field to the development of functional face masks.[32] The entire scientific community concentrates maximum attention on designing intelligent face masks capable of responding to external stimulation (Figure 1b). Furthermore, in recent years, many companies have tried to solve the problem of the low efficiency of conventional electrospinning by developing new methods to increase production. Since then, it has become possible to use nanofibers in industrial applications; therefore, electrospun functional face masks have the potential to become a product available on a large scale; anyway, only face masks containing electrospun filters for passive filtration are available on the market at the moment.[33]

Several significant reviews have been published on the application of electrospun nanofibers for face mask production.[34,35] The recent use of electrospinning in combination with active and stimuli-responsive nanomaterials to develop functional, smart face masks has not yet been analytically discussed. In this review, we aim to offer an in-depth picture focusing on the most important steps taken by material science researchers in developing a next-generation nanofiber-based functional face mask. First, a reasoned understanding of face mask principles, their historical development, and the electrospinning technique is provided. This is followed by a

https://doi.org/10.1021/acsami.2c10335
ACS Appl. Mater. Interfaces 2022, 14, 46123−46144

significant and inclusive review of the literature on the development of passive, active, and stimuli-responsive electrospun media to produce face masks, including the novel functional and on-demand activatable features. In addition, the vital importance of combining advanced techniques and novel materials with already-developed filtering protective devices is suggested, highlighting the future prospects and challenges in this dynamic field. Lastly, the review ends with a discussion of the valuable essential guidelines on the most effective pathways for developing a novel generation of face masks with brand-new, unique capabilities.

FACE MASKS: A HISTORICAL OVERVIEW

Face mask use and technological development are interwoven with scientific and technological progress and epidemiological and historical backgrounds.[36] From a historical standpoint, the use of face masks has been driven by the need for protection from possible contaminations deriving from the breath of other people.[37] Indeed, in the 13th century AD, the Venetian merchant Marco Polo, in his book *Il Milione*,[38] reported on the use of an archetypal face mask. Noble people, in charge of preparing meals for the emperor Kublai Khan, kept their mouths and noses bandaged with drapes of gold and silk to prevent contaminating the emperor's meals.[38]

According to a popular-science visual trope, the use of face masks for medical purposes dates back to the prototypical pandemic, namely the "Black Death" bubonic plague (1346–1353). During that period, doctors did not wear any personal protective devices; nevertheless, "plague doctors" were depicted, in retrospective artistic representations, wearing a costume complete with a beaked mask.[39] In reality, the beak mask was designed and fabricated by Charles de l'Orme in 1619, shown in section 1619 of Figure 2, to protect doctors from the plague outbreak in Paris. The mask's beak was filled with perfumes, spices, and garlic, which were expected to neutralize the "miasma" considered responsible for the plague outbreaks.[40]

However, in 1897, Polish surgeon Johann Mikulicz, shown in a portrait in section 1867 of Figure 2,[36,40] was the first researcher to suggest a scientific approach to the use of face masks. The scientific landscape of the second half of the 19th century was marked by remarkable signs of progress in the field of microbiology. Indeed, in 1867, Louis Pasteur's studies on the spread of diseases due to microorganisms inspired Joseph Lister to implement the concept of asepsis.[41,42] Asepsis consisted of using chemical substances to prevent the contamination of surgical wounds with germs transmitted by instruments, hands, sponges, and gauzes.[41] Thirty years later, driven by the results obtained through his cooperation with bacteriologist Carl Flügge, surgeon Johann Mikulicz wore a face mask in an operating room for the first time. Indeed, Carl Flügge demonstrated that very small respiratory droplets (Flügge droplets) contain culturable bacteria and, therefore, can be an additional cause of postsurgical infections.[40]

The extension of face mask use to patients and the population is historically associated with the outbreak of the Manchurian Plague (1910). Such a practice was promoted by Doctor Wu Lien-the, who was appointed by the Chinese Imperial court to coordinate the efforts against the plague outbreak.[39] Doctor Wu advanced the breakthrough hypothesis of direct airborne transmission of the plague between humans, thus encouraging the widespread use of protective face masks. The "anti-plague mask" shown in section 1910 of Figure 2 was claimed to be Doctor Wu's personal invention. It was made of several protective layers and required a complex tying procedure, resembling the current surgical face mask.[39]

The use of protective face masks was mandatory for medical personnel and police forces (Figure 2, section 1918) during the influenza pandemic in 1918–1919, the so-called Spanish Flu. The widespread use of face masks was considered effective in decreasing the number of deaths.[40]

Since the 1960s, disposable face masks have been used by medical personnel and the population of some densely populated Asian countries such as China, Japan, and South Korea. Disposable masks (IIR type), represented in Figure 2, section 1960, are made of nonwoven synthetic fibers organized in three layers made of nonwoven polypropylene, resulting in an efficient network for filtrating the wearer's respiratory emissions.[43]

Respirators, on the other hand, can avoid the spread of respiratory emissions both from and to the wearer. The N95 (Figure 2, section 1995) is probably the most well-known and commonly used respirator. Its filtering efficiency is 94% for viruses and almost 100% for bacteria.[44] The technology behind the N95 filtering efficiency was conceived in 1992 and patented by Prof. Peter Tsai three years later. The trapping of hazardous substances, including dust, bacteria, and viruses, relies on the electrostatic attraction promoted by positive and negative charges inherent in the N95 material.[45]

The spread since December 2019 of the SARS-CoV-2 virus (Figure 2) has made the use of face masks one of the necessary global countermeasures against the transmission of COVID-19. Face masks have been strongly recommended by the WHO.[46] The impact of the SARS-CoV-2 outbreak was so severe that the general public was encouraged to use face cloths and surgical masks as an alternative to N95 respirators.[47]

Scientists promptly contributed to tackling the COVID-19 pandemic and the issues related to the face mask shortage[48] by advancing challenging solutions that were not limited to improving the filtration efficiency of face masks and respirators but could also endow face masks and respirators with new capabilities. Thanks to original nanotechnology-based approaches, face masks can now boast antimicrobial activity, sensing ability, greater comfort, and filtration efficiency.

Indeed, a filter medium for face masks, functionalized with Cu nanowires swaddled by a metal–organic framework, demonstrated antibacterial activity and antiviral properties against the SARS-CoV-2 virus.[49] Antiviral activity can also be achieved by coating face masks with a nanocomposite obtained from Cu nanoparticles embedded in shellac[50] or by directly depositing Ag nanoparticles onto textiles,[51] as will be discussed later.

During the COVID-19 pandemic, face masks were also viewed as a system suitable for analyte sampling. Vaquer et al., inferring that SARS-CoV-2 antigens accumulate in the inner hydrophobic polypropylene layer of medical face masks, fabricated a point-of-need biosensor that can be applied to the inward layer of face masks.[52] This biosensor is made of filter paper endowed with a reservoir containing Au nanoparticles functionalized with a mouse monoclonal antibody anti-SARS-CoV-2 N-protein. The antibody recognizes SARS-CoV-2 antigens, thus triggering a color change that a smartphone app can quantify.[52]

Face masks can also be conceived as wearable sensing devices for wireless patient monitoring. A respiratory rate mask was proposed as a wearable sensor to monitor the respiratory

https://doi.org/10.1021/acsami.2c10335
ACS Appl. Mater. Interfaces 2022, 14, 46123–46144

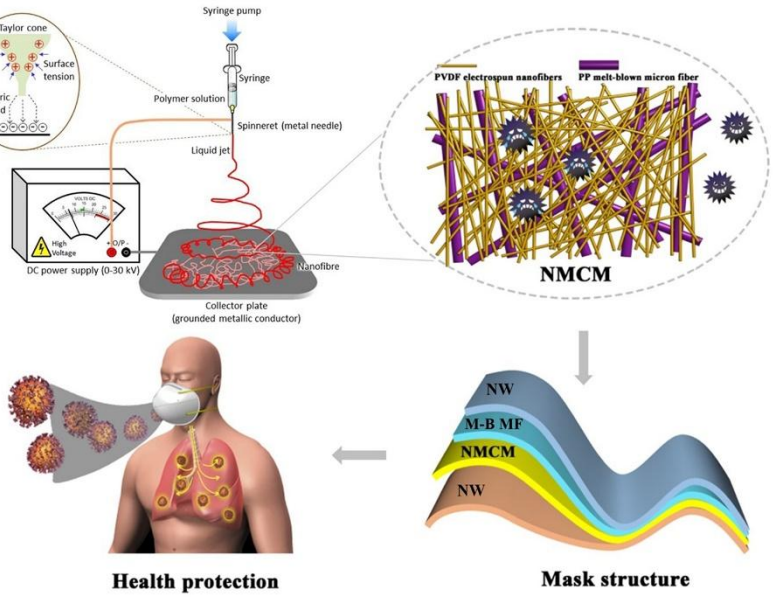

Figure 3. Electrospinning apparatus setup and nanofiber/microfiber composite membrane (NMCM) spun on polypropylene melt-blown micrometers fibers (M-B MF). Reproduced from ref 74 under a CC-BY license. Copyright 2018 the authors. The filtration mask structure contains additional protective nonwoven layers (NW), and its final application shows protection against viruses. Reproduced from ref 73 under a CC-BY license. Copyright 2021 the authors.

rate based on an impedance alteration detected in a humidity sensor containing $CsPbBr_3$ perovskite nanoparticles.[53]

Electrospinning-based nanotechnologies, however, offer outstanding opportunities for integrating multiple functions in face masks. An inspiring perspective for developing next-generation face masks has been proposed by De Sio et al.[18] The Authors proposed the design of a face mask based on multifunctional membranes. The membrane is made of electrospun nanofibers that offer more comfort to the wearer via two strategies. The first is the generation of a nanofiber architecture able to dissipate the humidity (moisture pump technology). The second is the design of a face mask which is adapted to the physical characteristics of users' face by an additive manufacturing technology. Moreover, the incorporation of Cu nanoclusters (outside the electrospun nanofibers) and Au bipyramids (inside the electrospun nanofibers) provides bactericidal and on-demand self-disinfecting properties, thus making the face mask reusable.

■ ELECTROSPINNING: A HISTORICAL OVERVIEW

The very first experiments related to electrospinning can be found as far back as the 16th century, when attempts were made to understand electrostatic phenomena.[57,58] At that time, William Gilbert (physicist of Queen Elizabeth I) observed that a charged piece of amber, at a sufficient distance away from a water droplet lying on a dry surface, attracted the droplets and pulled them into a cone shape.[58] With the growing use of the electrospinning technique in industry, in the 20th century, John Francis Cooley filed the first electrospinning patent for a method using different nozzles: conventional, coaxial, and airflow-assisted, and a spinneret featuring a rotating distributor.[59] Methods for the parallel spinning of multiple cellulose acetate fibers with simultaneous yarn formation attracted the interest of Anton Formhals, resulting in the patenting of numerous solutions in both the field of spinning nozzle construction and the process of fiber-winding devices.[60] Those inventions in fiber formation contributed to the filtration area when in 1939, Nathalie D. Rozenblum and Igor V. Petryanov-Sokolov developed highly efficient filtering materials now widely known as Petryanov filters.[61] This filtering cloth is used for fine and superfine cleaning of air and other gases from fine aerosols in gas masks. Later in the 1990s, research interest gained momentum. With the development of a theoretical basis for the spinning process, the spread of this technique increased sharply in both the industrial and scientific communities[62] A detailed historical outline of the development of spinning technology over the centuries can be found in a few comprehensive reviews.[57,58,60,61]

■ ELECTROSPINNING PROCESS

The basic principle of electrospinning is based on a polymer solution being sprayed in an electric field to form continuous fibers.[62,63] During the electrospinning of a polymer solution, an electric current applied to a metal nozzle leads to the repulsion of unipolar charges in the solution droplet.[64] When the charge limit is exceeded, the surface tension forces are overcome. As a result, a stream of polymer is ejected and stretched. If the solution viscosity is too low, the polymer jet will break apart and form droplets (electrospray).[65] Uniform charges repel each other, causing the polymer jet to spin and stretch further. At the same time, viscoelastic forces prevent the jet from breaking apart. On its way to the collector, the solvent evaporates from

https://doi.org/10.1021/acsami.2c10335
ACS Appl. Mater. Interfaces 2022, 14, 46123−46144

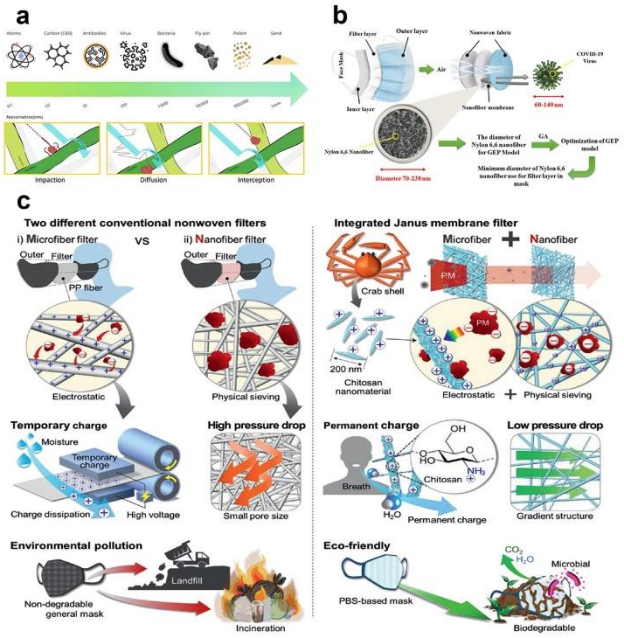

Figure 4. Passive filtering membranes. (a) Comparison of the size of naturally occurring particles and illustration of possible filtration mechanisms in membrane systems made of electrospun nanofibers. Reproduced from ref 88 under a CC-BY license. Copyright 2021 the authors. (b) Flowchart of the study for optimizing the nylon-6 electrospinning process using gene expression programming and genetic algorithms. Thus, the obtained nanofibrous membrane can capture coronavirus particles. Reproduced from ref 101 under a CC-BY-NC-ND license. Copyright 2021 the authors. (c) Comparison of particle capture mechanisms, user comfort, and environmental impact of conventional nonwoven filters and the integrated Janus filter developed by Choi et al. The use of conventional filters (left) results in a temporary charge or high-pressure drop and, as a disposable product, the filters pollute the environment. The filter based on PBS nanofibers with chitosan (right) has a durable charge, causes low-pressure drops, and is biodegradable. Reproduced from ref 107 under a CC-BY license. Copyright 2021 the authors.

the fiber, leading to its solidification and collection on a grounded collector in the form of a nonwoven fabric. The type of collector depends on the purpose of the material. Using appropriate collector shapes makes it possible to create tubes, 3D scaffolds, yarns, or flat membranes with a large surface area and randomly oriented fibers (Figure 3). Over the years, typical metal electrode spinnerets have been replaced with needleless nozzles. This invention increased the fiber production rate and eliminated clogging.

The electrospinning technique has received a great deal of attention from science and engineering communities thanks to its easy operation and the possibility of an efficient production scale-up.[32,66] The structure and size of the nanofibers can be customized using electrospinning parameters and polymer formulations, resulting in the fabrication of continuous fibers with diameters down to a few nanometers. Several parameters, such as applied voltage, polymer concentration, feeding rate, and distance between spinneret and collector, were identified as the most important. The applied voltage, as well as its polarity, can affect the reorientation of polymer chains that occur using electrospinning, allowing for control of the surface free energy of polymer fibers.[67,68] By adjusting the relative humidity, the internal porosity of a single fiber can be further enhanced to increase the specific surface area and tune the ultrafine porosity of the material.[69] Moreover, complex architectures, such as core−shell or hollow fibers, allow for the preparation of self-sterilizing,[70] antibacterial,[71] or highly porous fibers.[72] Therefore, as for its use in air filtration, it is the only technique capable of producing materials with low filter resistance for air and ultrafine particle capture.[73] Another advantage is its high surface-to-volume ratio, providing space for functionalization to efficiently remove numerous pollutants such as bacteria, viruses, and harmful gases.

■ ELECTROSPUN NANOFIBER-BASED FACE MASKS

Passive Filtering Membranes. Different face masks provide different levels of protection for the wearer, depending on the material of which they are made and their engineering design. The level of protection is closely related to the ability to filter pollutants and bacteria or viruses of varying sizes.[75−79] The porosity of the fibrous membrane plays a crucial role in the passive particulate matter filtration mechanism. High filtration efficiency is achieved by using thick layers of densely packed nanofibers. Materials with small pores catch smaller particles than materials with large pore sizes, such as cotton and synthetic fabrics.[80] Electrospinning is the most frequently used technique for producing nanofiber membranes of this type.[81]

Despite their high filtration efficiency, conventional face masks of melt-blown microfibers usually make breathing difficult.[82−84] Electrospun nanofibers are adequate substitutes

https://doi.org/10.1021/acsami.2c10335
ACS Appl. Mater. Interfaces 2022, 14, 46123−46144

for this masks because they provide high filtration efficiency, even close to 100%,[85] without causing respiratory distress.[86]

Essential parameters for assessing the user's comfort with a given filter medium are pressure drop and air or water vapor permeability.[87] The pressure drop determines the difference in total pressure between two points of the medium (e.g., fluid or air) flowing through the filter and results from the frictional forces that arise due to flow resistance.[88] Electrospun membranes have randomly arranged ultrafine fibers and a high surface-to-volume ratio. Moreover, they are nanoporous, vapor permeable and have good mechanical properties, so their use for personal protection face masks against minute particles, bacteria, and viruses can be particularly beneficial.[89−93] Moreover, nanofibers are considered especially effective in filtering submicrometer and nanometric contaminants, while having only a slight influence on the pressure drop.[88] The diameter of fibers and pores of the materials obtained by electrospinning polymer solutions can be easily controlled and regulated. The diameter of nanofibers can be 10−100 times smaller than conventional melt-blown microfibers.[88]

Possible particle trapping mechanisms (Figure 4a) explain how the high surface-to-volume ratio of electrospun fibers improves the filtration efficiency.[86,88] It is worth noting that the air filtration mechanism is in a steady and unsteady state. In the first one, the process efficiency and the pressure drop across the filter membrane depend only on the filter material, the properties of the particles, and the airflow. In the second state, with the filtration time and the deposition of pollutants on the filter surface, the filtration efficiency and airflow resistance change. However, the processes taking place in the unsteady state are so complex that they cannot be described in a simple way. Since the accumulation of particles on the surface of the electrospun mat does not significantly change its thickness, it is assumed that, in this case, the entire process is in a stable state.[94] Therefore, filtration can be achieved in five different ways, depending on particle size. These mechanisms include sieving, interception, inertia impaction, diffusion, and electrostatic attraction.[86,88]

If the particle size is larger than the pore size of the filter membrane, they are captured by sieving.[95,96] Commonly known electrospun filters use physical capture as the primary filtering mechanism, although this solution is insufficient in many cases.[97] When the polymer nanofibers are charged, they can attract particles having an opposite charge−according to the electrostatic attraction mechanism.[95,96] Accumulation of residual charges on the nanofiber mat during the electrospinning process changes its surface potential (V); therefore, the measurement of this parameter provides useful information on the process and the morphology of the membrane, i.e. the nanofiber diameter and the size of the pores between them. Liang et al. showed that an electrostatic voltmeter can be successfully used to online measure the V of the membrane during electrospinning; additionally, surface potential measurement, in combination with current measurements, is an efficient way to monitor the entire electrospinning process.[98] Another way to study the electrical properties of a wide range of materials is Kelvin probe force microscopy (KPFM). This technique combines the advantages of atomic force microscopy (AFM) and the Kelvin probe method. Due to the use of a conductive cantilevered beam with a sharp tip, KPFM is characterized by high spatial resolution, and the electrostatic surface potential of the sample can be measured from the micro- to the nanoscale. The analysis is carried out by detecting the movement of the conductive cantilever, which is due to the electrostatic force between the sample and the tip mounted on the cantilever.[99] The storage of residual charges in nanofibers is essential, especially for developing materials for filtration applications, as electrostatic forces can increase the adsorption or repulsion of pollutants.[98]

Other, smaller particles are filtered via the other three mechanisms. Particles with a size of 300−600 nm move with airflow. Since they are heavier than air, they are affected by an inertial impaction[95,96] and cannot separate in different directions, as air does when entering the fiber pores, so they hit them and deposit on their surface. Medium-sized particles are too small to have inertia and too large to diffuse in an airflow. Therefore, they are filtered by direct interception when the air stream deflects in the spaces between fibers.[88] The smallest particles, i.e., those with a size smaller than 300 nm, can diffuse in the airflow.[95,96] Moving randomly, they collide with the fibers on which they deposit. Therefore, as shown in Figure 4a, the smaller diameter of the electrospun filament corresponds to the higher filtration efficiency on particles of a specific size.

All the properties described above have led electrospun nanofibers to be increasingly used in the design and production of face masks all over the world.[48,100] Up to now, the following materials have been studied for use as passive filtration membranes in nanofiber mats: nylon-6.6,[101] nylon-6,[102−104] polycaprolactone,[105] poly(ethylene terephthalate),[17] silk fibroin,[17] polylactic acid,[106] poly(methyl methacrylate),[88] polybutylene succinate,[107] polyacrylonitrile,[86,100] and polyvinylidene fluoride.[48,108]

Polyamides. Polyamides are long-chain polymers in which the basic units are bound together through amide bonds (−C(O)−NH−). These compounds are classified as semicrystalline materials with a high melting temperature, stiffness, mechanical strength, and chemical resistance. However, they show considerable susceptibility to moisture. Moreover, polymer nanofibers with polar functional groups, e.g., nylon-6 (PA-6),[102,103] have a strong affinity for particulate matter (PM). This makes polyamides highly effective for eliminating pollutants with high efficiency at a low-pressure drop and sufficient air permeability.[102]

Zeraati et al. optimized nylon-6.6 (PA-66) electrospinning parameters so that the obtained nanofibers had a specific diameter and made it possible to prepare a membrane useful as a filter against the SARS-CoV-2 coronavirus.[101] The control of the size and morphology of electrospun nanofibers allows obtaining a material with the desired mechanical, electrical, optical, and biomedical properties. To determine the conditions of this process, researchers used artificial intelligence, including gene expression programming (GEP) and genetic algorithms (GA), as shown in Figure 4b. The results proved that the application of a 26 kV voltage makes it possible to obtain highly oriented nanofibers. In addition, by electrospinning a 16% solution using a working distance of 18 cm and a flow rate of 0.2 mL h^{-1}, nylon-6.6 nanofibers with a diameter of 55.8 nm can be obtained. It is worth mentioning that coronaviruses have a size of 60−140 nm, and their aerosols measure 0.3−2 μm. Scanning electron microscopy (SEM) measurements indicate that the surface of the obtained nanofibers is smooth, and they are arranged in a structure resembling a spider's web. Their porosity was 84.3%. The filtration efficiency (following ASTM standards) was 98.6%. The obtained diameter of nanofibers, their porosity, and the

https://doi.org/10.1021/acsami.2c10335
ACS Appl. Mater. Interfaces 2022, 14, 46123−46144

fact that they can attract viruses due to electrostatic interactions make it possible to use the developed structure as a filtering layer in face masks.[101]

Considering the importance of the thermal comfort of face mask users, Yang et al. developed a filter layer based on PA-6 that is highly efficient in particle trapping and effective radiative cooling.[102] Electrospun nanofibers were transferred to a nanoporous polyethylene substrate (PA-6/nanoPE fibers), thus increasing their mechanical strength. The prepared membrane had high mechanical strength compared to commercial face masks. Moreover, Yang and his collaborators showed that the structure could be further strengthened by providing additional support with two outside layers of cotton mesh. The nylon-6 nanofibers produced were characterized by a small diameter (<100 nm). Because they also had a large dipole moment, $PM_{2.5}$ particle filtering tests showed >99.0% efficiency for fibers with density reduced to about 85%. Particle trapping was accompanied by a low-pressure drop that characterizes air permeability. The polyethylene substrate is highly transparent to infrared radiation. Therefore, its use permitted an effective radiative cooling, ensuring thermal comfort for users on warm days. An additional advantage is that both materials used in this study are low-cost and readily available.[102]

Recently, another research group modified a nylon-6/PE membrane by electrospinning nylon-6 into a polyethylene nonwoven fabric.[104] Electrospun membranes have not been used alone as face masks yet due to their low mechanical properties caused by nanoscale diameters of fibers. Systems containing PE melt-blown nonwovens and PA-6 electrospun membrane could bear a tensile force of about 25 N, which is enough to be used as face masks. The new substrate proved better for face mask applications than prepunched nanoporous PE. In addition, the filter developed by Xu et al. had a two-level pore size of the electrospun mat providing gradient filtration. PE microfibers formed larger pores (~143 μm), while PA-6 nanofibers formed smaller pores (~6 μm). Due to the gradient filtration and the high dipole moment of nylon-6, the composites showed high efficiency in the filtration of a particulate matter (>99%) with a low-pressure drop (<100 Pa). They were also highly transmissive to mid-infrared radiation and thus able to remove heat effectively.[104]

Polyesters. Polyesters are polymers with multiple ester bonds (−C(O)−O−) in their main chain and due to the vast possibilities of synthesis, they are characterized by various properties. Polyesters are used primarily in the textile industry and for the production of plastics.

Polycaprolactone (PCL) is a biocompatible material,[109] and its nanofibers are successfully used in tissue engineering,[110] as well as in air filtering devices. However, Khandaker et al. investigated for the first time their use as a filter medium for use in face masks.[105] In this study, PCL nanofiber mats were fabricated by electrospinning on a drum collector for 3 or 10 min (PCL-3 and PCL-10, respectively). By selecting the parameters for electrospinning, the pore diameter could be controlled, which made it possible in the end to obtain an average pore value of 1.4 ± 0.3 μm for the PCL-10 sample. For comparison, the filtering layer from the Henry Schein Earloop surgical mask (as a control sample) was also tested. It was shown that, in this case, the average pore diameter was 5.7 ± 0.6 μm, which is almost 50 times the size of the average virus, whose diameter is approximately 120 nm. The values of the contact angles showed that all the mats—PCL-10, PCL-3, and the control sample—were highly hydrophobic. The contact angle, however, was the largest for the control sample, while PCL fabrics absorbed water droplets to a lesser extent. Moreover, they were resistant to extreme temperature conditions, and their properties did not change in the presence of a solvent. The PCL-10 fabric turned out to be the strongest mechanically, which shows that the difference in material thickness has an effect on the mechanical properties of PCL. In addition, PLC-10 was resistant to a pressure of 18 psi, and the filtration efficiency test proved that the double layer of the spun mat placed between fabrics is impermeable to particles smaller than 120 nm. Based on the results obtained, it can be said that PCL electrospun fibers may be a better filter medium for surgical masks than those currently used.[105]

Poly(ethylene terephthalate) is a semicrystalline thermoplastic polyester,[111] characterized by flexibility, high mechanical and thermal strength, and good chemical and electrical insulating properties,[112] enabling its wide application. Opálková Šišková et al. prepared a composite membrane based on PET with the addition of silk fibroin (SF), which could serve as a filter medium protecting against air-polluting particles, while ensuring a comfortable use.[17] Importantly, such a filter makes it possible to reuse plastics. Since SF can be obtained from natural silk cocoons, its production cost becomes negligible and hassle-free due to the easy availability of the necessary materials. In this study, electrospun membranes based on PET obtained from used bottles together with different SF contents were produced and tested. Micrographs taken with SEM showed that the fabricated mats were smooth, without defects, and the fibers were continuous and randomly oriented. SF-containing nanofibers were thinner than pure PET fibers, and the pore size of composite membranes was smaller than the pore size of the mats made of their pure components. The increase in silk fibroin content in the composites increased air permeability and improved their mechanical properties. Although pure SF shows poor mechanical resistance, it has a fibrous structure, and its inclusion in the composite provides high tensile strength and flexibility. The most effective filter from all those tested (with a filtration efficiency of 90.2%) belonged to the FFP1 class following the EN149 classification. Belonging to the FFP1 class makes it possible to use a filter as personal protective equipment in the form of a face mask.[17]

Polylactic acid (PLA) is a thermoplastic polymer belonging to aliphatic polyesters. This polymer is biocompatible, nontoxic, and safe for the environment. In addition, it has good mechanical properties, for which its use is very widespread. PLA is used in packaging for food, furniture, and clothes and in the medical and pharmaceutical industries.[113] Medical sutures, stents, and hygiene products for women are made from this polymer. Buluş et al. used the electrospinning technique to prepare a polylactic acid membrane and composites containing activated carbon (AC) as reinforcement.[106] A significant advantage of activated carbon, in this case, is the ability to adsorb gaseous pollutants in its deposits. In this way, it is possible to purify the air of volatile organic compounds, other gaseous pollutants, and unpleasant odors, such as the smell of cigarette smoke. Unfortunately, this material is insufficient for filtering particles such as dust and mold. In this study, four mats with the composition of 10% PLA, 10% PLA-1% AC, 10% PLA-5% AC, and 10% PLA-8% AC were obtained. Their structural, morphological, and mechanical analyses were then performed, and their filtration

https://doi.org/10.1021/acsami.2c10335
ACS Appl. Mater. Interfaces 2022, 14, 46123−46144

abilities were tested. The research showed that when the concentration of active carbon was increased, the electrical resistance of the solutions rose, the nanofibers obtained were thinner, and their mechanical strength was better. Their diameter was in the range of 80−240 nm. The best mat was obtained as a composite containing 10% PLA and 8% AC, for which the tensile strength was 60 MPa due to well oriented fibers and their small diameter. For all four membranes, the filtration efficiency of both bacteria and submicrometer particles was greater than 98%. Therefore, it has been proven that PLA-AC composites have ideal properties for use in the production of personal protective equipment and filtration applications.[106]

NanoLayr Ltd. developed a new type of filter membrane based on electrospun nanofibers. For this purpose, the company used poly(methyl methacrylate) and ethylene vinyl alcohol. The product is currently sold under the trade name FilterLayr.[88] Poly(methyl methacrylate) (PMMA) is a thermoplastic polyester with high transparency[114] and stiffness, commonly known as acrylic glass. Moreover, it is highly resistant to UV radiation. Ethylene-vinyl alcohol (EVOH), on the other hand, is a copolymer of ethylene and vinyl alcohol and is characterized by low oxygen permeability. For this reason, it is widely used in the production of food packaging. Karabulut et al. investigated the filtration efficiency of nanofiber materials similar to those marketed as FilterLayr.[88] Scientists produced more than 75 samples by electrospinning a PMMA/EVOH solution onto a PP nonwoven fabric. Tests were performed according to the following international standards: ASTM Test Method F2299 (for surgical masks), ASTM Test Method D3502 (for barrier masks), and NIOSH 42CFR84 (for respiratory masks, N95). In this study, researchers used various types and sizes of particles and variable air velocity for their tests. Results showed that nanofibers are highly homogeneous, and that as filters, they meet the requirements of each of the standards. Following the standard for respiratory masks, the filtration efficiency was 98.1% (pressure drop of 226 and 290 Pa at a rate of 85 and 120 l min^{-1}, respectively). According to the standard for surgical masks, the filtration efficiency was 99.9% (pressure drop of 44 Pa at a rate of 8 l min^{-1} with a filtered particle size of 100 nm), and for barrier masks, 99.7% (pressure drop 133 Pa at a rate of 60 l min^{-1}). Therefore, it has been shown that the materials based on electrospun PMMA/EVOH nanofibers produced by NanoLayr Ltd. meet all the requirements of face masks set out in three major, albeit quite different, international standards.[88]

Polybutylene succinate (PBS) is a thermoplastic polymer resin from the polyester family. This semicrystalline polymer is a biodegradable material. Choi et al. developed an electrospun PBS filter which wholly degrades in compost soil thanks to its biodegradability.[107] The produced filter consisted of two integrated mats−microfiber and nanofiber−obtained by the electrospinning method and covered with chitosan nanowires. Chitosan (Cs) is a biocompatible, biodegradable and nontoxic polysaccharide which, due to its properties, is ideally suited for the intended use, moreover, is considered an antibacterial material. Researchers used PBS solutions with different concentrations and, consequently, viscosity to obtain mats with varying fiber diameters. In this case, the particle capture mechanism combines physical sieving and electrostatic adsorption due to cationic sites and polar amide groups in chitosan. The efficiency of the obtained filter was comparable to the commercial N95 filter. It removed 98.3% of the 2.5 μm diameter solids ($PM_{2.5}$). PBS nanofibers screened contaminants, and microfibers ensured high breathability and low-pressure drop (59 Pa). Moreover, the resulting filter is reusable and fulfills its function even when the filter is wet, while the efficiency of the N95 filter drastically drops due to moisture, limiting its use to one time. Both materials used are biodegradable, and studies have shown that the obtained filter is wholly degraded in compost soil within one month. A comparison of conventional nonwoven filters and the integrated filter developed in this study is shown in Figure 4c.[107]

Polynitriles. Polynitriles are polymers composed of nitriles, i.e., organic compounds being derivatives of hydrogen cyanide of the general formula R−C≡N; the nitrile (−C≡N) group is attached to the remainder of the compound via a carbon atom.

Polyacrylonitrile (PAN) is a polar, stiff, and brittle duroplastic polymer. Nanofibers obtained from polymers such as PAN have reinforced polar groups on their surface.[103] They are often used as precursors to produce carbon nanofibers.[115] Lee and Jeon have developed a membrane made of PAN electrospun nanofibers, which apart from high filtration efficiency also made it possible to monitor the user's breathing.[86] This study examined a pure polymer PAN mat, while a mat containing an electrically conductive metal−organic framework (MOF), Ni-CAT-1. The $Ni(OAc)_2$ was synthesized directly on PAN nanofibers by a two-step hydrothermal reaction where the linking molecule is 2,3,6,7,10,11-hexahydroxytriphenylene (HHTP). The growth of Ni-CAT-1 crystals on the surface of nanofibers significantly influenced the latter's morphology, adhesion strength, and electrical resistance. As the concentration of MOF crystals increased, the diameter of the obtained fibers also increased, while the electrical resistance decreased as the thickness of the conductive armature increased. Filtration efficiency tests were conducted with the use of air polluted with dust particles $PM_{2.5}$ (~500 $\mu g\ m^{-3}$) and $PM_{10-2.5}$ (~1000 $\mu g\ m^{-3}$) and incense smoke containing $PM_{2.5}$ (~1500 $\mu g\ m^{-3}$) and $PM_{10-2.5}$ (~1000 $\mu g\ m^{-3}$). The particulate filtration efficiency from the air for both membranes was similar: >99%. The composite membrane, however, was a better filter for particulate matter from incense smoke than the pure PAN mat. In this case, the former's capture efficiency was 79% for $PM_{2.5}$ particles and 97% for $PM_{10-2.5}$, while for the pure PAN membrane, it was 59 and 90%, respectively. This was due to the fact that the oil droplets from incense burning had a higher affinity for MOF than for PAN nanofibers. Additionally, the electric resistance of the composite membrane changed with the change in the humid air flow rate, which makes this membrane serviceable for breath monitoring.[86]

The usefulness of such face masks should be as high as possible, so it would be good if their protective and filtering properties lasted longer and not were limited to a single use. However, for a given mask to be used again, it must be adequately prepared in advance to rid it of previously captured impurities. Mamun et al. verified whether the masks based on PAN nanofibers were reusable after washing them in a home washing machine.[100] Scientists produced electrospun PAN mats on a polypropylene substrate, which were then covered with another layer of PP, as is the case in a standard mask, and then tested their filtering capacity following the EN143 standard for respiratory masks. Filtration efficiency was retested after the composites were washed in a domestic

https://doi.org/10.1021/acsami.2c10335
ACS Appl. Mater. Interfaces 2022, 14, 46123−46144

washing machine at different temperatures (40 °C (short program), 40 °C, 60 °C, and 95 °C). Air permeability and resistance to evaporation were also tested. SEM analysis of PLA mats before washing showed that the nanofibers were relatively straight and without defects. Images from a confocal laser scanning microscope (CLSM) showed that washing actually did not change the surface of nanofiber membranes at all. It was found that this process affects air permeability and resistance to evaporation. As the washing temperature increases, air permeability increases, while the resistance to evaporation decreases. These changes, however, are so small that the effect of washing on air permeability and evaporation of the mats is negligible, thus making them reusable. Before washing, PP/PAN nanofibers/PP composites showed a filtration efficiency of 93.9%, while after washing at 60 and 95 °C, filtration efficiency was 86.1 and 88.6%, respectively. Therefore, their performance drops somewhat, but still remains high. There is a need for further research in this area, but it seems that washing masks in a domestic washing machine is an effective and promising method for achieving reusability.[100]

Polyfluoroolefins. Polyfluoroolefins represent vinyl polymers, i.e., polymers formed due to combining monomers containing −C═C− double bonds. Their backbones consist of carbon atoms linked by single −C−C− bonds and hydrogen and fluorine atoms.

Polyvinylidene fluoride (PVDF) is a thermoplastic polymer with a low chemical reactivity. Due to the smooth structure of nanofibers, uniform pore structure, and easy bonding with PET nanofibers, Ullah et al. chose PVDF to evaluate the reusability of filter membranes after an ethanol cleaning process.[48] These researchers compared a typical melt-blown (MB) filter with PP found in N95 masks and a filter made of PVDF nanofibers (NF) supported by PET (weight PET/weight PVDF = 98:2). The changes after cleaning in the filtration efficiency, morphological properties, and air permeability of both filters were assessed. Two different cleaning procedures were followed: in the first, membrane samples were immersed in, and in the second were sprayed with, 75% ethanol. The porosity of the MB filter (∼96%) was higher than that of the NF filter (∼80%), which probably resulted in twice better air permeability of the MB filter than that of the NF filter, before and after alcohol cleaning. Nevertheless, both membranes met the requirements for face masks in terms of air permeability, pressure drop, and morphology. Measurements of the contact angle of the analyzed filters, both before and after cleaning, showed that despite slight changes after exposure to ethanol, they remain hydrophobic. Therefore, it was concluded that the presented cleaning process of the filter materials does not affect their mechanical and chemical properties. When used once, they also showed a high and comparable filtration efficiency. However, the MB filter efficiency after treatment with ethanol proved to drop to 64%, while the NF filter efficiency was kept high at ∼97−99%, making its reuse possible. Moreover, it was shown that the NF filter is not cytotoxic to human cells.[48]

Leung and Sun decided to develop a filter membrane composed of PVDF nanofibers capable of filtering COVID-19 virus particles.[108] Using the electrospinning technique, the authors produced mats from electrostatically charged PVDF. SEM analysis showed that in prepared materials there are both smaller and larger fibers. It was concluded that the smaller ones can provide efficient filtration, while the larger ones give the mechanical resistance and low pressure drop of the filter medium. The obtained samples were arranged in two-, four-, and six-layer stacks, which increased the grammage of fibers in individual filtration membranes. Filtration efficiency tests were conducted using aerosols with a size of 20−300 nm, with the 100 nm aerosol being a representative example of an aerosol made of virus particles and carriers. The 50 nm particle size aerosol simulated the smallest possible aerosol event, and the 300 nm aerosol was selected for testing based on the standards set by NIOSH. The six-layer membrane of charged PVDF nanofibers achieved a filtration efficiency of 88, 88, and 96% for the 50, 100, and 300 nm aerosols, and 92, 94, and 98%, respectively, when tested with monodisperse NaCl aerosols. The pressure drop was 26 Pa in each case, so the obtained filter was 10 times more breathable than standard N95 masks. As the 300 nm NaCl aerosol test was 98% effective, the resulting filter could be qualified as an N98 respirator mask.[108]

■ ACTIVE NANOFIBROUS STRUCTURES FOR FACE MASK APPLICATION

Substantial efforts to produce higher-performance masks and respirators have been reported a number of times over the past few years. These include developing novel technologies to produce new or modified filter pieces and improving manufacturing protocols. Recently, researchers in the field of protection masks are working to include additional features in face masks, enabling an active filtration in protective equipment. This section focuses on the development of novel active filtering membranes that maintain constantly active properties over time.[116]

Active Thermal Dissipation for Wearability and Comfort Optimization. Wearing face masks remains the most effective protective measure against COVID-19 infection even after mass vaccination, but an inadequate comfort and low antibacterial/antiviral activities accelerate the frequency of surgical mask replacement, resulting in large amounts of medical waste. Several researchers have developed electrospun nanofiber layered masks with excellent wearing comfort to help solve this problem.

Xiong et al. proposed fabricating masks from electrospun fluorinated carbon nanofibers/carbon fibers (F-CNFs/CF).[116] These fibers were used to replace commercially available polypropylene nonwovens as the core layer in face masks. The through-plane and in-plane thermal conductivities of commercial PP nonwovens were only 0.12 and 0.20 W m^{-1} K^{-1}, but the fabricated nanofiber membranes achieved 0.62 and 5.23 W m^{-1} K^{-1}, representing an improvement of 380 and 2523%, respectively, providing better heat dissipation. The fabricated face masks provided outstanding comfort due to the mentioned thermal properties (Figure 5a).[116]

Yang et al. fabricated a highly breathable and thermally comfortable face mask combining the asymmetric wettable skin layer with the nanofiber membrane via the electrospinning technique.[117] In electrospinning, the electret process and fiber construction could be integrated into one process, as Yang et al. demonstrated. Thus, a desired composite face mask with a hierarchical structure and decent filtration performance was fabricated by combining electrospun nanofibers and nanoparticles. However, practically no effort has been made to investigate the wearing comfort of an electrospun composite membrane, and especially the relationship between membrane structure and wearability. To create a multilayer structure for filter application, Yang et al. synthesized an asymmetric wettable skin layer made of an electrospun PAN/poly(ether imide) membrane with high $PM_{2.5}$ removal efficiency, desirable

https://doi.org/10.1021/acsami.2c10335
ACS Appl. Mater. Interfaces 2022, 14, 46123−46144

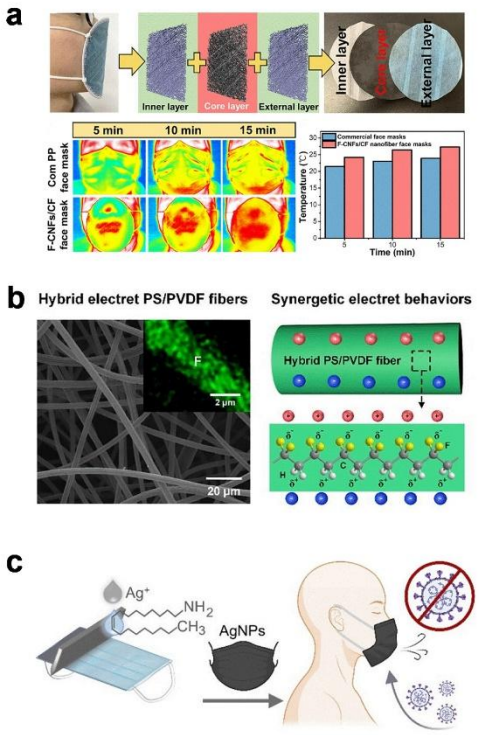

Figure 5. Various strategies applied to broaden the applications of respirators by enhancing and/or adding novel features. (a) Structure of nanocomposite fiber masks made of commercially available PP surgical masks and F-CNFs/CF nanocomposite fibers as well as the thermal analysis results obtained for the fibrous masks. Reproduced with permission from ref 116. Copyright 2022 Elsevier. (b) SEM image of the electret PS/PVDF-2 (the inset shows an elemental distribution map of fluorine atoms into a single electrospun fiber collected by energy-dispersive X-ray spectroscopy). Schematic representation of the contribution of PVDF to the electret effect. An N95 respirator with PS/PVDF-2 fibers as its core material. Reproduced with permission from ref 119. Copyright 2020 Elsevier. (c) Schematic representation of the coating procedure on a face mask with functionalized silver nanoparticles to inhibit viral infectivity and the final PPE application. Reproduced with permission from ref 51. Copyright 2021 American Chemical Society.

air permeability, and good radiation cooling properties. A low air permeability resistance and a uniform directional moisture transfer were observed for the composite membrane with a wetting gradient throughout its thickness. In addition, the multilayer structured nanofibrous membrane with outstanding radiative cooling is expected to significantly improve heat dissipation under extreme environmental conditions.[117]

Xiong et al. fabricated a novel face mask with excellent wearing comfort consisting of PP ultrafine fiber nonwovens and antibacterial functionalized nanoparticles of hexagonal boron nitride (h-BN).[118] After the antibacterial functionalization of h-BN, a simultaneous improvement in the thermal conductivity and antibacterial activity of PP ultrafine fiber nonwovens was observed. Organic chains of quaternary ammonium salt (QAC) with an extended spectrum of antibacterial activities were immobilized on the surface of the hydroxylation of h-BN nanoparticles by forming covalent bonds. The activated PP ultrafine fibrous webs were then impregnated with the QAC/h-BN nanoplatelet suspension. QAC/h-BN/PP nanocomposite fiber membranes overcome the poor thermal comfort and antibacterial activity issues inherent in commercial PP nonwovens. The antibacterial efficiency of the fabricated masks was 99.3% for *E. coli* and 96.1% for *S. aureus*, and the antibacterial mechanism of the samples was based on contact killing. The authors claimed that the new QAC/h-BN/PP nanocomposite fiber membranes could find application in a broad range of personal health protective equipment.[118]

Charge Surface Improvement for Higher Filtration Performance. Electret technology mitigates the conflict between filtration efficiency and pressure drop by providing fibers with an electrostatic effect that contributes to particle adsorption while generating negligible airflow effects. Compared to current electret technologies, electrospinning can perform the *in situ* charging and fiber formation, by making it possible to produce electret fibers in one step.

Li et al. fabricated hybrid electret consisting of polystyrene (PS) and polyvinylidene fluoride electrospun nanofibers by investigating the supplementation of electrical responses between polymer hybrid nanofibers.[119] The crossbreeding of the electrical polarization performances of PS and PVDF, two different polymers with low and high dielectric constants, led to the hybrid PS/PVDF nanofiber architecture, which showed an improved performance of electret effect and higher porosity (Figure 5b). This electret effect transpired on behalf of the movement of charges into polymer traps and dipole orientations, respectively. The fabricated face masks, including PS/PVDF hybrid nanofibers as the central layer in the N95 facepiece, had a higher filtration performance of 99.8%, a lower pressure drop of 72 Pa, and a longer mean life.[119]

Wang et al. developed a hybrid face mask consisting of PAN electrospun nanofibers for air filters, by refining the design of the existing surgical masks.[120] The structure of the proposed face mask consisted of a PAN nanofibrous layer over the face mask, to be covered by a bilayer of poly(3,4-ethylenedioxythiophene):polystyrenesulfonate (PEDOT:PSS) and polypropylene. As a result of their sandwich structure, the obtained masks achieved high filtration efficiency, with a filtration performance increase in the particle with a size range between 11.5 nm and 2.5 μm. In addition, with the aid of a tribo-charge applied via the PEDOT:PSS coated PP layer, capture efficiency increased by 7%. The implementation of tribo-charged took advantage of enhanced mechanical interception and electrostatic forces, which facilitated improvement in the filtration efficiency of particles. Stability and significantly extended mean life were validated by interception efficiencies of 94% ($PM_{0.25}$) and 99% ($PM_{2.5}$), without deterioration after 2 days. Lastly, an effective sterilization of the face mask surface could also be achieved with the aid of the generated tribo-charges.[120]

The human body is a great energy source, and the mechanical energy generated by body movements such as walking and inhalation is sufficient to power many wearable devices. Flexible electret nanogenerators with the primary operating mechanism of electrostatic induction caused by excess charges in the electret materials are characterized by considerable output power and a wide range of applications.

https://doi.org/10.1021/acsami.2c10335
ACS Appl. Mater. Interfaces 2022, 14, 46123−46144

Cheng et al. presented a self-driven smart face mask consisting of a sandwich structure using electrospun poly(ether imide) fibers as an active electret material.[121] As a result of the excess charges retained in the nonwoven poly(ether imide) fabric, this smart face mask effectively removes particles during breathing and collects the energy generated during the outbreath. The fabricated electrospun layer had a high filtration efficiency for submicrometer particles (99.6%) and a correspondingly low-pressure drop (10 Pa). The smart mask can act as a stand-alone sensor to detect the breathing rate; the durability of the smart face mask is outstanding, being able to work continuously for 40 h. This study offers an approach for fabricating high-efficiency face masks, advancing the progress of self-powered wearable electronics.[121]

Antiviral Activities of Functional Membranes. The rapid advancement of disinfecting materials and their incorporation into personal protective equipment is a critical necessity that will significantly contain the spread of the SARS-CoV-2 virus and other pathogens. Extensive research has been conducted to prepare antiviral materials for face masks, such as inorganic or organic nanoparticles incorporated into electrospun nanofibers.[19,51,122−126] Antimicrobial face masks activated by photo/electrothermal or photosensitizing agents have shown a high and functional inactivation of viruses and long durability. There are several different methods for effectively disinfecting material surfaces to prevent the transmission of pathogenic microbes, especially viruses, during pandemics. Most of the available disinfection procedures today require several steps and cannot be easily applied to the face masks that are currently available.

Abulikemu et al. investigated *in situ* assemblies of antiviral metal nanoparticles on a rigid surface and commercial nonwoven and woven textile face masks (Figure 5c).[51] By taking advantage of blade coating, silver nanoparticles (AgNPs) were synthesized in situ on a glass substrate and then transferred onto the surface of face masks with a roll-to-roll technique. Abulikemu et al. stated that a precise antiviral mechanism of AgNPs is not fully identified yet. The results showed a disinfection performance of 99.98% on the face masks and 99.99% on glass substrates against a surrogate virus of SARS-CoV-2.[51]

In another study, Hashmi et al. focused on electrospun nanofibers of PAN using copper oxide for antiviral applications in respiratory filters.[122] Copper(II) oxide is hydrophilic and has potential applications for magnetic storage purposes. The authors claimed the first-time use of copper oxide nanoparticles for antiviral respiratory masks. The membranes were fabricated by electrospinning a nanocomposite solution of PAN and copper oxide nanoparticles in different concentrations. The fabricated nanofibrous mat showed antiviral activity as well as release properties. MTT analysis also showed that more than 50% of the total cells survived after 120 h of incubation. Copper oxide nanoparticles also improved the tensile strength (8.45 MPa) of the produced nanofibrous membrane. However, the authors did not provide data on virus removal efficiency and pressure drop.[122]

Khanzada et al. demonstrated the antiviral activity of aloe vera (AV) incorporated within poly(vinyl alcohol) (PVA) electrospun nanofibers for protective clothing.[123] This research focused on developing electrospun AV/PVA nanofibers using electrospinning to form a cross-linked PVA/AV nanofibrous membrane. The study of the AV release supported the authors' claim regarding the serviceability of the protective clothing produced. Furthermore, the antiviral activity of the electrospun nanofibers was used to study the effect of the proposed nanofibrous membranes. The antiviral activity of the membranes is a result of anthraquinones isolated from Aloe Vera. The research showed a valid antiviral activity in different concentrations of AV incorporated into PVA.[123] The Authors did not report data on antiviral efficacy and pressure drop.

Nanostructured Face Masks with Antibacterial Properties. Research on nanofibrous materials for active face masks has improved various possible features. One of the methods for increasing the effectiveness of face masks is to reduce the activity of the bacteria filtered through the layers of face masks actively over time.

Pardo-Figuerez et al. fabricated face masks using PAN nanofibers in the middle layer of masks to improve their filtering capacity.[127] The implementation of ZnO in the PAN matrix produced nanocomposite fibers, resulting in solid antimicrobial properties of face masks against *E. coli* and *S. aureus*. The antimicrobial mechanism of ZnO particles is wielded by different methods, such as the generation of reactive oxygen species (ROS) and the release of ions to the surface, which could result in membrane dysfunction and obstruction of transmembrane electron carriage. The highest reduction ($R > 3$) against both types of bacteria was observed in the case of the PAN-ZnO at 3 wt %. As for filtration capacity, ZnO nanoparticles did not affect filtration performance, and although they slightly increased breathing resistance, the values obtained remained low and in line with the required European standard EN149 for FFP2 type PPE.[127]

Abbas et al. proposed a degradable multifunctional hybrid composite consisting of three electrospun nanofiber layers as a filter material, offering the potential to solve some of the challenges presented by face mask filters.[128] The outer active layer of the filter, a composite of TiO_2 nanotubes incorporated into the electrospun nanofiber matrix of Cs/PVA, acted as an antibacterial agent. The middle layer is Cs/PVA, which also serves to achieve natural air filtration and the inactivation of pathogens. The inner layer of the face mask filter is made of silk/PVA nanofibers, which improve the filter mechanical properties and heat dissipation while offering the wearer greater skin comfort. The filtration efficiency of these face masks increased by about 20% compared to commercial competitors. Cesium displayed antimicrobial activities against various microbes and pathogens by a mechanism involving alteration of biochemical pathways and membrane permeability, along with the damage of the bacterial cell wall and of organelles, consequently leading to cell death. Furthermore, *in vitro* tests showed the efficient role played by TiO_2 nanotubes, and Cs nanofibers in eliminating pathogenic bacteria.[128]

He et al. fabricated nanofibrous membranes with an enhanced filtration performance and solid antibacterial properties using bromosalicylic acid (BSA)/polyvinyl butyral (PVB) and electrospinning technology.[129] The incorporation of BSA in the membrane effectively eliminated 99.1% of both Gram-positive and Gram-negative *E. coli* and *S. aureus* in less than 8 h, taking advantage of the contact killing mechanism. The authors also investigated the germ-killing activity of the membrane produced, which showed to have a 99.9% germ-killing efficiency. It is noteworthy that the authors used BSA and PVB as green polymers and selected eco-friendly solvents and techniques.[129]

Hiragond et al. enhanced the quality of commercial face masks in terms of their antibacterial performance by treating

https://doi.org/10.1021/acsami.2c10335
ACS Appl. Mater. Interfaces 2022, 14, 46123−46144

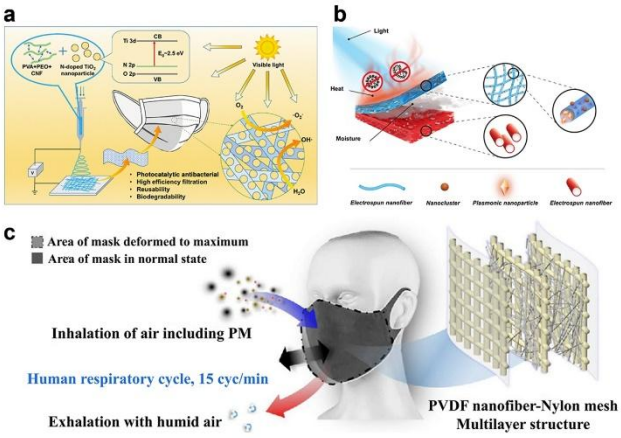

Figure 6. Different approaches developed for fabricating stimuli-responsive face masks. (a) Reusable masks with a functional design responsive to visible light. The nanofiber structure fabricated by electrospinning affords excellent breathability and particle filterability. Nitrogen-doped TiO_2 nanoparticles efficiently activate the mask upon irradiation with sunlight to destroy bacteria. Reproduced with permission from ref 142. Copyright 2021 American Chemical Society. (b) Sketch showing the morphology of a multifunctional light-responsive electrospun membrane for smart filtration. Light irradiation can trigger the active layer on demand to destroy pathogens and dissipate the trapped moisture, while the electrospun layer is an effective filtering and desiccant membrane. Reproduced with permission from ref 18. Copyright 2021 Wiley−VCH. (c) Scheme showing the electrostatic charge retention membrane features used by an electrospun PVDF layer inserted into a filter membrane multilayer structure. Reproduced with permission from ref 146. Copyright 2021 MDPI.

masks with silver nanoparticles.[130] First, the authors synthesized a starch-stabilized colloidal stock solution of Ag nanoparticles. Surgical masks were then treated with colloidal Ag nanoparticle solutions. The antibacterial activity of treated and untreated masks was tested against both Gram-positive and Gram-negative bacteria via the inhibition of bacteria growth method. The dual antimicrobial mechanism of Ag nanoparticles embedded in face masks followed by the entry of the Ag nanoparticles into the cytoplasm led to bacterial cell damage via an attack on the DNA.[130]

Salam et al. developed antiviral and antibacterial electrospun nanofiber membranes by incorporating HeiQ Viroblock (VB) and ZnO nanoparticles into a PAN electrospinning solution.[131] The authors claimed that the zinc oxide nanoparticles' high surface energy and surface area could be a key factor responsible for effectively eliminating viruses and bacteria by VB-loaded nanofibers. The encapsulated electrospun nanofibers can be used for protective clothing against bacteria (both Gram-negative and Gram-positive).[131]

Patil et al. fabricated a cotton/PLA-based biodegradable mask with improved antibacterial and respiration properties.[132] Their study focused on the fabrication of a three-layer mask whose upper and lower layers were made of cotton, and the middle layer was made of an electrospun nanofibrous PLA functionalized with traditional Indian herbal extracts. The use of traditional herbal extracts effectively neutralizes the effect of bacteria. It is known that they are sources of various substances, many of which have antimicrobial and radical-scavenging properties. The computational analysis of phytochemicals using the advanced scoring function showed the improved performance of herbal extracts in neutralizing bacteria. The results obtained from bacterial filtration efficiency (BFE) showed a noticeable efficiency of 97.9%. Furthermore, the achievement of 35.78 Pa cm^{-2} in the differential pressure of the masks confirmed the study's success.[132]

Zhang et al. fabricated a nanofiber membrane based on water-soluble PVA loaded with drugs to endow it with drug-loaded antibacterial properties using electrospinning.[133] The proposed electrospun layer not only improved filtration efficiency, moisture absorption, and air permeability but also increased the mechanical properties of the fabricated masks. These membranes successfully eliminated *S. aureus* and *E. coli*. The membrane's filtration performance was improved by 80−87%, depending on the width of the electrospun layer compared to commercial surgical masks.[133]

Alshabanah et al. developed an antimicrobial membrane made of electrospun biodegradable and synthetic nanofibers that could be used as a functional layer in PPE.[134] The developed nanofibers were made of PVA and thermoplastic polyurethane (TPU), loaded with Ag nanoparticles, and characterized and evaluated for their antiviral and antibacterial activities. Tests were performed using several viruses, including SARS-CoV-2, and several strains of bacteria, including *S. aureus*, *E. coli*, *Acinetobacter*, and *Klebsiella-Pneumoniae*. The results confirmed the successful development of antimicrobial materials.[134]

Qin et al. produced an antibacterial electrospun membrane with a mixture of PVB and berberine hydrochloride (BH).[135] The authors investigated the effects of BH concentration on the fabricated membranes, including morphology, antibacterial properties, and filtration efficiency. The reported filtration efficiency of the membrane reached 96.4% for $PM_{0.3}$ and 100% for $PM_{2.5}$, with a low-pressure drop of 108 Pa. The antibacterial examination of membranes for *S. aureus* showed an effective inhibition zone of the membranes against bacteria.[135]

https://doi.org/10.1021/acsami.2c10335
ACS Appl. Mater. Interfaces 2022, 14, 46123−46144

STIMULI-RESPONSIVE AND MULTIFUNCTIONAL FACE MASKS

Stimuli-responsive materials (SRMs) can be fabricated or integrated to enhance the function of multifunctional devices that possess desirable properties such as alertness to favorable stimuli.[136] When SRMs are exposed to external stimuli (e.g., temperature, light, and electromagnetic field), the molecular conformation, polarity, connectivity, or solubility changes from the initial state to a responsive form, resulting in a change in the materials' properties.[137] SRMs have been extensively studied as components in wearable devices, including sensors, actuators, drug delivery systems, and self-repairable devices. Despite their ability to improve protective properties, the study of SRMs for use in smart face masks is still in the early stages, as their development and applicability face many challenges.

Light-Responsive Face Masks. Disposable surgical masks can prevent environmental pollutants and other people's respiratory droplets from entering our respiratory system and help reduce infection risk. However, there are limitations to the existing masks. A nontrivial issue is that although the surfaces of surgical masks are hydrophobic, water droplets containing dangerous viruses may remain on them.[138] To overcome this concern, employing SRMs to provide a self-cleanable surface can be an excellent strategy (Figure 6a). Consequently, easily sterilizable and reusable face masks will offer a new deterrent against spreading pathogens and aid in the reduction of the influence of pandemic situations in the future.[139]

SARS-CoV-2 could be inactivated if exposed to a temperature of 56 °C for 15 min. One of the most widely available sources of energy to humans is solar radiation, a portion of electromagnetic radiation containing infrared, visible, and ultraviolet light. By taking advantage of the broad-spectrum absorption properties of SRMs, it is expected that the temperature necessary to inactivate pathogens can be achieved by irradiating photothermal responsive material with sunlight. Soni et al. produced a spray-coated layer of carbon nanotubes (CNT) on the outer layer of the melt-blown face mask.[140] The produced layer formed a superhydrophobic coating which increased the water contact angle of the surgical face mask from 113.6° ± 3.0° to 156.2° ± 1.8°. CNT-coated surgical masks also showed an outstanding photothermal response by increasing their surface temperature upon irradiation. The reported ΔT was higher than 55 °C within 30 s after exposure to sunlight. This increase in temperature leads to 99.9% elimination of *E. coli* compared to pristine conditions. These results confirm the ability to self-sterilize face masks by using SRMs.[140]

A self-sterilizing, recyclable, and high-performance face mask based on electrospinning was fabricated by Xiong et al.[141] The authors developed a needleless-electrospinning/spraying-netting technology to create a nanofibrous network. The proposed nanoarchitecture consists of a PAN nanofiber skeleton as a framework to maintain a network made of CNT@polyvinylpyrrolidone (FVPV) as the active part. This structure enabled a consistent and rapid photothermal sterilization (in 5 min) under solar radiation and an electrothermal self-sterilization (in 2 min) in sunless environments. This is also noteworthy that the potential of photothermal conversion and self-sterilization allowed the recycling of the fibrous materials as high-performance solar vapor generators to remove the salt from seawater. The results demonstrated the potential to reduce both the consumption of resources to combat disease transmission and the severe environmental impact of mask waste.[141]

Li et al. enhanced a prototype face mask by the ability of photocatalysis to sterilize bacteria on the surface of the mask by light irradiation.[142] Instead of PP, the authors initially used poly(vinyl alcohol), poly(ethylene oxide) (PEO), and nanocellulose, which are biodegradable polymers. The biodegradability of these polymers can reduce the environmental pollution caused by present-day masks made of synthetic plastics. The next step taken by the authors was to use electrospinning to produce composites with porous structures, which give the mask improved breathability and filtration. The authors later claimed that nanocellulose abundantly formed hydrogen bonds with PVA and PEO, while PEO served as a plasticizer in the electrospinning dopes. Both effects significantly improved the electrospinnability and mechanical performance of the resulting facepieces. Afterward, by introducing nitrogen-doped TiO_2 nanoparticles into the structure of the nanofibers, photosensitivity was also achieved in the face mask prototype. The photoactivity of TiO_2 nanoparticles can decrease the energy band gap toward the conductive band that is capable of enabling their efficient excitation under the sunlight. Subsequently, the generated free radicals can damage the cell membranes of the pathogens, leading to the killing of bacterial. The resulting nanofibrous face masks showed exceptional disinfection features against *E. coli* and *S. aureus* under sunlight, a considerable advancement in the technologies for producing the next generation of face masks.[142]

Li et al. created a nanofiber membrane containing the electroactive polymer of poly(vinylidene fluoride-*co*-hexafluoropropylene) (PVDF-HFP) as the matrix for electrospinning and the photosensitizer Rose Bengal (RB) as the dopant.[143] The multilayer porous structure of nanofibers with dopant promoted the trapping of pathogenic droplets and aerosols. Upon sunlight irradiation for 5−10 min, the fabricated membrane generated a considerable amount of reactive oxygen species. The efficient generation of ROS and particle interception ability of the proposed structure played a vital role in the main mechanisms of sterilization of the surface of the mask. The developed device showed a powerful inactivation by sunlight against various microbes (e.g., *S. aureus*, *E. coli*, *C. Albicans*, and *S. cerevisiae*).[143]

The impact of the rise in particulate matter index levels in the urban environment has driven the development of face masks toward novel targets. In addition, another environmental aspect, ultraviolet radiation (UV), is considered a significant risk factor; indeed, the UV index has been increasing continuously in recent years, with harmful effects on human health. Nevertheless, none of the filter materials or face masks have taken this problem into account.

To combat fine flying ashes and UV radiation, Chen et al. explored a class of electrospun nanofibers employing SRMs.[144] The authors constructed a filter made of electrospun PAN nanofibers filled with TiO_2. The induced antibacterial photocatalytic effect of the masks produced is achieved by UV light irradiation; bacteria such as *E. coli* and *staphylococcus* decomposed within a few hours of radiation. Thus, the prevention or reduction of UV irradiation and the deodorizing and/or antibacterial ability were simultaneously achieved by simply adding TiO_2 into the filter material, where TiO_2 has the function of decomposing bacteria and blocking UV rays. The Authors claimed that the antibacterial mechanism of the TiO_2

https://doi.org/10.1021/acsami.2c10335
ACS Appl. Mater. Interfaces 2022, 14, 46123−46144

in the filters is based on the absorption of UV light, which provoked the electron to jump from their valence band to their conduction band. The photogenerated electrons led to the production of radicals. These radical species oxidize the membrane of bacteria and later decompose the bacteria cells. Moreover, the presence of TiO_2 beads demonstrated a beneficial impact on filtration properties, in addition to photocatalytic and antibacterial activity.[144]

The disposable face masks currently available can neither inactivate pathogens nor eliminate viruses. Therefore, easily sterilizable and reusable masks with antiviral properties could be an effective prevention tool against the spread of pathogens and, especially, respiratory diseases.

Horváth et al. developed filters and facepieces based on TiO_2 nanowires (TiO_2 NWs).[139] The proposed PPE is made of a layer of TiO_2 NWs of a desirable thickness, affording different physical and chemical properties. The high efficiency of the fabricated filters is achieved thanks to the photogeneration of ROS under UV illumination. The authors estimated that a light-sterilizable mask based on the mentioned TiO_2 NWs could be reused more than 1000 times.[139]

De Sio et al. conceptualized a next-generation face mask with photoactive properties (Figure 6b).[18] Employing drop-casting technique, the authors achieved a water dispersion of gold nanorods (AuNRs), which can be used to create a uniform layer of plasmonic nanoparticles on the surface of the face masks. The assembled film of AuNRs can absorb near-infrared light, which subsequently lead to an electron excitation of AuNRs. The proposed layer over the face mask can be quickly activated on demand by light, to destroy pathogens and desorb the water entrapped between the human skin and the face mask, thus enhancing the equipment's wearability. This disinfection mechanism is based on localized thermal eradication of pathogens by exposing the outer layer of the face mask to a specific temperature level reached by irradiation of AuNRs.[18]

Impact of Charge on the Smart Features of Responsive Nanofibrous Face Masks. Surgical masks with functions such as a comfortable fit and rapid self-disinfection have been developed by changing the structure of surgical masks to avoid using expensive and nonportable disinfection devices.

Wang et al. fabricated an electret electrospun poly(ether sulfone)/barium titanate ($PES/BaTiO_3$) nanofibrous composite membrane with enhanced breathability and cooling properties.[145] The adjustment of morphology, porous structure, air penetrability, and water vapor transmittance rate (WVTR) was tuned by the concentration of nanoparticles. The comprehensive filtration measurements of the resulting membrane showed outstanding breathability. The polarization of $BaTiO_3$ nanoparticles conferred high injection energy and enhanced charge storage stability to the membrane, making it possible for the electret filter to trap $PM_{2.5}$ by electrostatic attraction. The performance of the membrane was unchanged even after being treated at 200 °C for 45 min. In addition, the composite nanofibrous membrane with remarkable cooling properties improved the thermal radiation dissipation even at abnormal temperatures. Furthermore, the membrane showed a high filtration efficiency (99.9%) and a lower pressure drop of 67 Pa with the proposed structure.[145]

Piezoelectric materials have been introduced into the structure of nanofibrous filters to improve the filtration efficiency without the polarization of nanofibers or using the energy of the quasi-permanent charge. Several research groups have designed nanofibrous membranes by electrospinning piezoelectric PVDF to benefit from electric charges on the filter surface.

Kang et al. also studied an electrostatic air filter for face masks that exhibited self-electrostatic charge generation and retention properties under cyclic air blowing and moist air infiltration.[146] Bending and vibration can even enhance the electrostatic charge density of the nanonet structure on the filter. By taking advantage of triboelectric charges, the proposed nanofibrous filter was used for fine dust filtration. A membrane was fabricated by electrospinning PVDF on a nylon network layer to preserve the nanofibrous structure (Figure 6c). The pores of the nanofibrous filter trapped the electric charges regardless of the direct contact with the ground state. The number of nylon networks of the filter membrane was adjusted to increase the PM filtration efficiency and improve the pressure drop. A three-layer electrospun filter structure has improved electrostatic charge generation in an environment that mimics breathing, a beneficial feature for face masks. The authors mentioned that a filter mask could generate electrostatic charges during breathing due to the unique multilayer structure of the membrane, overcoming the current limitation in PM filtration of face masks.[146]

Le et al. developed a novel smart face mask based on the concept that poly-L-lactic acid (PLLA) electrospun nanofibers can generate a piezoelectric charge when an airflow (such as human breathing) is applied.[147] This piezoelectric charge creates an electrostatic shielding layer that prevents the penetration of particles or pollutant droplets. The piezoelectric effect improves the removal of particulate matter by enhancing electrostatic charge adsorption and enables the PLLA piezoelectric nanofiber filter to overcome the existing problems of conventional face masks, such as moisture susceptibility, nondegradability, and poor reusability. The PLLA nanofiber filter can also be sterilized by standard means such as an ultrasonic bath or autoclave, making it possible for users to disinfect and reuse the filter. In addition, Le et al. created a prototype of a biodegradable face mask made of the piezoelectric PLLA nanofibrous membrane. This filter has a high filtration performance (99% for $PM_{2.5}$ and 91% for $PM_{1.0}$), while offering a promising pressure drop ($\approx$ 91 Pa at regular inhalation rate) for human respiration, thanks to the piezoelectric charge that is naturally stimulated by breathing through the face mask. The authors also mentioned that the electrospun PLLA piezoelectric membrane could be cost-effective compared to N95 respirators and surgical masks due to the reusability of the masks.[147]

■ FUTURE PERSPECTIVE AND CHALLENGES

Face masks have played a pivotal role in the recent COVID-19 pandemic. We have learned that although they are crucial to protecting people's lives, they also have a variety of downsides.[148] Before a new pandemic arrives, it is necessary for fundamental/advanced research and the relevant industries to engage in synergistic cooperation to develop innovative solutions that can be tested, scaled up, and manufactured in time.

- In the past two years, scientists worldwide have begun to focus on ideas for creative and ingenious face masks that can offer novel and exciting solutions. Innovative textile materials, biopolymers, nanostructured materials, 3D

https://doi.org/10.1021/acsami.2c10335
ACS Appl. Mater. Interfaces 2022, 14, 46123−46144

bioprinting, artificial intelligence, and stimuli-responsive nanoparticles are now considered the prime ingredients for tackling the challenge of producing intelligent, reusable face masks in the coming years. In all preliminary studies, it appears that this new direction can offer brilliant opportunities that must be investigated further.[149] To be successful in the next years to come, innovative approaches must rely on dealing with the following essential aspects for key innovations: cross-disciplinary expertise, international research projects, young researchers' exchange programs, and bi- and multilateral agreements between universities and research centers are solid and galvanizing approaches that can contribute to speeding up innovation. However, scientists and researchers cannot be left alone in this race. The support of governments, international organizations, and industrial partners is still crucial for supporting and scaling up the most promising new technologies developed so far. In addition to investing money in projects aimed at vaccine development, disease diagnosis, and treatment, more nonpharmaceutical activities should also be funded, highlighting smart textiles as part of face masks.[150]

- A group of scientists from MIT and Harvard is currently working together to develop a face mask capable of detecting the coronavirus. Their concept is based on the preparation of a sensor made of genetic material capable of binding viruses, which, after lyophilization on the face mask fabric, will be stable for a long time. Detection of the coronavirus will be possible in the presence of moisture, e.g., the user's saliva, and the detection signal will be quantified with a fluorimeter and emitted from the material in the form of fluorescent light.[151]
- Global climate change, including global warming, is already affecting and modifying our environment and biodiversity. It is time to do an about-face and start adopting meaningful actions to preserve our health and that of the next generations. For these reasons, it is necessary to rethink the materials and the environmental impact producing innovative biomedical devices such as protective face masks. From this standpoint, biodegradable and compostable materials[152] must be adopted as a "gold standard" for making lightweight, comfortable, eco-friendly face masks. The elastic loops connected to face masks to hold them in place produce severe ear fatigue and rub the skin. Ear protection mask extensions made of innovative, flexible, and hypoallergenic materials are needed to reduce or minimize face mask discomfort.
- Advanced and high-precision technological processes such as 3D printing,[153] electrospinning,[154] and nanofabrication[155] must be considered among the preferential pathways for providing face masks with high filtration power, comfort, and innovative designs. Digital twin technology for intelligent manufacturing can offer original ways to solve challenges connected with customization. Indeed, optimized facial comfort can be improved by combining 3D printing and direct digital manufacturing.[156] For example, specific designs can be obtained from a library of 3D heads from 3D scans of the heads and necks of healthcare professionals.
- Green and exotic nanomaterials, primarily derived from biowaste,[157] have to be extensively explored to include stimuli-responsive capabilities such as photothermal and photocatalytic disinfection, thus providing long-term reusability. Colorimetric and ultrasensitive biosensors that can measure the presence of harmful pathogens in the environment and send remote alert signals to competent authorities can play a crucial role if adequately integrated into the newly produced face masks. Indeed, this innovative function can help identify and isolate areas with much higher risks. Moreover, integrating multiple sensors can turn new-generation face masks into smart devices for health monitoring.

The socio-economic impact of COVID-19 on young people has produced countless moral and material damages, forcing them to live in an isolated and virtual world. The coming generations deserve a better world, and the role that science and technology can play now is vital to prevent future pandemics from producing the same effects. Envisioning innovative face masks that meet all the mandatory protection, customization, capabilities, and sustainability requirements is a fundamental step in the right direction. This technology can be easily extended to other valuable PPE for healthcare professionals and the general population, such as smart gloves, reusable gowns, and recyclable sanitary caps.

CONCLUSIONS

The use of personal protective equipment, including face masks, plays a vital role in numerous aspects of our lives since an evident increase in the level of air pollution caused by particulate matter or commonly present bacteria and viruses. During the COVID-19 pandemic, face masks became integral to everyone's daily routine. New products of this type can protect us from the next pandemic or significantly reduce its spread worldwide.

The need to develop face masks with outstanding filtration efficiency, excellent mechanical properties, comfortable breathing, and reusability has become a primary target. Moreover, developing devices with unique user-friendly properties activated in response to specific stimuli has been recognized as the next step in developing the next generation of personal protective equipment.

This review provides a practical roadmap to help scientists and specialists conceive the next-generation face masks that integrate innovative filters based on electrospun nanofibers.

It has been demonstrated that nanofiber filters typically perform better than the previously used melt-blown filters and are their promising alternative. One of the main advantages is that face masks that rely on electrospinning technology can be reutilized and, at the same time, preserve high filtration efficiency. In addition, and most importantly, these devices can be used as the building blocks for fabricating innovative and "smart" respirators, thanks to the extraordinary versatility of electrospun nanofibers.

The specific properties of various electrospinnable polymers make it possible to produce passive filters with particular abilities, such as controlled heat dissipation and breathing monitoring. However, this paper highlights that researchers have proposed a new generation of face masks that perform better than the previous ones, because they can provide more benefits than passive filtration.

Scientists working in the field of protective masks are focusing on including other components in filters to obtain active working filtration. This type of particle separation can be divided into two classes. In the first class, functional nanofibers

https://doi.org/10.1021/acsami.2c10335
ACS Appl. Mater. Interfaces 2022, 14, 46123−46144

are used; therefore, there is no need for additional external intervention to force their specific action, but the performed activity is continuous, nonspecific, and not triggerable upon request. In the second class of filters, their activation occurs on demand, i.e., under the influence of an external stimulus. It has been discussed that enriching nanofiber materials with other particles can become active filters, increasing the usability of masks with their new properties, such as antibacterial or antiviral capability. Particular types of face masks can have the ability to store the energy generated by the wearer while breathing. This research provides a new high-efficiency "smart" air filter and demonstrates a unique and straightforward strategy for developing self-powered and multifunctional healthcare devices. "Smart" multifunctional filters can also make it possible for us to create features in addition to that of killing bacteria and viruses, such as sterilizing face masks after using them and responding to environmental or external stimuli, including light, temperature, pH, magnetic and electric field, and/or mechanical stimuli. Furthermore, harvesting energy from inhaling/exhaling airflow is a promising perspective that can be achieved by taking advantage of smart materials.

As highlighted in this review, scientists have recently become increasingly interested in studying filtration membranes that show specific effects in response to stimuli. Nevertheless, this topic has not been thoroughly investigated; therefore, more research is needed to discover new possibilities for nanofiber filters based on modifying their properties. Much effort must also be spent translating fundamental research results into the application of the designed materials. The described approaches are innovative and offer vast opportunities; therefore, the new types of face masks can become commercial products of large-scale availability.

Smart face masks will benefit society as a whole, providing adequate protection against pollution and pathogens while reducing the costs incurred up to now for purchasing disposable products. Furthermore, the development of these systems will also significantly impact the environment because they could be biodegradable and do not need to be replaced often.

AUTHOR INFORMATION

Corresponding Author

Filippo Pierini − *Department of Biosystems and Soft Matter, Institute of Fundamental Technological Research, Polish Academy of Sciences, Warsaw 02-106, Poland;* orcid.org/0000-0002-6526-4141; Email: fpierini@ippt.pan.pl

Authors

Anna Zakrzewska − *Department of Biosystems and Soft Matter, Institute of Fundamental Technological Research, Polish Academy of Sciences, Warsaw 02-106, Poland;* orcid.org/0000-0002-1764-8554

Mohammad Ali Haghighat Bayan − *Department of Biosystems and Soft Matter, Institute of Fundamental Technological Research, Polish Academy of Sciences, Warsaw 02-106, Poland;* orcid.org/0000-0003-2912-7163

Paweł Nakielski − *Department of Biosystems and Soft Matter, Institute of Fundamental Technological Research, Polish Academy of Sciences, Warsaw 02-106, Poland;* orcid.org/0000-0001-6194-701X

Francesca Petronella − *Institute of Crystallography CNR-IC, National Research Council of Italy, Monterotondo 00015 Rome, Italy;* orcid.org/0000-0003-1583-5564

Luciano De Sio − *Department of Medico-Surgical Sciences and Biotechnologies, Research Center for Biophotonics, Sapienza University of Rome, Latina 04100, Italy;* orcid.org/0000-0002-2183-6910

Complete contact information is available at: https://pubs.acs.org/10.1021/acsami.2c10335

Author Contributions

†A.Z. and M.A.H.B. contributed equally to this work.

Notes

The authors declare no competing financial interest.

ACKNOWLEDGMENTS

This work was supported by the National Science Centre (NCN) SONATA BIS Project 2020/38/E/ST5/00456. The authors are grateful for the support provided by the National Agency for Academic Exchange (NAWA) grant PPI/APM/2018/1/00045/U/001. P.N. and F.P. acknowledge the financial support from the Polish Ministry of Science and Higher Education through scholarships for outstanding young scientists. L.D.S. acknowledges the Sapienza University of Rome, grant RG12117A85EDBC02 (Progetto Ateneo 2021, Personalized Reusable Face Mask with Smart Nano-Assisted Destruction of Pathogens).

REFERENCES

(1) Partridge, L.; Fuentealba, M.; Kennedy, B. K. The Quest to Slow Ageing through Drug Discovery. *Nat. Rev. Drug Discovery* **2020**, *19* (8), 513−532.

(2) Siddique, F.; Abbas, R. Z.; Mansoor, M. K.; Alghamdi, E. S.; Saeed, M.; Ayaz, M. M.; Rahman, M.; Mahmood, M. S.; Iqbal, A.; Manzoor, M.; et al. An Insight Into COVID-19: A 21st Century Disaster and Its Relation to Immunocompetence and Food Antioxidants. *Front. Vet. Sci.* **2021**, *7*, 586637.

(3) Deng, W.; Sun, Y.; Yao, X.; Subramanian, K.; Ling, C.; Wang, H.; Chopra, S. S.; Xu, B. B.; Wang, J.-X.; Chen, J.-F.; et al. Masks for COVID-19. *Adv. Sci. (Weinh)* **2022**, *9* (3), No. e2102189.

(4) Rinoldi, C.; Zargarian, S. S.; Nakielski, P.; Li, X.; Liguori, A.; Petronella, F.; Presutti, D.; Wang, Q.; Costantini, M.; De Sio, L.; et al. Nanotechnology-Assisted RNA Delivery: From Nucleic Acid Therapeutics to COVID-19 Vaccines. *Small Methods* **2021**, *5* (9), No. e2100402.

(5) Talic, S.; Shah, S.; Wild, H.; Gasevic, D.; Maharaj, A.; Ademi, Z.; Li, X.; Xu, W.; Mesa-Eguiagaray, I.; Rostron, J.; et al. Effectiveness of Public Health Measures in Reducing the Incidence of Covid-19, SARS-CoV-2 Transmission, and Covid-19 Mortality: Systematic Review and Meta-Analysis. *BMJ.* **2021**, *375*, No. e068302.

(6) Catching, A.; Capponi, S.; Yeh, M. T.; Bianco, S.; Andino, R. Examining the Interplay between Face Mask Usage, Asymptomatic Transmission, and Social Distancing on the Spread of COVID-19. *Sci. Rep.* **2021**, *11* (1), 15998.

(7) *What Are "Biologics" Questions and Answers*. U.S. Food and Drug Administration.https://www.fda.gov/about-fda/center-biologics-evaluation-and-research-cber/what-are-biologics-questions-and-answers (accessed 2022-04-04).

(8) Selvaranjan, K.; Navaratnam, S.; Rajeev, P.; Ravintherakumaran, N. Environmental Challenges Induced by Extensive Use of Face Masks during COVID-19: A Review and Potential Solutions. *Environmental Challenges* **2021**, *3*, 100039.

(9) Zhou, Y.; Liu, Y.; Zhang, M.; Feng, Z.; Yu, D.-G.; Wang, K. Electrospun Nanofiber Membranes for Air Filtration: A Review. *Nanomaterials* **2022**, *12* (7), 1077.

(10) Kisielinski, K.; Giboni, P.; Prescher, A.; Klosterhalfen, B.; Graessel, D.; Funken, S.; Kempski, O.; Hirsch, O. Is a Mask That Covers the Mouth and Nose Free from Undesirable Side Effects in Everyday Use and Free of Potential Hazards? *Int. J. Environ. Res. Public Health* **2021**, *18* (8), 4344.
(11) Torres, F. G.; De-la-Torre, G. E. Face Mask Waste Generation and Management during the COVID-19 Pandemic: An Overview and the Peruvian Case. *Sci. Total Environ.* **2021**, *786*, 147628.
(12) Valls, R. *Inorganic Chemistry: From Periodic Classification to Crystals*; Wiley-ISTE: Hoboken, NJ/London, 2017; pp 2−10.
(13) Crespo, C.; Ibarz, G.; Sáenz, C.; Gonzalez, P.; Roche, S. Study of Recycling Potential of FFP2 Face Masks and Characterization of the Plastic Mix-Material Obtained. A Way of Reducing Waste in Times of Covid-19. *Waste Biomass Valor* **2021**, *12* (12), 6423−6432.
(14) Shanmugam, V.; Babu, K.; Garrison, T. F.; Capezza, A. J.; Olsson, R. T.; Ramakrishna, S.; Hedenqvist, M. S.; Singha, S.; Bartoli, M.; Giorcelli, M.; et al. Potential Natural Polymer-based Nanofibres for the Development of Facemasks in Countering Viral Outbreaks. *J. Appl. Polym. Sci.* **2021**, *138* (27), 50658.
(15) Yu, B.; Chen, J.; Chen, D.; Chen, R.; Wang, Y.; Tang, X.; Wang, H.-L.; Wang, L.-P.; Deng, W. Visualization of the Interaction of Water Aerosol and Nanofiber Mesh. *Phys. Fluids (1994)* **2021**, *33* (9), 092106.
(16) Babaahmadi, V.; Amid, H.; Naeimirad, M.; Ramakrishna, S. Biodegradable and Multifunctional Surgical Face Masks: A Brief Review on Demands during COVID-19 Pandemic, Recent Developments, and Future Perspectives. *Sci. Total Environ.* **2021**, *798*, 149233.
(17) Opálková Šišková, A.; Mosnáčková, K.; Hrůza, J.; Frajová, J.; Opálek, A.; Bučková, M.; Kozics, K.; Peer, P.; Eckstein Andicsová, A. Electrospun Poly(Ethylene Terephthalate)/Silk Fibroin Composite for Filtration Application. *Polymers (Basel)* **2021**, *13* (15), 2499.
(18) De Sio, L.; Ding, B.; Focsan, M.; Kogermann, K.; Pascoal-Faria, P.; Petronela, F.; Mitchell, G.; Zussman, E.; Pierini, F. Personalized Reusable Face Masks with Smart Nano-Assisted Destruction of Pathogens for COVID-19: A Visionary Road. *Chem.—Eur. J.* **2021**, *27* (20), 6112−6130.
(19) Müller, W. E. G.; Neufurth, M.; Lieberwirth, I.; Muñoz-Espí, R.; Wang, S.; Schröder, H. C.; Wang, X. Triple-Target Stimuli-Responsive Anti-COVID-19 Face Mask with Physiological Virus-Inactivating Agents. *Biomater. Sci.* **2021**, *9* (18), 6052−6063.
(20) Boeing, C.; Sandten, C.; Hrincius, E. R.; Anhlan, D.; Dworog, A.; Hanning, S.; Kuennemann, T.; Niehues, C.; Schupp, T.; Stec, E.; et al. Decontamination of Disposable Respirators for Reuse in a Pandemic Employing In-Situ-Generated Peracetic Acid. *Am. J. Infect. Control* **2022**, *50* (4), 420−426.
(21) Mariello, M.; Qualtieri, A.; Mele, G.; De Vittorio, M. Metal-Free Multilayer Hybrid PENG Based on Soft Electrospun/-Sprayed Membranes with Cardanol Additive for Harvesting Energy from Surgical Face Masks. *ACS Appl. Mater. Interfaces* **2021**, *13* (17), 20606−20621.
(22) Naragund, V. S.; Panda, P. K. Electrospun Nanofiber-Based Respiratory Face Masks-a Review. *emergent mater* **2022**, *5*, 261−278.
(23) Nakielski, P.; Rinoldi, C.; Pruchniewski, M.; Pawłowska, S.; Gazińska, M.; Strojny, B.; Rybak, D.; Jezierska-Woźniak, K.; Urbanek, O.; Denis, P.; et al. Laser-Assisted Fabrication of Injectable Nanofibrous Cell Carriers. *Small* **2022**, *18* (2), No. e2104971.
(24) Pawłowska, S.; Rinoldi, C.; Nakielski, P.; Ziai, Y.; Urbanek, O.; Li, X.; Kowalewski, T. A.; Ding, B.; Pierini, F. Ultraviolet Light-assisted Electrospinning of Core−Shell Fully Cross-linked p(Nipaam-*Co* -nipmaam) Hydrogel-based Nanofibers for Thermally Induced Drug Delivery Self-regulation. *Adv. Mater. Interfaces* **2020**, *7* (12), 2000247.
(25) Ziai, Y.; Petronella, F.; Rinoldi, C.; Nakielski, P.; Zakrzewska, A.; Kowalewski, T. A.; Augustyniak, W.; Li, X.; Calogero, A.; Sabała, I.; et al. Chameleon-Inspired Multifunctional Plasmonic Nanoplatforms for Biosensing Applications. *NPG Asia Mater.* **2022**, *14* (1), 18.
(26) Pierini, F.; Lanzi, M.; Nakielski, P.; Pawłowska, S.; Zembrzycki, K.; Kowalewski, T. A. Electrospun Poly(3-Hexylthiophene)/Poly-(Ethylene Oxide)/Graphene Oxide Composite Nanofibers: Effects of Graphene Oxide Reduction. *Polym. Adv. Technol.* **2016**, *27* (11), 1465−1475.
(27) Pierini, F.; Lanzi, M.; Nakielski, P.; Kowalewski, T. A. Electrospun Polyaniline-Based Composite Nanofibers: Tuning the Electrical Conductivity by Tailoring the Structure of Thiol-Protected Metal Nanoparticles. *J. Nanomater.* **2017**, *2017*, 1−10.
(28) Nakielski, P.; Pawłowska, S.; Rinoldi, C.; Ziai, Y.; De Sio, L.; Urbanek, O.; Zembrzycki, K.; Pruchniewski, M.; Lanzi, M.; Salatelli, E.; et al. Multifunctional Platform Based on Electrospun Nanofibers and Plasmonic Hydrogel: A Smart Nanostructured Pillow for Near-Infrared Light-Driven Biomedical Applications. *ACS Appl. Mater. Interfaces* **2020**, *12* (49), 54328−54342.
(29) Xiong, R.; Hua, D.; Van Hoeck, J.; Berdecka, D.; Léger, L.; De Munter, S.; Fraire, J. C.; Raes, L.; Harizaj, A.; Sauvage, F.; et al. Photothermal Nanofibres Enable Safe Engineering of Therapeutic Cells. *Nat. Nanotechnol.* **2021**, *16* (11), 1281−1291.
(30) Li, B.; Zhao, J.; Lin, X.; Tu, D.; Meng, Y.; Li, Y.; Huang, P.; Zhang, H. Highly Efficient Sunlight-Driven Self-Cleaning Electrospun Nanofiber Membrane NM88B@HPAN for Water Treatment. *J. Clean. Prod.* **2022**, *355*, 131812.
(31) Xiong, R.; Xu, R. X.; Huang, C.; De Smedt, S.; Braeckmans, K. Stimuli-Responsive Nanobubbles for Biomedical Applications. *Chem. Soc. Rev.* **2021**, *50* (9), 5746−5776.
(32) Xue, J.; Wu, T.; Dai, Y.; Xia, Y. Electrospinning and Electrospun Nanofibers: Methods, Materials, and Applications. *Chem. Rev.* **2019**, *119* (8), 5298−5415.
(33) Omer, S.; Forgách, L.; Zelkó, R.; Sebe, I. Scale-up of Electrospinning: Market Overview of Products and Devices for Pharmaceutical and Biomedical Purposes. *Pharmaceutics* **2021**, *13* (2), 286.
(34) Zhang, Z.; Ji, D.; He, H.; Ramakrishna, S. Electrospun Ultrafine Fibers for Advanced Face Masks. *Mater. Sci. Eng. R Rep.* **2021**, *143*, 100594.
(35) Essa, W. K.; Yasin, S. A.; Saeed, I. A.; Ali, G. A. M. Nanofiber-Based Face Masks and Respirators as COVID-19 Protection: A Review. *Membranes (Basel)* **2021**, *11* (4), 250.
(36) Matuschek, C.; Moll, F.; Fangerau, H.; Fischer, J. C.; Zänker, K.; van Griensven, M.; Schneider, M.; Kindgen-Milles, D.; Knoefel, W. T.; Lichtenberg, A.; et al. Face masks: benefits and risks during the COVID-19 crisis. *Eur. J. Med. Res.* **2020**, *25* (1), 23.
(37) Howard, J.; Huang, A.; Li, Z.; Tufekci, Z.; Zdimal, V.; van der Westhuizen, H.-M.; von Delft, A.; Price, A.; Fridman, L.; Tang, L.-H.; et al. An Evidence Review of Face Masks against COVID-19. *Proc. Natl. Acad. Sci. U. S. A.* **2021**, *118* (4), No. e2014564118.
(38) Polo, M. *Il Milione*; Zanichelli: Bologna, 2009.
(39) Lynteris, C. Plague Masks: The Visual Emergence of Anti-Epidemic Personal Protection Equipment. *Med. Anthropol.* **2018**, *37* (6), 442−457.
(40) Strasser, B. J.; Schlich, T. A History of the Medical Mask and the Rise of Throwaway Culture. *Lancet* **2020**, *396* (10243), 19−20.
(41) Louis, F. K.-T. Great Names in the History of Orthopaedics XIV: Joseph Lister (1827−1912) Part 2. *Journal of Orthopaedics, Trauma and Rehabilitation* **2011**, *15* (1), 29−36.
(42) Newsom, S. W. B. Pioneers in Infection Control-Joseph Lister. *J. Hosp. Infect.* **2003**, *55* (4), 246−253.
(43) Alcaraz, J.-P.; Le Coq, L.; Pourchez, J.; Thomas, D.; Chazelet, S.; Boudry, I.; Barbado, M.; Silvent, S.; Dessale, C.; Antoine, F.; et al. Reuse of Medical Face Masks in Domestic and Community Settings without Sacrificing Safety: Ecological and Economical Lessons from the Covid-19 Pandemic. *Chemosphere* **2022**, *288* (1), 132364.
(44) de Araújo Andrade, T.; Nascimento Junior, J. A. C.; Santos, A. M.; Borges, L. P.; Quintans-Júnior, L. J.; Walker, C. I. B.; Frank, L. A.; Serafini, M. R. Technological Scenario for Masks in Patent Database During Covid-19 Pandemic. *AAPS PharmSciTech* **2021**, *22* (2), 72.
(45) *The Man Behind the Mask*. Tickle College of Engineering, Apirl 17, 2020. https://tickle.utk.edu/the-man-behind-the-mask/ (accessed 2022-04-05).
(46) World Health Organization. *Mask Use in the Context of COVID-19*; World Health Organization: Geneva, 2020.

(47) Ford, N.; Holmer, H. K.; Chou, R.; Villeneuve, P. J.; Baller, A.; Van Kerkhove, M.; Allegranzi, B. Mask Use in Community Settings in the Context of COVID-19: A Systematic Review of Ecological Data. *EClinicalMedicine* **2021**, *38*, 101024.
(48) Ullah, S.; Ullah, A.; Lee, J.; Jeong, Y.; Hashmi, M.; Zhu, C.; Joo, K. I.; Cha, H. J.; Kim, I. S. Reusability Comparison of Melt-Blown vs Nanofiber Face Mask Filters for Use in the Coronavirus Pandemic. *ACS Appl. Nano Mater.* **2020**, *3*, 7231.
(49) Kumar, A.; Sharma, A.; Chen, Y.; Jones, M. M.; Vanyo, S. T.; Li, C.; Visser, M. B.; Mahajan, S. D.; Sharma, R. K.; Swihart, M. T. Copper@ZIF-8 Core-Shell Nanowires for Reusable Antimicrobial Face Masks. *Adv. Funct. Mater.* **2021**, *31* (10), 2008054.
(50) Kumar, S.; Karmacharya, M.; Joshi, S. R.; Gulenko, O.; Park, J.; Kim, G.-H.; Cho, Y.-K. Photoactive Antiviral Face Mask with Self-Sterilization and Reusability. *Nano Lett.* **2021**, *21* (1), 337−343.
(51) Abulikemu, M.; Tabrizi, B. E. A.; Ghobadloo, S. M.; Mofarah, H. M.; Jabbour, G. E. Silver Nanoparticle-Decorated Personal Protective Equipment for Inhibiting Human Coronavirus Infectivity. *ACS Appl. Nano Mater.* **2022**, *5* (1), 309−317.
(52) Vaquer, A.; Alba-Patiño, A.; Adrover-Jaume, C.; Russell, S. M.; Aranda, M.; Borges, M.; Mena, J.; Del Castillo, A.; Socias, A.; Martín, L.; et al. Nanoparticle Transfer Biosensors for the Non-Invasive Detection of SARS-CoV-2 Antigens Trapped in Surgical Face Masks. *Sens. Actuators B Chem.* **2021**, *345*, 130347.
(53) Wu, Z.; Yang, J.; Sun, X.; Wu, Y.; Wang, L.; Meng, G.; Kuang, D.; Guo, X.; Qu, W.; Du, B.; et al. An Excellent Impedance-Type Humidity Sensor Based on Halide Perovskite CsPbBr3 Nanoparticles for Human Respiration Monitoring. *Sens. Actuators, B* **2021**, *337*, 129772.
(54) Hrvatin, K. Japanese Artists' Responses to COVID-19. *AS* **2022**, *10* (1), 183−209.
(55) Kuczkowski, J.; Stankiewicz, C.; Plichta, L.; Cieszyńska, J. Jan Mikulicz-Radecki (1850−1905): A Fundamental Contributor to World Surgery; Surgeon of the Head, Neck, and Esophagus. *Eur. Arch Otorhinolaryngol* **2012**, *269* (8), 1999−2001.
(56) Kaya, K.; Khalil, M.; Fetrow, B.; Fritz, H.; Jagadesan, P.; Bondu, V.; Ista, L.; Chi, E. Y.; Schanze, K. S.; Whitten, D. G.; et al. Rapid and Effective Inactivation of SARS-CoV-2 with a Cationic Conjugated Oligomer with Visible Light: Studies of Antiviral Activity in Solutions and on Supports. *ACS Appl. Mater. Interfaces* **2022**, *14* (4), 4892−4898.
(57) Guo, Y.; Wang, X.; Shen, Y.; Dong, K.; Shen, L.; Alzalab, A. A. A. Research Progress, Models and Simulation of Electrospinning Technology: A Review. *J. Mater. Sci.* **2022**, *57* (1), 58−104.
(58) Tucker, N.; Stanger, J. J.; Staiger, M. P.; Razzaq, H.; Hofman, K. The History of the Science and Technology of Electrospinning from 1600 to 1995. *J. Eng. Fiber. Fabr.* **2012**, *7* (2_suppl), 63−73.
(59) Nascimento, M. L. F.; Araújo, E. S.; Cordeiro, E. R.; de Oliveira, A. H. P.; de Oliveira, H. P. A Literature Investigation about Electrospinning and Nanofibers: Historical Trends, Current Status and Future Challenges. *Recent Pat. Nanotechnol.* **2015**, *9* (2), 76−85.
(60) Ghosal, K.; Agatemor, C.; Tucker, N.; Kny, E.; Thomas, S. Chapter 1. Electrical Spinning to Electrospinning: A Brief History. In *Electrospinning: From Basic Research to Commercialization*; Kny, E., Ghosal, K., Thomas, S., Eds.; Soft Matter Series; Royal Society of Chemistry: Cambridge, U.K., 2018; pp 1−23.
(61) *Electrospinning: Principles, Practice and Possibilities*; Mitchell, G. R., Ed.; Polymer Chemistry Series; Royal Society of Chemistry: Cambridge, U.K., 2015.
(62) Yarin, A. L.; Koombhongse, S.; Reneker, D. H. Bending Instability in Electrospinning of Nanofibers. *J. Appl. Phys.* **2001**, *89* (5), 3018−3026.
(63) Nakielski, P.; Pawłowska, S.; Pierini, F.; Liwińska, W.; Hejduk, P.; Zembrzycki, K.; Zabost, E.; Kowalewski, T. A. Hydrogel Nanofilaments via Core-Shell Electrospinning. *PLoS One* **2015**, *10* (6), No. e0129816.
(64) Greiner, A.; Wendorff, J. H. Electrospinning: A Fascinating Method for the Preparation of Ultrathin Fibers. *Angew. Chem. Int. Ed* **2007**, *46* (30), 5670−5703.
(65) Ma, C.; Liu, X. Formation of Nanofibrous Matrices, Three-Dimensional Scaffolds, and Microspheres: From Theory to Practice. *Tissue Eng. Part C Methods* **2017**, *23* (1), 50−59.
(66) Vass, P.; Szabó, E.; Domokos, A.; Hirsch, E.; Galata, D.; Farkas, B.; Démuth, B.; Andersen, S. K.; Vigh, T.; Verreck, G.; et al. Scale-up of Electrospinning Technology: Applications in the Pharmaceutical Industry. *Wiley Interdiscip. Rev. Nanomed. Nanobiotechnol.* **2020**, *12* (4), No. e1611.
(67) Stachewicz, U.; Stone, C. A.; Willis, C. R.; Barber, A. H. Charge Assisted Tailoring of Chemical Functionality at Electrospun Nanofiber Surfaces. *J. Mater. Chem.* **2012**, *22* (43), 22935.
(68) Wang, X.; Xiang, H.; Song, C.; Zhu, D.; Sui, J.; Liu, Q.; Long, Y. Highly Efficient Transparent Air Filter Prepared by Collecting-Electrode-Free Bipolar Electrospinning Apparatus. *J. Hazard. Mater.* **2020**, *385*, 121535.
(69) Szewczyk, P. K.; Stachewicz, U. The Impact of Relative Humidity on Electrospun Polymer Fibers: From Structural Changes to Fiber Morphology. *Adv. Colloid Interface Sci.* **2020**, *286*, 102315.
(70) Zou, Q.; Gai, Y.; Cai, Y.; Gai, X.; Xiong, S.; Wei, N.; Jiang, M.; Chen, L.; Liu, Y.; Gai, J. Eco-Friendly Chitosan@silver/Plant Fiber Membranes for Masks with Thermal Comfortability and Self-Sterilization. *Cellulose (Lond)* **2022**, *29* (10), 5711−5724.
(71) Nguyen, U. N. T.; Do, K. H.; Jang, B.; Kim, K.-S.; Kim, J.-H.; Lee, S.-M. Always-on Photocatalytic Antibacterial Facemask with Mini UV-LED Array. *Materials Today Sustainability* **2022**, *18*, 100117.
(72) Han, D.; Steckl, A. J. Coaxial Electrospinning Formation of Complex Polymer Fibers and Their Applications. *ChemPlusChem.* **2019**, *84* (10), 1453−1497.
(73) Kang, L.; Liu, Y.; Wang, L.; Gao, X. Preparation of Electrospun Nanofiber Membrane for Air Filtration and Process Optimization Based on BP Neural Network. *Mater. Res. Express* **2021**, *8* (11), 115010.
(74) Ghosal, K.; Chandra, A.; G., P.; S., S.; Roy, S.; Agatemor, C.; Thomas, S.; Provaznik, I. Electrospinning over Solvent Casting: Tuning of Mechanical Properties of Membranes. *Sci. Rep.* **2018**, *8* (1), 5058.
(75) Long, Y.; Hu, T.; Liu, L.; Chen, R.; Guo, Q.; Yang, L.; Cheng, Y.; Huang, J.; Du, L. Effectiveness of N95 Respirators versus Surgical Masks against Influenza: A Systematic Review and Meta-Analysis. *J. Evid. Based Med.* **2020**, *13* (2), 93−101.
(76) Davies, A.; Thompson, K.-A.; Giri, K.; Kafatos, G.; Walker, J.; Bennett, A. Testing the Efficacy of Homemade Masks: Would They Protect in an Influenza Pandemic? *Disaster Med. Public Health Prep.* **2013**, *7* (4), 413−418.
(77) Mueller, A. V.; Eden, M. J.; Oakes, J. M.; Bellini, C.; Fernandez, L. A. Quantitative Method for Comparative Assessment of Particle Removal Efficiency of Fabric Masks as Alternatives to Standard Surgical Masks for PPE. *Matter* **2020**, *3* (3), 950−962.
(78) van der Sande, M.; Teunis, P.; Sabel, R. Professional and Home-Made Face Masks Reduce Exposure to Respiratory Infections among the General Population. *PLoS One* **2008**, *3* (7), No. e2618.
(79) Rubbo, S. D.; Abbott, L. R. Filtration Efficiency of Surgical Masks: A New Method of Evaluation. *Aust. N. Z. J. Surg.* **1971**, *38*, 80−83.
(80) Chua, M. H.; Cheng, W.; Goh, S. S.; Kong, J.; Li, B.; Lim, J. Y. C.; Mao, L.; Wang, S.; Xue, K.; Yang, L.; et al. Face Masks in the New COVID-19 Normal: Materials, Testing, and Perspectives. *Research (Wash D C)* **2020**, *2020*, 7286735.
(81) Ahmed, F. E.; Lalia, B. S.; Hashaikeh, R. A Review on Electrospinning for Membrane Fabrication: Challenges and Applications. *Desalination* **2015**, *356*, 15−30.
(82) Liu, G.; Xiao, M.; Zhang, X.; Gal, C.; Chen, X.; Liu, L.; Pan, S.; Wu, J.; Tang, L.; Clements-Croome, D. A Review of Air Filtration Technologies for Sustainable and Healthy Building Ventilation. *Sustainable Cities and Society* **2017**, *32*, 375−396.
(83) Wang, X.; Kim, K.; Lee, C.; Kim, J. Prediction of Air Filter Efficiency and Pressure Drop in Air Filtration Media Using a Stochastic Simulation. *Fibers Polym.* **2008**, *9*, 34−38.

https://doi.org/10.1021/acsami.2c10335
ACS Appl. Mater. Interfaces 2022, 14, 46123−46144

(84) Zaatari, M.; Novoselac, A.; Siegel, J. The Relationship between Filter Pressure Drop, Indoor Air Quality, and Energy Consumption in Rooftop HVAC Units. *Building and Environment* **2014**, *73*, 151−161.
(85) Zhu, M.; Han, J.; Wang, F.; Shao, W.; Xiong, R.; Zhang, Q.; Pan, H.; Yang, Y.; Samal, S. K.; Zhang, F.; et al. Electrospun Nanofibers Membranes for Effective Air Filtration. *Macromol. Mater. Eng.* **2017**, *302* (1), 1600353.
(86) Lee, H.; Jeon, S. Polyacrylonitrile Nanofiber Membranes Modified with Ni-Based Conductive Metal Organic Frameworks for Air Filtration and Respiration Monitoring. *ACS Appl. Nano Mater.* **2020**, *3* (8), 8192−8198.
(87) Bagheri, M. H.; Khalaji, I.; Azizi, A.; Loibl, R. T.; Basualdo, N.; Manzo, S.; Gorrepati, M. L.; Mehendale, S.; Mohr, C.; Schiffres, S. N. Filtration Efficiency, Breathability, and Reusability of Improvised Materials for Face Masks. *Aerosol Sci. Technol.* **2021**, *55* (7), 817−827.
(88) Karabulut, F. N. H.; Höfler, G.; Ashok Chand, N.; Beckermann, G. W. Electrospun Nanofibre Filtration Media to Protect against Biological or Nonbiological Airborne Particles. *Polymers (Basel)* **2021**, *13* (19), 3257.
(89) Opálková Šišková, A.; Frajová, J.; Nosko, M. Recycling of Poly(Ethylene Terephthalate) by Electrospinning to Enhanced the Filtration Efficiency. *Mater. Lett.* **2020**, *278*, 128426.
(90) Leung, W. W. F.; Sun, Q. Electrostatic Charged Nanofiber Filter for Filtering Airborne Novel Coronavirus (COVID-19) and Nano-Aerosols. *Sep. Purif. Technol.* **2020**, *250*, 116886.
(91) Bortolassi, A. C. C.; Nagarajan, S.; de Araújo Lima, B.; Guerra, V. G.; Aguiar, M. L.; Huon, V.; Soussan, L.; Cornu, D.; Miele, P.; Bechelany, M. Efficient Nanoparticles Removal and Bactericidal Action of Electrospun Nanofibers Membranes for Air Filtration. *Mater. Sci. Eng. C Mater. Biol. Appl.* **2019**, *102*, 718−729.
(92) Molnár, K.; Mészáros, L. The Role of Electrospun Nanofibers in the Fight against the COVID-19. *Express Polym. Lett.* **2020**, *14*, 605.
(93) Qin, X.; Subianto, S. Electrospun Nanofibers for Filtration Applications. In *Electrospun Nanofibers*; Afshari, M., Ed.; Elsevier, 2017; pp 449−466.
(94) Lu, T.; Cui, J.; Qu, Q.; Wang, Y.; Zhang, J.; Xiong, R.; Ma, W.; Huang, C. Multistructured Electrospun Nanofibers for Air Filtration: A Review. *ACS Appl. Mater. Interfaces* **2021**, *13* (20), 23293−23313.
(95) Lee, K. W.; Liu, B. Y. H. On the Minimum Efficiency and the Most Penetrating Particle Size for Fibrous Filters. *J. Air Pollut. Control Assoc.* **1980**, *30* (4), 377−381.
(96) Tebyetekerwa, M.; Xu, Z.; Yang, S.; Ramakrishna, S. Electrospun Nanofibers-Based Face Masks. *Adv. Fiber Mater.* **2020**, *2* (3), 161−166.
(97) Deng, Y.; Lu, T.; Cui, J.; Ma, W.; Qu, Q.; Zhang, X.; Zhang, Y.; Zhu, M.; Xiong, R.; Huang, C. Morphology Engineering Processed Nanofibrous Membranes with Secondary Structure for High-Performance Air Filtration. *Sep. Purif. Technol.* **2022**, *294*, 121093.
(98) Liang, M.; Hébraud, A.; Schlatter, G. Modeling and On-Line Measurement of the Surface Potential of Electrospun Membranes for the Control of the Fiber Diameter and the Pore Size. *Polymer* **2020**, *200*, 122576.
(99) Lee, H.; Lee, W.; Lee, J. H.; Yoon, D. S. Surface Potential Analysis of Nanoscale Biomaterials and Devices Using Kelvin Probe Force Microscopy. *J. Nanomater.* **2016**, *2016*, 1−21.
(100) Mamun, A.; Moulefera, I.; Topuz, Y.; Trabelsi, M.; Sabantina, L. The Possibility of Reuse of Nanofiber Mats by Machine Washing at Different Temperatures. *Materials (Basel)* **2021**, *14* (17), 4788.
(101) Zeraati, M.; Pourmohamad, R.; Baghchi, B.; Singh Chauhan, N. P.; Sargazi, G. Optimization and Predictive Modelling for the Diameter of Nylon-6,6 Nanofibers via Electrospinning for Coronavirus Face Masks. *Journal of Saudi Chemical Society* **2021**, *25* (11), 101348.
(102) Yang, A.; Cai, L.; Zhang, R.; Wang, J.; Hsu, P.-C.; Wang, H.; Zhou, G.; Xu, J.; Cui, Y. Thermal Management in Nanofiber-Based Face Mask. *Nano Lett.* **2017**, *17* (6), 3506−3510.
(103) Kotresh, T. M.; Ramani, R.; Jana, N.; Minu, S.; Shekar, R. I.; Ramachandran, R. Supermolecular Structure, Free Volume, and Glass Transition of Needleless Electrospun Polymer Nanofibers. *ACS Appl. Polym. Mater.* **2021**, *3* (8), 3989−4007.
(104) Xu, Y.; Zhang, X.; Hao, X.; Teng, D.; Zhao, T.; Zeng, Y. Micro/Nanofibrous Nonwovens with High Filtration Performance and Radiative Heat Dissipation Property for Personal Protective Face Mask. *Chem. Eng. J.* **2021**, *423*, 130175.
(105) Khandaker, M.; Progri, H.; Arasu, D. T.; Nikfarjam, S.; Shamim, N. Use of Polycaprolactone Electrospun Nanofiber Mesh in a Face Mask. *Materials (Basel)* **2021**, *14* (15), 4272.
(106) Buluş, E.; Sakarya Buluş, G.; Yakuphanoglu, F. Production of Polylactic Acid-Activated Charcoal Nanofiber Membranes for COVID-19 Pandemic by Electrospinning Technique and Determination of Filtration Efficiency. *J. Mater. Electron. Devices* **2020**, *4*, 21−26.
(107) Choi, S.; Jeon, H.; Jang, M.; Kim, H.; Shin, G.; Koo, J. M.; Lee, M.; Sung, H. K.; Eom, Y.; Yang, H.-S.; et al. Biodegradable, Efficient, and Breathable Multi-Use Face Mask Filter. *Adv. Sci. (Weinh)* **2021**, *8* (6), 2003155.
(108) Leung, W. W.-F.; Sun, Q. Charged PVDF Multilayer Nanofiber Filter in Filtering Simulated Airborne Novel Coronavirus (COVID-19) Using Ambient Nano-Aerosols. *Sep. Purif. Technol.* **2020**, *245*, 116887.
(109) Malikmammadov, E.; Tanir, T. E.; Kiziltay, A.; Hasirci, V.; Hasirci, N. PCL and PCL-Based Materials in Biomedical Applications. *J. Biomater. Sci. Polym. Ed.* **2018**, *29* (7−9), 863−893.
(110) Khandaker, M.; Kotturi, H.; Progri, H.; Tummala, S.; Nikfarjam, S.; Rao, P.; Hosna, A.; Arasu, D. T.; Williams, W.; Haleem, A. M. In Vitro and in Vivo Effect of Polycaprolactone Nanofiber Coating on Polyethylene Glycol Diacrylate Scaffolds for Intervertebral Disc Repair. *Biomed. Mater.* **2021**, *16*, 045024.
(111) McKeen, L. W. Effect of Radiation on the Properties of Polyester Polymers. In *The Effect of Radiation on Properties of Polymers*; Elsevier, 2020; pp 93−128.
(112) Begum, S. A.; Rane, A. V.; Kanny, K. Applications of Compatibilized Polymer Blends in Automobile Industry. In *Compatibilization of Polymer Blends*; Ajitha, A. R., Sabu, T., Eds.; Elsevier, 2020; pp 563−593.
(113) Buluş, E.; Ismık, D.; Mansuroğlu, D. S.; Fındıkoğlu, M. S.; Bozkurt, B.; Şahin, Y. M.; Doğancı, E.; Doğancı, M. D.; Sakarya, G. Electrohydrodynamic Atomization (EHDA) Technique for the Health Sector of Polylactic Acid (PLA) Nanoparticles. In *2019 Scientific Meeting on Electrical-Electronics & Biomedical Engineering and Computer Science (EBBT)*; IEEE, 2019; pp 1−4.
(114) Chen, X. Y.; Romero, A.; Paton-Carrero, A.; Lavin-Lopez, M. P.; Sanchez-Silva, L.; Valverde, J. L.; Kaliaguine, S.; Rodrigue, D. Functionalized Graphene-Reinforced Foams Based on Polymer Matrices. In *Functionalized Graphene Nanocomposites and their Derivatives*; Jawaid, M., Bouhfid, R., Qaiss, A. el K., Eds.; Elsevier, 2019; pp 121−155.
(115) Moulefera, I.; Trabelsi, M.; Mamun, A.; Sabantina, L. Electrospun Carbon Nanofibers from Biomass and Biomass Blends-Current Trends. *Polymers (Basel)* **2021**, *13* (7), 1071.
(116) Xiong, S.-W.; Zou, Q.; Wang, Z.-G.; Qin, J.; Liu, Y.; Wei, N.-J.; Jiang, M.-Y.; Gai, J.-G. Temperature-Adjustable F-Carbon Nanofiber/Carbon Fiber Nanocomposite Fibrous Masks with Excellent Comfortability and Anti-Pathogen Functionality. *Chem. Eng. J.* **2022**, *432*, 134160.
(117) Yang, Y.; He, R.; Cheng, Y.; Wang, N. Multilayer-Structured Fibrous Membrane with Directional Moisture Transportability and Thermal Radiation for High-Performance Air Filtration. *e-Polym.* **2020**, *20* (1), 282−291.
(118) Xiong, S.-W.; Fu, P.-G.; Zou, Q.; Chen, L.-Y.; Jiang, M.-Y.; Zhang, P.; Wang, Z.-G.; Cui, L.-S.; Guo, H.; Gai, J.-G. Heat Conduction and Antibacterial Hexagonal Boron Nitride/Polypropylene Nanocomposite Fibrous Membranes for Face Masks with Long-Time Wearing Performance. *ACS Appl. Mater. Interfaces* **2021**, *13* (1), 196−206.

https://doi.org/10.1021/acsami.2c10335
ACS Appl. Mater. Interfaces 2022, 14, 46123−46144

(119) Li, Y.; Yin, X.; Si, Y.; Yu, J.; Ding, B. All-Polymer Hybrid Electret Fibers for High-Efficiency and Low-Resistance Filter Media. *Chem. Eng. J.* **2020**, *398*, 125626.
(120) Wang, L.; Bian, Y.; Lim, C. K.; Niu, Z.; Lee, P. K. H.; Chen, C.; Zhang, L.; Daoud, W. A.; Zi, Y. Tribo-Charge Enhanced Hybrid Air Filter Masks for Efficient Particulate Matter Capture with Greatly Extended Service Life. *Nano Energy* **2021**, *85*, 106015.
(121) Cheng, Y.; Wang, C.; Zhong, J.; Lin, S.; Xiao, Y.; Zhong, Q.; Jiang, H.; Wu, N.; Li, W.; Chen, S.; et al. Electrospun Polyetherimide Electret Nonwoven for Bi-Functional Smart Face Mask. *Nano Energy* **2017**, *34*, 562−569.
(122) Hashmi, M.; Ullah, S.; Kim, I. S. Copper Oxide (CuO) Loaded Polyacrylonitrile (PAN) Nanofiber Membranes for Antimicrobial Breath Mask Applications. *Current Research in Biotechnology* **2019**, *1*, 1−10.
(123) Khanzada, H.; Salam, A.; Qadir, M. B.; Phan, D.-N.; Hassan, T.; Munir, M. U.; Pasha, K.; Hassan, N.; Khan, M. Q.; Kim, I. S. Fabrication of Promising Antimicrobial Aloe Vera/Pva Electrospun Nanofibers for Protective Clothing. *Materials (Basel)* **2020**, *13* (17), 3884.
(124) Deng, C.; Seidi, F.; Yong, Q.; Jin, X.; Li, C.; Zhang, X.; Han, J.; Liu, Y.; Huang, Y.; Wang, Y.; et al. Antiviral/Antibacterial Biodegradable Cellulose Nonwovens as Environmentally Friendly and Bioprotective Materials with Potential to Minimize Microplastic Pollution. *J. Hazard. Mater.* **2022**, *424* (Pt A), 127391.
(125) Saikaew, R.; Intasanta, V. Versatile Nanofibrous Filters against Fine Particulates and Bioaerosols Containing Tuberculosis and Virus: Multifunctions and Scalable Processing. *Sep. Purif. Technol.* **2021**, *275*, 119171.
(126) Lee, S.; Nam, J.-S.; Han, J.; Zhang, Q.; Kauppinen, E. I.; Jeon, I. Carbon Nanotube Mask Filters and Their Hydrophobic Barrier and Hyperthermic Antiviral Effects on SARS-CoV-2. *ACS Appl. Nano Mater.* **2021**, *4* (8), 8135−8144.
(127) Pardo-Figuerez, M.; Chiva-Flor, A.; Figueroa-Lopez, K.; Prieto, C.; Lagaron, J. M. Antimicrobial Nanofiber Based Filters for High Filtration Efficiency Respirators. *Nanomaterials (Basel)* **2021**, *11* (4), 900.
(128) Abbas, W. A.; Shaheen, B. S.; Ghanem, L. G.; Badawy, I. M.; Abodouh, M. M.; Abdou, S. M.; Zada, S.; Allam, N. K. Cost-Effective Face Mask Filter Based on Hybrid Composite Nanofibrous Layers with High Filtration Efficiency. *Langmuir* **2021**, *37* (24), 7492−7502.
(129) He, P.; Wu, F.; Yang, M.; Jiao, W.; Yin, X.; Si, Y.; Yu, J.; Ding, B. Green and Antimicrobial 5-Bromosalicylic Acid/Polyvinyl Butyral Nanofibrous Membranes Enable Interception-Sterilization-Integrated Bioprotection. *Composites Communications* **2021**, *25*, 100720.
(130) Hiragond, C. B.; Kshirsagar, A. S.; Dhapte, V. V.; Khanna, T.; Joshi, P.; More, P. V. Enhanced Anti-Microbial Response of Commercial Face Mask Using Colloidal Silver Nanoparticles. *Vacuum* **2018**, *156*, 475−482.
(131) Salam, A.; Hassan, T.; Jabri, T.; Riaz, S.; Khan, A.; Iqbal, K. M.; Khan, S. U.; Wasim, M.; Shah, M. R.; Khan, M. Q.; et al. Electrospun Nanofiber-Based Viroblock/ZnO/PAN Hybrid Antiviral Nanocomposite for Personal Protective Applications. *Nanomaterials (Basel)* **2021**, *11* (9), 2208.
(132) Patil, N. A.; Gore, P. M.; Jaya Prakash, N.; Govindaraj, P.; Yadav, R.; Verma, V.; Shanmugarajan, D.; Patil, S.; Kore, A.; Kandasubramanian, B. Needleless Electrospun Phytochemicals Encapsulated Nanofibre Based 3-Ply Biodegradable Mask for Combating COVID-19 Pandemic. *Chem. Eng. J.* **2021**, *416*, 129152.
(133) Zhang, L.; Zhou, Y.; Wu, Q.; Han, Z.; Zhao, Z.; Li, F.; Wang, C.; Wei, K.; Li, G. A Functional Polyvinyl Alcohol Fibrous Membrane Loaded with Artemisinin and Chloroquine Phosphate. *J. Polym. Res.* **2021**, *28* (6), 232.
(134) Alshabanah, L. A.; Hagar, M.; Al-Mutabagani, L. A.; Abozaid, G. M.; Abdallah, S. M.; Shehata, N.; Ahmed, H.; Hassanin, A. H. Hybrid Nanofibrous Membranes as a Promising Functional Layer for Personal Protection Equipment: Manufacturing and Antiviral/Antibacterial Assessments. *Polymers (Basel)* **2021**, *13* (11), 1776.
(135) Qin, M.; Liu, D.; Meng, X.; Dai, Z.; Zhu, S.; Wang, N.; Yan, X. Electrospun Polyvinyl Butyral/Berberine Membranes for Antibacterial Air Filtration. *Materials Letters: X* **2021**, *10*, 100074.
(136) Pierini, F.; Guglielmelli, A.; Urbanek, O.; Nakielski, P.; Pezzi, L.; Buda, R.; Lanzi, M.; Kowalewski, T. A.; De Sio, L. Thermoplasmonic-activated Hydrogel Based Dynamic Light Attenuator. *Adv. Opt. Mater.* **2020**, *8* (12), 2000324.
(137) Wang, S.; Liu, Q.; Li, L.; Urban, M. W. Recent Advances in Stimuli-Responsive Commodity Polymers. *Macromol. Rapid Commun.* **2021**, *42* (18), No. e2100054.
(138) Zhong, H.; Zhu, Z.; Lin, J.; Cheung, C. F.; Lu, V. L.; Yan, F.; Chan, C.-Y.; Li, G. Reusable and Recyclable Graphene Masks with Outstanding Superhydrophobic and Photothermal Performances. *ACS Nano* **2020**, *14* (5), 6213−6221.
(139) Horváth, E.; Rossi, L.; Mercier, C.; Lehmann, C.; Sienkiewicz, A.; Forró, L. Photocatalytic Nanowires-Based Air Filter: Towards Reusable Protective Masks. *Adv. Funct. Mater.* **2020**, *30*, 2004615.
(140) Soni, R.; Joshi, S. R.; Karmacharya, M.; Min, H.; Kim, S.-K.; Kumar, S.; Kim, G.-H.; Cho, Y.-K.; Lee, C. Y. Superhydrophobic and Self-Sterilizing Surgical Masks Spray-Coated with Carbon Nanotubes. *ACS Appl. Nano Mater.* **2021**, *4* (8), 8491−8499.
(141) Xiong, J.; Li, A.; Liu, Y.; Wang, L.; Qin, X.; Yu, J. Multi-Scale Nanoarchitectured Fibrous Networks for High-Performance, Self-Sterilization, and Recyclable Face Masks. *Small* **2022**, *18* (2), No. e2105570.
(142) Li, Q.; Yin, Y.; Cao, D.; Wang, Y.; Luan, P.; Sun, X.; Liang, W.; Zhu, H. Photocatalytic Rejuvenation Enabled Self-Sanitizing, Reusable, and Biodegradable Masks against COVID-19. *ACS Nano* **2021**, *15* (7), 11992−12005.
(143) Li, M.; Wen, H.; Li, H.; Yan, Z.-C.; Li, Y.; Wang, L.; Wang, D.; Tang, B. Z. AIEgen-Loaded Nanofibrous Membrane as Photodynamic/Photothermal Antimicrobial Surface for Sunlight-Triggered Bioprotection. *Biomaterials* **2021**, *276*, 121007.
(144) Chen, K.-N.; Sari, F. N. I.; Ting, J.-M. Multifunctional TiO2/Polyacrylonitrile Nanofibers for High Efficiency PM2.5 Capture, UV Filter, and Anti-Bacteria Activity. *Appl. Surf. Sci.* **2019**, *493*, 157−164.
(145) Wang, N.; Cai, M.; Yang, X.; Yang, Y. Electret Nanofibrous Membrane with Enhanced Filtration Performance and Wearing Comfortability for Face Mask. *J. Colloid Interface Sci.* **2018**, *530*, 695−703.
(146) Kang, D. H.; Kim, N. K.; Kang, H. W. Electrostatic Charge Retention in PVDF Nanofiber-Nylon Mesh Multilayer Structure for Effective Fine Particulate Matter Filtration for Face Masks. *Polymers (Basel)* **2021**, *13* (19), 3235.
(147) Le, T. T.; Curry, E. J.; Vinikoor, T.; Das, R.; Liu, Y.; Sheets, D.; Tran, K. T. M.; Hawxhurst, C. J.; Stevens, J. F.; Hancock, J. N.; et al. Piezoelectric Nanofiber Membrane for Reusable, Stable, and Highly Functional Face Mask Filter with Long-Term Biodegradability. *Adv. Funct. Mater.* **2022**, *32*, 2113040.
(148) Bakhit, M.; Krzyzaniak, N.; Scott, A. M.; Clark, J.; Glasziou, P.; Del Mar, C. Downsides of Face Masks and Possible Mitigation Strategies: A Systematic Review and Meta-Analysis. *BMJ. Open* **2021**, *11* (2), No. e044364.
(149) El-Atab, N.; Mishra, R. B.; Hussain, M. M. Toward Nanotechnology-Enabled Face Masks against SARS-CoV-2 and Pandemic Respiratory Diseases. *Nanotechnology* **2022**, *33* (6), 062006.
(150) Ivanoska-Dacikj, A.; Stachewicz, U. Smart Textiles and Wearable Technologies − Opportunities Offered in the Fight against Pandemics in Relation to Current COVID-19 State. *REVIEWS ON ADVANCED MATERIALS SCIENCE* **2020**, *59* (1), 487−505.
(151) Goel, S.; Hawi, S.; Goel, G.; Thakur, V. K.; Agrawal, A.; Hoskins, C.; Pearce, O.; Hussain, T.; Upadhyaya, H. M.; Cross, G.; et al. Resilient and Agile Engineering Solutions to Address Societal Challenges Such as Coronavirus Pandemic. *Mater. Today Chem.* **2020**, *17*, 100300.
(152) Luckachan, G. E.; Pillai, C. K. S. Biodegradable Polymers- A Review on Recent Trends and Emerging Perspectives. *J. Polym. Environ.* **2011**, *19* (3), 637−676.

https://doi.org/10.1021/acsami.2c10335
ACS Appl. Mater. Interfaces 2022, 14, 46123−46144

(153) Shahrubudin, N.; Lee, T. C.; Ramlan, R. An Overview on 3D Printing Technology: Technological, Materials, and Applications. *Procedia Manufacturing* **2019**, *35*, 1286−1296.
(154) Huang, Z.-M.; Zhang, Y. Z.; Kotaki, M.; Ramakrishna, S. A Review on Polymer Nanofibers by Electrospinning and Their Applications in Nanocomposites. *Composites science and technology* **2003**, *63* (15), 2223−2253.
(155) Chen, Y. Nanofabrication by Electron Beam Lithography and Its Applications: A Review. *Microelectron. Eng.* **2015**, *135*, 57−72.
(156) Holmström, J.; Holweg, M.; Khajavi, S. H.; Partanen, J. The Direct Digital Manufacturing (r)Evolution: Definition of a Research Agenda. *Oper. Manag. Res.* **2016**, *9* (1−2), 1−10.
(157) Jjagwe, J.; Olupot, P. W.; Menya, E.; Kalibbala, H. M. Synthesis and Application of Granular Activated Carbon from Biomass Waste Materials for Water Treatment: A Review. *Journal of Bioresources and Bioproducts* **2021**, *6* (4), 292−322.

https://doi.org/10.1021/acsami.2c10335
ACS Appl. Mater. Interfaces 2022, 14, 46123−46144

Biomaterials Science

ROYAL SOCIETY OF CHEMISTRY

PAPER

View Article Online
View Journal

Cite this: DOI: 10.1039/d3bm01125a

Engineering surgical face masks with photothermal and photodynamic plasmonic nanostructures for enhancing filtration and on-demand pathogen eradication†

Mohammad Ali Haghighat Bayan, [a] Chiara Rinoldi,[a] Daniel Rybak,[a] Seyed Shahrooz Zargarian,[a] Anna Zakrzewska, [a] Olga Cegielska, [b] Kaisa Põhako-Palu,[c] Shichao Zhang,[d] Agata Stobnicka-Kupiec,[e] Rafał L. Górny,[e] Paweł Nakielski, [a] Karin Kogermann, [c] Luciano De Sio, [f] Bin Ding [d] and Filippo Pierini *[a]

Received 5th July 2023,
Accepted 28th December 2023

DOI: 10.1039/d3bm01125a

rsc.li/biomaterials-science

The shortage of face masks and the lack of antipathogenic functions has been significant since the recent pandemic's inception. Moreover, the disposal of an enormous number of contaminated face masks not only carries a significant environmental impact but also escalates the risk of cross-contamination. This study proposes a strategy to upgrade available surgical masks into antibacterial masks with enhanced particle and bacterial filtration. Plasmonic nanoparticles can provide photodynamic and photothermal functionalities for surgical masks. For this purpose, gold nanorods act as on-demand agents to eliminate pathogens on the surface of the masks upon near-infrared light irradiation. Additionally, the modified masks are furnished with polymer electrospun nanofibrous layers. These electrospun layers can enhance the particle and bacterial filtration efficiency, not at the cost of the pressure drop of the mask. Consequently, fabricating these prototype masks could be a practical approach to upgrading the available masks to alleviate the environmental toll of disposable face masks.

Introduction

In recent years, there has been an increasing focus on the health impacts of microbial components and particulate matter (PM), particularly since the onset of the COVID-19 pandemic.[1–3] When we breathe, cough, or sneeze, many respiratory secretions and saliva are released into the surrounding environment, creating infectious aerosols. These aerosols contain pathogenic particles that can deposit in living spaces and infect susceptible populations, leading to respiratory infections.[4,5] Numerous pathogenic bacteria and viruses have been shown to spread *via* aerosols, rapidly transmitting respiratory infectious diseases, particularly in enclosed spaces.[6] As a result, ensuring personal protection from infection is crucial and is a global issue.[7] Airborne PM is now recognized as one of the most harmful air pollutants significantly impacting air quality, public health, and ecosystems.[8,9] PM is classified as $PM_{0.3}$, PM_1, $PM_{2.5}$, and PM_{10} based on particle sizes smaller than 0.3, 1, 2.5, and 10 μm, respectively.[10] The most dangerous particles are those with aerodynamic diameters between 1.0 μm (PM_1) and 0.3 μm ($PM_{0.3}$), as they can travel long distances in the air and have a large surface area.[11,12] The mentioned features enable these particles to carry numerous pathogens and penetrate lung tissues and the blood-circulation system, resulting in respiratory and cardiovascular diseases. Face masks today are the potential means of protection from airborne pollutants emitted into the air.[13,14]

The primary issue with the available face masks is the short duration of functionality.[15] Personal protective equipment (PPE) has been severely in short supply during the COVID-19 coronavirus crisis.[16] Many techniques have been explored for

[a]Department of Biosystems and Soft Matter, Institute of Fundamental Technological Research, Polish Academy of Sciences, Warsaw 02-106, Poland. E-mail: fpierini@ippt.pan.pl
[b]Laboratory of Polymers and Biomaterials, Institute of Fundamental Technological Research Polish Academy of Sciences, Warsaw 02-106, Poland
[c]Institute of Pharmacy, Faculty of Medicine University of Tartu, Nooruse 1, 50411 Tartu, Estonia
[d]Innovation Center for Textile Science and Technology, College of Textiles, Donghua University, Shanghai 201620, China
[e]Laboratory of Biohazards, Department of Chemical, Aerosol and Biological Hazards, Central Institute for Labour Protection – National Research Institute, Warsaw 00-701, Poland
[f]Department of Medico-Surgical Sciences and Biotechnologies, Research Center for Biophotonics, Sapienza University of Rome, Latina 04100, Italy
†Electronic supplementary information (ESI) available. See DOI: https://doi.org/10.1039/d3bm01125a

the quick and frequent disinfection of these masks and other PPE to address the difficulty of safely reusing face masks.[17–20] Over the past three years, gigantic mask consumption generated huge biomedical waste (BMW), mainly released into the environment without proper sterilization. Moreover, the massive production of BMW on a comprehensive level of society led to the merging of BMW with municipal solid waste.[18,21,22] Exposure of hazardous and contagious waste to municipal waste in the environment will be one of the most significant environmental issues. The urgent need to find a feasible solution for an antibacterial face mask has received less scientific study.[23,24]

One of the approaches is employing nanotechnology and nanomaterials to modify the available face masks. Electrospinning is a technique capable of fabricating fibers with the desired dimension and morphology.[25–28] This technique is widely used to manufacture fibers for filtration. Furthermore, stimuli-responsive nanomaterials have been fabricated *via* this technique for various applications.[29–31] Using this strategy to advance existing respirators/masks has been previously illustrated as a feasible roadmap,[32] introducing an adjustable layer with a desired porosity over the already-available face masks, which is scalable and achievable.

Plasmonic nanoparticles can decorate the surface of fibrous materials for their physically driven antipathogenic activity.[17,33] This decoration enables an active pathway for reducing the accumulation of harmful and living pathogens in the pores of the fibers.[34] Such photothermally effective nanoparticles can induce light-triggered photothermal disinfection (on request) and have a broadband absorption range to eradicate any potentially lingering germs.[35–37]

Among plasmonic nanoparticles, gold nanoparticles (Au NPs) have been widely used in numerous scientific domains in recent years due to their optical and thermo-optical features.[31,38–40] Localized surface plasmon resonance (LSPR), a physical phenomenon, enables Au NPs to produce a strong electromagnetic field at the nanoscale level.[41] The coherent and dipolar oscillation of free electrons localized at the metal/dielectric interface is related to LSPR.[42,43] The LSPR oscillation produces a significant temperature increase on the surface of the Au NP when it is exposed to an appropriate (resonant) light source, converting the Au NP into a focused nanosource of heat.[44,45] It was abundantly evident that influential LSPR absorption, followed by quick energy conversion and dissipation, could efficiently heat the immediate environment and kill microorganisms.[46,47]

Researchers have studied and reported air filters and masks endowed with photo-responsive properties.[48–51] Li *et al.* investigated the potential of metal–organic frameworks (MOFs) for air pollution control and personal protection, focusing on a zinc-imidazolate MOF with photocatalytic bactericidal properties.[48] The fabricated MOF-based air filters not only achieve efficient particulate matter removal but also demonstrate remarkable photocatalytic antibacterial behavior. In another research, Kumar and co-workers presented the development of modified polycotton fabrics with molybdenum disulfide (MoS_2) nanosheets.[49] The modified fabric offered self-disinfection, antibacterial, and photothermal properties for reusable protective masks. The study highlighted the potential for cost-effective, large-scale production of nanosheet-modified antibacterial fabrics. Shao *et al.* explored the antibacterial properties of gold nanomaterials, including gold nanospheres (Au NSs) and gold nanorods (Au NRs), as well as silver nanoparticles (Ag NPs) under incandescent light exposure.[51] The results reveal that Au NSs do not exhibit significant antibacterial activity, while Au NRs demonstrate substantial bactericidal effects against various bacterial strains. This antibacterial effect is enhanced by the photodynamic and photothermal properties of Au NRs when exposed to near-infrared light (NIR), leading to bacterial inactivation.

We developed and optimized a strategy to introduce homogenous defectless electrospun sandwich-like layers. This architecture will be a good candidate for indoor bactericidal eradication upon NIR light. The structured layers stayed on the outer layer of the surgical face mask. The introduced layer was then decorated with Au NRs. The nanorods have encapsulated between layers of electrospun nanofibers to avoid their leakage. These nanofibrous layers can capture fine particles and maintain the applicability and performance of commercial surgical face masks. The decorated nanofibers introduced an on-demand antibacterial feature that can activate under the face masks' NIR region light irradiation. The design of the face mask is intended for bacterial elimination after each wearing through the NIR irradiation process. The antibacterial activity and electrospun layer simultaneously can improve the face mask's bacterial and PM filtration efficiency. This innovative face mask is designed to eliminate surface bacteria on face masks effectively. This key feature not only answers the needs of the general public but also holds particular significance for those in contact with hospital patients, helping prevent cross-contamination and the spread of diseases.

Results and discussion

Development and structural features of the platform

A feasible modification would extend their duration of functionality, aimed at designing new functionalities for commonly used masks. Therefore, the first step of fabricating the prototype face mask was to electrospin the first layer of polymer nanofibers on the surgical mask. An optimized electrospun polyacrylonitrile (PAN) layer was deposited on the surgical mask's outer layer. Afterward, the Au NRs alcosol suspension was electrosprayed on the surface of the PAN nanofibers. To make a protective layer for the electrosprayed nanoparticles on the as-decorated PAN electrospun nanofibers, an additional layer of pristine PAN nanofibers covered the Au NRs-PAN electrospun layer. Au NRs in this platform provide stimuli-responsiveness for the fabricated masks upon NIR light. The selected Au NRs for this study have the maximum absorption peak at 810 nm, which is the NIR region of the electromagnetic spectrum.[52,53] The gold nanoparticles triggered by NIR light

excite their free electron from the plain state of S_0 to the excited S_1 electronic states.[54] After this excitation, gold nanoparticles, to come back to the equilibrium state, will release thermal energy at the nanoscale. In the developed platform, taking advantage of generated heat can lead to an on-demand feature for eliminating the potential bacteria on the surface of the face mask. Fig. 1 illustrates material preparation and the schematic response of gold nanoparticles. Regarding the general performance of face masks, surgical masks have low $PM_{0.3}$ and bacterial filtration efficiency (discussed further below). However, they are not capable of antibacterial activities. While the proposed modification of face masks illustrated a significant improvement in bacterial and particle filtration efficiency, they are equipped with on-demand antibacterial properties.

Characterization and properties of gold nanorods

Au NRs were introduced onto the nanofiber-layered masks to equip them with antibacterial properties enabling photoresponseability. The transmission electron microscope (TEM) image of the Au NRs used for this study can be seen in Fig. 2a. Two Au NRs are presented in the TEM micrograph. In Fig. S1,† the TEM image displayed that the average length of nanorods is 50.8 ± 5 nm. Moreover, the TEM image analysis revealed that the gold nanorods' average width is 12.1 ± 0.8 nm with an average aspect ratio of 4.2 ± 0.6. The elemental mapping under a TEM (Fig. 2b) confirmed the presence of gold nanorods. As shown in Fig. 2c, Au NRs displayed strong absorbance in the NIR light region (810 nm). This absorbance is related to the length and aspect ratio of the Au NRs. The dynamic light scattering (DLS) curve of Au NRs in Fig. 2d shows an average hydrodynamic diameter of 50 nm, confirming the morphology of the gold nanoparticles used for this research.

Face mask modification procedure

To prepare the electrospinning solution, first, PAN was dissolved and transferred to a syringe to fabricate an electrospun layer over the outer layer of the surgical face mask. The next step was to decorate the as-spun PAN layer. Due to the high hydrophobicity of polypropylene (PP) melt-blown fibers and PAN electrospun layer (Fig. S2†), depositing uniform Au NRs was impossible. Soliwoda *et al.* proposed using alcosol of Au NRs instead of an aqueous solution to overcome this matter.[55] Subsequently, after the preparation of Au NRs alcosol, the as-spun PAN layer was decorated with Au NRs by electrospraying technique to equip the mask with photodynamic and photothermal properties. Finally, we employed electrospinning of PAN on the decorated layer to fabricate a protective layer for the decorated fibers. The described strategy allows the nanoparticles to be incorporated onto the electrospun layer and maintain their functionality without leaching. The binding forces between citrate-capped gold nanoparticles primarily involve electrostatic forces and coordination bonds. Citrate ions (from citrate molecules) are commonly used to stabilize and cap AuNPs. Additionally, citrate molecules can form coordination bonds with gold atoms on the nanoparticle surface. This contributes to the stability of the citrate-capped AuNPs.[56] Furthermore, due to the robust entrapment of the nanoparticles within the layers, the chance of escape or inhalation of gold nanoparticles is minutest. Consequently, the functionality of Au NRs is retained, and they can effectively exhibit photodynamic and photothermal activities without creating potential health risks. In Fig. 3a, the process of preparing antibacterial face masks is illustrated. The available surgical face

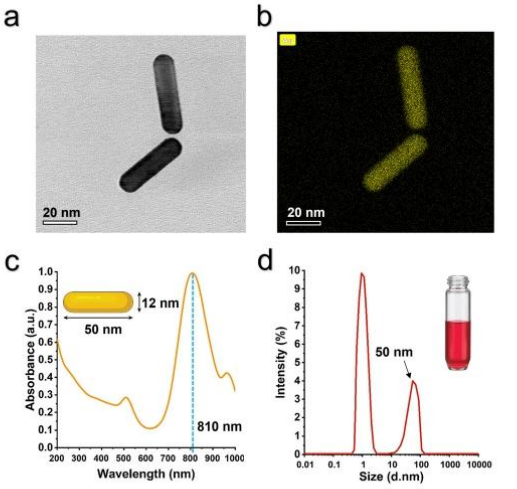

Fig. 2 Characterization of Au NRs utilized for this study. (a) High-resolution TEM image of two gold nanoparticles. (b) EDX elemental mapping image confirming the presence of gold. (c) UV-Vis spectrum of Au NR solution exhibiting the sharp absorbance peak at 810 nm related to the morphology and aspect ratio of the employed nanorods. (d) DLS plot presenting the hydrodynamic radius of nanorods approximately at 50 nm and an additional peak centered at 1 nm related to the nanorod rotational diffusion.

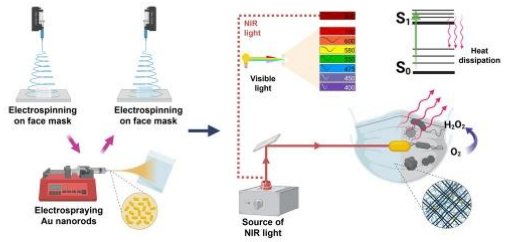

Fig. 1 Stratagem of modified face mask and novel features given by electrospinning and electrospraying. The schematic illustration shows the concept and structure design of the photo-response and photodynamic face mask fabrication. PAN nanofibers are formed firstly by electrospinning on a surgical mask, followed by Au NRs electrospraying procedure, and finally, PAN electrospun again on the decorated mask to create a protective layer for the nanoparticles. The nanostructured platform can efficiently be activated under the NIR irradiation.

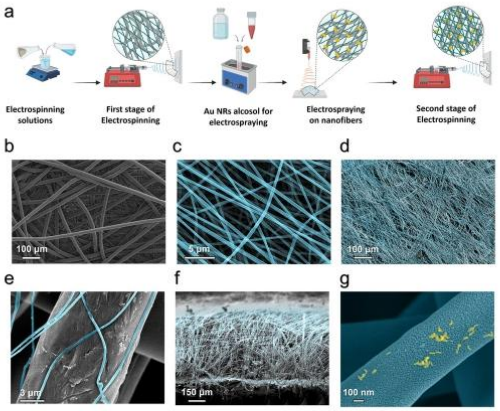

Fig. 3 Procedure of fabrication of nanostructured layer and morphological characterizations of the surgical mask (gray), PAN electrospun nanofibers (blue), and gold nanoparticles (yellow) fabricated for this study. (a) The nanostructured face mask fabrication scheme consisted of two electrospinning steps and one electrospraying stage. (b) SEM image of PP melt-blown surgical mask fibers. (c) SEM micrograph of standalone PAN nanofibers. (d) FE-SEM image of deposited PAN nanofibers on the outer layer of the face mask. (e) SEM image showing anchorage of a PAN electrospun nanofiber on the surface of PP melt-blown fiber. (f) Cross-section microscopic image of fabricated nanostructured face mask. (g) FE-SEM image of PAN nanofibers decorated with Au NRs.

masks mainly consist of three melt-blown layers of PP. As the structure of surgical masks has been shown in Fig. S3a,† the SEM micrographs show that the thickness of the internal and external layers are approximately 334 ± 23 μm and the thickness of the mid-layer is approximately 233 ± 16 μm (Fig. S3b†). Additionally, the PP melt-blown fibers used for commercial face masks have an average diameter of 18 ± 0.83 μm, as is shown in Fig. 3b. The morphology of the fabricated PAN electrospun nanofibers has been shown in Fig. 3c. The electrospun fibers of PAN are beadless, uniform, and have an average diameter of 387 ± 49 nm. Fig. 3d shows the SEM micrograph of the surgical mask's PP fibers covered with PAN nanofibers. Herein, the comparison of surgical mask microfibers with the PAN nanofibers is visible and illustrates a significant increase in the potential of PM filtration (Fig. 3d). The electrospinning of PAN over the face mask provided a physical entanglement between the melt-blown and nanofibers. The SEM image of the entanglement can be seen in Fig. 3e. In Fig. 3f, the SEM image of the cross-section of the prototype face mask showing the thickness (about 8.45 μm) of the electrospun layer of PAN can be seen. The FE-SEM image of Au NRs decorated nanofibers is presented in Fig. 3g, indicating the presence of Au NRs with an average length of 50 nm on the surface of electrospun PAN fibers is visible in this panel. In our previous study we demonstrated the stability of electrospun nanofibers decorated with Au NRs.[31] The electrospun mats were immersed in water, stirred vigorously, and irradiated with an NIR laser. Subsequent UV-Vis measurement of the immersion in liquid revealed no trace of released Au NRs, indicating system stability and non-release during use. SEM micrographs, the connected EDAX gold elemental mapping, and their EDAX spectra collected from three different representative areas of decorated face masks can be seen in Fig. S4.† The central area and two other zones localized in the face mask's corners are visualized to appreciate the homogeneous distribution along the electrosprayed samples' area.

Photo-responsiveness of the fabricated masks

The photothermal property of modified masks was evaluated under laser irradiation. A NIR laser source operating at 810 nm wavelength was irradiated on the samples passing through a custom-designed optical path to investigate the photo-responsiveness of the fabricated face masks. The schematic of photoresponse studies is illustrated in Fig. 4a. Any temperature change of the samples during irradiation was recorded and saved on the computer using a thermal camera. To observe the effect of NIR light on a surgical mask, plots of the temperature–time of untreated face masks under different powers of NIR light are reported in Fig. S5a.† The NIR light with 0.5 W cm^{-2} power increased the temperature of the outer layer of the face mask by 1 °C in 5 min of irradiation. Moreover, 3.0 W cm^{-2} and 4.0 W cm^{-2} NIR lasers were able to raise in temperature of the surgical mask respectively by 7.2 °C and 10.6 °C. Decorated face masks were irradiated by laser for 5 min with different NIR powers (Fig. S5b†) to find the optimum laser power for the self-sterilizing mask. Applying a 0.5 W cm^{-2} laser was able to reach 41.5 °C on the surface of the face mask. On the other hand, a 4.0 W cm^{-2} NIR light could increase the temperature to 115.0 °C. At the same time, a 3.0 W cm^{-2} laser was the optimum power, which raised the temperature to 113.2 °C, which can eradicate the pathogens *via* photothermal and photodynamic effects.[57,58]

The temporal plots of decorated face masks were graphed (Fig. 4b) to optimize the concentration of Au NRs alcosol and find the proper duration for electrospraying. The material was designed to reach sufficient temperature to eradicate the bacteria for the dry and wet face masks (Fig. 4c). To mimic the operative conditions of the surgical face mask, *i.e.*, accounting for the moisture that resides in the human exhale, the fabricated face mask can increase the temperature in a semi-wet scenario. The line profile plot module of the outer layer of the face mask shows a temperature of 113.5 °C along the surface of the mask (Fig. 4d). Furthermore, due to the application of decorated masks as wearable photoresponsive face masks, in Fig. 4e and f, the effect of laser irradiation on both sides of the platform has been studied. Meanwhile, the temperature of the inner layer, which is in contact with the user's skin, is about 29.5 °C showing the usability and safety of the fabricated platform. Fig. 4g is the thermographic image of decorated face masks under a 3.0 W cm^{-2} NIR laser. Images captured by the thermal camera showed a rapid rise in platform temperature, regarded as the direct responsiveness rate. In Fig. S6,† the thermographic image of a non-decorated face mask is visible.

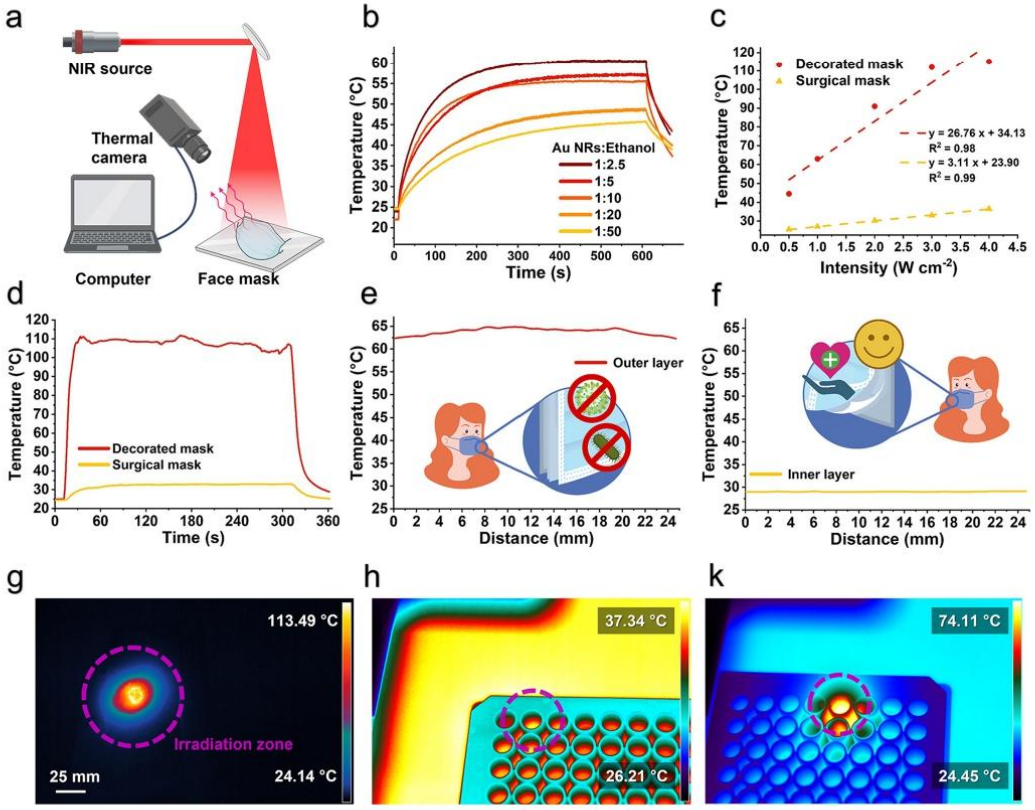

Fig. 4 The fabricated nanostructured face mask's photothermal representing the fabricated platform's fast responsiveness. (a) Scheme displaying the experimental setup designed to analyze the photo-response of the modified face mask under NIR irradiation. The temperature change was recorded during the analysis using a thermal camera. (b) Temporal plot of face masks decorated with different concentrations of Au NRs. The legends represent the volume ratio of the Au NRs solutions to ethanol in electrosprayed alcosol. Each sample was electrosprayed for 20 minutes. (c) Linear correlation between the maximum temperature sensed by the thermal camera and the intensity of the NIR-laser for dry surgical and decorated face masks. (d) Temperature vs. time plots of the nanostructured face mask decorated with Au NRs and untreated surgical mask under NIR-light irradiation for 5 min. (e) Temperature distribution graphs of the outer layer of the nanostructured face mask. (f) Temperature distribution graphs of the inner layer of the irradiated mask showing the temperature of 29.5 °C and safe for the user's skin. (g) Thermograph image of the nanostructure face mask under NIR light irradiation (intensity of 3.0 W cm^{-2}) showing a maximum temperature of 113.5 °C. (h) Thermal image of circular cut surgical mask treated with bacteria suspension showing the temperature of the sample and hot plate for the study was steady around 37 °C. (k) Thermogram of the nanostructured face mask cultured with bacteria under NIR-laser, in which the temperature reached 74 °C.

This figure indicates that the maximum reached temperature of a surgical mask under laser irradiation can be 32.56 °C which is not enough to eradicate pathogens.[36] To prepare and investigate specimens we utilized later for antibacterial studies (to be discussed whereafter), face masks were cut in circles and fixed at the bottom of 96-well plates. Fig. 4h and k show the thermographic images of the cut face masks during the antibacterial studies inside well plates. For this study, a hot plate was used to maintain the temperature of the samples at 37.0 °C imitating the wearer's face temperature. In Fig. 4h, the thermographic images of face masks during the antibacterial studies show that the temperature of the surgical mask was steady at 37.3 °C under NIR light irradiation. Meanwhile, in Fig. 4k, the decorated face mask displayed a rise in temperature to 74.1 °C under NIR irradiation for 15 min, which can be associated with the photothermal feature of Au NRs.

ROS generation of plasmonic nanoparticles

Recent research has focused on developing new and innovative methods for killing bacteria. One such method involves generating reactive oxygen species (ROS) generation with Au NRs. Gold nanorods can be utilized to generate ROS when irradiated with light. These generated ROS can damage bacterial cell walls and membranes, ultimately leading to cell death.[59,60]

This approach has the potential to be highly effective in eliminating bacteria. The reactivity of Au NRs and their potential to generate ROS was determined in PBS over time.[61–63] Deacetylation and purification of $DCFH_2$ in the present study were performed from an aqueous NaOH solution and purified by liquid phase extraction. The schematic of the preparation and purification steps is shown in Fig. 5a illustrating the different steps to prepare the $DCFH_2$ solution. Remarkably, during and after the preparation of $DCFH_2$, the solution was shielded from light to avoid oxidation upon light exposure. The absorption spectrum of $DCFH_2$ dissolved in methanol is shown in Fig. S7.† The spectrum has an absorption maximum at λ = 231 nm. The spectrum of dissolved $DCFH_2$ shows the identification of organic functional groups.[64] The scheme in Fig. 5b shows the ROS generation upon NIR light irradiation *via* Au NRs. A significant increase in DCF fluorescence occurred after the NIR laser irradiation of the Au NRs decorated face mask sample (Fig. 5c) in both decorated samples. In contrast, the fluorescence increase in the mentioned sample without laser irradiation was marginal, the same for the face mask without Au NRs. Similarly, DSC fluorescence of the surgical mask did not have a tangible change upon laser irradiation.

Biocompatibility of the face masks

Different approaches were used in this study to evaluate the breath safety of the fabricated face masks. According to the ISO guidelines (109993-5), cell cytotoxicity was measured by indirect and direct methods to follow the cells' viability, proliferation, and morphology changes on or in close contact with the mask.[65] The schematic of the direct and indirect cell viability methods can be seen in Fig. 6a. In the case of the indirect method for evaluating cell viability, cells were seeded onto the well plate, and their growth medium was replaced with the medium where the mask samples were soaked for 24 h. The indirect method results showed that the nanostructured masks did not leach any cytotoxic substances (or did not reach high enough concentrations of substances) into the aqueous medium during the experiment and therefore had no toxic effect on cells. In Fig. 6b, no statistical difference in cell viability was found between the nanostructured face masks tested (single and double electrospun layer on the surgical mask) and traditional surgical face masks. The results of the direct cell viability evaluation can be seen in Fig. 6c. Similar to the indirect cell viability method, there were no statistically significant

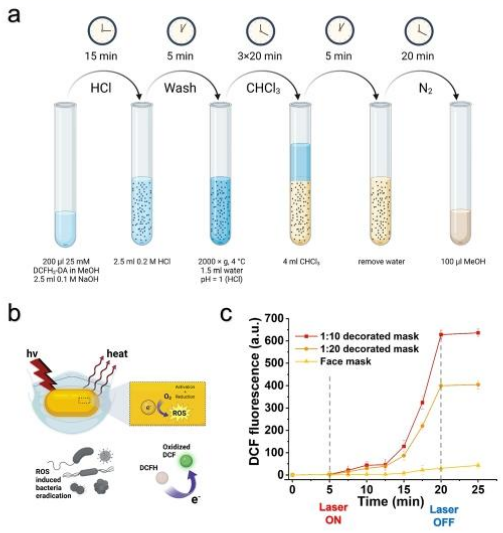

Fig. 5 ROS generation ability of Au NRs decorated face masks (a) Standard procedure for the preparation and purification of $DCHF_2$. (b) Schematic of ROS generation upon NIR-light triggered *via* Au NRs. (c) DCF fluorescence of different samples. Face mask decorated with two different concentrations of Au NRs and surgical face mask fluorescence changes over time.

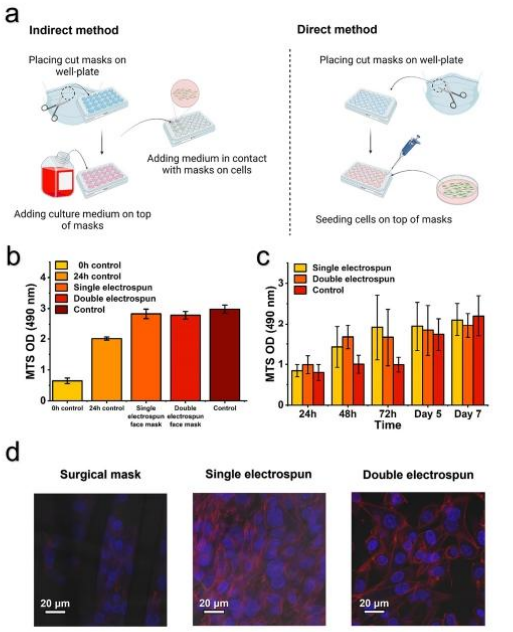

Fig. 6 Cell viability evaluation of BHK-21 exposed to different face mask samples. (a) Schematic illustrating the steps for indirect and direct methods. (b) Indirect cell viability assay results, showing no statistically significant difference between analyzed face masks and the control sample after 48 h. The control sample is cells on the well plate. (c) Results of direct cell viability method. Untreated cells grown at the bottom of the 24-wallplate were a control sample. (d) Confocal microscope images of BHK-21 cells on face mask samples. The blue color in the microscopic images stands for the nucleus, which was stained with DAPI, while red actin filaments stained are with Phallodine conjugated Alexa 568.

differences between tested masks and the controls at different time points, indicating the safety of tested masks.

In addition to the MTS direct cell viability assay, confocal microscopy was used to evaluate the safety and direct effect of nanostructured material of surgical mask on cell viability and proliferation. Fig. 6d shows confocal microscopy images of cells grown on tested masks for 48 h. No morphological changes in cells were observed when tested masks were compared to the control sample (cells cultured on round microscopy glass). It is possible to see even cell divisions, and the latter also indicates the well-being of the cells on top of the developed masks. Live cell staining and microscopy analyses were performed (ESI, Fig. S8†) to confirm that the fixation process during the sample preparation for imaging did not affect the cells on masks. Similarly, no morphological changes of the BHK-21 cells were observed when these cells were grown on the masks containing fibers and Au NRs on top compared to the surgical mask.

Bacteria and particle filtration performance

Bacterial filtration efficiency (BFE) and particle filtration efficiency (PFE) are test methods to evaluate face masks, respirators, and filtration media performance efficiency.[66,67] Fig. 7a shows the schematic of BFE and PFE tests and the fabricated face mask structure. BFE and PFE tests were conducted to evaluate the functionality of the face masks. Moreover, the results of these tests could be beneficial to optimize the thickness of the fabricated electrospun layers. The BFE testing method was assessed following the EN 14683:2019+AC standard. In Tables S1–3,† the total number of *Staphylococcus aureus* (*S. aureus*) bacteria that permeate the masks and their BFEs calculated following the mentioned standard can be found. To evaluate the effect of electrospinning, surgical mask, and electrospun face masks with single and double electrospun layers were analyzed. As can be seen in Fig. 7b, the BFEs were calculated as 55.24% ± 2.64, 90.16% ± 2.93, and 92.22% ± 3.53 for the surgical mask, single electrospun layer, and double electrospun layer, respectively. The results indicate that applying a layer of nanofibers to surgical face masks results in a statistically significant increase in the bacterial filtration efficiency of available surgical face masks. Additionally, to further investigate the effect of electrospun modification on the surgical mask, a PFE test was conducted with $PM_{0.3}$-like NaCl particles. As shown in Fig. 7c, the measured PFE of surgical face mask is about 37% ± 1.04, while the filtration efficiency of single and double electrospun layer masks are 67% ± 5.14 and 71% ± 5.62, respectively. The PFE test exhibited that the modified electrospun face mask can enhance the $PM_{0.3}$ filtration twofold with a double electrospun layer structure. Finally, Fig. 7d shows the pressure drop of the surgical and electrospun-modified face masks. The double electrospun layer face mask exhibited high BFE efficiency and escalated the $PM_{0.3}$ filtration while maintaining a similar pressure drop. In addition, the double-layer electrospun face mask pressure drop was 30.3 Pa, while the pressure drop of the surgical face mask was 25.1 Pa revealing the superior performance of fabricated face masks.

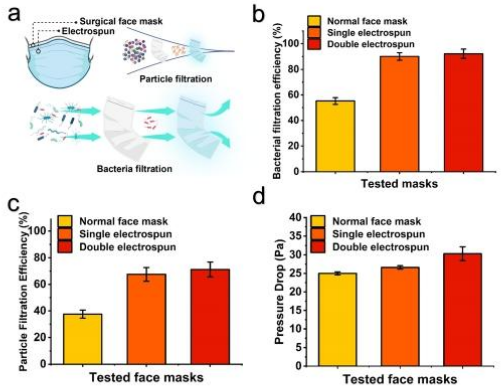

Fig. 7 (a) Schematic of BFE and PFE tests. (b) BFE of surgical masks compared with fabricated nanostructured platforms, showing enhancement in bacterial filtration. (c) PFE performance of surgical masks, single and double electrospun layer face masks, presenting a considerable improvement in particle filtration efficiency. (d) Pressure drop of fabricated single and double electrospun layer compared with surgical face mask showing maintain in pressure drop.

Bacteria eradication of the face mask

Photothermal and photodynamic bacterial inactivation properties of the materials are performed upon NIR laser irradiation. The antibacterial tests were evaluated using bacterial suspensions of *S. aureus*. This species was selected since it is one of the most common microorganisms, and it is responsible for a wide range of clinical infections.[68]

Antibacterial analysis was performed to evaluate the antibacterial properties of fabricated face masks. The test schematic is reported in Fig. 8a. The photothermal effect of Au NRs on bacteria suspension was observed after approximately 15 min of irradiation (Fig. 8b). During this time, in the presence of the Au NRs-coated masks, *S. aureus* were inactivated to the detection limit of 3 log units, demonstrating bacterial survival below 0.1% (Fig. 8c). No colonies were also observed in the representative plates, demonstrating effective inactivation of 99.95% of bacteria in the suspension, thus proving the self-sterilizing properties of the face masks under NIR light-radiation conditions. By contrast, no bacterial inactivation was observed for Au NRs-free masks upon illumination and for any tested samples without irradiation. Additionally, no effect of irradiation on control bacterial suspension was detected.

The bactericidal performance of the Au NRs-coated masks towards *S. aureus* was caused by the synergistic effect of the hydrophobicity of the masks and the photothermal performance of Au NRs, as reported in Fig. 4k. Various shapes of Au nanoparticles belong to a group of photosensitizers, which generate excited triplet states when exposed to light. These interact with molecular oxygen and create singlet oxygen,

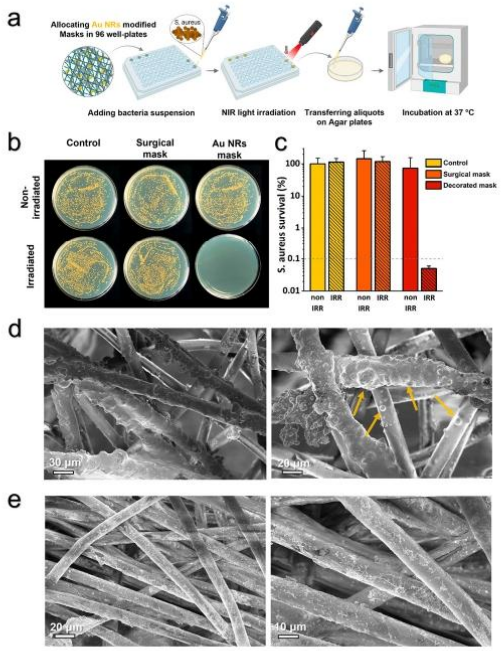

Fig. 8 Photothermal and photodynamic inactivation of *S. aureus* on Au NR-masks. (a) Schematic representation of the antibacterial test procedure. (b) Macroscopic pictures of bacterial colonies grown on LB agar. (c) Percent of bacteria survival after contact with bacterial suspension (control), mask, and Au NR-coated mask under NIR irradiation (IR) or dark incubation (n = 3). The detection limit at 103 CFU mL^{-1} is marked with the dashed line. Data points below the detection limit are set as 0.05% bacteria survival. Data are reported on a logarithmic scale as mean ± standard deviation. (d) SEM micrographs of face mask fibers cultured with bacteria; bacteria are marked with yellow arrows. (e) SEM images of fabricated face mask after NIR irradiation showing the elimination of bacteria on the surface of the mask.

damaging cell walls, plasma membranes, and DNA and eventually leading to the death of the microbial cells.[69,70] As the irradiation provided by the source of NIR light is continuous or recurring, the pathogens remaining on the surface of Au NRs-coated face masks can be easily eliminated in a repeated manner. Besides, the exposure time and temperature achieved during the experiments were also reported as sufficient to accomplish 4 log decays of SARS-CoV-2.[71]

The effect of Au NRs to eliminate the bacteria on the surface of fabricated face masks was further visualized using electron microscopy. For this purpose, two representatives decorated face masks with Au NRs cultured with *S. aureus* bacteria were examined. The first face mask was cultured with bacteria but was not irradiated by NIR light. The non-irradiated face mask did not show antibacterial activities. The colonies of *S. aureus* are visible in the image and marked with yellow arrows (Fig. 8d). On the other hand, the on-demand antibacterial effect of NIR irradiated Au NRs decorated face masks is visible on the micrographs (Fig. 8e) showing the elimination of the bacteria on the face mask.

Conclusions

This study displays a strategy to fabricate face masks with on-demand pathogen eradication capability. The strategy illustrated a way to decrease the environmental impact of many contaminated waste masks and the risk of spreading infections. The face mask's active layer consists of PAN electrospun nanofibers sandwiching Au NRs. The plasmonic nanoparticles electrospraying process offered the platform a combination of photothermal and photodynamic features. The antibacterial property of the platform is activated upon exposure to the NIR light and can eliminate 99.95% of bacteria on the surface of the face masks. Furthermore, the electrospinning technique improved nearly twice the face masks' particle and bacterial filtration efficiency. The study proved that obtaining a self-sterilizing face mask with boosted filtration properties has the potential for practical application. This developed structure will be an innovation for indoor bactericidal eradication applications as for hospital purposes. We engineered the face mask to have the capability to eliminate surface bacteria upon laser irradiation between wearing. Our findings pave the way toward realizing innovative face masks with light-assisted sterilization, high filtration efficiency, preventing cross-contamination, and long-lasting functionalities. The proposed concept could revolutionize next-generation face masks, drastically reducing the waste generated by face masks while improving the performance of conventional surgical masks.

Experimental

Materials

Ethanol (99.5%, Sigma Aldrich), *N*,*N*-dimethylformamide (DMF, 99.0%, Sigma Aldrich), hydrochloric acid (HCl, 37.0%, Sigma Aldrich), dimethyl sulfoxide (DMSO, 99.9%, Sigma Aldrich), hexamethyldisilane (HDMS, 99.0% Sigma Aldrich), formaldehyde (36.0%, Sigma Aldrich), glutaraldehyde (GTA, Sigma Aldrich), polyacrylonitrile (PAN, M_w = 150 kDa, Sigma Aldrich), sodium chloride fine particles (NaCl, 0.3 μm), phosphate buffered saline (PBS, pH ~7.4, Sigma Aldrich), gold nanorods (Au NRs, λ_a = 810 nm, O.D. = 50, Au NR ≈ 1 mg mL^{-1} nanoComposix, USA), nonwoven protective face mask (TZMO SA), DMEM/F-12 (Sigma Aldrich), FBS (F9665, Sigma Aldrich), penicillin (Sigma Aldrich), streptomycin (Sigma Aldrich), baby hamster kidney cell (BHK-21, ThermoFisher Scientific), Glascow's MEM (GMEM, ThermoFisher Scientific), tributyl phosphate (TBP, Sigma Aldrich), 4-(2-hydroxyethyl)-1-piperazineethanesulfonic acid (HEPES, ThermoFisher Scientific), *Staphylococcus aureus* (*S. aureus*, ATCC® 6538™, Pol-AURA), tryptic soy agar (TSA, bioMérieux SA, Marcy-l'Etoile, France), 2,4,5-Trimethylthiazole (TMS, 98.0%, Sigma Aldrich),

MTS cell proliferation reagent (BioVision), FM™ 4–64 (Invitrogen, ThermoFisher Scientific), ROTI® Mount FluorCare DAPI (Carl Roth), and Alexa Flour 568 (ThermoFisher Scientific), lysogeny broth (LB) and lysogeny agar (LB agar, A&A Biotechnology).

Fabrication of nanostructured mask

A 10% w/w solution of PAN in DMF was prepared at room temperature *via* a magnetic stirrer. Subsequently, the PAN solution was homogenously dissolved overnight and transferred to a 1 mL syringe equipped with a 26-G metal blunt-end needle. A surgical mask was fixed on a stationary collector at a distance of 12 cm from the tip of the needle and connected to the negative pole of the voltage source. The electrospinning conditions were as follows: a flow rate of 500 μL h^{-1} and an applied voltage of 12 kV. The environmental conditions of the procedure were kept at a temperature of 24 °C and relative humidity of 44%. To decorate the as-spun PAN nanofibers on the surgical mask *via* electrospraying, an alcosol suspension of Au NRs was prepared—briefly, 10 μL of 50 O.D. Au NRs were dispersed in a 100 μL water and ethanol solution with a volume ratio of 1 : 1 and ultrasonicated. An ultrasonic bath was utilized for 15 min to disperse the alcosol for electrospraying. Next, the electrospraying process of Au NRs alcosol was carried out using a 1 mL syringe with a 22-G needle. The electrospraying conditions were as follows: a flow rate of 200 μL h^{-1} and an applied voltage of 7 kV at a needle-collector distance of 6 cm. The PAN solution was used again to electrospun the nanostructured face mask's second layer to protect the as-prepared decorated PAN nanofibers. The fabrication and environmental parameters were the same used for the first layer of electrospun PAN fibers.

To calculate the amount of sprayed Au NRs content, we used eqn (1). The following equation, with assuming a continuous flow rate:

$$M = \mathrm{OD} \times V \times (A_{\mathrm{fm}}/A_{\mathrm{es}}) \quad (1)$$

where, the optical density of the nanoparticles (OD), volume of gold nanorods in electrospraying alcosol (V), A_{fm} as the face mask area, and A_{es} as the electrospraying area. In, the Table S4,† amount of gold nanorods in each sample has been reported.

Chemical characterizations

To measure the UV-Vis spectra of Au NRs solution from 200 to 1000 nm with a step of 5 nm, a Multiskan GO spectrophotometer (Thermo Scientific, USA) was utilized. The hydrodynamic diameter of Au NRs was measured using a dynamic light scattering (DLS) zeta sizer Nano ZS (Malvern Panalytical, UK).

Morphological studies

The morphological properties of the Au NRs solution used for this study were investigated using the transmission electron microscopy (TEM) method. On the other hand, scanning electron microscopy (SEM) and field-emission electron microscopy (FE-SEM) were carried out to study the morphology of fabricated and decorated nanofibers. SEM investigations were conducted using a JEOL JSM-6390LV microscope. The accelerating voltage was 10 kV at a working distance of 10 mm. TEM, FE-SEM, and Energy-dispersive X-ray spectroscopy (EDAX) were performed using the FEI Nova NanoSEM 450 microscopes. The accelerated voltage for TEM and FE-SEM microscopy was at 10 kV, and for EDAX, the operating voltage was at 15 kV. Before SEM and FE-SEM microscopic imaging, the samples were coated with a 4 nm thick layer of gold using SC7620 Polaron micro sputter coater (Quorum Technologies Ltd, Ashford, UK).

Thermal-activity and antibacterial testing of mask

The Coherent Powerline CW diode laser, which operates at 810 nm in the high absorption range of Au NRs, was used in the thermo-optical setup. Under laser irradiation, the temporal temperature profile and spatial heating distribution were measured and identified using a high-resolution thermal camera (FLIR, A655sc). With an accuracy of 0.2 °C, the camera generates thermal images with a resolution of 640 × 480 pixels. It smoothly integrates with specialized software (FLIR ResearchIR Max) to capture and process the thermal data that the camera has collected.

Deacetylation and purification of DCFH2

The 2′,7′-dichlorodihydrofluorescein diacetate ($DCFH_2$-DA) deacetylation to 2′,7′-dichlorodihydrofluorescein ($DCFH_2$) and further purification was conducted following the protocol reported by Reiniers *et al.*[71] Briefly, the methanol stock solution of $DCFH_2$-DA was neutralized with 0.1 M sodium hydroxide (NaOH). An equal volume of 0.2 M HCl to the NaOH fraction was gradually added to precipitate DCFH2. The precipitated pellet was centrifuged at 2000*g* for 15 min at 4 °C. After the supernatant collection, 4 mL of ice-cold acidified MiliQ water (pH = 1) was added, and the centrifugation preceded by acidified MiliQ addition was repeated two more times. Chloroform was used to extract DCFH2 and remove the aqueous phase. The organic phase was evaporated under a continuous stream of argon gas at room temperature. Pellet was dissolved in methanol up to a concentration of 0.05 M. The stock solution was purged with argon gas and stored at −20 °C. All the steps were performed using a probe covered with aluminum foil to shield the sample from light exposure.

Spectrofluorometric DCFH2 oxidation assay in a cell-free system

Deacetylated and purified DCFH2 was used to determine the oxidant-generating potential of Au NRs on the surface of the face mask in the cell-free environment. The face mask with Au NRs was placed in a 96-well plate and poured with 198 μL PBS (pH = 7.4) and 2 μL of $DCFH_2$ (50 μM final concentration). The oxidizing potential during NIR laser irradiation (3.0 W cm^{-2}) and in the absence of laser was assessed spectrofluorimetrically (λ_{ex} = 485 nm and λ_{em} = 538 nm). Time points T = 0–2.5 min and T = 15–20 min were performed without laser

irradiation, whereas time points T = 2.5–15 min were assessed using continuous laser irradiation.

Bacterial filtration efficiency

A six-stage cascade impactor (WES-710, Westech Instrument, Upper Stondon, Great Britain) was implemented to fix the face masks for bacterial filtration efficiency (BFE) tests. Also, an aerosol chamber using a collision nebulizer (MRE CN25, BGI Incorporated, Waltham, MA, USA) was used for the BFE test. The absorbance of cells was measured using a microplate reader (Tecan Sunrise, Tecan Group Ltd, Männedorf, Switzerland) at the optical density (O.D.) of 490 nm.

Before each experiment, the tested masks were conditioned at 21 ± 0.5 °C and 85 ± 5% relative humidity for a minimum of 4 h to bring them into equilibrium with the atmosphere before testing. BFE was determined for each set of tested masks according to the European Standard EN 14683:2019+AC. Briefly, a tested mask was clamped between an inlet and the first stage of a six-stage cascade impactor (WES-710, Westech Instrument, Upper Stondon, Great Britain). An aerosol of *Staphylococcus aureus* (ATCC 6538) was introduced (from suspension in peptone water) into an aerosol chamber using a Collision nebulizer (MRE CN25, BGI Incorporated, Waltham, MA, USA) and subsequently drawn through the tested mask and the impactor under vacuum loaded with six Petri plates filled with tryptic soy agar (TSA, bioMérieux SA, Marcy-l'Etoile, France). The flow rate through the impactor during testing was equal to 28.3 L min^{-1}, and the duration of each test was 2 min. The testing was performed with the inside of the mask in contact with the bacterial challenge aerosol. The tested area of each mask was equal to 52.78 cm^2. For each tested mask, its BFE was given by the number of colony-forming units (CFU) passing through the mask material expressed as a percentage of the CFU present in the challenge aerosol. To calculate BFE, the following eqn (2) was used:

$$\mathrm{BFE} = ((C - T))/(C) \times 100 \quad (2)$$

where: C is the mean of the total plate counts for the two positive control runs, T is the total plate count for the tested mask.

Negative and positive control runs supplemented each test with the mask. A negative control run was performed by passing air, without adding the bacterial challenge, through the cascade impactor for 2 min. Positive control run without a tested mask was done twice, before and after tests using an impactor fully loaded with TSA plates. The first positive control run was carried out at the beginning of the tests. After the last mask was tested, the second positive control run was performed. The duration of each of them was also 2 min.

After each aerosol sampling, the Petri plates were incubated at 37 ± 2 °C for 20 to 52 h. After incubation, the number of bacterial colonies on each impactor plate was counted (considering the 'positive hole' conversion table provided by the impactor manufacturer), and the counts were added to the total number of CFU collected by the impactor.

Filterability and breathability measurements

An automated filter tester provided by Zhaohui Filter Technology Co. Ltd, China, was used to measure filtration efficiency and airflow resistance. The tester could deliver charge-neutralized monodisperse solid NaCl aerosol particles that had a mass mean diameter of 300–500 nm and a geometric standard deviation not exceeding 1.92. The neutralized NaCl aerosol particles were fed into a filter holder and down through the filter with 100 cm^2 of effective area.

Cell study

Confocal microscope LSM710 (Carl Zeiss, Munich, Germany) and Zen software (Zeiss) was used to visualize cells on the mask and verify the MTS assay results. Using the goniometer Data Physics OCA 15EC (Filderstadt, Germany), water contact angle measurements were used to determine the face mask's hydrophobicity.

Cell culture

Baby hamster kidney cells (BHK-21) were grown on a GMEM medium supplemented with 10% FBS, 2% TPB, 10 mL of 1M HEPES, 100 μg mL^{-1} penicillin, and 100 μg mg^{-1} streptomycin. Cells were maintained at 37 °C in a 5% CO_2 incubator.

Indirect cell viability

Cells were seeded onto a 24-well plate at a density of 50 000 cells in a volume of 500 μL medium per well. The pieces of masks with the size of 1.5 × 1.5 cm were cut out and incubated in 1 mL of the cell growth medium. Cells were cultured at 37 °C and 5% CO_2 for 24 h. Then the culture medium of cells was replaced with 0.5 mL of the medium in contact with the mask samples. Untreated cells growing on the bottom of the 24-well plate were used as a control. After 24 h of incubation at 37 °C and 5% CO_2, 50 μL of MTS cell proliferation reagent (Biovision) was added to all the wells. Medium cultured in the absence of cells was used as a background and subtracted from the results. Samples were incubated for 1 h until a color change was visible. 200 μL of samples from the 24-well plate were transferred to the 96-well plate, making technical duplicates for each condition. The absorbance was measured using a microplate recorder (Tecan Sunrise) at the O.D. of 490 nm.

Direct cell viability

Mask samples of 1.5 × 1.5 cm^2 were cut out and put into CellCrown™ 24-well plate inserts. Cells at density 50000 cells in a volume of 500 μL medium were seeded onto each mask sample. An additional 750 μL of the medium was added into the wells and incubated at 37 °C and 5% CO_2. Incubation times were 24 h, 48 h, 72 h, 5days, and 7 days. 500 μL of the medium was replaced with a fresh medium every 48 h. As a control, untreated cells growing at the bottom of the 24-well plate wells were selected. Background conditions were created by adding 1.25 mL of the fresh medium into the empty walls. After incubation, 125 μL of MTS Cell Proliferation reagent was added to the cells, control, and background wells. After 1 h of

incubation, the O.D. measurements were performed following the same protocol reported for the indirect method.

Cell morphology

Confocal microscope LSM710 (Carl Zeiss, Munich, Germany) and Zen software (Zeiss) was used to visualize cells on the mask after direct cell viability testing (masks were replaced between CellCrown™ inserts) and confirm the MTS assay results. The only difference was that the cells were seeded onto the mask samples at the density of 100 000 cells in 500 μL medium per well and incubated at 37 °C and 5% CO_2 for 48 h. After the incubation, the mask pieces with cells were removed from the inserts and washed with 1× PBS solution, after which they were fixed with 3.7% formaldehyde for 10 min at room temperature. After fixation, mask pieces with cells were washed with 1× PBS and permeabilized with 0.1% Triton-X solution for 3 min at room temperature. After permeabilization, the mask pieces were again washed with 1× PBS. Then the mask pieces with cells were placed on the microscopy slide and stained with 10 μL of the staining solution containing DAPI and Alexa 568 in 1× PBS. A drop of ROTI®Mount FluorCare DAPI (Carl Roth, Karlsruhe, Germany) was added. The sample was covered with microscopy cover glass and sealed with nail polish. Samples were visualized under the microscope. In addition, microscopy analyses were performed to confirm that the fixation process did not affect the cells on mask staining without fixation (ESI, Fig. S8†). For this analysis, the same protocol as above was used, but after 48 h of incubation, the samples seeded with cells were removed from the inserts, washed in 1× PBS solution, and treated with 50 μL of 10 μg mL^{-1} FM 4–64 (Invitrogen, ThermoFisher, USA) staining solution in DMSO. After 2 min, the mask pieces were placed on a microscope slide and visualized under the microscope.

Bacterial culture

S. aureus (ATCC 6538) was cultured on lysogeny broth (LB) agar and isolated with a streak plate method. An isolated colony was inoculated in 3 mL of fresh LB broth for a test and grown overnight at 37 °C in an orbital shaker.

NIR-light-activated bacterial inactivation

NIR Inactivation studies were performed in sterile flat-bottom 96-well plates. Briefly, the materials were cut into 6 mm diameter circles, sterilized under UV light on both sides for one hour (30 min per side) to reduce the bioburden, and glued to the bottom of the wells. *S. aureus* bacteria were cultured overnight in LB broth. Afterward, the bacterial culture was adjusted to 5 × 105 colony-forming units (CFU mL^{-1}) by adding fresh PBS. 100 μL of the bacterial solution was added to each well onto the materials' surface. The 96-well plate was subjected to NIR irradiation for 15 minutes upon reaching the target temperature of 60 °C. The pure bacterial suspension was used as a positive control. The test was conducted in triplicate for each material, while non-irradiated control samples were incubated in the dark at room temperature for 20 min. After irradiation or dark incubation, 100 μL of sterile PBS was added to each well to resuspend the bacteria. Then, 100 μL aliquots were transferred to another 96-well plate and serially diluted. Each dilution was plated on LB agar in 3 technical repetitions. The plates were then incubated at 37 °C overnight, and afterward, the bacterial colonies were counted to estimate the bacteria's survival.

The plating technique limited the highest degree of inactivation detectable and amounted to 3 log units of detection in CFU mL^{-1}, starting from 5×10^5 CFU mL^{-1}, thus allowing for the detection of survival rates ≥0.1%.

Finally, to provide high-quality macroscopic observations and the possibility to detect bacteria at a survival rate as low as 0.05%, each suspension was further diluted 10 more times, and 100 μL of each dilution was spread evenly on LB agar plates (representative plates) and incubated at 37 °C overnight.

Statistical analysis for filtration efficiency

The data on filtration efficiency for each group of tested masks were checked for the normality of their distribution. In the three tested cases (*i.e.*, A, B, and C), the Kolmogorov–Smirnov, Lilliefors, and Shapiro–Wilk's W tests revealed that all analyzed data in each group had a normal distribution. Hence, the analysis of the variance (ANOVA) was carried out to check the differences between groups of tested masks. The ANOVA showed that the BFE for surgical masks significantly differed from BFE for masks fabricated samples (Scheffe tests: in both cases $p < 0.000001$). There was no significant statistical difference between BFE calculated for single and double electrospun layer masks ($p > 0.05$).

Statistical analysis for cell viability

To calculate live cell population percentages, the following equations were used.

Eqn (3):

$$\text{Cell viability}(\%) = (\text{sample O.D.} - \text{background O.D.})/(\text{control O.D.} - \text{background O.D.}) \times 100 \quad (3)$$

Eqn (4):

$$\text{Cell viability } (\%) = (\text{sample O.D.})/(\text{control O.D.}) \times 100 \quad (4)$$

All experiments were performed once in three replicates. Results are expressed as an arithmetic mean ± SD. Statistical analysis was performed using one-way ANOVA and *post hoc* pairwise *t*-tests with MS Excel 365 software ($p < 0.05$). Holm's method was used for adjusting in the case of multiple comparisons.

Author contributions

F.P. and L.D.S. convinced the idea. F.P., P.N., and M.A.H.B. designed the experiment. M.A.H.B. fabricated the platforms and performed chemical characterization and photothermal characterizations. C.R. and O.C. conducted bacterial studies. D.R. and S.S.Z. Performed the photodynamic experiment. M.A.

H.B., A.Z., and P.N. performed the morphological characterization. K.P.P. and K.K. carried out *in vitro* tests. S.Z. and B.D. Performed particle filtration tests. A.S-K. and R.L.G. carried out the bacterial filtration tests. M.A.H.B. wrote the manuscript. All authors discussed the results and commented on the manuscript. F.P. supervised the project.

Conflicts of interest

There are no conflicts to declare.

Acknowledgements

This work was supported by the National Science Centre (NCN) SONATA BIS Project No. 2020/38/E/ST5/00456. This research was supported by the Estonian Research Council grant PRG1507 (K. Kogermann). Fig. 1, 3a, 4a, 5a, 5b, 6a, 7a, and 8a were created with Biorender; Fig. 5c, S3, and S5† were partially created with Biorender. C. R., P. N., and F. P. acknowledge the financial support from the Polish Ministry of Science and Higher Education through scholarships for outstanding young scientists.

References

1 P. Piscitelli, A. Miani, L. Setti, G. De Gennaro, X. Rodo, B. Artinano, E. Vara, L. Rancan, J. Arias, F. Passarini, P. Barbieri, A. Pallavicini, A. Parente, E. C. D'Oro, C. De Maio, F. Saladino, M. Borelli, E. Colicino, L. M. G. Gonçalves, G. Di Tanna, A. Colao, G. S. Leonardi, A. Baccarelli, F. Dominici, J. P. A. Ioannidis and J. L. Domingo, The Role of Outdoor and Indoor Air Quality in the Spread of SARS-CoV-2: Overview and Recommendations by the Research Group on COVID-19 and Particulate Matter RESCOP Commission, *Environ. Res.*, 2022, **211**, 113038, DOI: **10.1016/J.ENVRES.2022.113038**.

2 J. L. Domingo and J. Rovira, Effects of Air Pollutants on the Transmission and Severity of Respiratory Viral Infections, *Environ. Res.*, 2020, **187**, 109650, DOI: **10.1016/J.ENVRES.2020.109650**.

3 H. R. Lee, L. Liao, W. Xiao, A. Vailionis, A. J. Ricco, R. White, Y. Nishi, W. Chiu, S. Chu and Y. Cui, Three-Dimensional Analysis of Particle Distribution on Filter Layers inside N95 Respirators by Deep Learning, *Nano Lett.*, 2021, **21**(1), 651–657, DOI: **10.1021/ACS.NANOLETT.0C04230**.

4 V. Stadnytskyi, P. Anfinrud and A. Bax, Breathing, Speaking, Coughing or Sneezing: What Drives Transmission of SARS-CoV-2?, *J. Intern. Med.*, 2021, **290**(5), 1010–1027, DOI: **10.1111/JOIM.13326**.

5 S. Niazi, R. Groth, K. Spann and G. R. Johnson, The Role of Respiratory Droplet Physicochemistry in Limiting and Promoting the Airborne Transmission of Human Coronaviruses: A Critical Review, *Environ. Pollut.*, 2021, **276**, 112450, DOI: **10.1016/J.ENVPOL.2020.115767**.

6 V. S. Salian, J. A. Wright, P. T. Vedell, S. Nair, C. Li, M. Kandimalla, X. Tang, E. M. Carmona Porquera, K. R. Kalari and K. K. Kandimalla, COVID-19 Transmission, Current Treatment, and Future Therapeutic Strategies, *Mol. Pharm.*, 2021, **18**(3), 754–771, DOI: **10.1021/ACS.MOLPHARMACEUT.0C00608**.

7 Y. Cho, Y. Son, J. Ahn, H. Lim, S. Ahn, J. Lee, P. K. Bae and I. D. Kim, Multifunctional Filter Membranes Based on Self-Assembled Core-Shell Biodegradable Nanofibers for Persistent Electrostatic Filtration through the Triboelectric Effect, *ACS Nano*, 2022, **16**(11), 19451–19463, DOI: **10.1021/ACSNANO.2C09165**.

8 X. Xu, S. U. Ha and R. Basnet, A Review of Epidemiological Research on Adverse Neurological Effects of Exposure to Ambient Air Pollution, *Front. Public Health*, 2016, **4**, 157, DOI: **10.3389/FPUBH.2016.00157**.

9 S. Han, J. Kim, Y. Lee, J. Bang, C. G. Kim, J. Choi, J. Min, I. Ha, Y. Yoon, C. H. Yun, M. Cruz, B. J. Wiley and S. H. Ko, Transparent Air Filters with Active Thermal Sterilization, *Nano Lett.*, 2022, **22**, 524–532, DOI: **10.1021/ACS.NANOLETT.1C02737**.

10 X. Wang, Z. Xu, H. Su, H. C. Ho, Y. Song, H. Zheng, M. Z. Hossain, M. A. Khan, D. Bogale, H. Zhang, J. Wei and J. Cheng, Ambient Particulate Matter PM1, PM2.5, PM10 and Childhood Pneumonia: The Smaller Particle, the Greater Short-Term Impact?, *Sci. Total Environ.*, 2021, **772**, 145509, DOI: **10.1016/J.SCITOTENV.2021.145509**.

11 S. Zhang, H. Liu, N. Tang, N. Ali, J. Yu and B. Ding, Highly Efficient, Transparent, and Multifunctional Air Filters Using Self-Assembled 2D Nanoarchitectured Fibrous Networks, *ACS Nano*, 2019, **12**, 2663–2673, DOI: **10.1021/ACSNANO.9B07293**.

12 H. Liu, J. Yu, S. Zhang and B. Ding, Air-Conditioned Masks Using Nanofibrous Networks for Daytime Radiative Cooling, *Nano Lett.*, 2022, **22**, 9485–9492, DOI: **10.1021/ACS.NANOLETT.2C03585**.

13 J. K. Kodros, K. O'Dell, J. M. Samet, C. L'Orange, J. R. Pierce and J. Volckens, Quantifying the Health Benefits of Face Masks and Respirators to Mitigate Exposure to Severe Air Pollution, *GEOHealth*, 2021, **5**, 482, DOI: **10.1029/2021GH000482**.

14 X. Jin, F. Gao, M. Qin, Y. Yu, Y. Zhao, T. Shao, C. Chen, W. Zhang, B. Xie, Y. Xiong, L. Yang and Y. Wu, How to Make Personal Protective Equipment Spontaneously and Continuously Antimicrobial Incorporating Oxidase-like Catalysts, *ACS Nano*, 2021, 7755–7771, DOI: **10.1021/ACSNANO.1C11647**.

15 S. Ullah, A. Ullah, J. Lee, Y. Jeong, M. Hashmi, C. Zhu, K. Il Joo, H. J. Cha and I. S. Kim, Reusability Comparison of Melt-Blown vs Nanofiber Face Mask Filters for Use in the Coronavirus Pandemic, *ACS Appl. Nano Mater.*, 2020, **3**, 7231–7241, DOI: **10.1021/ACSANM.0C01562**.

16 K. Iheduru-Anderson, Reflections on the Lived Experience of Working with Limited Personal Protective Equipment

during the COVID-19 Crisis, *Nurs. Inq.*, 2021, **28**, 12382, DOI: **10.1111/NIN.12382**.

17 L. De Sio, B. Ding, M. Focsan, K. Kogermann, P. Pascoal-Faria, F. Petronela, G. Mitchell, E. Zussman and F. Pierini, Personalized Reusable Face Masks with Smart Nano-Assisted Destruction of Pathogens for COVID-19: A Visionary Road, *Chem. – Eur. J.*, 2021, **27**, 6112–6130, DOI: **10.1002/CHEM.202004875**.

18 A. Tuñón-Molina, K. Takayama, E. M. Redwan, V. N. Uversky, J. Andrés and Á. Serrano-Aroca, Protective Face Masks: Current Status and Future Trends, *ACS Appl. Mater. Interfaces*, 2021, 56725, DOI: **10.1021/ACSAMI.1C12227**.

19 N. El-Atab, N. Qaiser, H. Badghaish, S. F. Shaikh, M. M. Hussain and M. M. Hussain, Flexible Nanoporous Template for the Design and Development of Reusable Anti-COVID-19 Hydrophobic Face Masks, *ACS Nano*, 2020, 7659, DOI: **10.1021/ACSNANO.0C03976**.

20 Z. Ye, Y. Ling, M. Yang, Y. Xu, L. Zhu, Z. Yan and P. Y, A Breathable, Reusable, and Zero-Power Smart Face Mask for Wireless Cough and Mask-Wearing Monitoring, *ACS Nano*, 2022, 5874, DOI: **10.1021/ACSNANO.1C11041**.

21 F. G. Torres and G. E. De-la-Torre, Face Mask Waste Generation and Management during the COVID-19 Pandemic: An Overview and the Peruvian Case, *Sci. Total Environ.*, 2021, 147628, DOI: **10.1016/J.SCITOTENV.2021.147628**.

22 G. Varghese, P. J. Deepthi, A. David, A. Karuth, J. Fatima, M. Jafferali, S. Begum, J. George, B. Rasulev and P. Raghavan, Experimental and Simulation Studies on Nonwoven Polypropylene– Nitrile Rubber Blend: Recycling of Medical Face Masks to an Engineering Product, *ACS Omega*, 2022, 4791, DOI: **10.1021/acsomega.1c04913**.

23 S. Sangkham, Face Mask and Medical Waste Disposal during the Novel COVID-19 Pandemic in Asia, *Case Stud. Chem. Environ. Eng.*, 2020, 100052, DOI: **10.1016/J.CSCEE.2020.100052**.

24 M. Yousefi, V. Oskoei, A. Jonidi Jafari, M. Farzadkia, M. Hasham Firooz, B. Abdollahinejad and J. Torkashvand, Municipal Solid Waste Management during COVID-19 Pandemic: Effects and Repercussions, *Environ. Sci. Pollut. Res.*, 2021, 32200–32209, DOI: **10.1007/S11356-021-14214-9**.

25 J. Xue, T. Wu, Y. Dai and Y. Xia, Electrospinning and Electrospun Nanofibers: Methods Materials and Applications, *Chem. Rev.*, 2019, 5415, DOI: **10.1021/ACS.CHEMREV.8B00593**.

26 P. Nakielski and F. Pierini, Blood Interactions with Nano- and Microfibers: Recent Advances, Challenges and Applications in Nano- and Microfibrous Hemostatic Agents, *Acta Biomater.*, 2019, **84**, 63–76, DOI: **10.1016/J.ACTBIO.2018.11.029**.

27 Y. Ziai, F. Petronella, C. Rinoldi, P. Nakielski, A. Zakrzewska, T. A. Kowalewski, W. Augustyniak, X. Li, A. Calogero, I. Sabała, B. Ding, L. De Sio and F. Pierini, Chameleon-Inspired Multifunctional Plasmonic Nanoplatforms for Biosensing Applications, *NPG Asia Mater.*, 2022, **14**, 1–17, DOI: **10.1038/s41427-022-00365-9**.

28 M. A. Haghighat Bayan, F. Afshar Taromi, M. Lanzi and F. Pierini, Enhanced Efficiency in Hollow Core Electrospun Nanofiber-Based Organic Solar Cells, *Sci. Rep.*, 2021, **11**, 1–11, DOI: **10.1038/s41598-021-00580-4**.

29 C. Huang, S. J. Soenen, J. Rejman, B. Lucas, K. Braeckmans, J. Demeester and S. C. De Smedt, Stimuli-Responsive Electrospun Fibers and Their Applications, *Chem. Soc. Rev.*, 2011, 2417, DOI: **10.1039/C0CS00181C**.

30 D. Han, X. Yu, Q. Chai, N. Ayres and A. J. Steckl, Stimuli-Responsive Self-Immolative Polymer Nanofiber Membranes Formed by Coaxial Electrospinning, *ACS Appl. Mater. Interfaces*, 2017, 11858, DOI: **10.1021/ACSAMI.6B16501**.

31 M. A. Haghighat Bayan, Y. J. Dias, C. Rinoldi, P. Nakielski, D. Rybak, Y. B. Truong, A. L. Yarin and F. Pierini, Near-Infrared Light Activated Core-Shell Electrospun Nanofibers Decorated with Photoactive Plasmonic Nanoparticles for on-Demand Smart Drug Delivery Applications, *J. Polym. Sci.*, 2023, **7**, 521–533, DOI: **10.1002/POL.20220747**.

32 A. Zakrzewska, M. A. Haghighat Bayan, P. Nakielski, F. Petronella, L. De Sio and F. Pierini, Nanotechnology Transition Roadmap toward Multifunctional Stimuli-Responsive Face Masks, *ACS Appl. Mater. Interfaces*, 2022, **14**(41), 46123–46144, DOI: **10.1021/ACSAMI.2C10335**.

33 C. Rinoldi, Y. Ziai, S. S. Zargarian, P. Nakielski, K. Zembrzycki, M. A. Haghighat Bayan, A. B. Zakrzewska, R. Fiorelli, M. Lanzi, A. Kostrzewska-Księżyk, R. Czajkowski, E. Kublik, L. Kaczmarek and F. Pierini, In Vivo Chronic Brain Cortex Signal Recording Based on a Soft Conductive Hydrogel Biointerface, *ACS Appl. Mater. Interfaces*, 2022, **15**, 6283–6298, DOI: **10.1021/ACSAMI.2C17025**.

34 D. Annur, Z. K. Wang, J. Der Liao and C. Kuo, Plasma-Synthesized Silver Nanoparticles on Electrospun Chitosan Nanofiber Surfaces for Antibacterial Applications, *Biomacromolecules*, 2015, 3248, DOI: **10.1021/ACS.BIOMAC.5B00920**.

35 C. A. S. Ballesteros, D. S. Correa and V. Zucolotto, Polycaprolactone Nanofiber Mats Decorated with Photoresponsive Nanogels and Silver Nanoparticles: Slow Release for Antibacterial Control, *Mater. Sci. Eng., C*, 2020, 110334, DOI: **10.1016/J.MSEC.2019.110334**.

36 M. Aravind, M. Amalanathan, S. Aslam, A. E. Noor, D. Jini, S. Majeed, P. Velusamy, A. A. Alothman, R. A. Alshgari, M. S. Saleh Mushab and M. Sillanpaa, Hydrothermally Synthesized Ag-TiO2 Nanofibers NFs for Photocatalytic Dye Degradation and Antibacterial Activity, *Chemosphere*, 2023, 138077, DOI: **10.1016/J.CHEMOSPHERE.2023.138077**.

37 M. Mariello, A. Qualtieri, G. Mele and M. De Vittorio, Metal-Free Multilayer Hybrid PENG Based on Soft Electrospun/-Sprayed Membranes with Cardanol Additive for Harvesting Energy from Surgical Face Masks, *ACS Appl. Mater. Interfaces*, 2021, 20606, DOI: **10.1021/ACSAMI.1C01740**.

38 D. A. Giljohann, D. S. Seferos, W. L. Daniel, M. D. Massich, P. C. Patel and C. A. Mirkin, Gold Nanoparticles for Biology and Medicine, *Angew. Chem., Int. Ed.*, 2010, 3280, DOI: **10.1002/ANIE.200904359**.

39 H. H. Jeong, E. Choi, E. Ellis and T. C. Lee, Recent Advances in Gold Nanoparticles for Biomedical Applications: From Hybrid Structures to Multi-Functionality, *J. Mater. Chem. B*, 2019, 3480, DOI: 10.1039/C9TB00557A.

40 J. Kang, G. Yeom, H. Jang, J. Oh, C. J. Park and M. G. Kim, Development of Replication Protein A-Conjugated Gold Nanoparticles for Highly Sensitive Detection of Disease Biomarkers, *Anal. Chem.*, 2019, 10001, DOI: 10.1021/ACS.ANALCHEM.9B01827.

41 Q. Wang, Z. H. Ren, W. M. Zhao, L. Wang, X. Yan, A. S. Zhu, F. M. Qiu and K. K. Zhang, Research Advances on Surface Plasmon Resonance Biosensors, *Nanoscale*, 2022, 564, DOI: 10.1039/D1NR05400G.

42 Y. Wang, Y. Wang, I. Aravind, Z. Cai, L. Shen, B. Zhang, B. Wang, J. Chen, B. Zhao, H. Shi, J. M. Dawlaty and S. B. Cronin, In Situ Investigation of Ultrafast Dynamics of Hot Electron-Driven Photocatalysis in Plasmon-Resonant Grating Structures, *J. Am. Chem. Soc.*, 2022, 3517, DOI: 10.1021/JACS.1C12069.

43 A. R. Peringath, M. A. H. Bayan, M. Beg, A. Jain, F. Pierini, N. Gadegaard, R. Hogg and L. Manjakkal, Chemical Synthesis of Polyaniline and Polythiophene Electrodes with Excellent Performance in Supercapacitors, *J. Energy Storage*, 2023, 108811, DOI: 10.1016/J.EST.2023.108811.

44 A. Guglielmelli, F. Pierini, N. Tabiryan, C. Umeton, T. J. Bunning and L. De Sio, Thermoplasmonics with Gold Nanoparticles: A New Weapon in Modern Optics and Biomedicine, *Adv. Photonics Res.*, 2021, 2000198, DOI: 10.1002/ADPR.202000198.

45 P. Nakielski, S. Pawłowska, C. Rinoldi, Y. Ziai, L. De Sio, O. Urbanek, K. Zembrzycki, M. Pruchniewski, M. Lanzi, E. Salatelli, A. Calogero, T. A. Kowalewski, A. L. Yarin and F. Pierini, Multifunctional Platform Based on Electrospun Nanofibers and Plasmonic Hydrogel: A Smart Nanostructured Pillow for Near-Infrared Light-Driven Biomedical Applications, *ACS Appl. Mater. Interfaces*, 2020, 54328, DOI: 10.1021/ACSAMI.0C13266.

46 M. R. Younis, R. B. An, Y. C. Yin, S. Wang, D. Ye and X. H. Xia, Plasmonic Nanohybrid with High Photothermal Conversion Efficiency for Simultaneously Effective Antibacterial/Anticancer Photothermal Therapy, *ACS Appl. Bio Mater.*, 2019, 3942, DOI: 10.1021/ACSABM.9B00521.

47 Y. Zhong, X. T. Zheng, S. Zhao, X. Su and X. J. Loh, Stimuli-Activable Metal-Bearing Nanomaterials and Precise On-Demand Antibacterial Strategies, *ACS Nano*, 2022, 19840, DOI: 10.1021/ACSNANO.2C08262.

48 P. Li, J. Li, X. Feng, J. Li, Y. Hao, J. Zhang, H. Wang, A. Yin, J. Zhou, X. Ma and B. Wang, Metal-Organic Frameworks with Photocatalytic Bactericidal Activity for Integrated Air Cleaning, *Nat. Commun.*, 2019, **10**, 1–10, DOI: 10.1038/s41467-019-10218-9.

49 P. Kumar, S. Roy, A. Sarkar and A. Jaiswal, Reusable MoS2-Modified Antibacterial Fabrics with Photothermal Disinfection Properties for Repurposing of Personal Protective Masks, *ACS Appl. Mater. Interfaces*, 2021, 12912, DOI: 10.1021/ACSAMI.1C00083.

50 W. Guo, W. Gao, Q. Li, S. Qu, L. Zhang, L. L. Tan and L. Shang, Plasmon-Enhanced Visible-Light Photocatalytic Antibacterial Activity of Metal–Organic Framework/Gold Nanocomposites, *J. Mater. Chem. A*, 2023, 2391, DOI: 10.1039/D2TA09061A.

51 L. Shao, S. Majumder, Z. Liu, K. Xu, R. Dai and S. George, Light Activation of Gold Nanorods but Not Gold Nanospheres Enhance Antibacterial Effect through Photodynamic and Photothermal Mechanisms, *J. Photochem. Photobiol., B*, 2022, 112450, DOI: 10.1016/J.JPHOTOBIOL.2022.112450.

52 S. Gao, W. Yue, C. S. Park, S. S. Lee, E. S. Kim and D. Y. Choi, Aluminum Plasmonic Metasurface Enabling a Wavelength-Insensitive Phase Gradient for Linearly Polarized Visible Light, *ACS Photonics*, 2017, 322, DOI: 10.1021/ACSPHOTONICS.6B00783.

53 Z. Lan, Y. Lei, W. K. E. Chan, S. Chen, D. Luo and F. Zhu, Near-Infrared and Visible Light Dual-Mode Organic Photodetectors, *Sci. Adv.*, 2020, **6**, 5, DOI: 10.1126/SCIADV.AAW8065.

54 W. Yang, B. Xia, L. Wang, S. Ma, H. Liang, D. Wang and J. Huang, Effects of Gold Nanoparticles in Photothermal Cancer Therapy, *Mater. Today Sustainability*, 2021, 100078, DOI: 10.1016/J.MTSUST.2021.100078.

55 K. Soliwoda, M. Rosowski, E. Tomaszewska, B. Tkacz-Szczesna, G. Celichowski and J. Grobelny, Electrospray Deposition of Gold Nanoparticles from Aqueous Colloids on Solid Substrates, *Colloids Surf., A*, 2015, 211, DOI: 10.1016/J.COLSURFA.2015.09.035.

56 H. Aldewachi, T. Chalati, M. N. Woodroofe, N. Bricklebank, B. Sharrack and P. Gardiner, Gold Nanoparticle-Based Colorimetric Biosensors, *Nanoscale*, 2017, **10**, 18–33, DOI: 10.1039/C7NR06367A.

57 E. Passaglia, B. Campanella, S. Coiai, F. Cicogna, A. Carducci, M. Verani, I. Federigi, B. Casini, B. Tuvo and E. Bramanti, Agri-Food Extracts Effectiveness in Improving Antibacterial and Antiviral Properties of Face Masks: A Proof-of-Concept Study, *ChemistrySelect*, 2021, 2288, DOI: 10.1002/SLCT.202004678.

58 S. W. Xiong, P. G. Fu, Q. Zou, L. Y. Chen, M. Y. Jiang, P. Zhang, Z. G. Wang, L. S. Cui, H. Guo and J. G. Gai, Heat Conduction and Antibacterial Hexagonal Boron Nitride/Polypropylene Nanocomposite Fibrous Membranes for Face Masks with Long-Time Wearing Performance, *ACS Appl. Mater. Interfaces*, 2021, 196, DOI: 10.1021/ACSAMI.0C17800.

59 A. Chompoosor, K. Saha, P. S. Ghosh, D. J. MacArthy, O. R. Miranda, Z. J. Zhu, K. F. Arcaro and V. M. Rotello, The Role of Surface Functionality on Acute Cytotoxicity, ROS Generation and DNA Damage by Cationic Gold Nanoparticles, *Small*, 2010, 2246, DOI: 10.1002/SMLL.201000463.

60 Y. Higashi, J. Mazumder, H. Yoshikawa, M. Saito and E. Tamiya, Chemically Regulated ROS Generation from

Gold Nanoparticles for Enzyme-Free Electrochemiluminescent Immunosensing, *Anal. Chem.*, 2018, 5773, DOI: **10.1021/ACS.ANALCHEM.8B00118**.

61 U. N. T. Nguyen, K. H. Do, B. Jang, K. S. Kim, J. H. Kim and S. M. Lee, Always-on Photocatalytic Antibacterial Facemask with Mini UV-LED Array, *Mater. Today Sustainability*, 2022, 100117, DOI: **10.1016/J.MTSUST.2022.100117**.

62 P. Tang, Z. Zhang, A. Y. El-Moghazy, N. Wisuthiphaet, N. Nitin and G. Sun, Daylight-Induced Antibacterial and Antiviral Cotton Cloth for Offensive Personal Protection, *ACS Appl. Mater. Interfaces*, 2020, 49442, DOI: **10.1021/ACSAMI.0C15540**.

63 A. Kumar, A. Sharma, Y. Chen, M. M. Jones, S. T. Vanyo, C. Li, M. B. Visser, S. D. Mahajan, R. K. Sharma and M. T. Swihart, Copper@ZIF-8 Core-Shell Nanowires for Reusable Antimicrobial Face Masks, *Adv. Funct. Mater.*, 2021, 2008054, DOI: **10.1002/ADFM.202008054**.

64 A. Ray Chowdhuri, S. Tripathy, S. Chandra, S. Roy and S. K. Sahu, A ZnO Decorated Chitosan–Graphene Oxide Nanocomposite Shows Significantly Enhanced Antimicrobial Activity with ROS Generation, *RSC Adv.*, 2015, 49420, DOI: **10.1039/C5RA05393E**.

65 X. Chen, T. Yu, Q. Kong, H. Xu, Z. Zhao, G. Li, H. Fan and Y. Wang, A Chlorogenic Acid Functional Strategy of Anti-Inflammation, Anti-Coagulation and Promoted Endothelial Proliferation for Bioprosthetic Artificial Heart Valves, *J. Mater. Chem. B*, 2023, 2663, DOI: **10.1039/D2TB02407A**.

66 M. Scungio and G. Parlani, Determining the Filtration Effectiveness of Non-Standard Respiratory Protective Devices by an Ad-Hoc Laboratory Methodology, *Atmos. Environ.*, 2023, 119731, DOI: **10.1016/J.ATMOSENV.2023.119731**.

67 T. A. Sipkens, J. C. Corbin, A. Oldershaw and G. J. Smallwood, Particle Filtration Efficiency Measured Using Sodium Chloride and Polystyrene Latex Sphere Test Methods, *Sci. Data*, 2022, **9**, 1–7, DOI: **10.1038/s41597-022-01860-y**.

68 S. Y. C. Tong, J. S. Davis, E. Eichenberger, T. L. Holland and V. G. Fowler, Staphylococcus Aureus Infections: Epidemiology, Pathophysiology, Clinical Manifestations, and Management, *Clin. Microbiol. Rev.*, 2015, 603, DOI: **10.1128/CMR.00134-14**.

69 M. Okkeh, N. Bloise, E. Restivo, L. De Vita, P. Pallavicini and L. Visai, Gold Nanoparticles: Can They Be the Next Magic Bullet for Multidrug-Resistant Bacteria?, *Nanomaterials*, 2021, 312, DOI: **10.3390/NANO11020312**.

70 S. Seifer and M. Elbaum, Thermal Inactivation Scaling Applied for SARS-CoV-2, *Biophys. J.*, 2021, 1054, DOI: **10.1016/J.BPJ.2020.11.2259**.

71 M. J. Reiniers, R. F. Van Golen, S. Bonnet, M. Broekgaarden, T. M. Van Gulik, M. R. Egmond and M. Heger, Preparation and Practical Applications of 2′,7′-Dichlorodihydrofluorescein in Redox Assays, *Anal. Chem.*, 2017, 3853, DOI: **10.1021/ACS.ANALCHEM.7B00043**.

RESEARCH ARTICLE

ADVANCED MATERIALS TECHNOLOGIES
www.advmattechnol.de

Solar-to-NIR Light Activable PHBV/ICG Nanofiber-Based Face Masks with On-Demand Combined Photothermal and Photodynamic Antibacterial Properties

*Mohammad Ali Haghighat Bayan, Chiara Rinoldi, Alicja Kosik-Kozioł, Magdalena Bartolewska, Daniel Rybak, Seyed Shahrooz Zargarian, Syed Ahmed Shah, Zuzanna J. Krysiak, Shichao Zhang, Massimiliano Lanzi, Paweł Nakielski, Bin Ding, and Filippo Pierini**

Hierarchical nanostructures fabricate by electrospinning in combination with light-responsive agents offer promising scenarios for developing novel activable antibacterial interfaces. This study introduces an innovative antibacterial face mask developed from poly(3-hydroxybutyrate-*co*-3-hydroxyvalerate) (PHBV) nanofibers integrated with indocyanine green (ICG), targeting the urgent need for effective antimicrobial protection for community health workers. The research focuses on fabricating and characterizing this nanofibrous material, evaluating the mask's mechanical and chemical properties, investigating its particle filtration, and assessing antibacterial efficacy under photothermal conditions for reactive oxygen species (ROS) generation. The PHBV/ICG nanofibers are produced using an electrospinning process, and the nanofibrous construct's morphology, structure, and photothermal response are investigated. The antibacterial efficacy of the nanofibers is tested, and substantial bacterial inactivation under both near-infrared (NIR) and solar irradiation is demonstrated due to the photothermal response of the nanofibers. The material's photothermal response is further analyzed under cyclic irradiation to simulate real-world conditions, confirming its durability and consistency. This study highlights the synergistic impact of PHBV and ICG in enhancing antibacterial activity, presenting a biocompatible and environmentally friendly solution. These findings offer a promising path for developing innovative face masks that contribute significantly to the field of antibacterial materials and solve critical public health challenges.

1. Introduction

Public health concerns are increasingly directed toward issues caused by disease-causing microorganisms, with the COVID-19 pandemic as a prominent example of their global impact.[1–3] The control and prevention of pathogen transmission are critical in averting infections and halting epidemic spread, highlighting the need for effective methods to eradicate these microorganisms. Face masks and protective garments commonly provide a protective barrier, preventing these microbial entities from reaching the human body.[4]

Fabrics and clothing that interact with infected persons are significant carriers of pathogens.[5] Remarkably, even thoroughly cleaned fabrics can accumulate millions of bacteria within hours of use, leading to the risk of cross-infection.[6] These events underscore the critical role of antibacterial textiles in daily life. Such fabrics offer an efficient means to thwart bacterial infections and lessen the spread of bacteria.

M. A. Haghighat Bayan, C. Rinoldi, A. Kosik-Kozioł, M. Bartolewska, D. Rybak, S. S. Zargarian, S. A. Shah, Z. J. Krysiak, P. Nakielski, F. Pierini
Department of Biosystems and Soft Matter
Institute of Fundamental Technological Research
Polish Academy of Sciences
Warsaw 02–106, Poland
E-mail: fpierini@ippt.pan.pl

S. Zhang, B. Ding
Innovation Center for Textile Science and Technology
College of Textiles
Donghua University
Shanghai 201620, China

M. Lanzi
Department of Industrial Chemistry "Toso Montanari"
University of Bologna
Viale Risorgimento 4, Bologna 40136, Italy

F. Pierini
Department of Biosystems and Soft Matter
Institute of Fundamental Technological Research
Polish Academy of Sciences
ul. Pawińskiego 5B, Warsaw 02–106, Poland

The ORCID identification number(s) for the author(s) of this article can be found under https://doi.org/10.1002/admt.202400450

DOI: 10.1002/admt.202400450

Several innovative approaches, including photocatalytic, photodynamic, and phototherapy, are being developed to tackle bacterial infections.[7–12] These techniques are particularly noteworthy for their swift and potent antibacterial effects and address issues related to bacterial resistance and environmental impact. Thanks to its adaptability and practicality, phototherapy is a promising technique for creating antibacterial fabrics.[13–17] Specific class of materials responsive to light can be activated by specific light wavelengths, which produce antibacterial agents. This process leverages light energy to generate ROS and/or induce hyperthermia, quickly eradicating bacteria upon activation.[18–21]

PHBV, an FDA-approved biodegradable aliphatic polyester, is renowned for its wide-ranging use in pharmaceutical and biomedical fields.[22] PHBV is remarkably esteemed as a semicrystalline polymer for its excellent biocompatibility, environmental friendliness, and non-toxic properties. Its remarkable flexibility and moldability make it an ideal candidate for polymer-based matrices, especially in pharmaceuticals and textile manufacturing.[23,24]

ICG is a well-regarded near-infrared fluorescent dye approved by the FDA and is extensively used in pharmaceutical and biomedical applications.[25] Its standout features include high biocompatibility, quick bodily elimination, minimal toxicity, and responsiveness to NIR light.[26] These attributes render ICG an invaluable asset in various applications.[27] Its distinctive spectral qualities and safety profile are noteworthy, establishing ICG as an optimal candidate for photodynamic photosensitization under near-infrared or solar irradiation.[28]

Recently, several photoresponsive materials have been engineered to eliminate bacteria through phototherapy. These include plasmonic nanoparticles, metallic oxides, and various organic compounds.[17,29–35] Inorganic materials are often favored for photothermal applications. However, they present significant limitations concerning safety and integration into fibrous matrices. The inhalation of inorganic nanoparticles is a serious concern, particularly in face mask applications. Conversely, organic materials, such as PHBV and ICG, offer notable advantages. Organic materials eliminate nanoparticle inhalation risks and can be seamlessly embedded within the fibrous matrix, ensuring uniform distribution and consistent performance without the risk of nanoparticle release. This makes organic materials safer and more practical for developing photothermal face masks designed for prolonged and direct human use. Their functionality can be primarily divided into 2 categories: photodynamic therapy (PDT) and photothermal therapy (PTT). PDT operates by inducing electron-hole pairs in the photoresponsive materials when exposed to specific light wavelengths.[36] These electron-hole pairs interact with oxygen or water molecules nearby to produce ROS, breaking down bacterial structures like cell membranes, DNA, and proteins. On the other hand, PTT works through the interaction of photons with the material's lattice structure, causing vibrations that increase the material's temperature, thus deactivating bacteria. A key aspect of PTT is managing the rise in temperature to prevent damage to surrounding healthy tissues.[37–41] Temperatures exceeding 60 to 100 °C effectively kill most bacteria, depending on the species and exposure time.[42] Wang et al. demonstrated the effectiveness of various substances, including plasmonic nanomaterials and metal oxides, in antibacterial applications.[43] However, challenges such as potential toxicity and environmental concerns remain.[44–45] Our study contributes to this field by proposing a biocompatible and environmentally friendly solution that leverages the unique properties of PHBV and ICG.

Electrospinning, an evolving technique, is gaining attention for producing ultrafine fibers from polymers and their composites. This technology finds diverse applications, including in the energy field, wound dressings, drug delivery systems, and protective clothing.[46–50] The nanofibers produced through electrospinning form a 3D network characterized by interlinked pores. This structure uniquely combines mechanical robustness, a vast surface area, and the inherent flexibility of polymers and composites.[51–53] Electrospinning with photoresponsive materials opens the potential for developing wearable fabrics endowed with safe and efficient antibacterial properties. This technique facilitates the fabrication of photoresponsive fibers, thereby enabling the fabrication of nanofibers tailored for filtration applications.

This study hypothesizes that integrating light-responsive agents into electrospun nanofibers can significantly enhance the antibacterial properties of face masks. The rationale behind this hypothesis is that electrospun materials' fibrous structure can create a dense network capable of effectively capturing airborne particles. By incorporating photothermal agents like ICG, which can generate heat and ROS upon light exposure, we aim to develop a mask that filters particles and actively eradicates pathogens.

This research introduced a biocompatible nanofibrous textile made from PHBV and ICG. This nanofibrous structure, created through electrospinning, suggests major progress in fabricating antibacterial face masks. Briefly, a solution containing PHBV and ICG was subjected to an electric field, resulting in the elongation of the mixture into nanofibers, which were then collected on a rotating drum. Upon exposure to NIR light or solar light, these nanofibers generate ROS and a rise in temperature. The synergistic effect of ROS production and temperature increase proved highly effective in eradicating 99.95% of *E. Coli* as a gram-negative bacterium and 99.94% of *S. Aureus* as a gram-positive bacterium. The fabricated mask also ensured biological safety, improved particle filtration efficiency, and possessed desirable mechanical properties.

2. Experimental Section

2.1. Materials

Poly(3-hydroxybutyric acid-*co*-3-hydroxyvaleric acid) (PHBV, Mw = 580.9 kDa, Sigma Aldrich), Indocyanine Green (ICG, Pharmaceutical Primary Standard, Sigma Aldrich), Sodium Hydroxide (NaOH, 97.0%, Sigma Aldrich), 2,2,2-Trifluoroethanol (TFE, 99.0%, Sigma Aldrich), 2-Propanol (99.5%, Sigma Aldrich), N,N-dimethylformamide (DMF, 99.0%, Sigma Aldrich), 1,1,1,3,3,3-Hexafluoro-2-propanol (HFIP, 99.0%, Sigma Aldrich), 1-Methyl-2-pyrrolidinone (NMP, 99.0%, Sigma Aldrich), Methanol (99.6%, Sigma Aldrich), Ethanol (96.0%, Sigma Aldrich), Hydrochloric Acid (HCl, 37.0%, Sigma Aldrich), Chloroform (99.5%, Sigma Aldrich), 2,7-Dichlorofluorescein ($DCFH_2$-DA,90%, Sigma Aldrich), Glutaraldehyde (GTA, 50%, Sigma Aldrich), Surgical Face Mask (Mobiclinic SA), Dulbecco's modified Eagle's medium

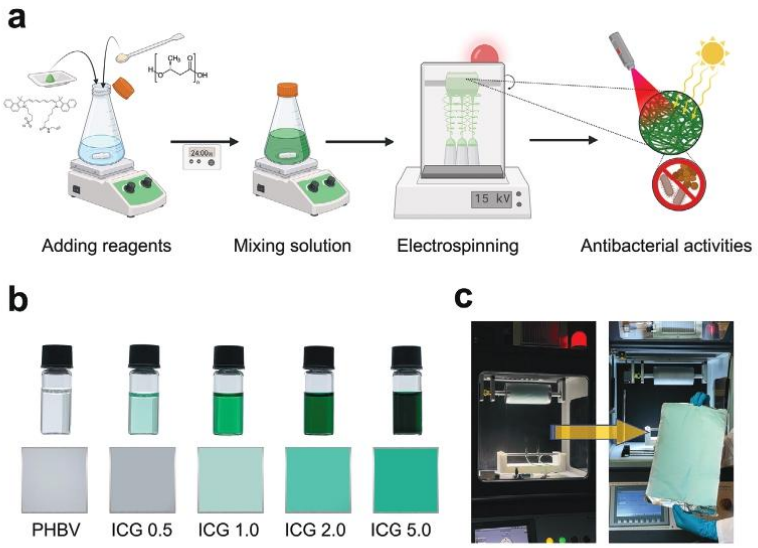

Figure 1. a) Schematic of the preparation of the solution from PHBV and ICG followed by the fabrication process for on-demand photothermal antibacterial eradication. b) Comparison of the appearance of the 5 ICG/PHBV solutions adopted in this study alongside the final spun textile, and c) Photographs representing the fabricated textile of ICG 2.0 during and after the electrospinning process.

(DMEM), Fetal Bovine Serum (FBS), Penicillin-Streptomycin (PS, Gibco Invitrogen), EDTA-trypsin (Gibco Invitrogen), Presto-Blue reagent (Thermo-Fisher Scientific), live/dead cytotoxicity kit assay (Thermo-Fisher Scientific), Phosphate buffer saline (PBS, Sigma Aldrich), hexamethyldisilane (HMDS, Sigma Aldrich), Lysogeny broth (LB, A&A Biotechnology), lysogeny agar (LB agar, A&A Biotechnology), Gram-negative bacteria *Escherichia Coli* (*E. Coli*, ATCC 25 922, Pol-AURA), and gram-positive *Staphylococcus Aureus* (*S. Aureus*, ATCC 6538, Pol-AURA). The CAS number of the chemicals used can be found in Table S1 (Supporting Information).

2.2. Methods

2.2.1. Electrospinning of PHBV Nanofibers

A 2% (w/w) solution of PHBV was prepared by dissolving the polymer in a TFE solvent. The solution was stirred continuously overnight at room temperature for the complete dissolution of the polymer. The electrospinning process was conducted using an Inovenso Nanospinner 24-nozzle Electrospinning Machine. The rotary drum of this machine is situated on the top of its chamber, while the syringe pump and the polymeric solutions are on the bottom in a semi-pilot scale. The key parameters for the electrospinning process were as follows: The PHBV solution's flow rate through the electrospinning setup was maintained at 400 µL h^{-1}. This flow rate was optimal for testing from 200 to 2000 µL h^{-1} to form a consistent polymer jet without causing solution dripping. The distance between the needle tip and the collector was 15 cm. An electrical potential of 15.0 kV was applied to the system, and negative voltage was applied to the collector. A 26-gauge needle was equipped for the process. The electrospinning was performed at room temperature with a relative humidity (RH) of 65%, and the nanofibers were collected on a grounded rotating drum collector, which was covered with aluminum foil. The face mask was stuck on the drum collector, and the electrospinning was conducted on the surface of the face mask. For the alternative structure, the middle layer of the face mask was put on the collector. The fabrication procedure can be seen in **Figure 1**a. To investigate the effect of ICG on the antibacterial properties of PHBV nanofibers, 5 different sample compositions were prepared (Figure 1b) as follows: pure PHBV, PHBV with 0.5% w/w of ICG, PHBV with 1% w/w ICG, PHBV with 2% w/w ICG, and PHBV with 5% w/w ICG, codenamed as PHBV, ICG 0.5, ICG 1.0, ICG 2.0, and ICG 5.0, respectively. Each formulation was electrospun using the Inovenso machine under the same conditions. The photograph of the electrospun mat during the electrospinning process and after the completion of spinning is also presented in Figure 1c.

2.3. Characterization of the Fibrous Materials

2.3.1. Morphological Studies

A comprehensive investigation was conducted using scanning electron microscopy (SEM). SEM analysis explored the morphological structure of the fabricated nanofibrous textile of PHBV and ICG-incorporated samples. Moreover, it confirmed the range

of cells spreading across the samples. This imaging technique was essential in revealing the complicated structural details of the samples under study. The SEM examinations were carried out using a high-precision JEOL JSM-6390LV microscope. The parameters set for this analysis included an accelerating voltage of 15 kV and a carefully adjusted working distance of 14 mm to ensure clear, detailed images. Before SEM, the samples were coated with layers of gold with a Quorum Technologies SC7620 Polaron mini sputter coater.

2.3.2. Chemical Characterizations

ATR-FTIR, UV–Vis, and Raman spectrometry characterized the chemical composition and structures. The Raman spectra were acquired with Labram 800 HR Raman spectrometer (laser excitation: 532 nm) (Horiba Jobin Yvon), observing the Raman shifts from 450 to 2080 cm^{-1}. Attenuated Total Reflectance Fourier Transform Infrared (ATR-FTIR) spectroscopy was used to identify and analyze the functional groups of the materials. This was achieved using a Bruker Vertex70 FT-IR Spectrometer, which measured the material's transmittance across the wavenumber spectrum ranging from 4000 to 400 cm^{-1}. The spectrometer was set to a resolution of 2 cm^{-1}, ensuring detailed and accurate spectral data. For each sample, the measurement process was repeated 8 times (eight scans) to enhance the reliability and reproducibility of the results. The UV–Vis absorption spectra of ICG solutions varied in concentration, solvents, and solvent temperatures and were measured using a Multiskan GO spectrophotometer (Thermo Scientific, USA). Similarly, the kinetics of ICG release into water over time was measured by this method. This instrument measured absorption across the wavelength range of 300 to 1000 nm, employing a wavelength increment of 5 nm for each step.

2.3.3. Thermogravimetry Characterization

Differential scanning calorimetry (DSC) analysis was conducted using a Perkin Elmer PYRIS-1 instrument, with the subsequent data interpretation being conducted via OriginPro software. The DSC temperature sweep was set from 20 to 200 °C with a heating rate of 10 °C min^{-1}, and the samples tested had a mass of ≈30 mg each under a nitrogen atmosphere. In parallel, thermogravimetric analysis (TGA) was undertaken with a Q5000 instrument from TA Instruments under a nitrogen atmosphere to prevent oxidation. The TGA protocol involved heating the samples from 20 to 800 °C at a rate of 10 °C min^{-1}, allowing for assessing the materials' thermal stability and decomposition characteristics over a wide temperature range.

2.3.4. Physical and Mechanical Characterizations

To investigate the hydrophobicity of the electrospun mats, their static water contact angles were precisely measured using optical contact angle measurement equipment from Kruss GmbH. This method involves observing and quantifying the angle formed at the point of contact between a droplet of water and the surface of the electrospun material. The mechanical characteristics of the PHBV nanofibers were assessed using tensile testing, which was conducted on a CTX Texture Analyzer (AMETEK Brookfield) by a uniaxial testing machine equipped with a 50 N load cell. The machine was set to a cross-head speed of 5 mm min^{-1}. For the analysis, rectangular specimens measuring 100 by 20 mm were secured in the device's holder. The thickness of each nonwoven sample was measured, and the average value was calculated and incorporated into the subsequent analysis. Key mechanical parameters such as Young's modulus, tensile strength, and elongation at break were calculated from the stress-strain curves obtained during the tests. Each specific formulation of the nanofibers underwent 3 separate tests under ambient conditions and in a dry state to ensure the reliability of the data.

2.3.5. In Vitro Study

L929 murine fibroblast cells were cultured in DMEM supplemented with 10% FBS and 1% PS in an incubator set at 37 °C with a 5% CO_2 atmosphere until they reached ≈80% confluence. Afterward, cell detachment was performed by exposing the cells to 0.05% EDTA-trypsin for 3 min in the incubator. Subsequent steps involved collecting the cells in a Falcon tube, centrifuging samples at 1200 rpm for 5 min to form a visible cell pellet, and resuspending samples in 1 mL of culture medium for counting. Two groups of fibrous samples in 24-well plates, labeled as PHBV and ICG 2.0, each with a diameter of 1.5 cm, were sterilized using UV light exposure (30 min per side). The sterilized samples were seeded with L929 fibroblasts by placing 50 µL of media containing 10000 cells on top. The media was added to seeded samples every 30 min with 50 µL of warm media for 2 h. Following this, supplemented DMEM media in 1 mL was added to each well.[54] The same procedures were carried out for cells seeded on 20 mm circular glass slides – without fibrous material (further referred to as TCP – tissue culture plate). The medium was changed every 2 days, and the culture was maintained for 7 days.

A PrestoBlue assay was performed to assess the cell's viability quantitatively. The nanofibrous samples and the tissue culture plate (TCP) seeded with L929 fibroblasts were treated with a 10% (v/v) solution of PrestoBlue reagent in culture medium, followed by a 2-h incubation at 37 °C in a 5% CO_2 environment. Five replicates of each sample were examined at 3 specific time points: 1, 3, and 7 days after cell seeding. Following the 2-h PrestoBlue incubation, each group's sample triplicates were transferred to a 96-well plate. Fluorescence was measured at an excitation wavelength of 530 nm and an emission wavelength of 620 nm using a fluorometer plate reader (Fluoroskan Ascent TM Microplate Fluorometer, Thermo Scientific).

A Live/Dead assay was conducted on the 7th day of the culture for a qualitative evaluation of cell viability. The cells were rinsed with PBS and then incubated for 10 min in a dye solution consisting of 0.5 µL of calcein (to stain live cells green) and 2 µL of ethidium homodimer (to stain dead cells red), dissolved in 1 mL of sterile PBS. After washing the cell samples 3 times with PBS, they were visualized using a confocal microscope (Leica TCS SP5 X).

The morphology of L929 fibroblasts seeded on the PHBV and ICG 2.0 samples was assessed using SEM. Their shape was

analyzed through SEM on triplicates at days 1, 3, and 7 of cell culture to examine the evolution of cell morphology during incubation. The samples were initially fixed in 3% ice-cold GTA for 3 h. After 3 washes in DI water, the samples were dehydrated by immersing them in solutions with increasing ethanol concentrations (50%, 70%, 90%, and 100%) for 15 min each. Subsequently, HMDS was introduced to the constructs, and the samples were air-dried overnight under a fume hood. Finally, the samples were sputter-coated with a thin layer of gold and examined using a SEM.

2.3.6. Filtration Performance

The evaluation of filtration efficiency and airflow resistance of the filters was measured according to ISO guidelines (29463-1:2017) using an automated filter tester by Zhaohui Filter Technology Co. Ltd. This device is capable of generating charge-neutralized, monodisperse solid NaCl aerosol particles, specifically of $PM_{0.3}$ size, which are utilized as test particles. The system delivers these aerosol particles at 32 liters per minute airflow rate. These neutralized NaCl aerosol particles are then directed into a filter holder, passing through the filter material with an effective filtration area of 100 cm^2.

2.3.7. Water vapor transmission

The electrospun nanofibers' water vapor permeability (WVTR) was assessed using the AS 82/220.X2 PLUS Analytical Balance, following the procedures outlined in ASTM E96. The water vapor transmission rate (WVTR), also known as water vapor permeability, was subsequently calculated based on the measurements obtained in Equation 1:

$$\mathrm{WVTR} = \frac{\Delta \mathrm{W}}{\Delta \mathrm{t}\, \mathrm{A}} \left(mgh^{-1}cm^{-2}\right) \quad (1)$$

where $\frac{\Delta W}{\Delta t}$ is the amount of water loss (milligrams) per hour of moisture transfer, and A is the evaporation exposure area in cm^2.

2.3.8. Photothermal Characterization

In the thermo-optical experiments, a Laser MDL-H-808 from CNI, operating at a wavelength of 808 nm, which overlaps with the area of maximum absorbance of ICG-incorporated PHBV nanofibers, was utilized to investigate the thermal response of these materials. Additionally, to assess the light-responsive behavior of the samples under conditions simulating one sun irradiation condition, an Abet Technologies model 10 500 solar simulator was used. The detailed thermal response of the samples, including both the temporal temperature changes and the spatial distribution of heat, was accurately recorded and analyzed using a high-resolution FLIR A655sc thermal camera. This camera can capture thermal images with a resolution of 640 × 480 pixels and works with an accuracy of 0.2 °C, making it suitable for observing subtle thermal variations in this research. The camera is seamlessly integrated with FLIR ResearchIR Max software, facilitating the comprehensive capture and analysis of thermal data. The experiments also included a cyclic analysis, where the samples were irradiated for 2 min, followed by a 1-min cooling period for 10 consecutive cycles. This cyclic protocol was designed to study the materials' thermal behavior under repeated thermal stress, providing more evidence of their thermal stability and potential for repeated application use.

2.3.9. ROS Generation

The conversion of 2,7-dichlorodihydrofluorescein diacetate ($DCFH_2$-DA) to 2,7-dichlorodihydrofluorescein ($DCFH_2$) and its subsequent purification followed a procedure outlined by Haghighat Bayan et al.[17] Initially, a methanol solution containing $DCFH_2$-DA was neutralized using 0.1 M NaOH. To this neutralized solution, an equal volume of 0.2 M HCl was added slowly to induce the precipitation of $DCFH_2$. The resultant precipitate was centrifuged at 2 000 rpm for 15 min at 4 °C to separate the pellet. The supernatant was removed, and the pellet was resuspended in 4 mL of ice-cold MiliQ water acidified to a 1.0 pH. This resuspension and centrifugation process was repeated twice to ensure thorough purification. Then, chloroform was employed to extract $DCFH_2$ by separating it from the aqueous phase. The chloroform layer containing the $DCFH_2$ was then carefully evaporated under a gentle stream of argon gas at ambient temperature to avoid oxidative degradation. The dry pellet obtained was reconstituted in methanol to achieve a final concentration of 0.05 M. This methanol solution of $DCFH_2$ was then purged with argon to remove any dissolved oxygen and stored at −20 °C to prevent any degradation. Throughout the process, the samples were protected from light by covering the probe with aluminum foil, as the compounds involved are photosensitive and can degrade upon light exposure.

$DCFH_2$ was used to evaluate the ability of ICG-incorporated PHBV nanofibers to generate ROS. To conduct this test, the control face mask, and the face mask with the nanofibers were positioned within wells of a 96-well plate. Each well was then filled with 198 µL of PBS at 7.4 pH, to which 2 µL of the $DCFH_2$ solution was added, achieving a final concentration of 200 µM. The potential of the ICG to induce oxidative reactions was monitored spectrofluorometrically, both in the presence and absence of NIR laser and solar irradiation. The spectrofluorometer settings were adjusted to an excitation wavelength (λ_{ex}) of 485 nm and an emission wavelength (λ_{em}) of 538 nm to detect the fluorescence signal indicative of $DCFH_2$ oxidation. The assay included various time points to differentiate between the effects with and without laser and solar light irradiation. A systematic and controlled experimental setup was employed to assess the generation of ROS in the samples quantitatively. Each sample was exposed to 2 distinct light sources: an NIR laser and a solar simulator. The experimental protocol was methodically designed to include 6 conditions: a nonirradiated control and irradiation periods of 1, 2, 3, 4, and 5 min, respectively, with 3 repeats. This methodical approach facilitated a comprehensive investigation into the temporal dynamics of ROS generation under each illumination platform, highlighting the effects of photothermal activation on ROS generation in the system.

2.3.10. Antibacterial Performance

E. Coli (ATCC 25 922) and *S. Aureus* (ATCC 6538) were cultured on lysogeny broth (LB) agar and isolated with a streak plate method. For the test, 1 isolated colony was inoculated in fresh LB broth (3 mL) and grown at 37 °C overnight in an orbital shaker.

NIR and solar irradiations were carried out in sterile flat-bottom 96-well plates. Briefly, the materials were shaped in disks with a diameter of 6 mm, sterilized under UV light for 30 min per each side to decrease the bioburden, and glued on the bottoms of the wells. Sterile PBS diluted the bacterial culture to 10^7 colony-forming units (CFU)/mL for *E. Coli*. At the same time, the concentration of *S. Aureus* was set to 10^8 CFU mL^{-1}. The following day, 150 µL of the bacterial suspension are added to each well containing the material. Samples were subjected to NIR or solar irradiation for 5 min. The pure bacterial suspension was analyzed as a positive control. NIR and solar irradiation tests were performed in triplicate for each material. On the other hand, control samples subjected to no irradiation were incubated at room temperature (RT) in the dark for 5 min. Subsequently, 100 µL of sterile PBS was added to each well irradiated or incubated at RT, and the present bacterium was resuspended. Afterward, 100 µL aliquots were transferred to a new 96-well plate and serially diluted. Three technical repetitions of each dilution were then plated on LB agar plates. Plates were incubated overnight at 37 °C. The following day, bacterial colonies were counted to evaluate the Bacterial Survival.

The plating technique limited the highest inactivation degree and detected at 3 log units of CFU/mL, thus permitting the detection of survival rates ≥ 0.1%.

Lastly, to macroscopically visualize bacteria at a 0.05% survival rate, bacteria suspensions in contact with each sample were diluted 10 times. Then, 100 µL of the resulting diluted suspensions were spread evenly on LB agar (representative plates) using a glass spreader and incubated overnight at 37 °C. The initial concentration of *S. Aureus* and *E. Coli* on the representative plates was 10^7 CFU mL^s.

2.3.11. Statistical Analysis

Data were statistically analyzed through a one-way ANOVA analysis followed by Tukey's multiple pairwise comparisons test calculated by OriginPro software. The data are presented as mean ± SD of triplicates from at least $n = 5$ samples per group at each time point. The statistics show differences in construct properties and cell viability between groups at each time point. Significance was set at the 0.05 level.

3. Results and Discussion

3.1. Morphology and Structure of the Platform

A SEM microscope was utilized to show the morphological characteristics of the fabricated fibers, as shown in **Figure 2**. Depicted in Figure 2a are fibers composed of PHBV, characterized by their smooth texture. This panel demonstrates PHBV fibers with incremental concentrations of ICG, ranging from 0% to 5%. The histograms of fiber diameter distribution of PHBV nanofibers were created to analyze the effect of increasing concentrations of ICG on fiber morphology in Figure S1 (Supporting Information). With higher percentages of ICG in the samples, the histograms shifted toward thinner fiber diameters. This trend indicates a correlation between ICG content and fiber size. However, the change in diameter is less than 10 nm, which will not lead to the properties of the fibers. Moreover, the calculated porosity of the samples is in Table S2 (Supporting Information). Figure 2b focuses on the fibrous composition of surgical masks, predominantly polypropylene (PP). The average size of the melt-blown fibers is 34 ± 6 µm. Figure 2c, along with a magnified inset provided in Figure 2d, illustrates the application of PHBV fibers onto the PP fibers of the surgical mask. Figure 2e highlights the anchorage of PHBV fibers to the PP fibers of the mask. The SEM image vividly illustrates the intricate anchorage between electrospun PHBV nanofibers and PP melt-blown fibers within the structure of a face mask. This micrograph highlights the integration of the 2 materials, showcasing the nanofibers' uniform coating over the melt-blown substrate, thereby suggesting an enhanced interface for improved filtration efficiency and mechanical stability. Finally, Figure 2f conceptualizes the integration of PHBV nanofibers within a surgical mask as a middle layer, suggesting a structural modification.

3.2. Chemical and Thermal Properties

The ATR-FTIR spectra of the nanofibers are illustrated in **Figure 3**a. The spectrum of the surgical mask not coated with PHBV, comprising polypropylene, exhibits a shoulder at 2875 cm^{-1} (–CH_3 symmetric stretching) and asymmetric and symmetric in-plane C–H (–CH_3) bending at 1455 cm^{-1} with a shoulder at 1358 cm^{-1} (–CH_3 and –CH_2 deformations), confirming its composition.[55,56] The PHBV is characterized by a C=O stretching vibration at 1720 cm^{-1}, with C–O stretching bands at 1278 and 1054 cm^{-1} and C–H stretching bands ≈2974 and 2935 cm^{-1}. C–H bending vibrations are observed at 1453 and 1380 cm^{-1}.[57,58] The PHBV integrated with ICG demonstrates bands related to ICG's aromatic planes, with C–H vinyl out-of-plane bending from 900 to 1100 cm^{-1} and aromatic C=C stretches between 1400 and 1500 cm^{-1}.[59] In Figure 3b, Raman spectroscopy reveals distinct vibration patterns in the surgical mask with a biocompatible nanofibrous mat made from PHBV and ICG. In the fingerprint region (500–1500 cm^{-1}), prominent peaks at 809 and 973 cm^{-1} are related to C–C stretching and CH_3 rocking. Additionally, the peak at 1169 cm^{-1} indicates C–C stretching and CH bending, while the peak at 1330 cm^{-1} corresponds to CH stretching, CH_2 wagging, and CH_3 bending. Furthermore, the peak at 1460 cm^{-1} is associated with CH_2 bending and CH_3 asymmetric bending.[60–62] The stretching bands originate from the polypropylene component.[61,62] An isolated signal at 1725 cm^{-1} in the PHBV polymer is linked to C=O groups.[63] The peak ≈1613 cm^{-1}, associated with C=C stretching, suggests the presence of aromatic compounds or carbon-carbon double bonds, indicative of ICG, a cyanine dye with aromatic rings, mainly detected in 1600–1700 cm^{-1} range.[63] Figure S2a (Supporting Information) presents the UV–Vis spectra of ICG in various solvents, while Figure S2b shows the absorbance peaks of

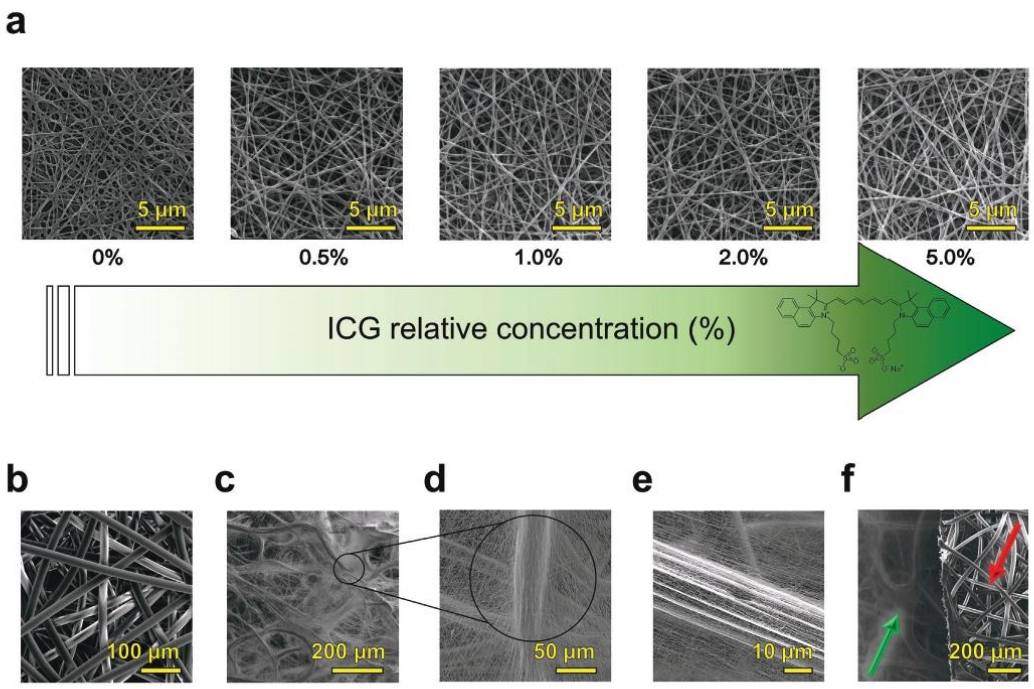

Figure 2. Comprehensive SEM analysis of electrospun fibers and surgical mask integration. a) Uniform PHBV nanofibers with varying ICG content from 0% to 5%. b) Microstructure of polypropylene melt-blown fibers in a surgical mask. c) Overlay of PHBV nanofibers on PP mask fibers, with d) providing a detailed zoomed-in view. e) Close-up of the anchorage between PHBV nanofibers and PP mask fibers, and f) Micrograph of PHBV nanofibers incorporated within a surgical mask (the mask incorporating nanofibers is indicated with a green arrow on the left, while the surgical neat face mask is marked with a red arrow on the right).

ICG after 24 h, highlighting ICG's stability in different solvents. After analysis of the diverse behaviors exhibited by ICG in various solvents, TFE emerged as the optimal choice due to its capacity to dissolve both PHBV and ICG. Additionally, as depicted in Figure 3c, the UV–Vis absorbance peaks of ICG at varying concentrations were observed. Figure 3d displays the normalized absorption spectra of (2.0% w/w) ICG in TFE, revealing 2 peaks at ≈780 and 700 nm, corresponding to monomer and H-type aggregated forms, respectively.[64] Temperature-induced spectral changes in ICG are also observed, with a switch in the central peaks and a decrease in the shoulder intensity, indicating the transformation of ICG forms. The thermal stability of PHBV nanofibers with ICG was examined using TGA. Results in Figure 3e indicate that ICG addition leads to decreased degradation onset temperatures for ICG 2.0 and ICG 5.0 samples. PHBV nanofibers with ICG show initial weight losses ≈200 °C, and DTG analysis (Figure S3, Supporting Information) confirms a decrease in degradation temperature, attributed to ICG's faster degradation compared to PHBV.[65,66] This finding is corroborated by DSC analysis results (Figure 3f), indicating potential material degradation at the end of the first heating scan at 200 °C. Figure 3f shows the melting point of PHBV is 171.90 °C and the melting enthalpy of 34.40 J g^{-1}.

3.3. Physical and Mechanical Properties

In the context of potential biomedical applications for the engineered nanofibers, their surface hydrophilicity is a critical parameter, given that numerous prior studies have established a correlation between surface hydrophilicity and cellular behaviors such as adhesion, proliferation, and migration.[67–69] The hydrophilicity of the surgical face mask, PHBV, and ICG-incorporated PHBV nanofibers was systematically evaluated using the water contact angle measurement technique, with the findings delineated in **Figure 4**. At the moment of dropping, angle measurements indicated that the contact angles for PHBV and ICG-incorporated samples were ≈120°, progressively decreasing to ≈100° for samples with the highest ICG concentration (Figure 4a). Figure S4 (Supporting Information) showcases the contact angle measurement for all samples at each time point. The initial water contact angle for the surgical mask was observed to be ≈140°. Observations made at one and 2-min intervals post-droplet application revealed negligible changes in the contact angles for the PHBV nanofibers and the surgical mask (Figure 4b,c). In contrast, samples incorporating 0.5 and 1 percent ICG exhibited less change in contact angle than those with 2.0 and 5.0 percent ICG. After ≈5 min, the water contact angle for the face mask was reduced to

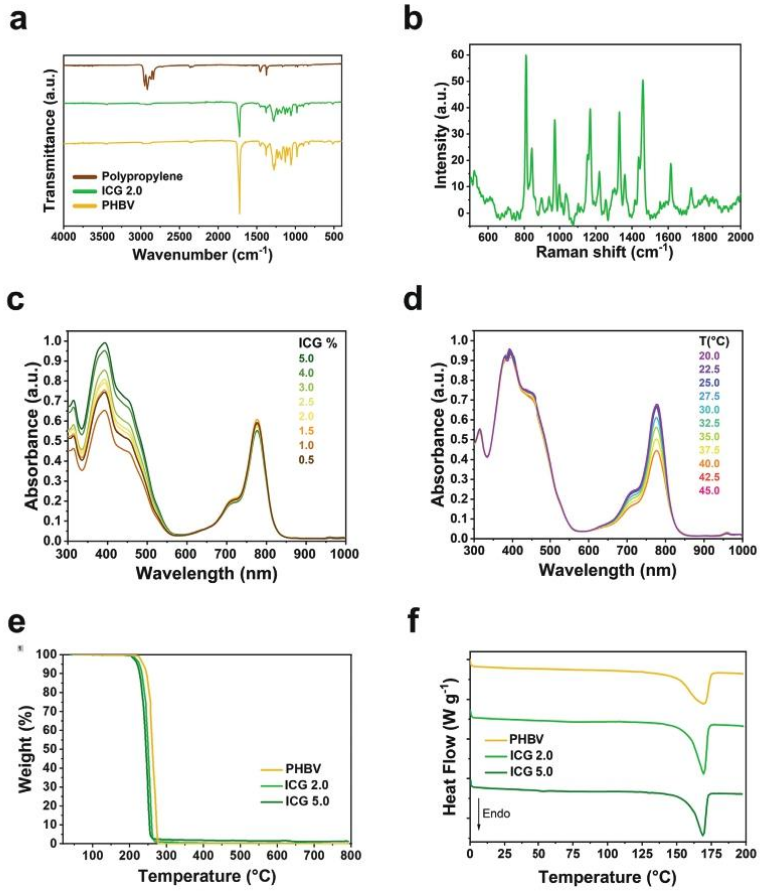

Figure 3. Comprehensive spectroscopic analysis of nanofibers and composite materials. a) ATR-FTIR spectra showcasing the chemical characteristics of samples. b) Raman spectroscopy results reveal unique vibrational patterns indicative of the incorporation of ICG in PHBV nanofibers over the face mask. c) UV–Vis spectra of ICG in TFE at different concentrations. d) Normalized absorption spectra of ICG in TFE in different temperatures. e) TGA analysis demonstrating the thermal degradation profiles of PHBV nanofibers with varying concentrations of ICG, and f) DSC analysis revealing the thermal behavior of PHBV nanofibers.

≈120°, for PHBV to ≈100°, and for ICG 0.5 and ICG 1.0 to ≈90°. Notably, for ICG 2.0 and ICG 5.0 samples, the contact angle experienced a significant reduction, ≈3 fold, and 5 fold, respectively, after the same duration (Figure 4d). These observations suggest that the contact angle of ICG-incorporated nanofibers decreases over time. To explain the mechanism driving this phenomenon, the extent of ICG leaching into water from the electrospun mats was quantified. After conducting a detailed analysis, the decrease in contact angle on ICG-loaded nanofibers correlated with the release of ICG into water. Figure S5 (Supporting Information) illustrates the temporal profile of ICG release into water. This phenomenon underscores the impact of ICG's hydrophilic properties on altering the surface characteristics of the nanofibers upon its release.[70]

Tensile testing was employed to assess their modulus, strength, and elongation performance in investigating the mechanical properties of PHBV nanofibers integrated with variable concentrations of ICG. Tensile testing was conducted on PHBV nanofibers and a series of ICG-incorporated PHBV nanofibers, as illustrated in Figure 4e. Representative stress-strain curves for these materials are depicted in Figure 4f. Critical mechanical properties, including tensile modulus, tensile strength, and elongation-at-break, were quantitatively evaluated with 3 replicate measurements for each sample. The incorporation of ICG at concentrations of 0.5, 1.0, 2.0, and 5.0 wt% resulted in a sequential decrease in the elastic modulus of PHBV by 5.0%, 12.0%, 13.0%, and 14.0%, respectively, as shown in Figure 4g. Additionally, Figure 4h reveals a reduction in the ultimate strain of

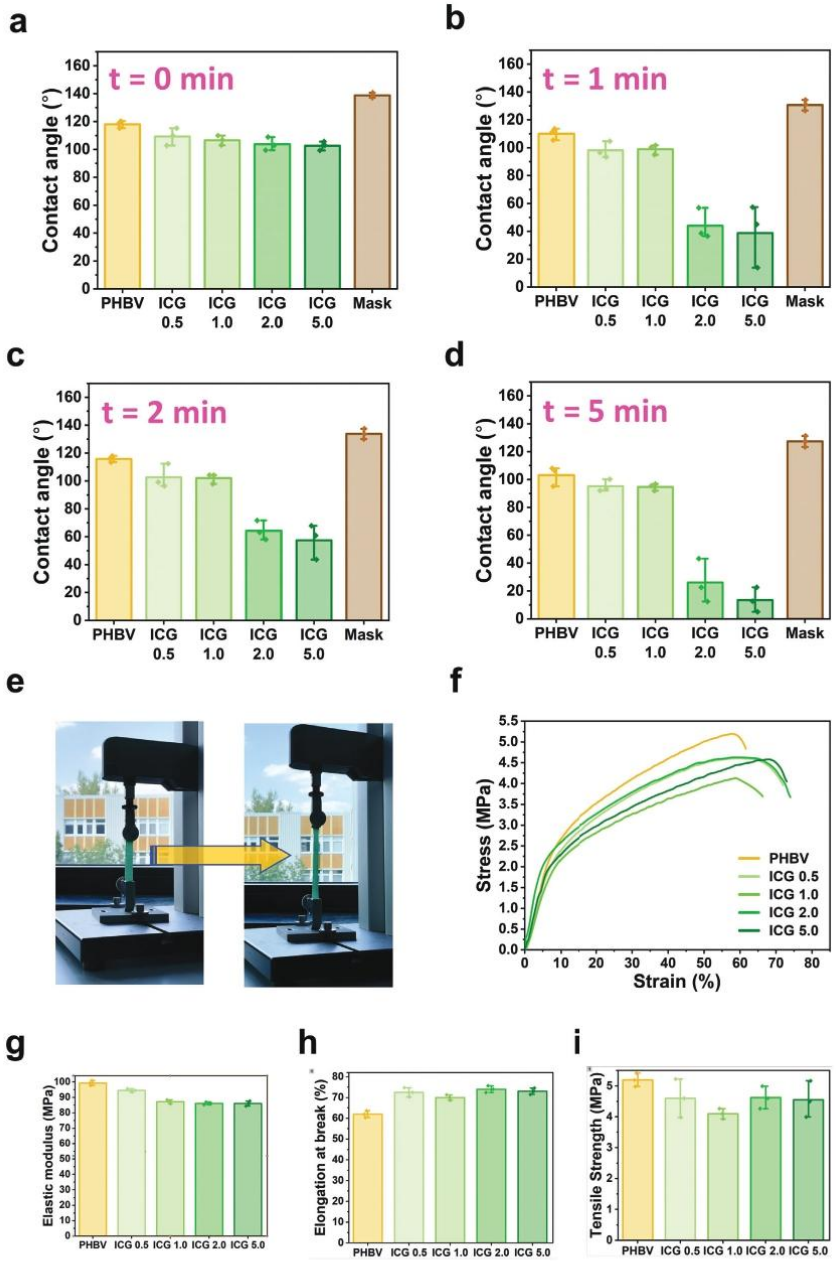

Figure 4. Analysis of surface hydrophilicity in nanofiber samples. a) Initial water contact angles for PHBV and ICG-integrated PHBV nanofibers and surgical masks. b) Stability of contact angles over a period of 1 min. c) Stability of contact angles over a period of 2 min for PHBV nanofibers and the surgical mask, indicating minimal changes, and d) Comparative analysis of the decrease in water contact angles after 5 min, highlighting a significant reduction in angles for ICG 2.0 and 5.0 samples. Mechanical Characterization of PHBV Nanofibers with ICG Integration. e) Setup for tensile testing

pure PHBV nanofibers with an increase in the percentage of ICG within the fibers. Conversely, Figure 4i indicates that the tensile strength of the composites filled with various ICG concentrations remained mainly comparable to that of the PHBV nanofibers without ICG integration.

3.4. In Vitro Studies

The in vitro biological response was evaluated by examining the viability of L929 fibroblast cells seeded on samples PHBV, ICG 2.0, and TCP over a 7-day culture period under ISO 10993–5:2009 (**Figure** 5a). A noticeable upward trend in viability was observed across all tested conditions as the culture time progressed. Comparing samples containing ICG molecules with scaffolds without ICG showed a significant increase in cell proliferation on day 1, day 3, and the 7th day of incubation, suggesting that the ICG stimulates cell growth (Figure 5b). SEM images captured at each time point of cell culture (Figure 5c) revealed visible cell spreading and proliferation on the sample surface, with no noticeable differences among the tested conditions. On the first day after seeding with cells, the scaffolds exhibit a round morphology with visible attachment points to the substrate. During incubation, the cells multiply and completely cover the surface of the fibrous scaffolds, eventually forming multilayered cell colonies, as illustrated on the 7th day of incubation. The results of quantitative cell proliferation studies were complemented with qualitative assessments of cell viability. For this purpose, the viability was determined using a fluorescent live-dead assay, as illustrated in Figure 5d. The prevalence of living cells was observed on all scaffolds at day 7 of culture (Figure 5d), which aligns with the increasing signal from the fluorescent data obtained from the PrestoBlue assay (Figure 5b). The results demonstrate the biocompatibility of the fibrous structures, emphasizing their suitability for cell attachment, survival, spreading, and proliferation. The cells proliferated in both PHBV and ICG 2.0 cases, as evidenced by the morphology.

3.5. Filtration Performance

In this study, the efficacy of electrospun modifications on surgical masks was evaluated in terms of particle filtration efficiency (PFE) using $PM_{0.3}$-like NaCl particles, alongside an analysis of the associated pressure drop. As outlined in **Figure** 6a, the baseline PFE of a standard surgical face mask was measured at ≈81.2%. Moreover, the PFE of the N95 face mask was measured at 93.5%. In comparison, masks incorporating single, double, triple, and quadruple layers of electrospun PHBV nanofibers demonstrated enhanced PFEs of 83.5%, 95.2%, 98.9%, and 99.1%, respectively, indicating an enhancement in $PM_{0.3}$ filtration efficiency through thickening of electrospun layers. The thickness of these samples can be seen in Table S3 (Supporting Information). Correspondingly, the pressure drops across face mask samples were increasing, with an increase in the thickness of the samples. The mask with a double electrospun layer exhibited a high PFE efficiency and maintained an acceptable pressure drop of 87.9 Pa, according to the European standard (EN 14 683). Comparing the performance of all the studied systems, the superior filtration features of the electrospun nanofiber-based face masks are proved. Therefore, double-spun was chosen due to particle filtration results and the pressure drop. The filtration mechanism of electrospun nanofibers in face masks operates through several key processes: mechanical interception, inertial impaction, diffusion, and electrostatic attraction. The fine, fibrous structure of electrospun materials creates a dense network that can capture airborne particles effectively. The small fiber diameters also enhance the Brownian motion effect, improving the capture of smaller particles through diffusion. The electrospun nanofibers can also carry electrostatic charges, attracting and trapping particles more effectively. This combination of mechanical and electrostatic mechanisms significantly improved filtration efficiency, particularly for submicron particles. The water vapor transmission rate study was conducted to determine the breathability and permeability of the fabricated mask. In Figure 6b, the image of the setup is depicted. The results in Figure 6c show that the double-spun face mask decreased the value of WVTR and air permeability. As more moisture replaces the air in the pores, it permeates more slowly and eventually reaches a steady state until slightly between 2 and 5 h. The decrease in WVTR is attributed to high moisture content due to the filled interfacial gap. The double-spun mask demonstrated good breathability, positioning itself between the surgical mask and the N95 mask, and the nanofibers did not negatively impact the breathability.

3.6. Photothermal Response of Platform

Integrating renewable energy sources such as solar energy is crucial in addressing resource scarcity and environmental pollution challenges. In this context, developing textiles with photothermal properties represents an approach toward utilizing clean energy. This study investigates the photothermal characteristics of fabricated nanofibrous systems comprising PHBV, ICG 0.5, ICG 1.0, ICG 2.0, and ICG 5.0, with the findings presented in **Figure** 7. To evaluate the photothermal response of these samples under varying conditions, NIR light laser beams with intensities ranging from 10 to 3000 mW were utilized for 5 min. As illustrated in Figure 7a, the PHBV nanofibrous mat exhibited a surface temperature change (ΔT) of ≈6.5 °C across all laser power levels, starting from an ambient temperature of 25 °C. Conversely, the ICG 2.0 nanofibrous mat demonstrated a progressive increase in surface ΔT, reaching 6.0, 16.3, 17.0, 30.6, 31.8, 42.4, and 45.5 °C with ascending laser powers of 10, 500, 1000, 1500, 2000, 2500, and 3000 mW respectively. Comparative analysis, shown in Figure 7b, indicates that the surface temperatures of PHBV, ICG 0.5, ICG 1.0, ICG 2.0, and ICG 5.0 increased to 50, 53, 64, and 66 °C, respectively, underscoring the enhanced photothermal effect of the nanofibrous mats upon the incorporation of ICG under both NIR and solar light exposure. Additionally, Figure S6

of PHBV nanofibers and ICG-incorporated samples. f) Representative stress-strain curves illustrating the mechanical response of each sample. g) Comparative analysis of the elastic modulus for PHBV nanofibers with increasing ICG concentrations. h) Variation in ultimate strain of PHBV nanofibers with different ICG content, and i) assessment of tensile strength across all samples.

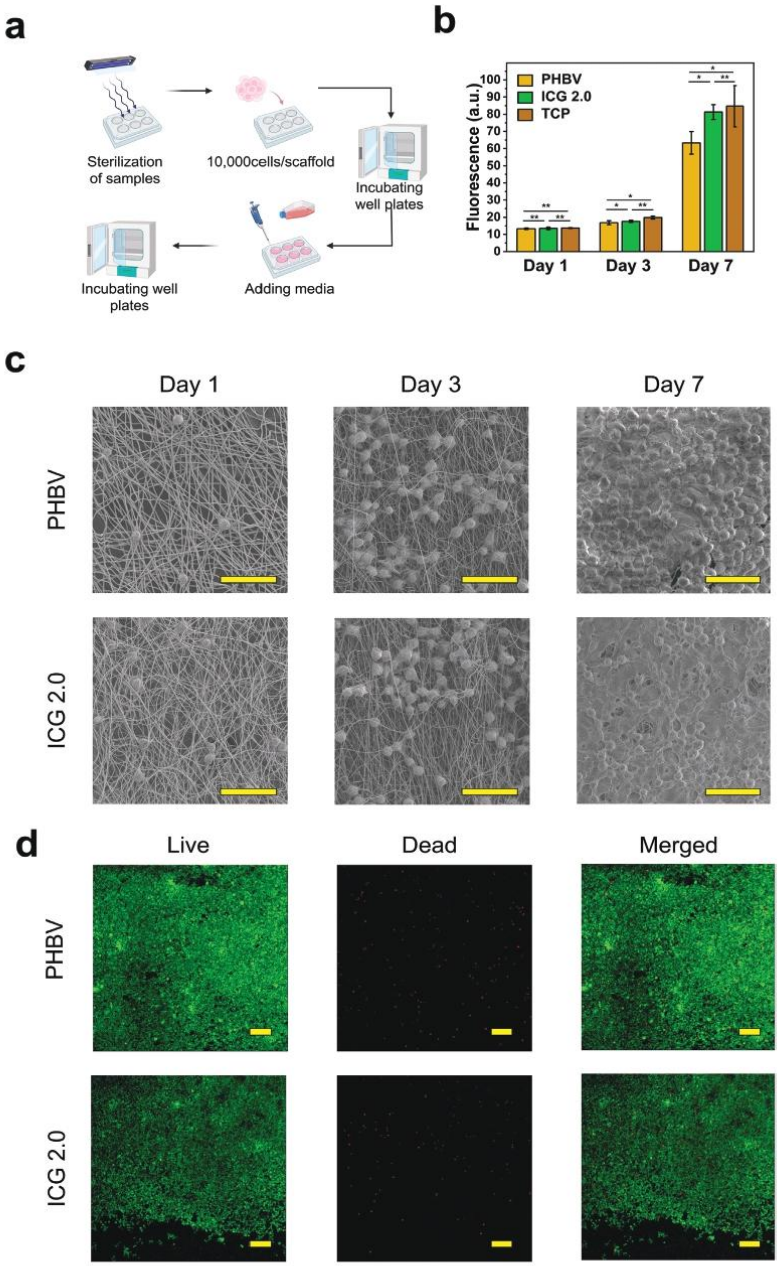

Figure 5. a) Schematic representation of sample sterilization and cell seeding. b) In vitro biological response: Quantitative viability of L929 fibroblast cells seeded on PHBV (ochre), ICG 2.0 (green), TCP (brown) up to 7 days of culture c) SEM images of cell spreading on PHBV and ICG 2.0 scaffolds performed on days 1, 3, and 7 of culture. Scale bar = 10 µm, and d) in vitro biological response: Qualitative viability of L929 fibroblast cells seeded on PHBV and ICG 2.0 fibrous scaffolds performed at day 7 of incubation-scale bar: 100 µm.

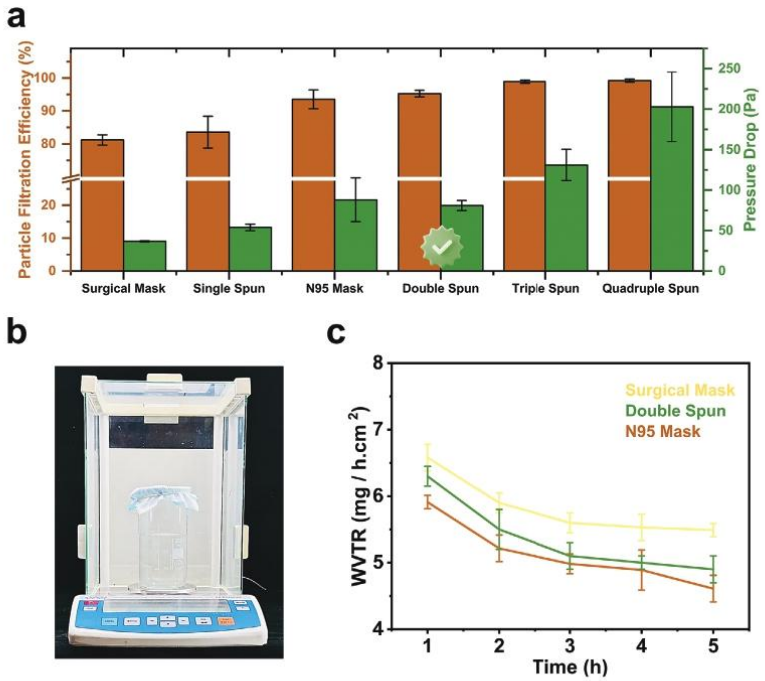

Figure 6. Evaluation of particle filtration efficiency, pressure drop, and WVTR in electrospun-modified face masks. a) PFE and pressure drop comparison between the standard surgical face mask, N95 mask, and masks with single, double, triple, and quadruple electrospun material layers demonstrates significant improvements in $PM_{0.3}$ particle filtration. The statistical analysis of PFE can be found in Table S4 (Supporting Information). b) Setup for WVTR testing of samples and c) WVTR rate of face masks.

(Supporting Information) presents the photothermal response of an alternative middle photothermal active layer integrated within a face mask. These experiments were conducted in triplicate for each sample type. Figure 7c displays the temperature–time curve for the ICG 2.0 nanofibers under 2500 mW NIR light exposure, with a photo inset showing the heating zone, where the maximum surface temperature reached 67 °C. After 2 min of solar light irradiation, the maximum temperature achieved by the ICG 2.0 fabric was ≈64 °C, as seen in Figure 7d. After evaluation of the photothermal efficiency of the face mask under both NIR laser and solar light simulator conditions, the results indicate that the PHBV/ICG nanofibers exhibit significant temperature increases when exposed to both light sources. Specifically, the ICG 2.0 nanofibrous mat demonstrated a desired temperature rise under NIR laser and solar light exposure. This demonstrates that the nanofibers effectively convert NIR and solar light into heat, highlighting their dual functionality for photothermal applications. The high photothermal efficiency under these conditions ensures that the face mask can effectively inactivate bacteria, such as *S. Aureus* and *E. Coli*. This dual capability enhances the mask's practical utility in environments where either NIR or natural sunlight can be harnessed for photothermal activation.

To assess the potential antibacterial applications of the electrospun mats, this study focuses on analyzing their response to cyclic irradiation. The rationale behind examining cyclic irradiation effects lies in understanding the durability and consistency of the mats' photothermal properties, which are crucial for effective and sustained antibacterial activity. Repeated irradiation cycles simulate practical conditions where intermittent exposure to light sources occurs, providing insights into the material's performance over extended use and its potential effectiveness in antibacterial applications. Figure 7e presents a schematic depiction of the cyclic irradiation process. Observations indicate that the surface temperature of the electrospun mats experiences a swift escalation within the initial 10 s of NIR irradiation and ≈30 s when subjected to solar simulation irradiation. Furthermore, the stabilized temperature for each irradiation intensity consistently reaches and maintains a plateau at ≈66 °C for NIR irradiation, as elucidated in Figure 7f. In the context of solar irradiation, the cyclic surface temperature of the ICG 2.0 mats, after undergoing 10 cycles, stabilizes at 63 °C, as demonstrated in Figure 7g. Notably, the electrospun mats exhibit a uniform photothermal temperature response in each cycle, suggesting their potential efficacy in applications such as photothermal deicing, where consistent heat distribution is dominant.

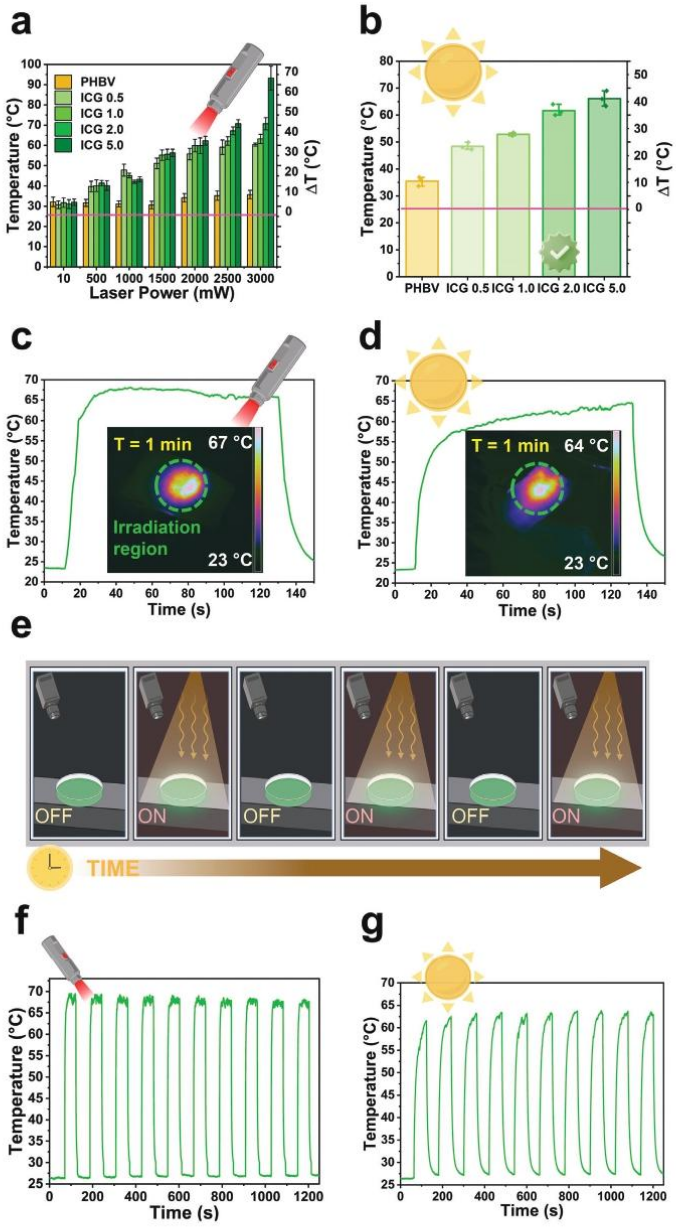

Figure 7. Photothermal properties of nanofibrous mats with varied ICG concentrations. a) Surface temperature change (ΔT) and maximum temperature of PHBV and ICG-integrated nanofibrous mats under different NIR laser power intensities. b) Comparative analysis of the surface temperature rises in PHBV, ICG 0.5, ICG 1.0, ICG 2.0, and ICG 5.0 mats under solar light. c) Temperature-time curve for ICG 2.0 under 2500 mW NIR light, with a photo inset showing the peak heating zone. d) Temporal plot of ICG 2.0 upon solar light. e) A schematic representation of the cyclic irradiation process, f) rapid increase in surface temperature of the electrospun mats during NIR irradiation for 10 cycles, and g) uniform cyclic surface temperature of ICG 2.0 mats at 63 °C after 10 cycles of solar irradiation.

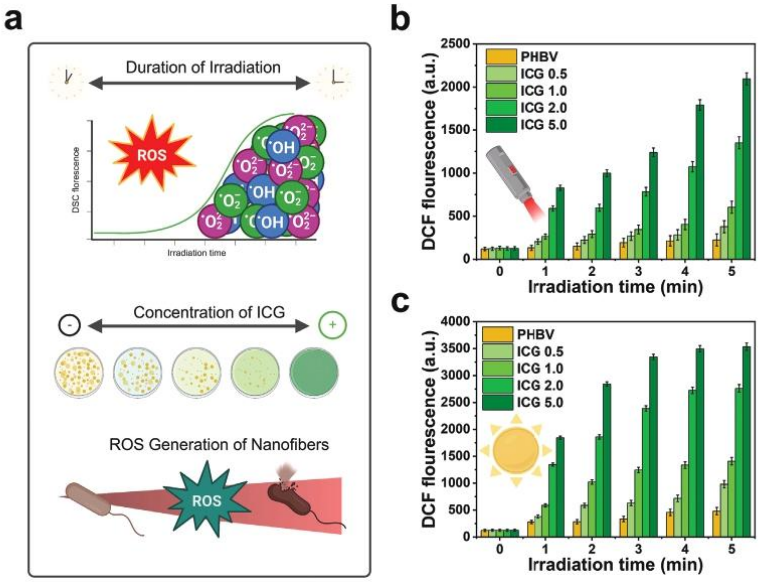

Figure 8. ROS generation of ICG-integrated nanofibers. a) Schematic representation illustrating the relationship between ROS generation, irradiation time, and different ICG concentrations in the nanofibers and how this leads to bacterial inactivation. b) Analysis of ROS generation in PHBV nanofibers with ICG upon NIR light irradiation, and c) evaluation of ROS generation under solar light irradiation in 6 different time points for each sample.

3.7. ROS Generation

Current research is increasingly directed toward the development of novel antimicrobial methodologies. A prominent way within this domain involves the induction of ROS via the incorporation of ICG into nanofibers. ICG is known to facilitate ROS generation upon light irradiation, with ROS capable of disrupting bacterial cell walls and membranes, culminating in bacterial cell death. This strategy is posited to be markedly efficacious in bacterial eradication. The efficiency of ROS generation by ICG was quantitatively assessed in a PBS medium over time. **Figure** 8a depicts a schematic correlation between the increase in ROS generation with irradiation time and varying ICG concentrations, elucidating the mechanism by which ROS induction leads to bacterial inactivation. Notably, during the preparation and subsequent handling of the $DCFH_2$ solution, measures were taken to cover it from light to preclude oxidation due to light exposure. The absorption spectrum of $DCFH_2$ in methanol, as shown in Figure S7 (Supporting Information), exhibits a peak absorption at $\lambda = 230$ nm, confirming the presence of specific organic functional groups as reported by Haghighat Bayan et al. Figure 8b presents data on ROS generation in response to NIR (2000 mW) light irradiation in ICG-enhanced samples. These samples were subjected to triple-replicate testing under various conditions, including no irradiation (control) and exposure for 1, 2, 3, 4, and 5 min. A pronounced increase in $DCFH_2$ fluorescence was observed post-NIR laser irradiation in the ICG-integrated PHBV samples. In contrast, the fluorescence increment in the same samples without laser exposure and in PHBV samples lacking ICG was negligible. $DCFH_2$ fluorescence in pure PHBV samples remained essentially unchanged upon laser irradiation. Additionally, ICG-incorporated samples were exposed to solar light to examine ROS generation over time (Figure 8c), with responses akin to those observed under NIR irradiation. Notably, the ICG 2.0 and ICG 5.0 samples demonstrated substantial ROS production. The SEM images of the samples, taken before and after the ROS generation studies, are depicted in Figure S8 (Supporting Information). These images provide an explicit visual confirmation that the ROS production and the associated temperature changes during the study did not adversely affect the structural integrity of the fibers. This observation is crucial as it indicates the resilience of the fiber structure under the conditions applied for ROS generation, a critical factor in their potential use in antimicrobial applications.

3.8. On-Demand Inactivation of Bacteria

The on-demand inactivation of bacteria in contact with samples exposed to NIR or solar irradiations was investigated using a bacterial suspension of gram-positive *S. Aureus* and gram-negative *E. Coli*. These strains were chosen because they are one of the most commonly used for the evaluation of microorganism response as well as the investigation of the antibacterial properties of a material.[71] *S. Aureus* and *E. Coli* are ideal for antibacterial studies due to their well-characterized genetics and ubiquitous presence in various environments, making them representative models for studying bacterial behavior and responses.

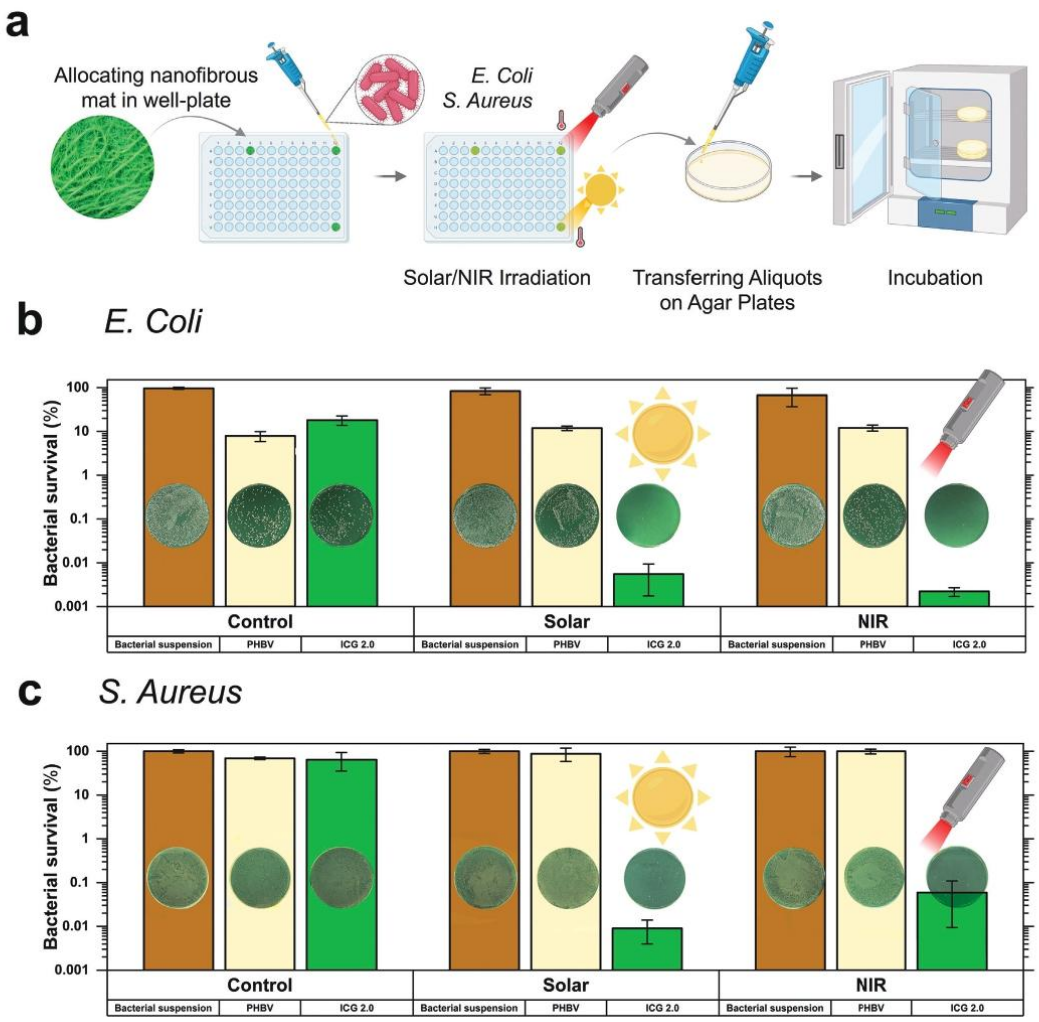

Figure 9. Antimicrobial activity of ICG-integrated nanofibers. a) Schematic of the experimental procedures applied to test the designed materials, and b) percentage of bacteria survival when in contact with PHBV and ICG 2.0 nanofibrous materials subjected to NIR or solar irradiations and incubation at RT in the dark for *E. Coli* and c) *S. Aureus* survival when in contact with PHBV and ICG 2.0 nanofibrous materials subjected to NIR or solar irradiations. Incubation at RT in the dark for *E. Coli* and *S. Aureus* pure bacteria suspension was tested as a control. Images of bacterial colonies grown on LB agar plates for each tested condition are displayed in each related bar. The bacterial survival percent below 0.01% is the detection limit of 10^3 CFU mL^{-1}. Measurements below the limit of detection are set as 0.05% bacteria survival. Data are presented on a logarithmic scale as mean ± standard deviation.

Additionally, both bacteria are common pathogens known to cause various infections.[72,75]

Figure 9a provides a comprehensive illustration of the step-by-step experimental methodologies implemented to evaluate the performance and efficacy of the designed materials under various irradiation conditions (solar or NIR). The outstanding photothermal and photodynamic properties of the ICG were evident after ≈5 min of NIR or solar light exposure (Figure 7). During the irradiation time, in the presence of the ICG, *E. Coli* was inactivated to 3 log units (the detection limit), thus proving 0.1% bacterial survival (Figure 9b). Additionally, representative agar plates related to this testing condition showed no colonies, evidencing the inactivation of bacteria to 99.95% (Figure 9b). We also achieved complete bacterial elimination on the representative plates for

S. Aureus at a 10^7 CFU mL^{-1} concentration. Therefore, we increased the bacterial concentration to 10^8 CFU mL^{-1} for the dilution test to ensure the data exceeded the detection limit and could be accurately represented on the graph. In Figure 9c, the ICG-incorporated masks effectively inactivated *S. Aureus* to the detection limit of 3 log units within just 5 min of both NIR or solar irradiation. Bacterial survival was reduced to 0.059%. This significant reduction, demonstrating bacterial survival below 0.1%, highlights the robust self-sterilizing properties of the ICG 2.0 face mask under these irradiation conditions. On the representative plates for *S. Aureus*, we successfully eliminated all bacteria at the bacteria concentration of 10^7 CFU mL^{-1}. On the other hand, it is possible to observe the *E. Coli* inactivation in 1 log unit in case of bacteria suspension in contact with ICG 2.0 and PHBV (aside from the irradiation/no irradiation condition). This is likely due to the antibacterial properties of PHBV, which have previously been demonstrated to possess interesting antimicrobial characteristics.[76] However, ICG 2.0 under NIR or solar irradiation could effectively inactivate bacteria 2 log units more, evidencing significantly higher performances. Besides, bacteria inactivation was not reported in the case of bacteria suspension subjected and not subjected to NIR or solar light, showing no effect of irradiation on *E. Coli* and *S. Aureus* suspension. Results showed how the photoactivable properties of the ICG 2.0 led to outstanding bactericidal performance toward *E. Coli* and *S. Aureus*. Indeed, when exposed to NIR and solar lights, the material can reach a temperature of up to 65 °C, damaging the cell membrane and thus leading to the death of bacteria.[77]

4. Conclusion

This comprehensive study explored developing, characterizing, and testing a novel antibacterial material composed of PHBV nanofibers integrated with ICG, which can be activated via different solar and NIR light sources. Our findings highlight the antibacterial properties, enhanced filtration efficiency, and mechanical strength of the nanofibrous mat when integrated directly into a face mask. This integrated approach demonstrates significant improvements and novel features for face masks, highlighting their enhanced protective capabilities, particularly crucial in public health contexts. Integrating this material into face masks elevates their effectiveness in filtering out pathogens. It imbues them with improved user safety, thereby establishing these enhanced masks as a promising option for protective clothing in combating viral transmission.

The investigation began with the electrospinning of PHBV nanofibers, incorporating varying concentrations of ICG to assess their impact on the antibacterial properties. We successfully prepared uniform nanofibers with incremental ICG concentrations, demonstrating effective integration of ICG into the PHBV matrix. The morphology and structure of the nanofibers were confirmed through SEM analysis. At the same time, their chemical and thermal properties were thoroughly examined, and the effective presence of both PHBV and ICG was confirmed. The water contact angle tests revealed that integrating ICG into PHBV nanofibers decreased their hydrophobicity, a desirable trait for biomedical applications. In vitro studies further endorsed the biocompatibility of the nanofibers, as evidenced by the attachment and proliferation of L929 fibroblast cells. A key focus of this research was the exploration of the photothermal properties of the nanofibrous mats. We demonstrated that upon NIR and solar light irradiation, the temperature of the mats increased significantly, indicating their potential use in photothermal and photodynamic applications.

Furthermore, the cyclic photo-response study highlighted the durability and consistency of the mats' PTT and PDT properties, which are crucial for their antibacterial activity. These aspects are essential for enduring recurrent exposure to light sources and simulating real-world usage scenarios. The generation of ROS upon light irradiation was a key feature of our material, with the ICG-incorporated PHBV nanofibers showing a marked increase in ROS generation, especially under NIR and solar light, leading to effective bacterial inactivation. Additionally, the photothermal effect, facilitated by the material's ability to convert light into heat, further contributed to the antibacterial efficiency. The SEM images post-ROS generation studies confirmed that these processes, encompassing both PDT and PTT mechanisms, did not compromise the structural integrity of the fibers, underlining their stability and suitability for antimicrobial applications. Our research also contained the photothermal inactivation of bacteria, using *E. Coli* and *S. Aureus* as model organisms. This choice was motivated by *S. Aureus* and *E. Coli*'s well-characterized genetics and their relevance as a common pathogen. The results were remarkable, showing a significant reduction in bacterial viability upon NIR and solar irradiation, thereby confirming the bactericidal efficacy of the material.

Our vision for future work involves further optimizing the composition and structure of these nanofibers to enhance their antibacterial efficacy and broaden their application scope. In the future, we also aim to explore the potential of these materials in diverse fields. Beyond face masks, the proposed technology holds significant potential for extension to other biomedical devices. Incorporating light-activated antibacterial properties into various materials could greatly impact wound dressings, medical gowns, and other protective garments, improving infection control in medical settings. Additionally, this technology could be adapted for use in air and water filtration systems, contributing to broader public health and environmental protection efforts. The scalability of the electrospinning process and the biodegradability of PHBV make this material a promising candidate for sustainable and eco-friendly applications in diverse biomedical and environmental fields.

In conclusion, this study introduces an approachable method for combating microbial infections on-demand, particularly relevant during health crises. Developing these innovative nanofibrous face masks addresses public health concerns and paves the way for future advancements in antibacterial materials.

Supporting Information

Supporting Information is available from the Wiley Online Library or from the author.

Acknowledgements

This work was supported by the National Center for Research and Development (NCBiR) (WPC2/NanoHealer/2021) and the Ministry of Science and Technology of China (2021YFE0105100). Figures 1a,5c,7,8,9, and

Figure S6 (Supporting Information) were partially created with BioRender. C.R., P.N., and F.P. acknowledge the financial support from the Polish Ministry of Science and Higher Education through scholarships for outstanding young scientists. S.S.Z. acknowledges the support of the European Union's Horizon 2021 research and innovation program under the Marie Sklodowska-Curie grant agreement no. 101068036, "SuSCoFilter".

Conflict of Interest

The authors declare no conflict of interest.

Data Availability Statement

The data that support the findings of this study are available from the corresponding author upon reasonable request.

Keywords

face masks, light-responsive electrospun nanofibers, pathogen eradication, photodynamic, photothermal

Received: March 19, 2024
Revised: July 23, 2024
Published online:

[1] R. E. Baker, A. S. Mahmud, I. F. Miller, M. Rajeev, F. Rasambainarivo, B. L. Rice, S. Takahashi, A. J. Tatem, C. E. Wagner, L. F. Wang, A. Wesolowski, C. J. E. Metcalf, *Nat. Rev. Microbiol.* **2021**, *20*, 193.
[2] H. O. Ukuhor, *J. Infect. Public Health* **2021**, *14*, 53.
[3] M. Everard, P. Johnston, D. Santillo, C. Staddon, *Environ. Sci. Policy* **2020**, *111*, 7.
[4] S. M. Imani, L. Ladouceur, T. Marshall, R. Maclachlan, L. Soleymani, T. F. Didar, *ACS Nano* **2020**, *14*, 12341.
[5] N. Karim, S. Afroj, K. Lloyd, L. C. Oaten, D. V. Andreeva, C. Carr, A. D. Farmery, I. D. Kim, K. S. Novoselov, *ACS Nano* **2020**, *14*, 12313.
[6] R. H. McQueen, B. L. Ehnes, *Infect. Prevent.* **2022**, 139.
[7] S. Bin Jeong, D. U. Lee, B. J. Lee, K. J. Heo, D. W. Kim, G. B. Hwang, A. J. MacRobert, J. H. Shin, H. S. Ko, S. K. Park, Y. S. Oh, S. J. Kim, D. Y. Lee, S. B. Lee, I. Park, S. B. Kim, B. Han, J. H. Jung, D. Y. Choi, *Chem. Eng. J.* **2022**, *440*, 135830.
[8] A. Cimini, A. Borgioni, E. Passarini, C. Mancini, A. Proietti, L. Buccini, E. Stornelli, E. Schifano, S. Dinarelli, F. Mura, C. Sergi, I. Bavasso, B. Cortese, D. Passeri, E. Imperi, T. Rinaldi, A. Picano, M. Rossi, *Polymers* **2023**, *15*, 4586.
[9] C. Zhang, H. Pan, X. Wang, S. K. Sun, *Biomater. Sci.* **2018**, *6*, 2750.
[10] S. Virlley, S. Shukla, S. Arora, D. Shukla, D. Nagdiya, T. Bajaj, S. Kujur, Garima, A. K., J. S. Bhatti, A. Singh, C. Singh, *J. Drug Deliv. Sci. Technol.* **2023**, *87*, 104842.
[11] S. G. Bown, *World J. Surg.* **1983**, *7*, 700.
[12] M. J. Maisels, *J. Perinatol.* **2002**, *21*, S93.
[13] F. Pierini, P. Nakielski, O. Urbanek, S. Pawlowska, M. Lanzi, L. De Sio, T. A. Kowalewski, *Biomacromolecules* **2018**, *19*, 4147.
[14] P. Tang, Z. Zhang, A. Y. El-Moghazy, N. Wisuthiphaet, N. Nitin, G. Sun, *ACS Appl. Mater. Interfaces* **2020**, *12*, 49442.
[15] A. Zakrzewska, M. A. Haghighat Bayan, P. Nakielski, F. Petronella, L. De Sio, F. Pierini, *ACS Appl. Mater. Interfaces* **2022**, *14*, 46123.
[16] M. A. Haghighat Bayan, Y. J. Dias, C. Rinoldi, P. Nakielski, D. Rybak, Y. B. Truong, A. L. Yarin, F. Pierini, *J. Polymer Sci.* **2023**, *61*, 521.
[17] M. A. Haghighat Bayan, C. Rinoldi, D. Rybak, S. S. Zargarian, A. Zakrzewska, O. Cegielska, K. Põhako-Palu, S. Zhang, A. Stobnicka-Kupiec, R. L. Górny, P. Nakielski, K. Kogermann, L. De Sio, B. Ding, F. Pierini, *Biomater. Sci.* **2024**, *12*, 949.
[18] M. P. Brynildsen, J. A. Winkler, C. S. Spina, I. C. MacDonald, J. J. Collins, *Nat. Biotechnol.* **2013**, *31*, 160.
[19] B. Pinegin, N. Vorobjeva, M. Pashenkov, B. Chernyak, *J. Cell. Physiol.* **2018**, *233*, 3745.
[20] L. De Sio, B. Ding, M. Focsan, K. Kogermann, P. Pascoal-Faria, F. Petronela, G. Mitchell, E. Zussman, F. Pierini, *Chem. A Eur. J.* **2021**, *27*, 6112.
[21] D. Rybak, Y. C. Su, Y. Li, B. Ding, X. Lv, Z. Li, Y. C. Yeh, P. Nakielski, C. Rinoldi, F. Pierini, J. M. Dodda, *Nanoscale* **2023**, *15*, 8044.
[22] F. G. Blanco, N. Hernández, V. Rivero-Buceta, B. Maestro, J. M. Sanz, A. Mato, A. M. Hernández-Arriaga, M. A. Prieto, *Nanomaterials* **2021**, *11*, 1492.
[23] D. Chouhan, S. Kaushik, D. Arora, *Biomaterials in Tissue Engineering and Regenerative Medicine: From Basic Concepts to State of the Art Approaches*, Springer, Singapore **2021**, 163.
[24] E. S. Hosseini, S. Dervin, P. Ganguly, R. Dahiya, *ACS Appl. Bio Mater.* **2021**, *4*, 163.
[25] M. B. Reinhart, C. R. Huntington, L. J. Blair, B. T. Heniford, V. A. Augenstein, *Surg. Innov.* **2015**, *23*, 166.
[26] J. S. Treger, M. F. Priest, R. Iezzi, F. Bezanilla, *Biophys. J.* **2014**, *107*, L09.
[27] J. A. Carr, D. Franke, J. R. Caram, C. F. Perkinson, M. Saif, V. Askoxylakis, M. Datta, D. Fukumura, R. K. Jain, M. G. Bawendi, O. T. Bruns, *Proc. Natl. Acad. Sci. U.S.A.* **2018**, *115*, 4465.
[28] Z. Sheng, D. Hu, M. Xue, M. He, P. Gong, L. Cai, *Nano-Micro Lett.* **2013**, *5*, 145.
[29] S. K. Singh, S. Mazumder, A. Vincy, N. Hiremath, R. Kumar, I. Banerjee, R. Vankayala, *ACS Appl. Nano Mater.* **2023**, *6*, 1508.
[30] H. F. Jiao, J. Guo, Y. Cui, X. Yu, Y. Liao, Y. Ying, Z. Li, K. Yao, H. Huang, *Adv. Ther.* **2022**, *5*, 2100202.
[31] M. R. Younis, R. B. An, Y. C. Yin, S. Wang, D. Ye, X. H. Xia, *ACS Appl. Bio Mater.* **2019**, *2*, 3942.
[32] R. Lubart, *Photomed. Laser Surg.* **2012**, *30*, 115.
[33] J. Prakash, S. B. N. Krishna, P. Kumar, V. Kumar, K. S. Ghosh, H. C. Swart, S. Bellucci, J. Cho, *Catalysts* **2022**, *12*, 1047.
[34] V. N. Nguyen, Z. Zhao, B. Z. Tang, J. Yoon, *Chem. Soc. Rev.* **2022**, *51*, 3324.
[35] T. Fedatto Abelha, A. Rodrigues Lima Caires, *Adv. Nanobiomed. Res.* **2021**, *1*, 2100012.
[36] M. M. Yawalkar, S. Menon, H. C. Swart, S. J. Dhoble, *Photophys. Nanophys. Therapeut.* **2022**, 51.
[37] B. Yang, Y. Chen, J. Shi, *Chem. Rev.* **2019**, *119*, 4881.
[38] L. Wang, Y. Li, L. Zhao, Z. Qi, J. Gou, S. Zhang, J. Z. Zhang, *Nanoscale* **2020**, *12*, 19516.
[39] S. Pon Janani, P. Thillai Arasu, I. U. Muzaddadi, A. Murugan, C. R. Ravikumar, N. N. Yadav, H. S. Yadav, *Emerging Nanomaterials and Nano-based Drug Delivery Approaches to Combat Antimicrobial Resistance*, Elsevier, Netherlands **2022**, 531.
[40] N. Singh, R. Sen Gupta, S. Bose, *Nanoscale* **2024**, *7*, 3243.
[41] H. P. Lee, A. K. Gaharwar, *Adv. Sci.* **2020**, *7*, 2000863.
[42] M. J. Blaser, P. F. Smith, H. J. Cody, W. L. L. Wang, F. M. LaForce, *J. Infect. Dis.* **1984**, *149*, 48.
[43] D. Wang, S. C. Pillai, S. H. Ho, J. Zeng, Y. Li, D. D. Dionysiou, *Appl. Catal. B* **2018**, *237*, 721.
[44] T. Naseem, T. Durrani, *Environ. Chem. Ecotoxicol.* **2021**, *3*, 59.
[45] G. K. Inwati, P. Kumar, F. Goutaland, P. Sharma, H. C. Swart, *Multifunctional Hybrid Semiconductor Photocatalyst Nanomaterials*, Springer, Germany **2023**, 289.
[46] M. A. Haghighat Bayan, F. Afshar Taromi, M. Lanzi, F. Pierini, *Sci. Rep.* **2021**, *11*, 1.
[47] C. Rinoldi, Y. Ziai, S. S. Zargarian, P. Nakielski, K. Zembrzycki, M. A. H. Bayan, A. B. Zakrzewska, R. Fiorelli, M. Lanzi, A. Kostrzewska-Księyk, R. Czajkowski, E. Kublik, L. Kaczmarek, F. Pierini, *ACS Appl. Mater. Interfaces* **2023**, *15*, 6283.

[48] P. Nakielski, D. Rybak, K. Jezierska-Woźniak, C. Rinoldi, E. Sinderewicz, J. Staszkiewicz-Chodor, M. A. Haghighat Bayan, W. Czelejewska, O. Urbanek, A. Kosik-Kozioł, M. Barczewska, M. Skomorowski, P. Holak, S. Lipiński, W. Maksymowicz, F. Pierini, *ACS Appl. Mater. Interfaces* **2023**, *15*, 58103.
[49] D. Rybak, C. Rinoldi, P. Nakielski, J. Du, M. A. H. Bayan, S. S. Zargarian, M. Pruchniewski, X. Li, B. Strojny-Cieślak, B. Ding, F. Pierini, *J. Mater. Chem. B* **2024**, *12*, 1905.
[50] A. R. Peringath, M. A. H. Bayan, M. Beg, A. Jain, F. Pierini, N. Gadegaard, R. Hogg, L. Manjakkal, *J. Energy Storage* **2023**, *73*, 108811.
[51] N. Bhardwaj, S. C. Kundu, *Biotechnol. Adv.* **2010**, *28*, 325.
[52] S. Agarwal, J. H. Wendorff, A. Greiner, *Polymer* **2008**, *49*, 5603.
[53] W. E. Teo, S. Ramakrishna, *Nanotechnology* **2006**, *17*, R89.
[54] A. Kosik-Kozioł, E. Graham, J. Jaroszewicz, A. Chlanda, P. T. S. Kumar, S. Ivanovski, W. Święszkowski, C. Vaquette, *ACS Biomater. Sci. Eng.* **2019**, *5*, 318.
[55] V. Mylläri, T. P. Ruoko, S. Syrjälä, *J. Appl. Polym. Sci.* **2015**, *132*, https://doi.org/10.1002/APP.42246.
[56] R. Morent, N. De Geyter, C. Leys, L. Gengembre, E. Payen, *Surf. Interface Anal.* **2008**, *40*, 597.
[57] B. Fei, C. Chen, H. Wu, S. Peng, X. Wang, L. Dong, *Eur. Polym. J.* **2003**, *39*, 1939.
[58] S. P. C. Gonçalves, S. M. Martins-Franchetti, *J. Polym. Environ.* **2010**, *18*, 714.
[59] Z. Chaudhary, G. M. Khan, M. M. Abeer, N. Pujara, B. Wan-Chi Tse, M. A. McGuckin, A. Popat, T. Kumeria, *Biomater. Sci.* **2019**, *7*, 5002.
[60] D. Puchowicz, M. Cieslak, D. Puchowicz, M. Cieslak, *Recent Developments in Atomic Force Microscopy and Raman Spectroscopy for Materials Characterization*, IntechOpen, England **2021**, https://doi.org/10.5772/INTECHOPEN.99731.
[61] E. Masaeli, M. Morshed, M. H. Nasr-Esfahani, S. Sadri, J. Hilderink, A. van Apeldoorn, C. A. van Blitterswijk, L. Moroni, *PLoS One* **2013**, *8*, e57157.
[62] J. Coates, *Encyclopedia of Analytical Chemistry*, Wiley, United States **2000**, https://doi.org/10.1002/9780470027318.A5606.
[63] Q. Tang, F. Xu, C. Zhang, C. Li, F. Liu, M. Shen, X. Liu, J. Lin, L. Zhu, T. Lin, D. Sun, *J. Incl. Phenom. Macrocycl. Chem.* **2022**, *102*, 735.
[64] D. Farrakhova, Y. Maklygina, I. Romanishkin, D. Yakovlev, A. Plyutinskaya, L. Bezdetnaya, V. Loschenov, *Photodiagnosis Photodyn. Ther.* **2022**, *37*, 102636.
[65] A. Schönbächler, O. Glaied, J. Huwyler, M. Frenz, U. Pieles, *J. Photochem. Photobiol. A Chem.* **2013**, *261*, 12.
[66] O. Demirel, S. O. Gundogdu, S. Yuce, H. Unal, *ACS Omega* **2023**, *8*, 37908.
[67] V. Leung, F. Ko, *Polym. Adv. Technol.* **2011**, *22*, 350.
[68] A. Ghajarieh, S. Habibi, A. Talebian, *Russ. J. Appl. Chem.* **2021**, *94*, 847.
[69] R. Rasouli, A. Barhoum, M. Bechelany, A. Dufresne, *Macromol. Biosci.* **2019**, *19*, 1800256.
[70] V. Saxena, M. Sadoqi, J. Shao, *Int. J. Pharm.* **2004**, *278*, 293.
[71] A. Singh, A. K. Dubey, *ACS Appl. Bio Mater.* **2018**, *1*, 3.
[72] Y. Wang, Y. Yang, Y. Shi, H. Song, C. Yu, *Adv. Mater.* **2020**, *32*, 1904106.
[73] M. R. Mangalea, B. A. Duerkop, *Infect. Immun.* **2020**, *88*.
[74] K. Hoelzer, N. Wong, J. Thomas, K. Talkington, E. Jungman, A. Coukell, *BMC Vet. Res.* **2017**, *13*, 211.
[75] F. Zaccagnini, D. De Biase, F. Bovieri, G. Perotto, E. Quagliarini, L. De Sio, *Small* **2024**, 2400531.
[76] Ł. Kaniuk, Z. J. Krysiak, S. Metwally, U. Stachewicz, *Mater. Sci. Eng., C* **2020**, *110*, 110668.
[77] W. Li, H. Zhang, X. Li, H. Yu, C. Che, S. Luan, Y. Ren, S. Li, P. Liu, X. Yu, X. Li, *ACS Appl. Mater. Interfaces* **2020**, *12*, 7617.

Received: 15 December 2022 | Revised: 24 January 2023 | Accepted: 24 January 2023

DOI: 10.1002/pol.20220747

RESEARCH ARTICLE

JOURNAL OF POLYMER SCIENCE WILEY

Near-infrared light activated core-shell electrospun nanofibers decorated with photoactive plasmonic nanoparticles for on-demand smart drug delivery applications

Mohammad Ali Haghighat Bayan[1] | **Yasmin Juliane Dias**[2] | **Chiara Rinoldi**[1] | **Paweł Nakielski**[1] | **Daniel Rybak**[1] | **Yen B. Truong**[3] | **Alexander L. Yarin**[2,4] | **Filippo Pierini**[1,3]

[1]Department of Biosystems and Soft Matter, Institute of Fundamental Technological Research, Polish Academy of Sciences, Warsaw, Poland

[2]Department of Mechanical and Industrial Engineering, University of Illinois at Chicago, Chicago, Illinois, USA

[3]Commonwealth Scientific and Industrial Research Organization (CSIRO) Manufacturing, Clayton, Victoria, Australia

[4]School of Mechanical Engineering, Korea University, Seoul, Republic of Korea

Correspondence
Filippo Pierini, Department of Biosystems and Soft Matter, Institute of Fundamental Technological Research, Polish Academy of Sciences, ul. Pawińskiego 5B, Warsaw 02-106, Poland.
Email: fpierini@ippt.pan.pl

Funding information
National Science Centre, Grant/Award Number: 2020/38/E/ST5/00456; Polish National Agency for Academic Exchange, Grant/Award Number: BPN/BEK/2021/1/00161; National Agency for Academic Exchange, Grant/Award Number: PPI/APM/2018/1/00045/U/001; Polish Ministry of Science and Higher Education

Abstract

Over the last few years, traditional drug delivery systems (DDSs) have been transformed into smart DDSs. Recent advancements in biomedical nanotechnology resulted in introducing stimuli-responsiveness to drug vehicles. Nanoplatforms can enhance drug release efficacy while reducing the side effects of drugs by taking advantage of the responses to specific internal or external stimuli. In this study, we developed an electrospun nanofibrous photo-responsive DDSs. The photo-responsivity of the platform enables on-demand elevated drug release. Furthermore, it can provide a sustained release profile and prevent burst release and high concentrations of drugs. A coaxial electrospinning setup paired with an electrospraying technique is used to fabricate core-shell PVA-PLGA nanofibers decorated with plasmonic nanoparticles. The fabricated nanofibers have a hydrophilic PVA and Rhodamine-B (RhB) core, while the shell is hydrophobic PLGA decorated with gold nanorods (Au NRs). The presence of plasmonic nanoparticles enables the platform to twice the amount of drug release besides exhibiting a long-term release. Investigations into the photo-responsive release mechanism demonstrate the system's potential as a "smart" drug delivery platform.

KEYWORDS

electrospun core-shell nanofibers, NIR-light activation, on-demand drug release, plasmonic nanoparticles, stimuli-responsive nanomaterials

1 | INTRODUCTION

The strategy of providing medication or other pharmacological substances to produce a long-lasting therapeutic effect is realized with drug delivery systems (DDSs).[1,2] Scientific discoveries revealed that controlled delivery of drugs could affect treatment efficacy.[3] Hence, DDSs have grown in importance in the pharmacological industry over the past few decades.[4–6] Controlled drug release is one of the methods of drug delivery and an essential topic in biomedical research.[7] In this process, a polymer, ceramic, or metal carrier is combined with a drug or active agent in a designed approach so that an active agent can be released into the human body in a predetermined and desired way.[8] By taking advantage of controlled releasing carriers as DDSs, the drug molecules could be sustainably released. Additionally, the carriers can maintain an effective drug concentration for the designated period.[9] The DDS optimization also avoids burst release reducing the side effects of high concentrations of drugs.[10] An ideal drug carrier should have the following characteristics: stable physical and chemical properties, biocompatibility, extremely low toxicity, and adjustable drug release.[11] In recent years, the research on DDSs has focused on enhancing the carrier's release kinetic, incorporating different techniques to produce new generations of carriers.[12,13] DDSs can efficiently target a specific living tissue and promote drug absorption. Moreover, they can release the drug on demand to achieve an effective and safe therapeutic effect; these novel systems are called stimuli-responsive DDSs or "smart" DDSs (SDDSs).[14–19]

Stimuli-responsive drug carriers can trigger drug release from the nanoplatforms.[20–22] One of the most exciting stimuli responses is the photo-responsiveness of photoactive material. Photoactive materials are chemical compounds in one or more spectrum bands sensitive to electromagnetic radiation. Electromagnetic radiation can cause chemical or physical changes in the material's structure. Among electromagnetic waves, UV and IR are the most used in biomedical applications.[23] UV light can damage tissues and cells due to high scattering and absorption by water and proteins in the human body through a one-photon mechanism. In contrast to UV, near-infrared (NIR) light can be absorbed through a two-photon process. The one-photon absorption of UV light and the two-photon absorption of NIR light supply enough energy to activate the photoreactions of photo-responsive material.[24,25] NIR light has no adverse effects on tissues or cells.[26] It can penetrate tissues up to several centimeters with slim scattering and absorption by water and endogenous proteins. Due to the characteristics mentioned above, the NIR-responsive polymeric SDDs are promising for on-demand drug administration.[27,28]

Plasmonic nanoparticles can efficiently convert the photons' energy into the energy of charge carriers in nanoparticles.[29] Among plasmonic nanoparticles, gold nanoparticles are of high interest due to their surface functional properties and the ability to generate heat through irradiation. Due to the localized surface plasmon resonance (LSPR) phenomenon, gold nanoparticles strongly absorb light and convert it into thermal energy. Therefore, a specific laser frequency stimulating gold particles can produce a hot zone with a radius a thousand times larger than their size. This effect can be used in various applications. For instance, gold nanoparticles' LSPR can damage cancer cells or bacteria with a process called photothermal therapy (PTT).[30,31] Thus, gold nanorods (Au NRs) are one of the most promising plasmonic PPT agents. The lowest light absorption in most body tissues is in the 700 to 900 nm wavelength band, called the "NIR tissue window."[32] As a result, using Au NRs, which possess plasmon resonance in this window, reduces the risk of damaging healthy cells.[33,34]

Electrospinning is a straightforward and economical technique for producing micro and nanofibers utilizing polymer solutions by applying an electrical field. Fibers fabricated by this method have large specific volumes, favorable mechanical properties, and extensive contact area, yielding numerous applications for materials produced.[17,35]

Electrospinning can produce sophisticated structures such as hollow, core-shell, or porous nanofibers.[36] Initially introduced in 2003, the coaxial electrospinning method made it possible to fabricate nanofibers from two or more types of polymer solutions with a broader range of morphologies.[37,38] This method aims to create more advanced nanofibers and nanostructures designed to improve the efficiency of targeted applications.[39–41]

Electrospraying is a technique similar to electrospinning but utilizes electrical force to produce nanoparticles instead of nanofibers. In electrospraying, the liquid at the outlet of a nozzle is exposed to electrical Maxwell stresses, pulling the surface normally and against the restraining surface tension effect. The Maxwell stresses arise in the air between the liquid meniscus affected by an inserted electrode or the nozzle being an electrode (at high DC voltage applied) and a grounded counter-electrode. One of the benefits of electrospraying is the ability to fabricate droplets on the micro-nano scale, regarding fabrication parameters.[42,43]

In the present study, we report the fabrication of photo-responsive PVA-PLGA core-shell nanofibers decorated with plasmonic Au NRs using a simultaneous electrospinning-electrospraying method. A coaxial electrospinning setup provided a shell of poly(lactic-co-glycolic acid) (PLGA) over a poly(vinyl alcohol) (PVA) core and a drug model.[44] PVA is a water-soluble

biocompatible polymer without toxicity to cells and is an ideal polymer for fabricating fibrous biomaterials. Therefore, PVA is selected as the core for loading a hydrophilic drug. PLGA is a hydrophobic synthetic polymer with outstanding biocompatibility.[45] Hence, PLGA can provide an efficient protective shell for the water-soluble core of the system. The as-spun fibers can be used as a drug carrier, combining the outstanding properties of both polymers. The present research focuses on designing and optimizing unique stimuli-response material. These materials can control the drug release kinetics on-demand by applying external stimulation. Simultaneous decoration of core-shell nanofibers with Au NRs provided photo-responsive properties to the assembled fibrous material. It is anticipated that the photo-responsive PVA-PLGA nanofibers matrix decorated by Au NRs holds great promise as on-demand drug carriers.

2 | RESULTS AND DISCUSSION

2.1 | Structure of the core-shell platform

Plasmonic nanoparticle decorated core-shell fibers were designed by coaxial electrospinning of PVA and PLGA solutions with simultaneous electrospraying of Au NRs alcosol. In Figure 1A, the schematic of the electrospinning-co-electrospraying technique is illustrated. The core-shell structure was observed already from the modified Taylor cone of electrospinning, and the fiber morphology was confirmed using TEM. The fiber fabrication with coaxial electrospinning of PVA and PLGA, decoration with electrospraying by Au NRs, and encapsulation of RhB as a drug model inside the polymer core structure were performed simultaneously. Plasmonic particles on the polymer core-shell fibers provided a well-designed hierarchical structure to the final platform. Due to the presence of Au NRs, fibrous drug carriers can produce heat in response to the NIR light triggering (Figure 1B). For this reason, it was advantageous to employ the photo-response ability of Au NRs to develop SDDSs for modulated drug release application. Starting from the principle that the induced temperature can accelerate the drug release kinetics of the core-shell system.

2.2 | Morphological characterizations

The schematic in Figure 2A represents the structure of the platform's core consisting of PVA and a shell of PLGA that form the final core-shell structure. Also, the placement of Au NRs is visualized in the schematic. The FE-SEM microscopy was conducted to visualize the presence of Au NRs, confirming the presence of nanoparticles on the fibers (Figure 2B). The in-depth morphology of the produced coaxial PVA-PLGA fiber is shown in the TEM micrograph in Figure 2C. The contrast, created by electron beam diffraction, represents the distinctive phase in the core-shell structure. The bright region represents the fiber's core, and the dark region indicates the shell. The diameters of the core and shell are approximately 634 and 981 nm, respectively.

Figure 2D presents SEM images of PVA, PLGA, and the core-shell fibers. The monolithic fiber fabrication process was optimized to achieve a fibrous structure similar to the core-shell fibers as a control for drug release studies. The associated diameter distribution of fabricated nanofibers reveals the average diameter of PVA nanofibers of 972 ± 76 nm (Figure S1). Similarly, the average thickness of PLGA fibers is 952 ± 41 nm,

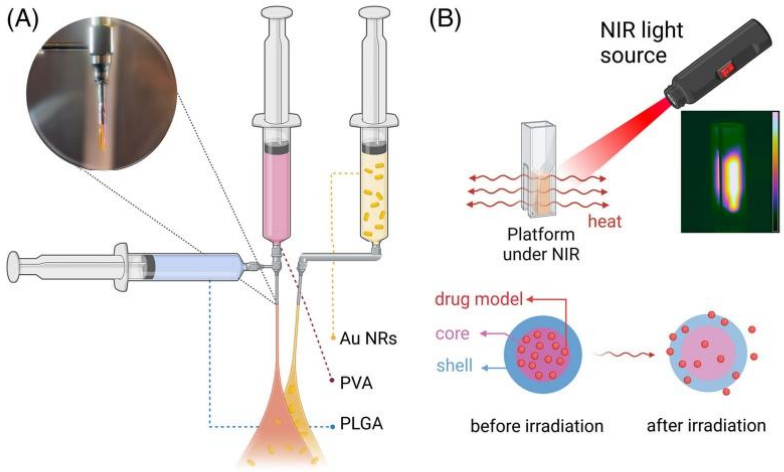

FIGURE 1 Illustration of material preparation.
(A) Schematic presenting the fabrication by coaxial electrospinning of PVA and RhB core and PLGA shell, concurrent with Au NRs electrospraying.
(B) Representative scheme of the photo-responsiveness of the fabricated material under the NIR light, highlighting that an increase in temperature can facilitate a drug release process.

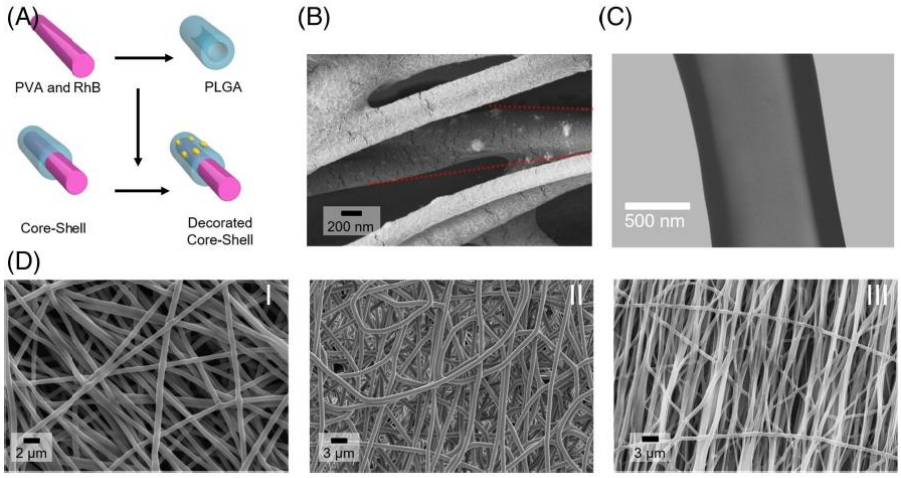

FIGURE 2 Morphological analysis of the electrospun fibers and the core-shell platform. (A) Schematic drawing representing fabrication of core-shell fibers composed of PVA and RhB core, PLGA shell, and decorated with Au NRs. (B) FE-SEM micrograph of Au NRs on the surface of the core-shell platform. (C) The inner core structure and the outer shell of the fiber are evident in the TEM micrograph of the core-shell platform. (D) SEM images of I- PVA electrospun fibers, II- PLGA monolithic fibers, and III- core-shell fibrous materials, demonstrating similar diameters of the monolithic fibers and the core-shell platform.

and of the core-shell platform, 993 ± 33 nm. The efforts to produce fibers with comparable thickness were undertaken to compare the drug release kinetics of the fibers mutually. Figure S2 reports different magnifications of SEM images of the fabricated fibers, highlighting the defect-free, beadless, and geometrical uniformity of the electrospun nanofibers.

2.3 | Physio-chemical characterizations

The ATR-FTIR (Figure 3A) was performed to characterize the chemical structure of the fabricated platform. As can be seen, in both PLGA and core-shell samples, at 1750 cm^{-1}, there are peaks related to the (—CO—) bonds. Also, at the wavenumber of 1080 cm^{-1}, the peak related to the (—C—O—C—) group in both PLGA and core-shell transmissions is visible. However, at 3445 cm^{-1}, the peak of the hydroxyl group is just displayed for PVA fiber. The absence of a hydroxyl group peak in core-shell fibers exhibits the lack of PVA in the platform's outer layer, indicating that the PLGA shell covers the PVA core.[46]

The PVA, PLGA, and core-shell fibers were analyzed using differential scanning calorimetry (DSC). The DSC thermograms represented the characteristic peaks of melting temperature (T_m) and glass transition temperature (T_g) (Figure 3B). The melting temperature of pure PVA is assigned to a reasonably large and sharp exothermic peak visible at about 180.5 °C. For the core-shell nanofibers—where PLGA is introduced—this peak is shifted to 174.2 °C. This gradual shift of the melting temperature to lower values occurs most probably because of the addition of PLGA in the fiber structure.

Thermogravimetric analysis (TGA) was performed to investigate the thermal properties of the PVA, PLGA, and PVA-PLGA core-shell fibers (Figure 3C). Derivative thermogravimetry (DTG) analysis was also carried out on neat PVA and PLGA fibers and the core-shell structure and reported in Figure S3. The PVA fibers presented a multi-step decomposition process with the central peak at 263 °C and a second stage at 414 °C. The first peak can be related to the release of acetyl groups transferred to acetic acid molecules and subsequent catalytic degradation of the main chain by in situ chains strapping at a higher temperature.[47] For the neat PLGA fibers, the TGA curve shows that the degradation starts at 245 °C and finishes at 360 °C with nearly 100% weight loss. The core-shell fiber's TGA curve showed that a shift had occurred at 320 °C. This peak provides additional evidence of the presence of PVA in the core-shell. The formation of the core-shell structure was evident when appropriate conditions were met during the platform fabrication.

The photo-responsivity of PVA-PLGA core-shell nanofibers results from the decoration of the fiber surface with Au NRs. The XRD pattern study was carried out to demonstrate the presence of Au NRs in the core-shell

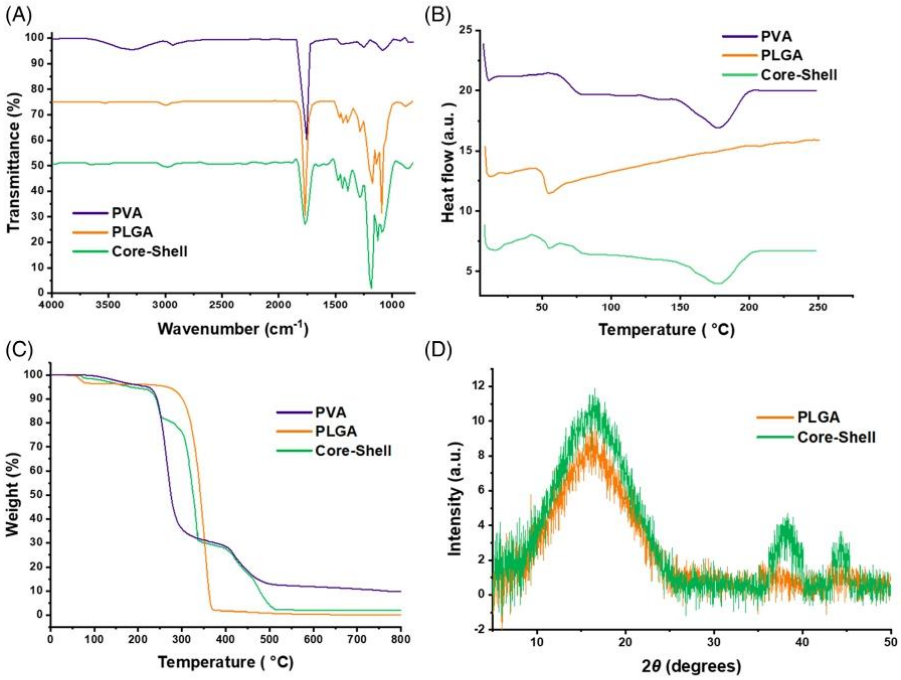

FIGURE 3 Chemical and physical properties of PLGA, PVA, and core-shell fibers. (A) ATR-FTIR spectra of PLGA and PVA fibers compared with the core-shell platform. (B) DSC graph of the core-shell system, showing the presence of both PVA and PLGA in the structure. (C) Weight percentage versus temperature TGA curves of monolithic fibers along with the core-shell platform. (D) XRD pattern of PLGA fiber compared with core-shell fibers decorated with Au NRs.

fibers (Figure 3D). XRD data revealed the characteristic peaks of Au NRs at 2θ scattered angles of 38.0 and 44.2°, which certifies the presence of Au NRs in the platform.[48]

2.4 | Cell studies

In order to verify the biocompatibility of the proposed electrospun substrates and their potential use for biomedical applications, L929 fibroblasts were seeded and cultured onto the fibrous constructs, as also reported in previous studies.[49,50] The presence of a PVA core in the PLGA-based core-shell fibers was investigated in terms of cell response and compared to PLGA pristine fibers and TCP controls. More specifically, cell-materials interactions were evaluated with regard to cell viability, proliferation, and morphology. A Live/Dead assay kit was used to stain the cells seeded onto the constructs and mark them in green or red color according to their live or dead state. Representative Live/Dead images showed a large majority of viable green cells on both days 1 and 3 of culture (Figure S4), demonstrating the high viability percentage of cells cultured on the proposed substrates (>87%, Figure 4A) and the cytocompatibility of the materials. No significant difference was detected among the selected conditions at any time point.

The cell proliferation is reported in Figure 4B, displaying the linear growth of cells during the culture time (1, 3, and 7 days) for all tested conditions. No evident difference between the fibrous samples was detected, while cells seeded onto tissue culture substrates showed a more significant proliferation at the initial stage of the culture (1 and 3 days). This is not surprising since TCPs are treated to be highly cell-friendly, promoting easy and efficient cell adhesion and growth. At the latest stage of culture (day 7), all the tested samples showed similar performance, proving the biocompatibility and suitability of the fibrous substrates for cell viability, activities, and proliferation.

Finally, cell morphological analysis was carried out by observing confocal images of Actin/DAPI stained

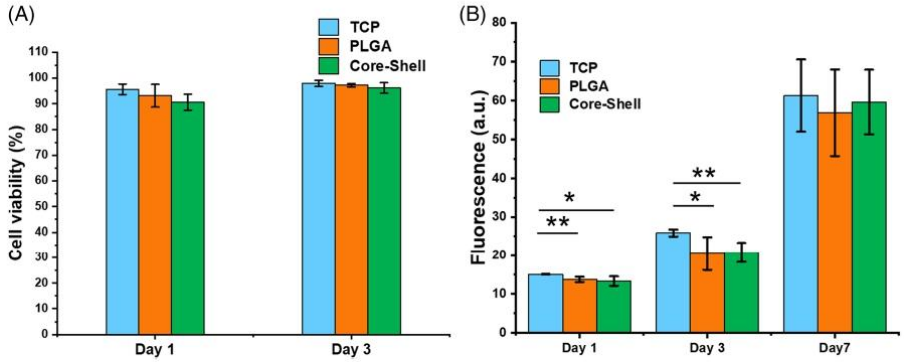

FIGURE 4 Cell viability of L929 fibroblasts seeded on PVA-PLGA core-shell fibers, PLGA fibers, and TCP. (A) Cell viability percentage calculated from Live/Dead images analysis, reporting cell viability >87% at days 1 and 3 of culture. (B) Cell proliferation up to 7 days of culture, showing the increasing trend during the culture time for all tested samples. Significant differences are reported as $^{*}p \leq 0.05$, $^{**}p \leq 0.01$.

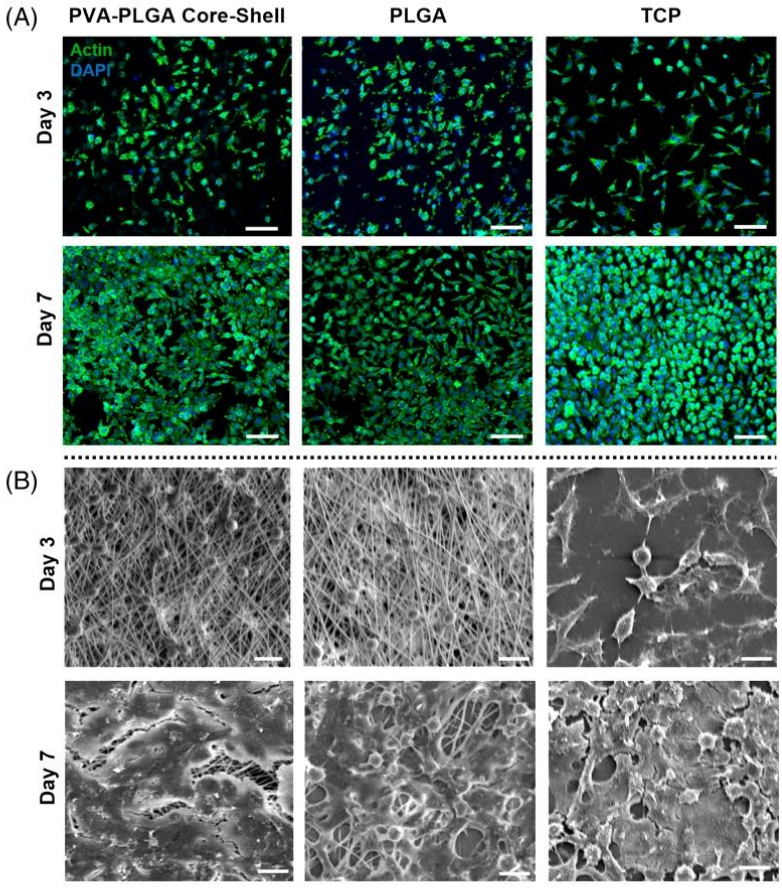

FIGURE 5 Cell morphology of L929 fibroblasts seeded on PVA-PLGA core-shell fibers, PLGA fibers, and TCP after 3 and 7 days of culture. (A) Cell cytoskeleton is stained green while nuclei are marked in blue (Actin/DAPI staining). Scale bar: 100 μm. (B) SEM images of the cells seeded on fibrous constructs versus TCP control. Scale bar: 20 μm. Data revealed the spreading and elongation of the cells during the culture time.

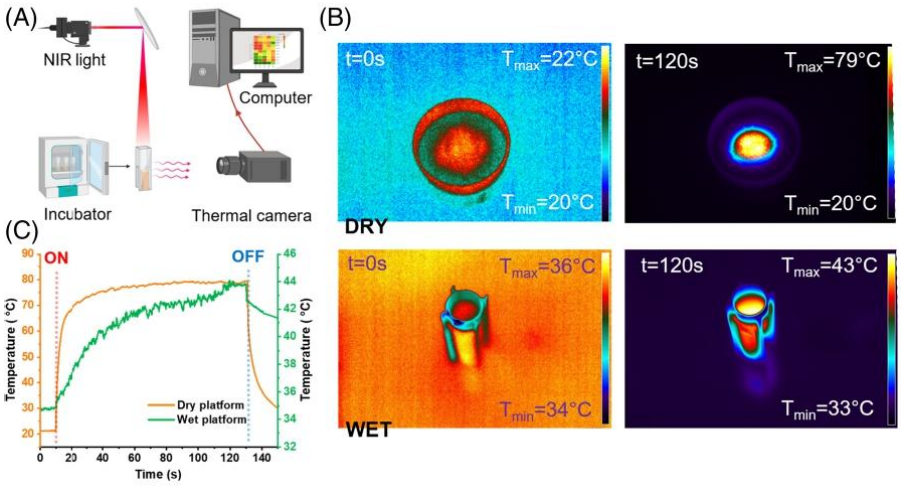

FIGURE 6 The photo-responsive platform features the fast and on-demand responsiveness of the fabricated material. (A) The schematic of the experimental setup illustrates a thermal camera capturing the temperature of the samples taken out from an incubator and irradiated by a NIR laser. (B) The IR thermogram images of the dry and wet platforms before and after 2 min of irradiation were captured with a thermal camera. Wet samples were analyzed on a hot plate to maintain the platform's temperature at around 37 °C. (C) Temporal plots of the platform's behaviors under the NIR illustration for wet and dry samples, showing the photo-response property of the material.

samples (Figure 5A) and SEM micrographs of the structures (Figure 5B) at days 3 and 7 of culture. At the early stage, the cell cytoskeleton appeared roundish and spherical on the fibrous samples compared to TCP control, most probably due to the lack of cell binding sites in the synthetic polymers. However, during the culture time, cells spread and became more elongated with the typical spindle shape, highlighting the efficient support for cell adhesion and spreading.

2.5 | Thermal-response characterizations

The nanofibrous system was decorated with the Au NRs and loaded by Rhodamine-B. The decoration of the platform with plasmonic nanoparticles provided a robust absorption of NIR light that can provide heat due to the outstanding photo-response efficiency.[29] The photo responsiveness to the irradiation of NIR light was confirmed using a thermal camera. The applied NIR laser power was fixed at 2.4 W cm^{-2} and irradiated directly on the system with an 808 nm wavelength.

Figure 6A shows a schematic of a NIR laser emitting beam irradiation on the platform (contained in a water-filled vial) and the experimental setup used to investigate the fiber's photothermal activity. Simultaneously with the illumination of samples, the thermal camera records the thermographic images of the photo-response of the irradiated samples.

Low-power lasers are common in clinical practice due to their bio-stimulating effect in treatment. A lower-power laser, however, results in less heat during the procedure. The heat produced by the SDDSs may not be enough to modulate the drug release if there is a considerable distance between the heat producer (in this case, NIR) and the stimuli-responsive material. The designated strategy was to locate the Au NRs on the surface of the nanofibers instead of putting them inside the core-shell system. The rods are either trapped between the fibers or deposited on their surface. The advantage of this method is the higher generated temperature compared to the particles inside the fibers and the reduction of side effects as the thermally-accelerated polymer matrix degradation.

As can be seen in Figure S5, the location of nanorods can improve the amount of induced heat for dry samples up to 9.6 °C in 2 min. Table S1 displays the temperature responses due to different structures and localization of Au NRs.

The PVA-PLGA core-shell fibers decorated with Au NRs show a strong NIR light absorption and conversion to thermal energy. Figure 6B shows the thermographic images of the platform in dry and wet states. The platform was studied first in the dry state to indicate the maximal potential of the response of the core-shell fiber to NIR light. Subsequently, they were analyzed in water

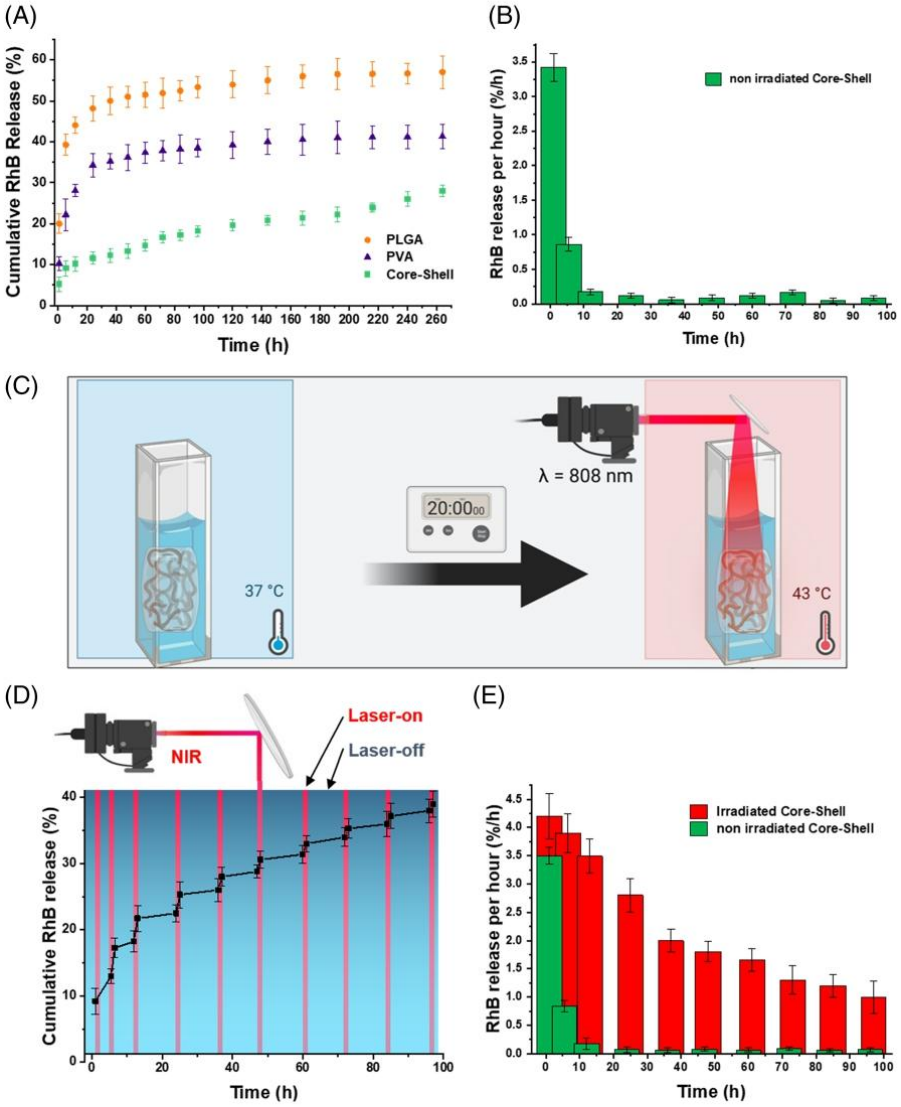

FIGURE 7 Drug delivery property of the core-shell platform. (A) Cumulative RhB release of three samples of monolith PLGA and PVA and non-irradiated core-shell, showing the burst release of the monolithic fibers. (B) Bar chart of non-irradiated core-shell RhB release per hour, demonstrating the release kinetic of non-irradiated platforms in different time stages. (C) The scheme represents the platform's induced temperature under NIR irradiation, helping to elevate the RhB release. (D) Cumulative RhB release after 10 NIR-light irradiation cycles. The red vertical lines represent a cycle of irradiation. (E) The bar graph of RhB release per hour while the platform was irradiated with NIR light for sequences of 20 min. The graph clearly shows the induced release of RhB upon the laser trigger, assisting the photo response behavior of the fabricated platform.

to reveal the applicable property of the platform for the drug delivery application. The fiber's temperature increased significantly and rapidly, increasing the surrounding water temperature. The highest temperature of samples was 80 °C for dry samples and 44 °C for fibers in water. (Figure 6C). The plasmonic system was successfully designed to achieve the targeted temperature that triggered the core-shell structure to modulate the drug

release and reach the typical temperature range for performing PTT.

2.6 | Drug release studies

This study aimed to develop a smart drug carrier to sustain the drug level in a therapeutic window by exploiting its photo-responsive properties. Sustained drug release can improve therapeutic consequences by reducing drug toxicity and dosing frequency while increasing efficiency. For this purpose, RhB, as a fluorescent dye, was selected as a drug model. Previous studies have demonstrated that developing core-shell structured nanofibers can reduce burst release and sustain long-term drug release.[51]

In Figure 7A, the drug release from PLGA, crosslinked PVA, and core-shell fibers were measured at 37 °C and not triggered by NIR light. The PVA fibers for this study were crosslinked since the monolith PVA can dissolve in water and are incomparable with PLGA and core-shell fibers. To emphasize the effect of morphology on drug release and avoid the dimension effect, the three mentioned fibers were produced with similar fiber size distributions. Considerable differences were observed for two different structures of monolithic and core-shell materials. The RhB release from the monolithic PLGA fibers exhibited an initial burst release. Similarly, in the case of the PVA, RhB was released burst in the early stages of the study. However, the release profile was sustained for core-shell fibers with near first-order release kinetics. As a result of the internal structure, the overall release rate of core-shell fibers was significantly slower, and the release trend constantly increased during the incubation time (Figure 7B). For the monolith fibers, the cumulative release did not increase after 4 days of the study.

The NIR irradiation process is illustrated in Figure 7C. This figure shows the increase in the platform temperature using a $\lambda = 808$ nm source of NIR. The platform reached 43 °C as a response to irradiating by laser. The RhB release from the irradiated platform utilizing NIR light is visible in Figure 7D. The duration of each irradiation sequence was 20 min. For samples not triggered with NIR light, a small amount of drug release was observed from the nanofibers, indicating that the Au nanorods played a vital role as a nanoscale heat-generating source. These findings appeared promising for biomedical applications that target a modulated drug release. The drug release intensity was elevated upon NIR irradiation after each timepoint of drug release measurement, and the release data were collected before and after each cycle. Figure 7E shows the on-demand release from the core-shell system with Au NRs. The structure of the core-shell fibrous materials led to a regulated and steady release compared to the monolithic counterparts. Introducing Au nanorods led to the fabrication of a photo-responsive polymer core-shell system to solve this problem. Taking advantage of the stimuli-responsive drug carrier, upon the NIR irradiation, the release kinetic of the vehicle is elevated in response to NIR light irradiation. At the first time point, the release from the core-shell fibers triggered by NIR is about 1.8 folds higher than the non-irradiated core-shell. The platform's exposure to NIR provided 39% of RhB release in the first 96 h of the study, while for the irradiation control sample, the release rate was 18%. The reported results imply the increase in RhB release from the core-shell fiber upon NIR irradiation that is associated with an increase in the temperature of the platform.

The mechanism of RhB release from electrospun nanofibers is based on the drug model's desorption from the nanofibers and its subsequent diffusion in water through the porous structure of the platform. Desorption is the limiting factor in drug release from nanofibers because dye diffusion in water occurs quicker than desorption. The temperature rise caused by the laser irradiation on the platform generates an increase in the kinetics of both desorption and diffusion.

The SEM images of fibers before and after submerging in water were acquired to study the platform's stability. In Figure S6 the SEM micrographs of electrospun platform after submerging in water are collected every 24 h timepoints. This figure exhibited the platform will not dissolve in water during the drug release process. Moreover, UV–vis spectroscopy was carried out to observe the effect of drug release and irradiation on the nanorod's detachment. The absorption spectra of samples before and after the irradiation were compared to Au NRs spectra to trace similarities. The spectra of platform media before and after NIR irradiation did not exhibit characteristic peaks of Au NRs at 514 and 808 nm. This result reveals the stability of the nanostructured platform by submerging it in water and even after irradiation (Figure S7). Accordingly, implementing plasmonic nanoparticles, which can be triggered upon a source of light (NIR), is a promising candidate for on-demand release applications. Consequently, the core-shell morphology is suitable for a steady and controlled drug release in the long term.

3 | CONCLUSION

The present work described the successful fabrication of a core-shell platform for smart drug delivery. This platform incorporated PVA and PLGA as biocompatible polymers, Rhodamine-B as the drug model, and gold nanorods as plasmonic agents to induce an on-demand platform response upon NIR irradiation.

Core-shell platform was fabricated by coaxial electrospinning of PLGA and PVA paired with electrospraying of Au NRs under controlled environmental conditions. The role of the PLGA shell is crucial for the platform because the PVA core can dissolve in water. Furthermore, the PLGA shell can protect the core from structural damage. In addition, the core-shell structure was proved to be biocompatible and provided sustained drug release kinetics. Moreover, the drug release from the core-shell nanofibrous material was performed under the NIR laser to demonstrate the on-demand performance of the "smart" drug delivery system. The RhB release of the activated platform by NIR light, compared to the non-irradiated system, exhibited successful elevation of the release resulting from response to the stimuli. Moreover, the nanostructured core-shell platform exhibited stability in the structure before and after irradiation with NIR light. The present work highlights that employing plasmonic nanoparticles elevates on-demand the release rate of the drug by increasing the temperature of the platform. The smart fabricated drug delivery system will be helpful in future clinical applications, emphasizing the photoactive feature of this platform.

4 | EXPERIMENTAL SECTION

4.1 | Materials

For the fabrication of the platform, Polyvinyl alcohol (PVA, 85,000–124,000 Da), Hydrochloric acid (HCl, 37%), Hexafluoro isopropanol (HFIP, 99.5%), acetone (99.5%), and Rhodamine B (RhB, 95%) were purchased from Sigma Aldrich. Poly (D, L-lactide-co-glycolide) (PLGA, Purasorb PDLG 5010) was obtained from Corbion Purac, and gold nanorods (Au NRs, $\lambda = 800$ nm, OD = 50, $C = 0.88$ mg mL^{-1}) from nanoComposix, USA. For the cell studies, Bovine serum albumin (BSA), hexamethyldisilane (HMDS) and phosphate buffer saline (PBS), glutaraldehyde (GTA), Triton X, DAPI, and L929 murine fibroblasts were bought from Sigma-Aldrich, Poland. "Dulbecco's modified" Eagle's medium (DMEM), fetal bovine serum (FBS), penicillin streptomycin (PS), and EDTA-trypsin were purchased from Gibco Invitrogen, USA. Alexa Fluor 488 Phalloidin and Live/Dead assay were obtained from Thermo-Fisher Scientific, USA.

4.2 | Platform preparation

The core polymer solution was prepared by dissolving 1.0 g of PVA in 10.0 mL of DI water, and the fibers' shell solution contained 11 wt% of PLGA in 10.0 mL HFIP. Furthermore, alcosol of Au NRs was prepared by dissolving 20 μL of 50 OD Au NRs (17.6 μg) in 100 μL of 1:1 ethanol and water solution (v:v). For the coaxial electrospinning setup, the spinneret consisted of a 21G needle for the core and a 16G needle for the shell solution. Core-shell fibers were electrospun by applying 12 kV voltage and a flow rate of 250 μL h^{-1} for the core solution and 650 μL h^{-1} for the shell solution. Fibers were collected on a grounded drum rotating at 450 rpm with an 18 cm needle-to-collector distance. The ambient parameters as temperature and humidity in electrospinning were 20 °C and 45%, respectively. Core-shell fibrous materials containing a drug model were fabricated using the same procedure by dissolving 5 mg of RhB in 5 mL of the core solution during the early stage of preparation. In addition, PVA and PLGA monolith nanofibers with similar structural features (e.g., fiber diameter, mat porosity, and thickness) and the same amount of RhB were prepared as control samples. To prepare monolith fibers of PLGA, a solution of 0.9 wt% RhB in shell solution was prepared. The electrospinning parameters for PLGA solution were using a 26G needle, 15 kV was the applied voltage, 800 μL h^{-1} was the flow rate, with a needle tip to rotor collector distance of 18 cm at a rotation speed rate of 450 rpm. The as-prepared PVA solution was processed with a 26G needle, applying 10 kV voltage, with a flow rate of 400 μL h^{-1} and similar drum collector parameters used to prepare the PLGA nanofibers. The ambient parameters for PVA electrospinning were 20 °C and 40% relative humidity. After the electrospinning procedure, the PVA fibers were soaked in a 10 mL solution of 2.5 wt% glutaraldehyde in acetone at 44 °C. The next step was adding 100 μL of HCl to the crosslinking solution and maintaining the fibers in the solution for 1 h. Finally, the electrospun mat was washed twice with acetone and water. For electrospraying of Au NRs, the prepared alcolsol was transferred to a 1 mL syringe equipped with a 26G needle. Electrospraying parameters were set at 12 kV positive voltage, 400 μL h^{-1} flow rate, needle-collector distance of 18 cm, 450 rpm of drum rotation, at a temperature of 20 °C, and humidity of 45%.

4.3 | Morphological characterizations

In order to study the morphology and dimension of the fabricated core-shell nanofibers, transmission electron microscopy (TEM) was performed. For the analysis of the core-shell fibers, electrospinning was performed directly on a TEM grid. The FE-SEM microscopy method was performed to show the presence of Au NRs on the surface of the platform. FE-SEM and TEM studies were conducted using FEI Nova NanoSEM 450 microscope at a working distance of 2 mm and accelerating voltage of

30 kV. Scanning electron microscopy (SEM) observations were performed using JEOL JSM-6390LV at a working distance of 10 mm and 10 kV accelerating voltage to investigate the structure of the monolith fibers. Before the SEM, materials were sputtered with approximately 5 nm thick layers of gold using an SC7620 Polaron mini sputter coater (Quorum Technologies Ltd., Ashford, UK).

4.4 | Chemical characterizations

ATR-FTIR spectroscopy was employed to characterize the presence of the material's functional groups. A Bruker Vertex70 FT-IR Spectrometer measured the transmittance of the material in the wavenumbers range of 4000–400 cm^{-1} with a resolution of 2 cm^{-1} and eight scans for each sample. Using Bragg-Brentano geometry, XRD measurements were completed with a Bruker D8 Discover diffractometer in the reflection mode. The analysis was conducted in the angular range (2 thetas, 2θ) between 5 and 50°. Data were collected with a step of 0.02° per second at each point. Moreover, XRD made it possible to confirm the presence of Au NRs in the platform. Ultraviolet–visible (UV–Vis) spectra were acquired using a Multiskan GO spectrophotometer (Thermo Scientific, USA) to scan over a range of 400 to 1000 nm with a step of 5 nm. In order to prove the absence of gold nanoparticles in the drug release solution and detect any potential nanoparticle leak caused by laser irradiation, UV–vis spectra were performed.

4.5 | Thermal characterizations

DSC analysis was performed with a Perkin Elmer PYRIS-1, and data were analyzed using OriginPro software. Measurements were performed from 0 to 250 °C, with a rate of 10 °C min^{-1} and the weight of the samples were approximately 20 mg. The thermogravimetric analysis (TGA) was performed by a Q5000 (TA Instruments) under the nitrogen purge. The analysis was conducted in the temperature range of 20–800 °C with a heating ramp of 10 °C min^{-1}.

4.6 | In vitro cell studies

L929 murine fibroblasts were cultured in DMEM modified with 10% FBS and 1% PS and incubated at 37 °C and 5% CO_2 until reaching ~80% confluence. The culture medium was changed every other day. During the seeding process, cells were detached by PBS washing and subsequent incubation in 0.05% EDTA-trypsin for 3 min at 37 °C and 5% CO_2. The harvested cells were centrifuged for 5 min at 1200 rpm, and the resulting cell pellet was resuspended in a suitable volume of culture medium to obtain the desired cell density in the seeding solution.

PVA-PLGA core-shell and PLGA fibers were electrospun onto coverslips with a diameter of 1.5 cm, sterilized under UV light for 30 min on both sides, and finally placed in 24-well plates. A tissue culture plate (TCP) was tested as a control condition. L929 fibroblasts were seeded on the samples with a cell density of 10^4 units cm^{-2} and cultured for up to 7 days.

Cells were stained using a Live/Dead assay kit to investigate the viability of L929 fibroblasts seeded on the samples. On days 1 and 3 of culture, the samples were washed with PBS and treated with the Live/Dead staining solution composed of 0.5 μL of calcein (for staining the viable cells in green color) and 2 μL of ethidium homodimer (for red staining of dead cells) in 1 mL of PBS. Three replicates of each sample were soaked in the staining solution and incubated for 10 min at 37 °C and 5% CO. Then, scaffolds were washed three times in PBS and imaged using a confocal microscope (Leica). Percentages of viable cells were counted using the Cell Counter plugin of ImageJ (National Institute of Health, USA).

The cell proliferation rate was assessed with PrestoBlue assay. Cells seeded on PVA-PLGA core-shell fibers, PLGA fibers, and TCPs were incubated for 1 h in 10% (v/v) PrestoBlue solution in a culture medium at 37 °C and 5% CO_2. Five replicates per each condition were tested after 1, 3, and 7 days of culture. The resulting solution was aliquoted in 100 μL aliquots, transferred to a 96-well plate, and analyzed with a fluorometer (Fluoroskan Ascent TM Microplate Fluorometer, Thermo Scientific) with excitation at 530 nm and emission at 620 nm.

The cell morphology was observed in confocal and SEM images of three sample replicates fixed after 3 and 7 days of culture. For the staining of cell cytoskeleton and nuclei, samples were washed with PBS and fixed in 4% paraformaldehyde for 15 min at room temperature. After washing, samples were first incubated in 0.3% (v/v) Triton X-100 solution for 15 min and then in 1% (w/v) BSA for 30 min. Subsequently, samples were treated with a solution of 1:40 Alexa Fluor 488 Phalloidin in PBS in the darkness for 40 min. Finally, cell nuclei were stained using a solution of 1:500 DAPI in PBS for 10 min. Samples were washed and imaged using a confocal microscope (Leica).

For SEM images, the constructs were washed in PBS and fixed in 3% ice-cold GTA for 3 hours. The substrates were then washed three times with deionized water and dehydrated in 50%, 70%, 90%, and 100% concentrated

ethanol solutions for 15 minutes each. Finally, samples were treated with HMDS and dried under a fume hood overnight.

4.7 | Photo-responsivity characterization

The NIR light source was a diode laser (EKSMA OPTICS) operating at 808 nm in the high absorption range of Au NRs (longitudinal plasmon band) with a rectangular profile. A high-resolution thermal camera (FLIR, A655sc) was employed to map and identify the spatial heating distribution and temperature profile under laser illumination. The camera produces thermal images of 640 by 480 pixels with an accuracy of ±0.2 °C. It works seamlessly with proprietary software (FLIR ResearchIR Max) to record and process the thermal data acquired by the camera.

4.8 | Drug-release analysis

The release of Rhodamine B from the monolith fibers of PLGA, PVA, and core-shell was analyzed at 37 °C. Circular electrospun mat samples with a diameter of 2 cm and containing approximately 50 μg of dye (Rhodamine-B) were immersed in 1 mL of PBS solution at 37 °C. The vial was sealed and wrapped with aluminum foil to prevent water evaporation and light exposure. The supernatant fluid was exchanged with fresh water and maintained at the incubator to maintain the same temperature as set for any specific test after 1, 4, 10, and 12 h of release. The sample temperature was checked by a FLIR thermal camera several times for each sample. Over the next 4 days, the release level of RhB was measured every 12 h. Subsequently, the measurement time points were reduced to once per day (over the following 7 days). Fluorescence signals were measured with a fluorometer (Fluoroskan Ascent TM Microplate Fluorometer, Thermo Scientific, USA) (excitation-emission 530–620 nm) and used to evaluate the concentration of released RhB based on a calibration curve.

The gold nanorods decorated systems release experiments were carried out using an 808 nm diode laser (EKSMA OPTICS) and a power density of 2400 mW cm^{-2}. The 1 cm circular decorated core-shell fibers were suspended in a vial filled with 1 mL of deionized water. The vial was additionally secured with a parafilm seal to protect the sample from water evaporation. The samples were irradiated with a NIR laser in periodic cycles of the ON/OFF mechanism of irradiation, and the duration of irradiation was 20 min, and they rested for 40 min for each sequence. Afterward, the supernatant was collected, and its concentration was measured using the fluorometer to evaluate the amount of RhB released.

4.9 | Statistical analysis

Data are presented as mean values ± *SD*. One-way ANOVA test was carried out, and differences were considered statistically significant when the *p*-value was ≤0.05: $*p \leq 0.05$, $**p \leq 0.01$, $***p \leq 0.001$, $****p \leq 0.0001$. Drug release measurements were performed six times for each platform.

ACKNOWLEDGMENTS

This work was supported by the National Science Centre (NCN) SONATA BIS Project No. 2020/38/E/ST5/00456 and the Polish National Agency for Academic Exchange (NAWA) under Bekker NAWA Programme, grant number: BPN/BEK/2021/1/00161. The Authors are grateful for the support provided by the National Agency for Academic Exchange (NAWA) grant no. PPI/APM/2018/1/00045/U/001. Figures 1, 6A, 7C, and S7a were created with Biorender; Figure 7D was partially created with Biorender. C.R., P.N., and F.P. acknowledge the financial support from the Polish Ministry of Science and Higher Education through scholarships for outstanding young scientists.

ORCID

Yen B. Truong https://orcid.org/0000-0003-2210-2414
Filippo Pierini https://orcid.org/0000-0002-6526-4141

REFERENCES

[1] A. Luraghi, F. Peri, L. Moroni, *J. Controlled Release* **2021**, *334*, 463.
[2] T. Sahu, Y. K. Ratre, S. Chauhan, L. V. K. S. Bhaskar, M. P. Nair, H. K. Verma, *J. Drug Deliv. Sci. Technol.* **2021**, *63*, 102487.
[3] C. Li, J. Wang, Y. Wang, H. Gao, G. Wei, Y. Huang, H. Yu, Y. Gan, Y. Wang, L. Mei, H. Chen, H. Hu, Z. Zhang, Y. Jin, *Acta Pharm. Sin. B* **2019**, *9*, 1145.
[4] D. Steinberg, M. Friedman, *Periodontol 2000* **2020**, *84*, 176.
[5] O. Veiseh, J. W. Gunn, M. Zhang, *Adv. Drug Deliv. Rev.* **2010**, *62*, 284.
[6] S. S. Silva, J. M. Gomes, R. L. Reis, S. C. Kundu, *ACS Appl. Bio Mater.* **2021**, *4*, 4000.
[7] Y. Xu, C. S. Kim, D. M. Saylor, D. Koo, *J. Biomed. Mater. Res. B Appl. Biomater.* **2017**, *105*, 1692.
[8] D. Mishra, J. R. Hubenak, A. B. Mathur, *J. Biomed. Mater. Res. A* **2013**, *101*, 3646.
[9] N. Kamaly, B. Yameen, J. Wu, O. C. Farokhzad, *Chem. Rev.* **2016**, *116*, 2602.
[10] K. S. Butler, P. N. Durfee, C. Theron, C. E. Ashley, E. C. Carnes, C. J. Brinker, *Small* **2016**, *12*, 2173.
[11] B. Felice, M. P. Prabhakaran, A. P. Rodríguez, S. Ramakrishna, *Mater. Sci. Eng., C* **2014**, *41*, 178.
[12] A. M. Inamuddin, A. M. Asiri, *Applications of Nanocomposite Materials in Drug Delivery*. UK: Woodhead Publishing; **2018**, p. 1.
[13] P. Jana, M. Shyam, S. Singh, V. Jayaprakash, A. Dev, *Eur. Polym. J.* **2021**, *142*, 110155.
[14] X. Tong, W. Pan, T. Su, M. Zhang, W. Dong, X. Qi, *React. Funct. Polym.* **2020**, *148*, 104501.

[15] M. Sheikhpour, L. Barani, A. Kasaeian, *J. Controlled Release* **2017**, *253*, 97.
[16] A. M. Vargason, A. C. Anselmo, S. Mitragotri, *Nat. Biomed. Eng.* **2021**, *5*, 951.
[17] A. L. Yarin, B. Pourdeyhimi, S. Ramakrishna, *Fundamentals and Applications of Micro and Nanofibers*. UK: Cambridge University Press; **2013**, p. 1.
[18] Y. Zhang, S. Sinha-Ray, A. L. Yarin, *J. Mater. Chem.* **2011**, *21*, 8269.
[19] Y. Zhang, A. L. Yarin, *J. Mater. Chem.* **2009**, *19*, 4732.
[20] J. K. Patra, G. Das, L. F. Fraceto, E. V. R. Campos, M. D. P. Rodriguez-Torres, L. S. Acosta-Torres, L. A. Diaz-Torres, R. Grillo, M. K. Swamy, S. Sharma, S. Habtemariam, H. S. Shin, *J. Nanobiotechnol.* **2018**, *16*, 1.
[21] Y. Wang, J. Yan, N. Wen, H. Xiong, S. Cai, Q. He, Y. Hu, D. Peng, Z. Liu, Y. Liu, *Biomaterials* **2020**, *230*, 119619.
[22] S. Mura, J. Nicolas, P. Couvreur, *Nat. Mater.* **2013**, *12*, 991.
[23] A. Liguori, S. Pandini, C. Rinoldi, N. Zaccheroni, F. Pierini, M. L. Focarete, C. Gualandi, *Macromol. Rapid Commun.* **2022**, *43*, 2100694. https://doi.org/10.1002/MARC.202100694
[24] G. Liu, W. Liu, C. M. Dong, *Polym. Chem.* **2013**, *4*, 3431.
[25] B. Sana, A. Finne-Wistrand, D. Pappalardo, *Mater. Today Chem.* **2022**, *25*, 100963.
[26] H. Chu, J. Zhao, Y. Mi, Z. Di, L. Li, *Nat. Commun.* **2019**, *10*, 1.
[27] A. Tomitaka, H. Arami, A. Ahmadivand, N. Pala, A. J. McGoron, Y. Takemura, M. Febo, M. Nair, *Sci. Rep.* **2020**, *10*, 1.
[28] P. Nakielski, S. Pawłowska, C. Rinoldi, Y. Ziai, L. de Sio, O. Urbanek, K. Zembrzycki, M. Pruchniewski, M. Lanzi, E. Salatelli, A. Calogero, T. A. Kowalewski, A. L. Yarin, F. Pierini, *ACS Appl. Mater. Interfaces* **2020**, *12*, 54328.
[29] A. Guglielmelli, F. Pierini, N. Tabiryan, C. Umeton, T. J. Bunning, L. de Sio, *Adv. Photonics Res.* **2021**, *2*, 2000198.
[30] N. Sarfraz, I. Khan, *Chem. – Asian J.* **2021**, *16*, 720.
[31] B. Singh, N. Shukla, J. Kim, K. Kim, M. H. Park, *Pharmaceutics* **2021**, *13*, 1319.
[32] F. Pierini, A. Guglielmelli, O. Urbanek, P. Nakielski, L. Pezzi, R. Buda, M. Lanzi, T. A. Kowalewski, L. de Sio, *Adv. Opt. Mater.* **2020**, *8*, 20000324. https://doi.org/10.1002/ADOM.202000324
[33] S. Asadi, L. Bianchi, M. de Landro, S. Korganbayev, E. Schena, P. Saccomandi, *J. Biophotonics* **2021**, *14*, e202000161.
[34] I. Capek, *Adv. Colloid Interface Sci.* **2017**, *249*, 386.
[35] H. M. Ibrahim, A. Klingner, *Polym. Test.* **2020**, *90*, 106647.
[36] M. Badmus, J. Liu, N. Wang, N. Radacsi, Y. Zhao, *Nano Mater. Sci.* **2021**, *3*, 213.
[37] J. Yoon, H. S. Yang, B. S. Lee, W. R. Yu, *Adv. Mater.* **2018**, *30*, 1704765.
[38] M. Hou, X. Y. Zhao, C. Yang, Z. Q. Xue, H. Y. Chen, J. Vac Sci, B. Zaicheng Sun, E. Zussman, A. L. Yarin, J. H. Wendorff, A. Greiner, *Adv. Mater.* **2003**, *15*, 1929.
[39] D. Han, A. J. Steckl, *ChemPlusChem* **2019**, *84*, 1453.
[40] S. Pawłowska, C. Rinoldi, P. Nakielski, Y. Ziai, O. Urbanek, X. Li, T. A. Kowalewski, B. Ding, F. Pierini, *Adv. Mater. Interfaces* **2020**, *7*, 2000247.
[41] A. L. Yarin, M. W. Lee, S. An, S. S. Yoon, *Self-Healing Nanotextured Vascular Engineering Materials*. Switzerlan: Springer Nature; **2019**, p. 105. https://doi.org/10.1007/978-3-030-05267-6
[42] D. N. Nguyen, C. Clasen, G. van den Mooter, *J. Pharm. Sci.* **2016**, *105*, 2601.
[43] N. Bock, T. R. Dargaville, M. A. Woodruff, *Prog. Polym. Sci.* **2012**, *37*, 1510.
[44] S. Sett, M. W. Lee, M. Weith, B. Pourdeyhimi, A. L. Yarin, *J. Mater. Chem. B* **2015**, *10*, 2147.
[45] W. Ren, X. Yu, L. Chen, T. Shi, T. Bou-Akl, D. C. Markel, *J. Biomater. Appl.* **2022**, *37*, 712.
[46] E. García-Millán, M. Quintáns-Carballo, F. J. Otero-Espinar, *Data Brief* **2017**, *15*, 133.
[47] F. Reguieg, L. Ricci, N. Bouyacoub, M. Belbachir, M. Bertoldo, *Polym. Bull.* **2020**, *77*, 929.
[48] W. Chen, A. Palazzo, W. E. Hennink, R. J. Kok, *Mol. Pharmaceutics* **2017**, *14*, 459.
[49] P. Nakielski, C. Rinoldi, M. Pruchniewski, S. Pawłowska, M. Gazińska, B. Strojny, D. Rybak, K. Jezierska-Woźniak, O. Urbanek, P. Denis, E. Sinderewicz, W. Czelejewska, J. Staszkiewicz-Chodor, M. Grodzik, Y. Ziai, M. Barczewska, W. Maksymowicz, F. Pierini, *Small* **2022**, *18*, 2104971. https://doi.org/10.1002/smll.202104971
[50] C. Rinoldi, E. Kijeńska, A. Chlanda, E. Choinska, N. Khenoussi, A. Tamayol, A. Khademhosseini, W. Swieszkowski, *J. Mater. Chem. B* **2018**, *6*, 3116.
[51] M. Khodadadi, S. Alijani, M. Montazeri, N. Esmaeilizadeh, S. Sadeghi-Soureh, Y. Pilehvar-Soltanahmadi, *J. Biomed. Mater. Res. A* **2020**, *108*, 1444.

SUPPORTING INFORMATION

Additional supporting information can be found online in the Supporting Information section at the end of this article.

How to cite this article: M. A. Haghighat Bayan, Y. J. Dias, C. Rinoldi, P. Nakielski, D. Rybak, Y. B. Truong, A. L. Yarin, F. Pierini, *J. Polym. Sci.* **2023**, 1. https://doi.org/10.1002/pol.20220747

12- Statement of the Co-Authors

Doctoral student's statement on participation

in a scientific publication

I hereby confirm that my contribution to the preparation of **publication no. 1**, Anna Zakrzewska†, **Mohammad Ali Haghighat Bayan**†, Paweł Nakielski, Francesca Petronella, Luciano De Sio, and Filippo Pierini. "Nanotechnology transition roadmap toward multifunctional stimuli-responsive face masks." ACS Applied Materials & Interfaces 14, no. 41 (**2022**): 46123-46144, involved gathering literature data referring to 157 publications and analyzing them. Additionally, I was responsible for writing the literature review and preparing responses to reviewers.

Signature of the doctoral student

Signature of the supervisor

Doctoral student's statement on participation in a scientific publication

I hereby confirm that my contribution to the preparation of publication **no. 2**, **Mohammad Ali Haghighat Bayan**, Yasmin Juliane Dias, Chiara Rinoldi, Paweł Nakielski, Daniel Rybak, Yen B. Truong, Alexander L. Yarin, and Filippo Pierini. "Near-infrared light activated core-shell electrospun nanofibers decorated with photoactive plasmonic nanoparticles 26 for on-demand smart drug delivery applications." Journal of Polymer Science 61, no. 7 (**2023**): 521-533, involved the preparation and improvement of core-shell polymer nanofibers, decoration of core-shell nanofibers with plasmonic nanoparticles, preparation and analysis of SEM images showing the morphology of the fibrous materials, performing chemical analysis of the surface of the materials with the ATR-FTIR apparatus, measurement of photothermal response upon laser irradiation, measurement of drug release of the system over time with and without laser irradiation, as well as preparation of the discussion of the results obtained. Additionally, I was responsible for writing and editing the manuscript, preparing and adjusting figures, and preparing responses to the reviewers.

Signature of the doctoral student

Signature of the supervisor

Doctoral student's statement on participation in a scientific publication

I hereby confirm that my contribution to the preparation of publication **no. 3**, **Mohammad Ali Haghighat Bayan**, Chiara Rinoldi, Daniel Rybak, Seyed Shahrooz Zargarian, Anna Zakrzewska, and Filippo Pierini. "Engineering surgical face masks with photothermal and photodynamic plasmonic nanostructures for enhancing filtration and on-demand pathogen eradication." Biomaterials Science, no 12 (**2024**): 949-963., involved performing chemical analysis with the ATR-FTIR, UV-Vis, and DLS apparatus, the preparation of PAN nanofibers using electrospinning, decorating nanofibers with gold nanoparticles, preparation, and analysis of SEM images showing the morphology of the nanofibers, and face masks, measurement of the photo-thermal response of the mask upon NIR and solar lights, as well as preparation of the discussion of the results obtained. Additionally, I was responsible for writing and editing the manuscript, preparing and adjusting figures, and preparing responses to the reviewers.

Signature of the doctoral student

Signature of the supervisor

Doctoral student's statement on participation in a scientific publication

I hereby confirm my contribution to preparing publication **no. 4**, **Mohammad Ali Haghighat Bayan**, Chiara Rinoldi, Paweł Nakielski, Bin Ding, and Filippo Pierini. "Solar-to-NIR Light Activable PHBV/ICG Nanofiber-Based Face Masks with On-Demand Combined Photothermal and Photodynamic Antibacterial Properties." (**2024**) Advanced Materials Technologies involved the preparation of PHBV nanofibers, enhancing of nanofibers with introducing ICG to the samples, preparation, and analysis of SEM images showing the morphology of the nanofibers, and face masks, performing chemical analysis of the surface of the materials with the ATR-FTIR apparatus, measurement of the contact angle and tensile test of the nanofibers, measurement of ICG release over time, measurement of WVTR of the fabricated face masks, measurement of the photo-thermal response of the mask upon NIR and solar lights, as well as preparation of the discussion of the results obtained. Additionally, I was responsible for writing and editing the manuscript, preparing and adjusting figures, and preparing responses to the reviewers.

Signature of the doctoral student

Signature of the supervisor